INSTITUT POLYTECHNIQUE DE PARIS

NNT : 2024IPPAX008

Thèse de doctorat

Modèle de croissance cellulaire sous l'action d'un stress : Émergence d'hétérogénéité et impact de l'environnement

Thèse de doctorat de l'Institut Polytechnique de Paris
préparée à l'École polytechnique

École doctorale n°574 École doctorale de mathématiques Hadamard (EDMH)
Spécialité de doctorat : Mathématiques appliquées

Thèse présentée et soutenue à Palaiseau, le 9 février 2024, par

IGNACIO MADRID CANALES

Composition du Jury :

Marie Doumic Ingénieure en Chef des Ponts et Forêts, Directrice de recherche, Inria et École polytechnique (CMAP, UMR 7641)	Présidente
Jochen Blath Professor, Goethe-Universität Frankfurt (Institut für Mathematik)	Rapporteur
Marc Hoffmann Professeur, Université Paris-Dauphine PSL (CEREMADE, UMR 7534)	Rapporteur
Bertrand Cloez Chargé de recherche, INRAE Montpellier (UMR Mistea)	Examinateur
Tetsuya Kobayashi Professor, Institute of Industrial Science, The University of Tokyo	Examinateur
Sylvie Méléard Professeur, École polytechnique (CMAP, UMR 7641)	Directrice de thèse
Meriem El Karoui Professor, University of Edinburgh	Co-directrice de thèse

Remerciements

Dans les lignes qui suivent, je tiens à remercier l'ensemble des personnes qui, tout au long de ces trois années et demie de thèse, et bien avant également, ont contribué, peut-être à leur insu, à ce que ces pages voient le jour.

Je commence par remercier mes directrices de thèse, Sylvie et Meriem. Je les remercie toutes les deux de m'avoir offert l'opportunité de participer à ce beau projet de recherche. Je sais à quel point vous teniez à ce projet depuis sa conception. Merci de m'avoir permis de m'initier à ce métier guidé par vos précieux conseils, de votre soutien et confiance constants, et dans un véritable esprit de collaboration personnelle et scientifique, de vraie interdisciplinarité et de confrontation d'idées, qui n'ont fait qu'approfondir mon amour pour ce métier. Je ne me suis jamais senti seul, et je vous en suis très reconnaissant. Je tiens à remercier Sylvie, non seulement pour les heures passées au tableau (ou à l'écran lors des premiers mois encore sous l'ombre du Covid) qui ont profondément et à jamais façonné ma rigueur, mais aussi pour la générosité avec laquelle Sylvie a partagé avec moi son expérience, dans tout ordre de choses. À ce moment où je me livre à l'exercice de la rétrospection, je me rends compte de l'ampleur de la croissance professionnelle et humaine que tous nos échanges m'ont permis de vivre. Merci beaucoup ! De même, je remercie Meriem pour toute sa confiance et ses mots d'encouragement, venus toujours aux bons moments. Merci de m'avoir accueilli dans ton laboratoire à Édimbourg, et d'avoir contribué au façonnement mon esprit sous une autre rigueur, celle de la biologie, différemment exigeante, et qui m'a permis de faire adopter à cette thèse un regard attentif sur la biologie comme que je le souhaitais. Merci à toutes les deux de m'avoir accompagné en ce début de chemin.

Je tiens ensuite à exprimer ma reconnaissance envers Jochen Blath et Marc Hoffmann pour avoir accepté de rapporter cette thèse. Merci pour le temps que vous m'avez consacré, votre lecture attentive et pour l'enthousiasme avec lequel vous avez accueilli mes travaux. Je remercie particulièrement Jochen, qui, malgré des imprévus difficiles, a pu faire partie de ce jury de thèse. Un grand merci également à Bertrand Cloez, Marie Doumic, et Tetsuya Kobayashi d'avoir accepté d'être membres du jury. En paticulier, merci Marie d'en avoir été la présidente. Merci pour les enrichissantes discussions que j'ai eu la chance d'avoir avec vous tous.

Ceux qui s'aventureront dans les pages qui suivent sauront que les travaux présentés sont motivés par une série d'observations expérimentales effectuées au laboratoire El Karoui

de l'Université d'Édimbourg par Sebastián Jaramillo Riveri et James Broughton. En effet, malgré ce qui pourrait en transparaître au tableau ou dans les pages qui suivent, les données ne sont pas simplement données ! Je tiens donc à exprimer ma reconnaissance particulière envers James. Je suis vraiment reconnaissant et toujours impressionné par ses données impeccables, fruit d'un long et ardu travail, dont j'ai eu la chance d'être témoin ne serait-ce que d'une partie infinitésimale l'espace d'une semaine à Édimbourg. Merci également de m'avoir initié à la blouse blanche durant cette semaine, et plus généralement, pour tous nos échanges sur les données, les modèles, tes résultats et les miens. Thanks! Je tiens également à remercier l'équipe de Meriem pour les nombreuses et passionnantes discussions et séminaires, en particulier lors de ma première année de thèse.

Je remercie Maxime Estavoyer et Adil El Abdouni pour nos longues mais toujours très amusantes journées de travail au CIRM l'été 2022. Travailler avec vous a été un vrai plaisir. Je tiens également à remercier Vincent Calvez, Florence Hubert, Julien Olivier et Magali Tournus pour leur encadrement et leurs conseils tout au long de ce projet. Cela m'a permis d'élargir considérablement mes horizons de recherche et de rencontrer des sujets passionnants. J'en profite également pour remercier l'ensemble des organisateurs du CEMRACS 2022, grâce à qui cette expérience de collaboration et de belles rencontres ont pu exister.

Je remercie la Chaire MMB, ses membres et comité de pilotage, de m'avoir fait découvrir une panoplie de sujets fascinants lors de différents rencontres, séminaires et écoles de printemps à Aussois. Merci aussi pour tous les excellents moments passés ensemble, que ce soit à l'X, à la sortie du Museum et surtout aux pieds des Alpes. Ça me manquera ! Je tiens à remercier particulièrement Céline et Josué d'avoir profité de chaque rencontre pour m'encourager et m'aider à décompresser. Je remercie aussi Charline et Aline pour l'invitation à Grenoble et nos discussions.

Je remercie tous les membres du groupe PEIPS et de la toute nouvelle équipe MERGE pour nos échanges et pour tout ce que j'ai appris (peu à peu) dans les séminaires d'équipe (et aux after-works).

Je remercie plus généralement l'ensemble du CMAP pour tout le temps passé ensemble. Je remercie Nasséra, Roberta et toute l'équipe administrative pour leur soutien, disponibilité et patience. Je remercie aussi mes chers collègues et amis doctorants et jeunes docteurs rencontrés dans ces couloirs. Un grand merci à Claire, Dominik, Solange, Corentin et Eugénie de m'avoir si bien accueilli au bureau 2015. Je tiens à remercier Claire tout particulièrement, non seulement parce que c'était un plaisir de t'avoir comme co-bureau, mais aussi parce que tu as été une vraie grande sœur de thèse. J'ai beaucoup appris de toi, merci pour tous tes conseils. Je remercie aussi mes très chers nouveaux co-bureaux, Alexandre, Antoine(s), Vanessa, qui ont reinsufflé de la vie au bureau et avec qui j'adore pouvoir rire et discuter de tout et de rien. Merci Vanessa pour tes jeux et questions improbables. Merci Alexandre pour le temps passé à réfléchir à deux sur tes questions et les miennes. Ton enthousiasme a su me contagier quand j'en avais besoin. Merci aussi au reste de la fratrie, Ana et Anouar, pour les bons moments passés ensemble. Je vous souhaite à tous des belles continuations, et j'ai hâte de recroiser nos chemins. Je remercie finalement Madeleine pour son amitié sincère, nos tentatives de randonnée à Aussois, et toutes nos discussions, en passant par les maths et l'enseignement, mais aussi du futur, la vie et des bons plans !

Je remercie aussi Mme Coussot pour ses précieux conseils.

Je tiens à remercier ici les professeurs qui ont cultivé en moi l'amour des sciences et des maths, et qui surtout, par leur confiance et encouragement, m'ont poussé à rêver du plus loin depuis ma petite ville au Chili. Merci Mariela, David et M. Hormazábal. Je tiens aussi à remercier Rolando Rebolledo, dont la passion transmise dans ses cours et nos échanges, les écoles de "Biostochastique" et l'invitation à participer à un superbe workshop avec des biologistes et écologues chiliens et français, ont été décisifs dans ma décision de venir à l'École polytechnique pour faire des mathématiques appliquées à la biologie, et qui ont, par conséquent, conduit à ces magnifiques années.

À mes amis de toujours, David, Pancho et Daniela, et à mes amis de la faculté, Ignacio, Ignacia (oui, oui, je sais...), Gabriel, Pato, merci beaucoup d'avoir été toujours là et de votre indulgence (enfin j'espère) pour ne jamais répondre à vos messages comme il faut. Un merci particulier à Ignacia, dont la thèse à Grenoble m'a permis de voir plus souvent, et avec qui chaque rencontre me redonnait vie. Enfin, je remercie aussi Martín, échappé aux climats plus cléments, mais qui m'accompagne depuis le début de mon aventure en France et avec qui j'ai pu toujours compter comme sur un grand frère.

À Thomas, merci de ton soutien inconditionnel, d'être toujours à mes côtés, de me rappeler la beauté du monde les jours les plus rudes. Merci aussi à Lucie, Frédéric, Mathias, Clara et Martin d'être ma famille durant tout ce temps.

Je voudrais terminer en remerciant ceux qui ont toujours été là pour me soutenir dans mes choix me ramenant dans des pays lointains et vers des destins pas toujours très définis. Mes parents, Silvia et Renato, mes sœurs, Carla et Camila. Je remercie les efforts immenses de mes parents qui m'ont permis d'aboutir à ces lignes. Sans eux, sans ma chère *bueli*, je n'aurais pas su arriver ici. Gracias.

À tous, je dis un immense merci.

Résumé

Cette thèse porte sur l'analyse statistique et mathématique de la croissance cellulaire à l'échelle individuelle sous l'effet d'un stress. À partir de l'analyse des données recueillies par James Broughton et Sebastián Jaramillo sous la direction de Meriem El Karoui, nous avons construit différents modèles permettant une scompréhension à différents niveaux de l'impact que la réponse hétérogène au stress génotoxique (réponse SOS) a sur la croissance d'une population de bactéries *E. coli*. Pour modéliser la dynamique de ces populations on utilise des processus stochastiques à valeurs mesures.

Nous construisons tout d'abord un modèle stochastique basé sur le modèle "adder" de contrôle de la taille, étendu pour incorporer la dynamique de la réponse SOS et son effet sur la division cellulaire. Le cadre choisi est paramétrique et le modèle est ajusté par maximum de vraisemblance aux données de lignées individuelles obtenues en *mother machine*. Cela nous permet de comparer quantitativement les paramètres inférés dans différents environnements.

Nous nous intéressons ensuite aux propriétés ergodiques d'un modèle plus général que "adder", répondant à des questions ouvertes sur son comportement en temps long. On considère un flot déterministe général et un noyau de fragmentation non nécessairement autosimilaire. Nous montrons l'existence des éléments propres. Ensuite, une h-transformée de Doob avec la fonction propre nous ramène à l'étude d'un processus conservatif. Enfin, en montrant une propriété de *petite set* pour les compacts de l'espace d'états, nous obtenons alors la convergence exponentielle du modèle.

Finalement, nous considérons un modèle bitype structuré en âge modélisant la plasticité phénotypique observée dans la réponse au stress. Nous étudions la probabilité de survie et le taux de croissance de la population en environnement constant et périodique. Nous mettons en lumière un trade-off pour avoir la survie de la population, ainsi qu'une sensibilité par rapport aux paramètres du modèle qui n'est pas la même pour la probabilité de survie et pour le taux de croissance.

Nous concluons avec une section indépendante, initiée durant le CEMRACS 2022. Nous étudions numériquement la propagation spatiale des populations structurés en taille modélisant le mouvement collectif de clusters de *Myxobactéries* à travers de systèmes d'équations de réaction-diffusion.

Abstract

This thesis focuses on understanding individual-scale cell growth under stress. Starting from the analysis of the data collected by Sebastián Jaramillo and James Broughton under the supervision of Meriem El Karoui, we have developed various models to comprehend the impact of the heterogeneous response to genotoxic stress (SOS response) on the growth of a *Escherichia coli* bacteria populations. We employ measure-values stochastic processes to model the dynamics of these populations.

Firstly, we construct a stochastic model based on the "adder" size-control model, extended to incorporate the dynamics of the SOS response and its effect on cell division. The chosen framework is parametric, and the model is fitted by maximum likelihood to individual lineage data obtained in *mother machine*. This allows us to quantitatively compare inferred parameters in different environments.

Next, we explore the ergodic properties of a more general model than the "adder," addressing open questions about its long-time behaviour. We consider a general deterministic flow and a fragmentation kernel that is not necessarily self-similar. We demonstrate the existence of eigenelements. Then, a Doob h-transform with the foud eigenfunction reduces the problem to the study of a conservative process. Finally, by proving a "petite set" property for the compact sets of the state space, we obtain the exponential convergence.

Finally, we consider a bitype age-structured model capturing the phenotypic plasticity observed in the stress response. We study the survival probability of the population and the population growth rate in constant and periodic environments. We evince a trade-off for population establishment, as well as a sensitivity with respect to the model parameters that differs for survival probability and growth rate.

We conclude with an independent section, collaborative work initiated during CEMRACS 2022. We investigate numerically the spatial propagation of size-structured populations modeling the collective movement of *Myxobacteria* clusters via a system of reaction-diffusion equations.

Contents

Chapter 1

Introduction générale

"[W]hile I have sought to shew the naturalist how a few mathematical concepts and dynamical principles may help and guide him, I have tried to shew the mathematician a field for his labour,–a field which few have entered and no man has explored. Here may be found homely problems, such as often tax the highest skill of the mathematician, and reward his ingenuity all the more for their trivial associations and outward semblance of simplicity."

D'Arcy Thompson (*On Growth and Form*, 1917)

1.1 Brève revue du contexte

Cette thèse naît d'une collaboration étroite entre mathématiciens et biologistes établie à partir des observations réalisées par Sebastián Jaramillo et James Broughton dans le cadre de leurs thèses doctorales sous la direction de Meriem El Karoui à l'Université d'Édimbourg. Ils ont observé que lors de l'exposition des cellules bactériennes d'*Escherichia coli* à une faible concentration de ciprofloxacine (un antibiotique qui crée des cassures double-brin de l'ADN), la réponse individuelle au stress est significativement variable d'une cellule à l'autre, bien qu'elles soient isogéniques (partageant le même matériel génétique) et grandissent dans les mêmes conditions.

À l'intérieur d'*E. coli*, la détection d'endommagements de l'ADN provoque une réponse moléculaire complexe appelée **réponse SOS**, induisant la réparation des cassures double-brin et dont l'intensité peut être suivie au cours du temps grâce à des marqueurs fluorescents. Ces mesures d'intensité ont mis en évidence une importante hétérogénéité des réponses entre cellules individuelles, variant de très faibles à très fortes, avec d'importants impacts sur leur morphologie et croissance. En effet, la réponse SOS induit l'expression de protéines qui provoquent l'arrêt de la division, sans pour autant arrêter la croissance cellulaire. De ce fait, l'hétérogénéité des réponses SOS se voit ainsi traduite en hétérogénéité de tailles caractérisée par l'émergence d'une sous-population de très longues bactéries dites *filamenteuses*. De plus, en arrêtant leur division, ces bactéries peuvent être capables de persister après la fin du traitement antibiotique, ce qui fait de ce phénomène un phénomène d'importance cruciale pour la compréhension des mécanismes d'antibiorésistance, sujet majeur de la recherche biomédicale contemporaine et source de croissante préoccupation en santé publique.

Typiquement, lors de mesures de croissance de la population, c'est l'accroissement de la masse totale de la population qui est observée, et non le nombre de cellules. Ainsi les filaments, bien que peu nombreux (5-10% de la population totale en fonction du milieu de croissance [82]), contribuent de manière importante à la croissance observée de la population, beaucoup moins au nombre total de cellules. Il est donc nécessaire de comprendre l'évolution de la population à l'échelle des cellules individuelles pour tenir compte de ces différents comportements. Pour ce faire, il est fondamental de bien comprendre les mécanismes de la division cellulaire qui contrôlent l'évolution temporelle du nombre de cellules à l'échelle individuelle. C'est ensuite au mathématicien de traduire de tels mécanismes en **taux de division** dépendant des *traits* (taille, âge, constitution moléculaire, etc.) de la bactérie. Ce problème s'insère dans une quête plus large et aujourd'hui en plein essor, propulsée par l'explosion du développement de techniques de microscopie *single-cell*, et qui amène les biologistes à se poser une question naturelle : comment ces nouvelles observations *single-cell* se confrontent-elles aux comportements macroscopiques déjà connus ?

Cette question est néanmoins bien antérieure à l'avènement de ces nouvelles techniques de microscopie. Déjà au début du XX^{e} siècle, dans son aujourd'hui célèbre *On Growth and Form*, dont l'épigraphe porte quelques lignes, le biologiste écossais D'Arcy Thompson s'intéressa à l'émergence de la diversité morphologique du vivant à partir de mécanismes *microscopiques*. Il essaya d'expliquer à travers des modèles mathématiques simples la manière dont le *taux de croissance* façonne la *forme* des cellules, tissus, organes, et populations, reliant subtilement ces différentes échelles. Il souligna d'ailleurs avec finesse l'une des difficultés principales de la comparaison des données microscopiques et macroscopiques, en mettant en évidence ce que l'on appellerait aujourd'hui un *biais par l'âge*:

> *We must be very careful, however, how we interpret such a Table [montrant le ralentissement moyen de la croissance chez l'homme au cours de l'âge]; for it records the character of a population, and we are apt to read in it the life-history of the individual. The two things are not necessarily the same. That a man grows less as he grows older all old men know; but it may also be the case, and our Table may indicate it, that the short men live longer than the tall. ([137] p.92)*

L'observation de la croissance bactérienne étant bien plus élusive que l'observation de la croissance humaine, il a fallu atteindre le développement de techniques de microscopie avant que les microbiologistes puissent se poser les mêmes questions. La variabilité dans la prolifération cellulaire a été mise en évidence au moins depuis le papier de 1932 de Kelly et Rahn [88] chez *E. areogenes* et *B. cereus*. Dans ces travaux, ils suivirent à la main plus de 1700 individus durant 4 générations, montrant une considérable variation de leur taux de division (*rate of fission*). Ils remarquèrent la dépendance en âge de la distribution des temps de division et Rahn suggérera lui-même un modèle microscopique pour expliquer cette variabilité, à partir duquel il déduira un taux de division résultant de la convolution de lois exponentielles. David Kendall s'intéressera au sujet (voir [89] et les références citées dans cet ouvrage) et formalisant le modèle de Rahn comme un processus de Markov, essayera d'estimer les valeurs des paramètres du taux de division à l'aide du calcul du coefficient de variation (le ratio entre l'écart-type et la moyenne). Plus tard, une théorie générale des processus stochastiques de branchement avec des taux de division âge-dépendents sera développée par Bellman et Harris en 1948 et 1952 [13].

La suite est bien connue, et le célèbre processus de Bellman-Harris se convertira en outil classique. Néanmoins, la dérivation des liens entre ce type de modèle stochastique et des modèles de population équivalents, l'inférence des paramètres, et en particulier, la compréhension quantitative du *biais par l'âge* qu'il faut considérer en passant de l'un vers l'autre, demeurent un sujet majeur en mathématiques et en biologie. Ce n'est que récemment que le développement des probabilités modernes a permis la formulation rigoureuse des dynamiques stochastiques individu-centrées des populations structurées en âge [57, 140], et l'analyse de l'échantillonnage des lignées individuelles dans l'arbre généalogique d'une population [105]. Du côté de la biologie, le développement récent des techniques de *microfluidique* a permis de capturer, manipuler et suivre de très petits échantillons bactériens, que ce soit des petites populations ou des cellules individuelles, pendant des temps de plus en plus longs [142, 72, 116]. Un clair exemple est le montage expérimental dit *mother machine* [142], avec lequel J. Broughton, S. Jaramillo et M. El Karoui ont acquis les données que l'on analysera (travaux doctoraux de J. Broughton, non publiés à cette date).

1.2 Résultats principaux et synopsis de la thèse

Cette thèse est constituée de quatre chapitres suivant l'introduction. Les résultats résumés ci-dessous ont pour but commun de contribuer à la compréhension de l'impact quantitatif de l'hétérogénéité intercellulaire sur les observables macroscopiques d'une population de cellules sous l'action d'un stress. En combinant une fine observation des données *single-cell*, en étroite collaboration avec les biologistes du laboratoire de M. El Karoui, ainsi que l'utilisation des outils issus de la théorie de processus stochastiques à valeur mesures, de la théorie de semigroupes et de l'analyse d'équations aux dérivées partielles (EDP), cette approche interdisciplinaire vise à améliorer notre compréhension des dynamiques complexes au sein des populations cellulaires, dans ses différentes échelles.

1.2.1 Chapitre 2 : Modélisation et calibration du modèle « adder » à partir des données de cellules individuelles sous stress génotoxique

Dans le deuxième chapitre, nous construisons un modèle de la croissance d'une population de bactéries *E. coli* sous l'effet de stress antibiotique à la lumière des données recueillies par James Broughton, Sebastián Jaramillo et Meriem El Karoui [82, 24] en utilisant le montage microfluidique connu comme *mother machine* (MM) [142, 116], représentée par la Fig. 1.1. Dans ce dispositif, des bactéries isolées sont piégées dans des cavités étroites qui permettent le suivi des lignées cellulaires individuelles au cours du temps (Fig. 1.1A). Les données produites sont d'une grande résolution temporelle et d'échantillons. En effet, un seul dispositif peut comporter autour de 10^4 cavités, permettant l'acquisition d'un grand nombre de lignées indépendantes se développant dans les mêmes conditions et pendant de très longues périodes, réalisant ainsi ce que l'on pourrait considérer comme des *réelles expériences de Monte-Carlo*. Les acquisitions d'image sont effectuées à des intervalles de temps réguliers et permettent de suivre la taille et le niveau de fluorescence des cellules individuelles au fil du temps (Fig. 1.1B-C).

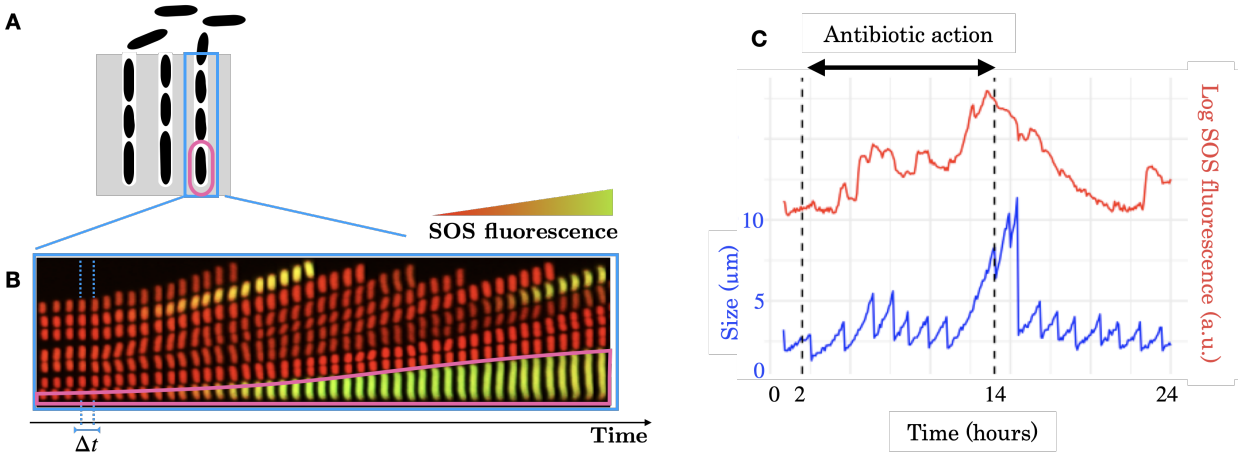

Figure 1.1: La *mother machine* (MM) A. Schéma représentant les cavités parallèles de la *mother machine*. **B**. Kymographe constitué des images de microscopie acquises par J. Broughton dans une cavité (par exemple, celle mise en évidence en bleu dans le panneau **A**). Les acquisitions sont effectuées à des intervalles équidistants de longueur $\Delta t = 5$ minutes. À chaque instant, la fluorescence mesurant l'intensité de la réponse SOS est mesurée. La lignée mère correspond à la trajectoire de la cellule au bas du dispositif (mise en évidence en rose). **C.** Exemple de la taille et de la fluorescence mesurées à partir de la lignée mère dans le kymographe.

À partir d'une analyse originale de ces données, nous proposons un modèle stochastique qui incorpore les sources de variabilité impactant la dynamique de croissance. En premier lieu, on considère une population des cellules en absence de stress, dont la dynamique de division est décrite par le modèle « adder » [133] de contrôle de la taille cellulaire. Sous ce modèle, le temps de division de chaque bactérie est décidé en fonction de la taille a qu'elle a

rajouté depuis sa naissance, et ce, indépendamment de sa taille initiale, i.e.

$$\mathbb{P}(\text{Taille ajoutée jusqu'à la division} \geq a) = S(a) = \exp\left(-\int_0^a B(s)ds\right), \tag{1.1}$$

où B est le taux de division qu'on cherchera à estimer. La surprenante précision de ce simple modèle phénoménologique pour prédire les distributions de taille de *E. coli* a été démontré à plusieurs reprises et sous diverses conditions lors de la dernière décennie [129, 28]. Avec cette simple règle, il a été possible d'expliquer les distributions de tailles stationnaires et de tailles à la division que des modèles plus classiques structurés seulement en taille ou en âge étaient incapables de récupérer fidèlement [133, 46].

On note $a > 0$ la taille ajoutée depuis la naissance et $y > 0$ la taille actuelle de la bactérie. On formule le modèle adder comme un processus stochastique Z_t à valeurs mesures, à support dans $\mathbb{R}_+^2$ (structuré en âge a et taille y) et déterministe par morceaux. On considère en effet que, entre deux divisions aléatoires, chaque cellule grandit à taux exponentiel $\lambda > 0$, commun pour toute la population. Suivant l'approche introduite par [57, 140], en utilisant une représentation trajectorielle de Z_t par rapport à une mesure ponctuelle de Poisson, on montre que pour toute fonction $f \in C_b^{1,1}(\mathbb{R}_+^2)$, Z_t s'écrit comme une semi-martingale de la forme

$$\langle Z_t, f\rangle \overset{\text{def}}{=} \int_{\mathbb{R}_+^2} f(\mathbf{x}) Z_t(d\mathbf{x}) = \langle Z_0, f\rangle + \int_0^t \langle Z_s, \mathcal{Q}f\rangle\, ds + \mathscr{M}_t^f, \tag{1.2}$$

où $\mathscr{M}_t^f$ est une martingale de carré intégrable, et le générateur infinitésimal $\mathcal{Q}$ est donnée pour toute fonction $f \in C_b^{1,1}(\mathbb{R}_+^2)$ par

$$\mathcal{Q}f(a,y) = \lambda y\left(\partial_a + \partial_y\right) f(a,y) + \lambda y B(a)\left(2\int_0^1 f(0,\rho y)F(\rho)\mathrm{d}\rho - f(a,y)\right), \tag{1.3}$$

où F est un noyau de probabilité à support dans $[0,1]$, décrivant une division auto-similaire, i.e. dont la loi dépend uniquement de la proportion entre la taille de la mère et sa fille, et non de la taille absolue de la mère.

L'inférence statistique des taux de division a été étudiée en détail dans d'autres modèles connexes et selon des approches complémentaires (voir, par exemple, le chapitre de revue de Doumic et Hoffmann sur le sujet [46]). On pourra citer en particulier les travaux de Osella et al. [117], Doumic et al. [47], Hoffmann et Olivier [78] et Van Heerden et al. [141], où à partir d'observations *single-cell* de MM, on infère le taux de division en utilisant des estimateurs non paramétriques. Concernant l'estimation de B dans notre cas, comme déjà remarqué par [46], l'hypothèse adder réduit le modèle structuré en taille et âge à un simple modèle de renouvellement, auquel on peut appliquer les techniques classiques d'analyse de survie (voir par exemple le livre [135]). Par exemple, si on dispose d'un échantillon $(A_i)_{i\in[\![1,N]\!]}$ i.i.d. de fonction de répartition $1-S$, on peut définir l'estimateur non-paramétrique classique :

$$\hat{B}(a) = \frac{\sum_{i=1}^N K_h(a-A_i)}{\sum_{i=1}^N \mathbb{1}_{A_i\leq a}}$$

avec $K_h = K(a/h)/h$, où K est un bon noyau (gaussien, par exemple) et $h > 0$ est une fenêtre donnée. La Proposition 4.1 de Doumic et Hoffmann [78] montre que si B es α-höldérienne, la valeur optimale de h donne un taux de converge d'ordre $N^{-\alpha/(2\alpha+1)}$ de $\hat{B}$ vers B. Dans notre cas, on cherche un cadre statistique qui permette non seulement l'estimation de B à partir des données, mais qui soit aussi capable de quantifier l'effet des covariables continues (intensité de fluorescence de la réponse SOS) et qualitatives (milieu de culture) que l'on rajoutera dans la seconde partie du chapitre. De même, on souhaite que le cadre choisi puisse permettre la prédiction (extrapolation) du taux de division, que l'on pourra réutiliser pour réaliser des simulations à partir du modèle ajusté. Ces raisons nous ont conduit naturellement vers un cadre statistique paramétrique. Du côte biologique, cette approche nous permet de fournir des résultats quantitatifs et biologiquement interprétables au moment de comparer les différents *setup* expérimentaux. De plus, nous apportons la preuve numérique que, pour le modèle proposé, la maximisation de vraisemblance est numériquement tractable. Cela peut également permettre des extensions pertinentes dans notre cadre paramétrique, telles que l'inclusion d'effets aléatoires (modèles dits de *fragilité* ou *frailty*, en anglais [79]), que nous discutons dans la conclusion du chapitre.

Finalement, la richesse des données acquises dans le laboratoire de M. El Karoui (à la fois en MM et en population, pour les mêmes souches et sous les mêmes conditions) nous permet de quantifier l'écart entre les données de population et de cellules individuelles. Ainsi, sous une hypothèse de stationnarité, que l'on démontre au Chapitre 3, on confronte les données *single-cell* à des données de population acquises en absence de stress. On met en évidence un décalage systématique qui peut être dû à un effet exogène limitant la croissance de *E. coli* en MM, par rapport aux mesures de population.

En second lieu, on s'intéresse à la croissance sous stress. On couple ce modèle à un modèle stochastique de diffusion représentant l'intensité de la réponse au stress (réponse SOS) comme une variable d'état réelle $(X_t)_{t\geq 0}$ évoluant en temps. En particulier on considère un modèle d'Ornstein-Uhlenbeck

$$\begin{cases} dX_t &= -\theta_{c(t)}\left(\mu_{c(t)} - X_t\right)dt + \zeta^2_{c(t)}dB_t \\ c(t) &= \mathbb{1}_{[\tau_0,\tau_1[}(t) \end{cases}$$

où $[\tau_0, \tau_1[$ est l'intervalle d'administration de l'antibiotique, les paramètres $\{\theta_i, \mu_i, \zeta_i^2\}_{i\in\{0,1\}}$ modélisent l'action de l'antibiotique sur la dynamique de la réponse au stress et B_t est un mouvement brownien standard. Motivé par les mesures expérimentales de X_t par marquage de fluorescence, on construit un nouveau modèle de branchement décrivant l'effet de cette variable sur la dynamique de croissance et division modélisée en premier lieu. À cet égard, on considère des taux de division de la forme $B(a, x)$ dépendant de la taille ajoutée et de la valeur $X_t = x$ au temps de division.

De plus, les observations montrent la présence des divisions asymétriques, dépendantes de la taille y de la mère, que l'on modélise par un noyau $k(y, \cdot)$ qui n'est donc plus autosimilaire. En effet, lorsque *E. coli* devient longue, un système de régulation intracellulaire agit pour définir la position de la division cellulaire, qui n'est plus nécessairement à la moitie de la cellule, mais peut aussi arriver de façon périphérique. À la lumière des données, on propose de modéliser $k(y, \cdot)$ comme un mélange uniforme de $N(y)$ lois Bêta dont le nombre

$N(y) \in \mathbb{N}$ représente le nombre de positions où la division pourrait avoir lieu dans une bactérie de taille y, s'écrivant ainsi

$$k(y,\rho) = \frac{1}{N(y)} \sum_{n=1}^{N(y)} F_n^{N(y)}(\rho), \tag{1.4}$$

où pour tout $N > 1$, $\{F_n^N, n \in [\![1, N]\!]\}$ est une famille de N densités de loi Bêta, dont on estime les paramètres par maximum de vraisemblance à partir des données. Ainsi, le nouveau processus est généré à tout temps $t \geq 0$ par le générateur non homogène

$$\begin{aligned}\tilde{\mathcal{Q}}_{(t)} f(a,y,x) = &- \theta_{c(t)}(\mu_{c(t)} - x)\partial_x f(a,y,x) + \frac{\zeta^2_{c(t)}}{2}\partial_{xx} f(a,y,x) \\ &+ \lambda y \left(\partial_a + \partial_y\right) f(a,y,x) + \lambda y B(a,x) \left(\int_0^1 f(0,\rho y, x) k(y,\rho) \mathrm{d}\rho - f(a,y,x) \right).\end{aligned}$$

En particulier, on utilise un modèle paramétrique flexible basé sur la distribution Gamma généralisé [131], qui permet de générer des fonctions $B(a,x)$ avec des propriétés et interprétations biologiques très vastes. Cela nous permettra de quantifier l'effet perturbatif de la réponse au stress sur les mécanismes de contrôle de la taille chez *E. coli*. De plus, on met en évidence que l'hétérogénéité de la réponse SOS peut biaiser le taux de division adder observé. Cela permet d'expliquer l'émergence apparente d'un régime de *perte de contrôle*, où le taux de division diminuerait pour les bactéries plus longues.

1.2.2 Chapitre 3 : Ergodicité exponentielle d'un modèle général structuré en taille et âge

Cette partie a été publiée sous forme d'article dans *Acta Applicandae Mathematicae* [103].

L'hypothèse de stationnarité qui est clé pour la comparaison des mesures individuelles et de populations est démontrée dans le troisième chapitre. Cela est fait pour une version plus générale du modèle déterministe par morceaux structuré en taille et âge introduit dans le chapitre 2. On étudie le comportement en temps long du semigroupe de transition $M_t : C_b^{1,1}(\mathbb{R}_+^2) \to C_b^{1,1}(\mathbb{R}_+^2)$ associé au processus Z_t défini par

$$M_t f(a,y) \overset{\text{def}}{=} \mathbb{E}_{\delta_{(a,y)}}\left[\langle Z_t, f\rangle\right] = f(a,y) + \int_0^t M_s\left(\mathcal{Q} f\right)(a,y)\mathrm{d}s$$

avec la méthode probabiliste dite *de Harris* [71, 69, 10, 14], suivant la théorie initiée par Doeblin [40], et largement développée et popularisée par Meyn et Tweedie [112]. À cette fin, on établit préalablement des estimations concernant les éléments propres du générateur infinitésimal $\mathcal{Q}$, grâce à des méthodes analytiques basées sur le théorème de Krein-Rutman, suivant les idées développés notamment par B. Perthame [119] pour l'étude des équations de transport.

On considère un modèle plus général que l'adder, caractérisé par un nouveau générateur $\mathcal{Q}$ défini pour toute $f \in C_b^{1,1}(\mathbb{R}_+^2)$ par

$$\mathcal{Q} f(a,y) = g(a,y)^\top \nabla f(a,y) + \beta(a,y)\left(\int_0^\infty f(0,z) k(a,y,z)\mathrm{d}z - f(a,y) \right),$$

où $g(a,y) = (g_1(a,y), g_2(a,y))$ contient le taux de vieillissement $g_1(a,y)$ et le taux d'élongation $g_2(a,y)$ d'un individu d'âge a et taille y, $\beta(a,y)$ est le taux de division d'un individu d'âge a et taille y, et $k(a,y,z)$ est un noyau à densité décrivant les tailles z de la descendance d'un individu d'âge a et taille y au moment de sa division. Ainsi, sont cas particuliers le modèle adder classique, donné par $g_1(a,y) = g_2(a,y) = \lambda y$ et $k(a,y,z) = k(y,z) = \frac{2}{y}F(z/y)$, et le modèle adder avec division asymétrique, où le noyau k est donné par (1.4).

On utilise la version du théorème ergodique de Harris formulée sous le nom de *Théorème d'ergodicité V-uniforme* par Meyn et Tweedie [111] comme suit:

Théorème 3.2.1 (Théorème 6.1 de [111]). *Soit $(X_t)_t$ un processus de Markov continu à droite aux valeurs dans un espace polonais localement compact E muni de sa tribu borélienne $\mathcal{B}(E)$, et soit $\mathcal{A}$ le générateur infinitésimal de X. Soit P_t le semigroupe de transition associé. Si les deux conditions suivantes sont vérifiées :*

(H1) ***Condition de minorisation (dite de Doeblin ou de petite set) pour les ensembles compacts de*** *E . Tout ensemble compact de E est petite pour un squelette de X, c'est à dire, pour tout compact $\mathcal{K} \subset E$ il existe une mesure de probabilité discrète $\mu = (\mu_n)_{n\in\mathbb{N}}$ sur $\mathbb{N}$ et un $\Delta > 0$ telle qu'il existe une mesure non-triviale ν (qui peut dépendre de Δ et μ) sur $\mathcal{B}(E)$ qui pour tout $\mathbf{x} \in \mathcal{K}$ vérifie la borne inférieure :*

$$\langle \mu, \delta_{\mathbf{x}} P_\cdot f\rangle = \sum_{n\in\mathbb{N}} \mu_n P_{n\Delta} f(\mathbf{x}) \geq \langle \nu, f\rangle .$$

(H2) ***Condition de Foster-Lyapunov***

Il existe une fonction coercive V, i.e. $V(\mathbf{x}) \to +\infty$ lorsque $||\mathbf{x}|| \to +\infty$, telle que $V(\mathbf{x}) \geq 1$ pour tout $\mathbf{x}$, et des constantes $c > 0$, $d < \infty$ telles que

$$\mathcal{A}V(\mathbf{x}) \leq -cV(\mathbf{x}) + d \quad \forall \mathbf{x} \in E.$$

Sous (H1) et (H2), il existe une unique mesure de probabilité non-triviale π et constantes $C, \omega > 0$ telles que pour tout $\mathbf{x} \in E$ et $t \geq 0$

$$||\delta_{\mathbf{x}} P_t - \pi||_V \leq CV(\mathbf{x}) \exp(-\omega t), \tag{1.5}$$

où $||\cdot||_V$ est une norme définie par

$$||\mu||_V := \sup_{g:||g||\leq V} |\langle \mu, g\rangle|$$

En particulier, $||\mu||_1 = ||\mu||_{TV}$ est la norme de variation totale.

Or, le semigroupe généré par $\mathcal{Q}$ n'est pas nécessairement conservatif. Bien que récemment Bansaye et al. aient établi dans [10] un résultat étendant le théorème de Harris aux semigroupes non conservatifs, il s'avère que les conditions dites de *contrôle du ratio de masses* (hypothèses (A3) et (A4) *ibidem*) sont assez difficiles à montrer dans le cas à deux dimensions continues (taille et âge). Ces conditions sont liées à l'irréductibilité du processus

et sont associées à l'existence d'un temps de couplage à partir duquel les trajectoires issues de toute condition initiale se croisent (voir par exemple la discussion dans [34]). La difficulté dans notre cas est de construire de telles trajectoires, car le flot déterministe déterminé par g ne peut explorer $\mathbb{R}_+^2$ que par des trajectoires unidimensionelles. Qui plus est, les transitions sont non locales et dégénérées : bien que les tailles de cellules filles suivent une loi à densité $k(a, y, \cdot)$, l'âge de cellules nouveau-nées est renvoyé de façon déterministe à 0. La condition de *petite set* établie par (H1) permet de contourner cette difficulté, car au lieu de demander un temps de couplage uniforme pour tout condition initiale, elle autorise à prendre une moyenne discrète en temps par rapport à la loi d'échantillonnage μ. Le lecteur habitué à d'autres versions aujourd'hui plus classiques du théorème de Harris peut se référer à la discussion faite au Chapitre 3, où l'on commente à propos de ces versions équivalentes.

Pour appliquer ce théorème on doit d'abord construire un bon semigroupe conservatif, qui nous permette ensuite de remonter au comportement ergodique de M_t. Pour ce faire, on montre d'abord que sous les hypothèses 3.3.3, il existe une unique fonction propre $h : \mathbb{R}^2 \to \mathbb{R}_+$ et valeur propre $\Lambda > 0$ solutions du problème aux valeurs propres

$$\mathcal{Q}h = \Lambda h. \tag{1.6}$$

Cela nous permet de construire un processus auxiliaire de générateur

$$\mathcal{A}f(a,y) = g(a,y)^\top \nabla f(a,y) + \beta(a,y)\left(\int_0^\infty (f(0,z) - f(a,y))\,\frac{h(0,z)}{h(a,y)} k(a,y,z)\mathrm{d}z\right)$$

dont le semigroupe associé P_t est Markovien et conservatif ($P_t 1 \equiv 1$) et peut donc être étudié avec les techniques de Meyn et Tweedie. Ensuite, on récupère le semigroupe associé au processus originel via une *h-transformée de Doob*:

$$M_t f(a,y) = e^{\Lambda t} h(a,y) P_t\left(\frac{f}{h}\right)(a,y).$$

Cela nous permet finalement d'obtenir le résultat principal du chapitre:

Théorème 3.2.4 (Ergodicité exponentielle)**.** *Sous les Hypothèses 3.3.3 et si la condition (H2) est vérifiée pour une fonction coercive $V : \mathbb{R}_+^2 \to \mathbb{R}_+$, alors il existe une unique mesure de probabilité π et des constantes $C, \omega > 0$ telles que pour toute condition initiale $\mu_0 \in \mathcal{M}_p(\mathbb{R}_+^2)$*

$$||e^{-\Lambda t}\mu_0 M_t - \langle \mu_0, h\rangle \pi||_V \leq C \langle \mu_0, V\rangle e^{-\omega t}. \tag{1.7}$$

Les idées des preuves sont les suivantes:

1. **Existence de h**

   a) On commence par réduire le problème (1.5) à un problème scalaire grâce à la propriété de renouvellement en a. Dans le Lemme 4.4.2 on montre que (Λ, h) est

solution de (1.5) (et d'une certaine condition limite) avec $\Lambda > 0$ et $h \in W^{1,\infty}_{loc}(\mathbb{R}^2_+)$ si et seulement si

$$h(a,y) = \int_0^\infty h(0,z)K_\Lambda(a,y,z)\mathrm{d}z$$

pour un certain noyau $K_\Lambda : \mathbb{R}^3_+ \to \mathbb{R}_+$ dont les propriétés spectrales déterminent celles de $\mathcal{Q}$. On considère donc l'opérateur $\mathcal{G}_\lambda$ définie pour toute fonction $f \in C^1(\mathbb{R}_+)$ par

$$\mathcal{G}_\lambda f(y) = \int_0^\infty f(z)K_\lambda(0,y,z)dz \quad \forall y > 0. \tag{1.8}$$

b) On démontre ensuite l'existence de $\Lambda > 0$ et $h \in W^{1,\infty}_{loc}(\mathbb{R}^2_+)$ solutions de (1.5) adaptant un schéma classique construit sur le théorème de Krein-Rutman, comme suit :

   i. On construit une version tronquée de $\mathcal{G}_\lambda$ qui est compacte. On applique ensuite le théorème de Krein-Rutman pour montrer que pour tout $\lambda \geq 0$ l'opérateur tronqué admet une unique valeur propre $\mu_\lambda \geq 0$ et fonction propre $h_\lambda \geq 0$, à une normalisation près.

   ii. On montre qu'il existe un unique $\lambda_0 > 0$ tel que $\mu_{\lambda_0} = 1$. De plus, on montre que la valeur de λ_0 est uniformément bornée pour toute troncature de $\mathcal{G}_\lambda$.

   iii. On passe à la limite et on montre que les éléments propres limites $(\lambda_0, h_{\lambda_0})$ de la famille de troncatures compactes de $\mathcal{G}_\lambda$ sont effectivement solutions du problème aux valeurs propres.

2. **Preuve de la condition de Doeblin (H1)**

   En conditionnant par rapport aux temps de division, on écrit l'action du semigroupe P_t comme la solution *mild* d'une équation recursive (formule de Duhamel (3.39)). Ensuite, pour toute fonction f mesurable et bornée, on peut minorer $P_t f(a,y)$ en faisant des itérations successives de la formule et gardant les termes que l'on sait contrôler sous les hypothèses 3.3.3. La preuve consiste donc essentiellement à estimer des bornes inférieures de ces termes sur toute trajectoire issue d'un compacte donné.

On conclut le chapitre avec l'application au modèle adder où $\mathcal{Q}$ est donné par (1.3), pour lequel on montre la convergence exponentielle vers sa mesure stationnaire. En particulier, pour le modèle adder avec croissance exponentielle les éléments propres sont explicites : $h(a,y) = y$ et $\Lambda = \lambda$ (le taux d'élongation), et la condition de Lyapunov (H2) est vérifiée par $V(a,y) = y^{-1} + y$. Le résultat général s'étend aussi au cas où la croissance n'est pas exponentielle ou les divisions ne sont pas symétriques. Cet ensemble de résultats permet de répondre ainsi à des questions ouvertes laissées par l'analyse de Gabriel et Martin [62].

1.2.3 Chapitre 4 : *Trade-offs* dans un modèle de prolifération bactérienne sous stress

Dans le quatrième chapitre, on cherche à introduire dans l'analyse un élément clé, délibérément délaissé dans nos premiers chapitres : la présence de *mort cellulaire*. En effet, même

aux doses supposées sous-létales de ciprofloxacine, on peut observer un nombre non négligeable de bactéries qui arrêtent totalement leur croissance et division. Or, l'induction de la réponse SOS devrait avoir un rôle protecteur. De fait, notre analyse des données montre que la réponse SOS n'est pas seulement hétérogène entre chaque cellule, mais également que, au cours de la vie d'une bactérie, l'intensité de la réponse peut fluctuer significativement, donnant émergence à un phénomène de *plasticité phénotypique*. À certains moments, de façon aléatoire mais dépendante de l'environnent et de l'intensité du stress, *E. coli* peut passer de son état normal d'apparente inactivité de réponse SOS à un état de forte activité. On observe ainsi, lorsque l'antibioitique est présent, des distributions bimodales dans le niveau de réponse SOS. Ensuite, après une ou plusieurs divisions, la progéniture d'une cellule qui a très fortement induit la réponse SOS est capable de retourner à l'état normal.

Dans le but d'améliorer la compréhension phénoménologique et quantitative de l'intérêt évolutif de cette stratégie de plasticité pour répondre au stress, nous formulons un modèle stochastique minimal qui préserve les éléments principaux du phénomène. Ainsi, nous gardons une structure en âge, tandis que la variabilité de la réponse SOS est résumée en deux traits discrets. Nous considérons ainsi des cellules *vulnérables* (type $i = 0$), susceptibles de mourir au moment de leur division avec probabilité $p \in (0, 1)$, et des cellules *tolérantes* (type $i = 1$), dont les temps de divisions sont néanmoins beaucoup plus longs. Les temps de divisions des deux phénotypes sont caractérisés par leur taux de division $\beta_0(a)$ et $\beta_1(a)$. Les cellules vulnérables peuvent devenir tolérantes à taux $\alpha > 0$. À leur tour, les cellules tolérantes ne peuvent redevenir vulnérables qu'après leur division, ce qui arrive avec une une probabilité de rétablissement $\gamma \in (0, 1)$. On formalise cette dynamique avec un processus stochastique Z_t à valeurs mesures à support sur $\mathbb{R}_+ \times \{0, 1\}$ tel que

$$Z_t(da, di) = Z_t(da, \{0\})\delta_0(di) + Z_t(da, \{1\})\delta_1(di)$$

et qui admet pour toute $f \in C^{1,\cdot}(\mathbb{R}_+ \times \{0, 1\})$ et $t \geq 0$ la décomposition en semimartingale

$$\begin{aligned}\int (f(a,0)Z_t(da,\{0\}) + f(a,1)Z_t(da,\{1\})) \\ = \int (f(a,0)Z_0(da,\{0\}) + f(a,1)Z_0(da,\{1\})) \\ + \int_0^t \int (\mathcal{Q}f(a,0)Z_s(da,\{0\}) + \mathcal{Q}f(a,1)Z_s(da,\{1\}))ds + \mathcal{M}_t^f,\end{aligned} \tag{1.9}$$

où $\mathcal{M}_t^f$ est une martingale de carré intégrable et le générateur $\mathcal{Q}$ est défini par

$$\begin{aligned}\mathcal{Q}f(a,i) = \partial_a f(a,i) + (1-i)\alpha(f(a,1) - f(a,0)) - \beta_i(a)f(a,i) \\ + 2(1-i)(1-p)\beta_i(a)f(0,0) + 2i\beta_i(a)(\gamma f(0,0) + (1-\gamma)f(0,1))\end{aligned} \tag{1.10}$$

On s'intéresse au comportement en temps long de Z_t. En premier lieu, on met en évidence un *trade-off* explicite entre le taux de switch phénotypique et la probabilité de récréer des individus vulnérables qui dépend du niveau de stress p. Si on note $\lambda_{\alpha,\gamma}$ le taux de croissance exponentielle de la population et $\pi_i^{\alpha,\gamma}$ la probabilité d'extinction de la population issue d'une cellule inviduelle d'âge 0 et type i on montre

Théorème 4.3.5 et 4.4.5. *Sous les hypothèses 4.2.1 on a*

$$\lambda_{\alpha,\gamma} > 0 \iff \pi_0^{\alpha,\gamma}, \pi_1^{\alpha,\gamma} < 1 \iff \left\{ p \leq \frac{1}{2} \right\} \cup \left\{ p > \frac{1}{2} \text{ and } \gamma < \frac{1}{2}\left(1 + \frac{q}{(2p-1)(1-q)}\right) \right\},$$

où $q = \int_0^{+\infty} \alpha \exp\left(-\int_0^a (\alpha + \beta_0(s))\mathrm{d}s\right) \mathrm{d}a$ *est la probabilité qu'une cellule de type* ***0*** *switche vers le type* ***1*** *avant se diviser.*

Ensuite, on analyse les sensibilités de $\lambda_{\alpha,\gamma}$ et de $\pi_i^{\alpha,\gamma}$ par rapport aux variations de α et γ. En contraste avec les résultats de Campillo et al. [27], qui s'intéressent aussi aux liens entre les deux mesures de fitness, mais pour un modèle mono-type structuré en taille, nous montrons que la présence de plasticité phénotypique permet de casser la monotonie espérée entre les variations du paramètre Malthusian et la probabilité de survie de la population. En effet on montre que des variations de α et γ qui font diminuer la probabilité de survie de la population, peuvent faire augmenter le taux de croissance global de la population. C'est le résultat principal suivant :

Théorème 4.5.6. *Sous les hypothèses 4.2.1 et 4.2.4, on a pour tout* $\alpha \geq 0$.

$$\partial_\gamma \pi_0^{\alpha,\gamma} > 0 \text{ et } \partial_\gamma \pi_1^{\alpha,\gamma} > 0$$

En revanche, pour tout $\alpha \geq 0$ *il existe une valeur critique* $\bar{p} \leq 1/2$ *tel que pour tout* $\gamma \in (0,1)$

$$\partial_\gamma \lambda_{\alpha,\gamma} > 0 \iff p < \bar{p},$$
$$\partial_\gamma \lambda_{\alpha,\gamma} < 0 \iff p > \bar{p}.$$

Ce résultat nous indique que seules les « stratégies extrémales » de plasticité phénotypique ($\gamma = 0$ ou $\gamma = 1$) sont optimales au sens Darwinien du maximum de fitness $\lambda_{\alpha,\gamma}$. Pour conclure, on montre que l'intérêt des stratégies de plasticité non triviales émerge quand l'environnement (i.e. la probabilité de mort p) est autorisé à fluctuer au cours du temps. Pour ce faire, nous considérons le cas où la probabilité de mort est une fonction du temps $p(t)$ continue et T-périodique. On étend nos résultats précédents en utilisant la théorie de Floquet [32]. Bien que l'on ne puisse pas exhiber le *trade-off* de façon aussi explicite que pour le cas où p est constant, on montre que le signe de la dérivée $\partial_\gamma \lambda_{\alpha,\gamma}$ peut changer de façon non-triviale en fonction des valeurs de $p(t)$. En particulier, on illustre numériquement que, en fonction de la période T, la valeur optimale de $\lambda_{\alpha,\gamma}$ est atteinte à l'intérieur de l'espace de paramètress, i.e. pour $\gamma \in (0,1)$ et $\alpha > 0$.

De façon intéressante, on peut comparer nos résultats mathématiques à des travaux expérimentaux précédents qui ont essayé de mesurer la fitness de populations de *E. coli* dont le taux d'induction et répression de la réponse SOS face aux endommagements de l'ADN sont manipulés à l'aide de modifications génétiques [92]. Cela permet aux auteurs d'inférer un paysage de fitness (*fitness landscape*) qui donne la valeur de λ en fonction des modifications génétiques réalisées. Ainsi, si on associe notre paramètre de switch α

à leur paramètre d'induction de réponse SOS (qui fait passer les cellules vulnérables en cellules tolérantes), et notre paramètre de rétablissement γ à leur paramètre de répression de réponse SOS (qui permet de revenir à l'état normal lorsque les endommagements de l'ADN ont été réparés), on peut comparer nos prédictions de $\lambda_{\alpha,\gamma}$ à leurs paysages de fitness. Nous discutons sur quelques comportements qualitatifs que nos résultats mathématiques permettent d'éclaircir.

1.2.4 Chapitre 5 : Changement de régime dans la vitesse de propagation d'une population de *Myxobactéries* structuré en taille de clusters

Ce chapitre a été élaboré au cours de l'école de recherche CEMRACS 2022, qui a eu lieu au CIRM (Marseille) pendant l'été 2022, en collaboration avec Vincent Calvez, Adil El Abdouni, Maxime Estavoyer, Florence Hubert, Julien Olivier and Magali Tournus. Ce chapitre a été soumis à publication dans *ESAIM: Proceedings and Surveys*.

Nous nous intéressons au phénomène de la propagation spatiale d'une population de bactéries structurée en taille et position spatiale. Bien qu'il s'agisse cette fois-ci de *Myxococcus xanthus*, bactérie terrestre prédatrice d'*E. coli* dont le comportement et très diffèrent de celui de sa proie, l'étude vise pareillement à analyser l'effet de la structure en taille sous-jacente sur le comportement macroscopique de la population. Cette fois ce n'est pas le taux de croissance que l'on regarde comme indicateur de *fitness* de la population, mais la vitesse de sa propagation spatiale. En effet, en présence des proies, *M. xanthus* se déplace de façon collective à travers des fronts de propagation constitués de *clusters* de bactéries de diverses tailles, pouvant contenir d'une bactérie isolée à plusieurs milliers de bactéries chimiquement recollées les unes aux autres. De façon intéressante, cet attroupement a un effet synergique et le coefficient de diffusion spatiale des *clusters* est plus élevé que celui des bactéries isolées.

On considère un modèle minimal de réaction-diffusion avec une structure de taille très simplifiée, consistant en *clusters* de 1 ou 2 bactéries seulement. Pour $i \in \{1,2\}$, on note $p_i(x,t)$ la densité de nombre de clusters de i bactéries à la position spatiale $x \in \mathbb{R}$ au temps $t \geq 0$. On note aussi $p = p_1 + 2p_2$ la densité du nombre total de bactéries. On se place dans l'échelle de grandes populations et on suppose toutes les cellules bien mélangées, de façon que p_1 et p_2 sont solutions du système de réaction-diffusion

$$\partial_t p_1 = \theta_1 \Delta p_1 - \tau_1 p_1^2 + 2\tau_2 p_2 + \alpha p_1 \left(1 - \frac{p}{K}\right), \tag{5.1}$$

$$\partial_t p_2 = \theta_2 \Delta p_2 + \frac{\tau_1}{2} p_1^2 - \tau_2 p_2, \tag{5.2}$$

Le premier terme de (5.1) et (5.2) est un terme de diffusion, décrivant le mouvement spatial aléatoire de bactéries isolées et de paires de bactéries. On suppose que $\theta_2 > \theta_1$, i.e. que les clusters se diffusent plus rapidement que les bactéries isolées. Le terme non linéaire $\tau_1 p_1^2$ représente la coagulation de 2 bactéries isolées qui deviennent 1 cluster de 2 bactéries à taux $\tau_1 > 0$. De même, le terme $\tau_2 p_2$ corresponds à la fragmentation de 1 cluster de 2 bactéries qui devient 2 bactéries individuelles à taux $\tau_2 > 0$. On suppose que seules les bactéries isolées peuvent se diviser. On suppose que cette croissance est de type logistique, avec un taux de croissance $\alpha > 0$ et une capacité de charge $K > 0$. Ainsi, le système

(5.1)-(5.2) est une extension de l'Équation de Fisher-KPP [54, 90]. En particulier, on peut obtenir Fisher-KPP en faisant $\tau_2 = 0$, ce qui découple les deux équations.

Nous explorons numériquement le comportement en temps long du modèle en fonction des valeurs des taux de coagulation τ_1 et fragmentation τ_2 de clusters, et du rapport entre les coefficient de diffusion de clusters θ_2/θ_1. Les simulations numériques de ce système nous permettent de conclure l'existence de solutions d'onde pour toutes les valeurs positives de paramètres. De plus, nous observons deux régimes distincts séparés par un seuil constant θ^* pour le rapport θ_2/θ_1. Lorsque $\theta_2/\theta_1 < \theta^*$, le front de propagation consiste en ondes dites "tirées". Cela signifie que la vitesse de propagation est égale à la vitesse du modèle Fisher-KPP. Dans ce cas, la propagation de la population est limitée par la motilité des bactéries isolées, de sorte que l'attroupement n'affecte pas en réalité la vitesse. Cependant, lorsque $\theta_2/\theta_1 > \theta^*$, le front de propagation consiste en ondes dites "poussées". Dans ce cas, la vitesse de propagation est strictement supérieure à la vitesse de Fisher-KPP, grâce à l'effet non négligeable de la non-linéarité introduite par le terme de coagulation. Autrement dit, nous concluons que lorsque la motilité des clusters est suffisamment grande par rapport à la motilité des bactéries isolées, le comportement collectif de *M. xanthus* permet à l'ensemble de la population de se propager plus rapidement que dans le cas sans *clusterisation*. Nous observons également que θ^* est indépendant des taux de coagulation et de fragmentation. En particulier, nous pouvons réduire le système au cas $\tau_1, \tau_2 \to +\infty$, ce qui nous donne une équation scalaire que nous étudions numériquement, et dont nous donnons quelques heuristiques pour son étude analytique.

Ensuite nous nous intéressons à un modèle plus général, à structure de taille continue, apparenté au modèles de population structurée formulés aux chapitres précédents. On étend le système (5.1)-(5.2) à un modèle général de Diffusion-Croissance-Fragmentation-Coagulation décrit par (5.3)-(5.5) ci-dessous, où $\rho(t,x,z)$ est la densité de nombre de clusters de taille $z \in [0, z_{max}]$ en position spatiale $x \in \mathbb{R}$ au temps $t \geq 0$. On modélise ρ comme la solution du système intégro-différentiel suivant

$$\partial_t \rho(t,x,z) = \partial_{xx}\left[\theta(z)\rho(t,x,z)\right] - \partial_z\left[v(z,m)\rho(t,x,z)\right] + \mathcal{F}[\rho](t,x,z) + \mathcal{G}[\rho](t,x,z), \quad (5.3)$$

où $m(t,x) = \int_0^{z_{\max}} z'\rho(t,x,z')\,dz'$ est la densité locale du nombre de bactéries, $v(z,m) \geq 0$ est la vitesse de croissance de clusters de taille z quand le nombre local de bactéries alentour est m, $\mathcal{F}$ l'opérateur de fragmentation défini par

$$\mathcal{F}[\rho](t,x,z) = 2\int_z^{z_{\max}} \beta(z')k(z',z)\rho(t,x,z')\,dz' - \beta(z)\rho(t,x,z), \quad (5.4)$$

et $\mathcal{G}$ l'opérateur de coagulation défini par

$$\begin{aligned}\mathcal{G}[\rho](t,x,z) = \frac{1}{2}\int_0^z \gamma(z-z',z')\rho(t,x,z-z')\rho(t,x,z')\,dz' \\ - \rho(t,x,z)\int_0^{z_{\max}-z} \gamma(z',z)\rho(t,x,z')dz'. \quad (5.5)\end{aligned}$$

L'existence de fronts de propagation dans des modèles de populations structurés a été étudiée dans des cas particuliers [49, 21, 2, 67]. L'étude numérique du cas avec un opérateur de coagulation est nouveau. Nos expériences numériques montrent que la solution du

système integro-différentiel admet aussi des solutions en forme d'onde. De plus, comme pour le modèle à 2 types, on remarque l'existence d'un seuil pour le coefficient de diffusion à partir duquel la vélocité c est plus grandd que la vélocité de Fisher-KPP.

On conclut le chapitre avec des expériences numériques d'une extension du modèle à 2 types où l'on rajoute proie dans le milieu. Au contact de leur proie, les bactéries peuvent *switcher* vers un état dit d'alimentation, où elles consomment la proie en arrêtant de se diffuser. L'idée est de récupérer, au moins de façon qualitative, les données d'avancement du front de propagation de *M. xanthus* sur une gouttelette de *E. coli* (proie), où l'on voit la décélération du front de propagation au contact de *E. coli*. Nos simulations montrent un accord qualitatif avec les expériences biologiques, ce qui permet de valider notre modèle très simplifié. Ainsi, nous concluons que la sociabilité et la forte diffusion des clusters de *M. xanthus* jouent un rôle prépondérant dans la vitesse de prédation et de propagation spatiale de la population.

1.2.5 Conclusion générale et perspectives

La discussion spécifique de ces résultats est donnée en anglais à la fin de chaque chapitre. Nous nous permettons de donner ici une conclusion synoptique à la lumière de ces quatre parties, ainsi que quelques perspectives ouvertes par ces travaux.

Du point de vue de la biologie, les résultats de cette thèse illustrent mathématiquement et numériquement l'effet positif que l'hétérogénéité cellulaire peut avoir sur diverses mesures de la *fitness* d'une population bactérienne, malgré les effets apparemment négatifs que cela peut avoir à l'échelle microscopique. Ainsi, la diminution du taux de division induite par la réponse SOS mise en évidence par inférence statistique dans le Chapitre 2, permettrait toutefois d'assurer un meilleur rendement malthusien si les cellules plus âgées deviennent en même temps tolérantes, comme les résultats du Chapitre 4 le montrent. De même, les résultats du Chapitre 5 montrent que la diffusion accélérée des agglomérés cellulaires peut accélérer la vitesse de propagation de la population globale, même si ce n'est que les cellules isolées qui sont capables de se nourrir et de se reproduire.

On voit néanmoins que ces effets sont souvent soumis à des *trade-off* associant le risque lié aux stratégies d'hétérogénéité, comme la probabilité de mourir p de cellules à division rapide du Chapitre 4. Ces *trade-offs* font émerger de résultats intéressants, et suggèrent des éléments de preuve de l'intérêt évolutif de l'apparition de telles stratégies. Ainsi, l'émergence de la filamentation chez *E. coli* peut être expliquée en partie par l'adaptation conjointe des taux d'induction et de répression de la réponse SOS (α,γ) et des taux de division (β_0, β_1) dans un environnement fluctuant.

De plus, les résultats mathématiques du Chapitre 4 suggèrent que certaines modifications de la réponse SOS (comme celles qui peuvent être provoquées par certaines molécules antibiotiques) peuvent diminuer la probabilité d'établissement de microcolonies, mais augmenter le taux de croissance asymptotique de la population. Cela soulève des questions méthodologiques sur la comparaison des résultats expérimentales où la mesure d'intérêt est la survie de la colonie et d'autres où la mesure d'intérêt est le taux de croissance de la population. Qui plus est, ces différences prennent source dans l'hétérogénéité sous-jacente et souvent mal ou pas prise en compte. Ainsi, des procédés de modélisation donnée-centrés qui

prennent en compte explicitement l'hétérogénéité face au traitement antibiotique et qui permettent de confronter données single-cell et de population, tel que l'on présente au Chapitre 2, deviennent de cruciale importance.

Cependant, on remarque la présence d'une hétérogénéité supplémentaire, qui n'est pas entièrement comprise par le niveau d'intensité SOS. Il serait très intéressant de modéliser cette hétérogénéité supplémentaire avec une approche à effets mixtes. Des avancées récentes de cette théorie pour l'étendre aux flots stochastiques, d'un côté, et aux lignées cellulaires, de l'autre, pourraient être adaptées à notre cas.

Du point de vue des outils mathématiques, nous donnons dans le Chapitre 3 notre contribution majeure. L'approche probabiliste choisie permet de contourner les problèmes liés au manque de compacité qui apparaissent dans l'estimation de bornes de hypocoercivité dans des approches plus analytiques. Cela nous permet de montrer des nouveaux résultats que, même pour le cas adder d'origine, n'étaient pas accessibles précédemment. De même, on contribue avec quelques idées originales pour la construction des éléments propres de l'opérateur $\mathcal{Q}$ associé (en absence d'hypothèse d'auto-similarité pour le noyau de fragmentation, par exemple) et pour la construction trajectorielle de la condition de Doeblin qui peuvent être applicables à d'autres contextes.

Pour conclure, nous avons traité la question de l'hétérogénité cellulaire sous une approche *coarse-grained* : les mécanismes derrière la variabilité intracellulaire ont été réduits en taux de division, types cellulaires et traits continus dont l'interprétation biomoléculaire est plutôt diffuse. Bien que cela nous permette déjà de lier les dynamiques au niveau de cellules individuelles et au niveau de population, une perspective intéressante est d'obtenir l'hétérogénéité cellulaire comme résultat d'une hétérogénéité métabolique, ce qui permettrait de lier les dynamiques biomoléculaires aux dynamiques de population. La régulation métabolique du contrôle de la taille cellulaire (pour expliquer le modèle adder, particulièrement) est un sujet actif de recherche en biologie, mais l'impact de ces mécanismes sur la croissance de populations est loin d'être clair. Ainsi, la question du contrôle de la taille et de l'hétérogénéité bactérienne constitue un champ d'application idéal pour des méthodes à l'interface de l'analyse et des probabilités. Qui plus est, l'avancement des techniques expérimentales et la richesse de données permettent la confrontation des résultats théoriques avec des résultats empiriques dans un niveau comparable à celui de la physique, ainsi que des questionnements sur le long terme et les adaptations évolutives. Beaucoup de biologistes et physiciens s'accordent à dire que le développement de la microbiologie des 80 dernières années est comparable à celui de l'astronomie et la physique à l'aube du XVII^{e} siècle [84]. De même, le besoin d'outils mathématiques adaptés ne devrait qu'augmenter, d'où la valeur des approches rigoureuses et robustes qui aident décortiquer la complexité du caractère intrinsèquement multi-échelle de ces phénomènes.

Chapter 1

General introduction

"[W]hile I have sought to shew the naturalist how a few mathematical concepts and dynamical principles may help and guide him, I have tried to shew the mathematician a field for his labour,–a field which few have entered and no man has explored. Here may be found homely problems, such as often tax the highest skill of the mathematician, and reward his ingenuity all the more for their trivial associations and outward semblance of simplicity."

D'Arcy Thompson (*On Growth and Form*, 1917)

1.1 Brief review of the context

This thesis arises from a close collaboration, based on observations made by Sebastián Jaramillo and James Broughton in the context of their doctoral theses under the supervision of Meriem El Karoui at the University of Edinburgh. They observed that during the exposure of *Escherichia coli* bacteria to a low concentration of ciprofloxacin (an antibiotic that causes double-strand breaks in DNA), the individual stress response is significantly variable from one cell to another, although they are isogenic (with the same genetic material) and grow under the same conditions.

Within *E. coli*, the detection of DNA damage triggers a complex molecular response called the **SOS response**, inducing the repair of double-strand breaks. The intensity of this

response can be monitored over time using fluorescent markers. These intensity measurements have revealed significant heterogeneity in the SOS response among individual cells, ranging from very weak to very strong, with significant impacts on their morphology and growth. Indeed, the SOS response induces the expression of proteins that cause cell division to stop without arresting cell growth. Consequently, the SOS heterogeneity is translated into size heterogeneity, characterised by the emergence of a subpopulation of abnormally long *filamentous* bacteria. Furthermore, by arresting their division, these bacteria may be capable of persisting after stopping the antibiotic treatment, making this phenomenon crucial for understanding antibiotic resistance mechanisms—a major topic in contemporary biomedical research and a growing concern in public health.

Typically, during population growth measurements, it is the increase of the population total mass that is observed, rather than the number of cells. Thus, filaments, although few in number (5-10% of the total population depending on the growth medium [82]), contribute significantly to the observed population growth, but less so to the total number of cells. To account for these different behaviours, it is essential to understand the population's evolution at the individual cell level. To achieve this, a fundamental understanding of the cell division mechanisms controlling is necessary. It then falls to the mathematician to translate such mechanisms into **division rates** dependent on the *traits* (size, age, molecular constitution, etc.) of the bacterium. This problem fits into a broader and active field, propelled by the explosion in the development of *single-cell* microscopy techniques, prompting biologists to ask themselves a natural question: how do these new *single-cell* observations align with known macroscopic behaviours?

This question, however, predates the advent of these new microscopy techniques. Already in the early 20th century, in his now-famous work *On Growth and Form*, Scottish biologist D'Arcy Thompson delves into the emergence of morphological diversity in living organisms based on *microscopic* mechanisms. He attempted to explain, through simple mathematical models, how the *growth rate* shapes the *form* of cells, tissues, organs, and populations, subtly connecting these different scales. He highlighted one of the main challenges in comparing microscopic and macroscopic data, pointing out what we would now call an *age bias*:

> *We must be very careful, however, how we interpret such a Table [showing the slowdown of human growth through age]; for it records the character of a population, and we are apt to read in it the life-history of the individual. The two things are not necessarily the same. That a man grows less as he grows older all old men know; but it may also be the case, and our Table may indicate it, that the short men live longer than the tall. ([137] p.92)*

The observation of bacterial growth being much more elusive than the observation of human growth, microbiologists had to wait until the development of microscopy techniques before posing similar questions. Variability in cell proliferation has been highlighted since at least the 1932 paper by Kelly and Rahn [88] on *E. areogenes* and *B. cereus*. In this work, they manually tracked over 1700 individuals for 4 generations, demonstrating a considerable variation in their *rate of fission*. They noted the age dependence of the distribution of

division times, and Rahn himself suggested a microscopic model to explain this variability. From this model, he derived a division rate resulting from the convolution of exponential laws. David Kendall took interest in the topic (see [89] and references cited therein) and, formalising Rahn's model as a Markov process, attempted to estimate the parameter values of the division rate using the coefficient of variation (the ratio of the standard deviation to the mean). Later, a general theory of branching stochastic processes with age-dependent division rates was developed by Bellman and Harris in 1948 and 1952 [13].

The subsequent developments are well-known, and the renowned Bellman-Harris process became a classic tool. Nevertheless, the derivation of links between such stochastic models and equivalent population models, parameter inference, and, in particular, the quantitative understanding of the *age bias* that must be considered when transitioning between them, remain major subjects in both mathematics and biology. Only recently has the development of modern probability allowed the rigorous formulation of stochastic individual-based models in age-structured populations [57, 140] and the analysis of the sampling of individual lineages in the genealogical tree of a population [105]. On the biological side, the recent development of *microfluidic* techniques has enabled the capture, manipulation, and tracking of very small bacterial samples, from small populations to individual cells, and for increasingly extended periods [142, 72, 116]. A clear example is the experimental setup known as the *mother machine* [142], with which J. Broughton, S. Jaramillo, and M. El Karoui have obtained data that will be analysed (J. Broughton's doctoral work, not yet published at this date).

1.2 Main results and thesis synopsis

This thesis consists of four chapters following this introduction. The summarised results below share the common goal of contributing to the understanding of the quantitative impact of intercellular heterogeneity on the macroscopic observables of a cell population under stress. By combining a detailed observation of *single-cell* data in close collaboration with the biologists from El Karoui Lab, along with the use of tools from the theory of measure-valued stochastic processes, semigroup theory, and PDE analysis, this interdisciplinary approach aims to enhance our understanding of complex dynamics within cell populations across various scales.

1.2.1 Chapter 2: Modelling and calibration of the "adder" model from individual cells under genotoxic stress data

In the second chapter, we construct a model of the growth of a population of *E. coli* bacteria under the influence of antibiotic stress based on the data collected by James Broughton, Sebastián Jaramillo, and Meriem El Karoui [82, 24], using the microfluidic setup known as *mother machine* (MM) [142, 116], depicted in Fig. 1.1. In this device, isolated bacteria are trapped in narrow cavities that allow tracking of individual cell lineages over time (Fig. 1.1A). The produced data have high temporal resolution and sampling. Indeed, a single device can have around 10^4 cavities, enabling the acquisition of a large number of

independent lineages developing under the same conditions for very extended periods, thus realising what could be considered as *real Monte Carlo experiments*. Image acquisitions are performed at regular time intervals, allowing the tracking of the size and fluorescence level of individual cells over time (Fig. 1.1B-C).

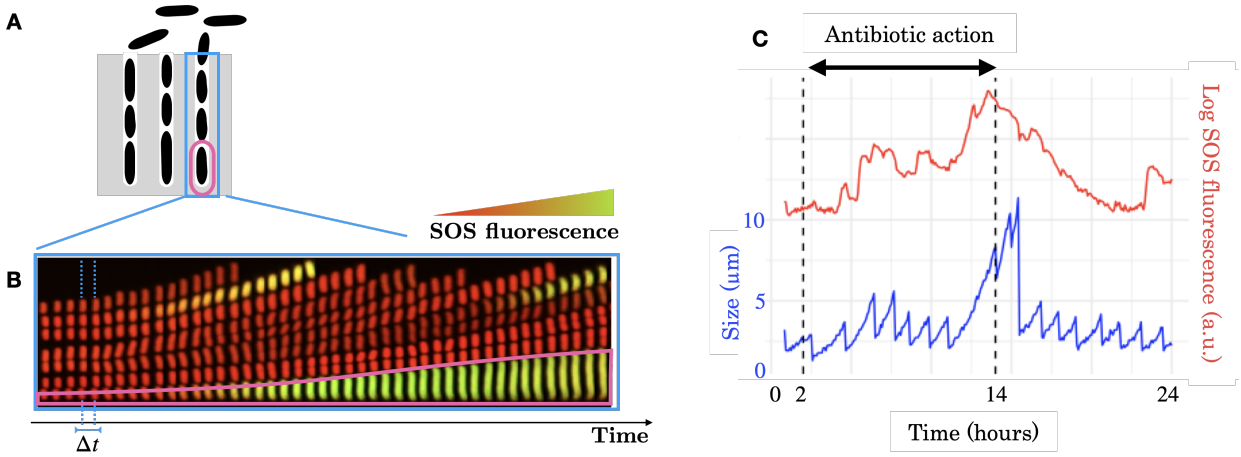

Figure 1.1: The *mother machine* (MM) A. Diagram representing the parallel cavities of the *mother machine*. **B**. Kymograph composed of microscopy images acquired by J. Broughton in a cavity (for example, the one highlighted in blue in panel **A**). Acquisitions are made at equidistant intervals of length $\Delta t = 5$ minutes. At each instant, fluorescence measuring the intensity of the SOS response is measured. The mother lineage corresponds to the trajectory of the cell at the bottom of the device (highlighted in pink). **C.** Example of size and fluorescence measured from the mother lineage in the kymograph.

Starting from an original analysis of these data, we propose a stochastic model that incorporates sources of variability impacting the growth dynamics. First, we consider a population of cells growing in absence of stress, where the division dynamics are described by the "adder" model [133] of size control. Under this model, the division time of each bacterium is decided based on the size a it has added since its birth, independently of its initial size, i.e.,

$$\mathbb{P}(\text{Added size until division} \geq a) = S(a) = \exp\left(-\int_0^a B(s)ds\right), \tag{1.1}$$

where B is the division rate that we will seek to estimate. The surprising accuracy of this simple phenomenological model in predicting the size distributions of *E. coli* has been demonstrated on several occasions and under various conditions over the last decade [129, 28]. With this simple rule, it has been possible to explain stationary size distributions and size-at-division distributions that more classical models structured only by size or age were unable to recover [133, 46].

We denote by $a > 0$ the size added since birth and $y > 0$ the current size of the bacterium. We formulate the adder model as a piecewise-deterministic measure-valued stochastic process Z_t supported in $\mathbb{R}_+^2$ (structured in age a and size y). We consider that, between two

random divisions, each cell grows at an exponential rate $\lambda > 0$, common for the entire population. Following the approach introduced by [57, 140], using a pathwise representation of Z_t with respect to a Poisson point measure, we show that for any function $f \in C_b^{1,1}(\mathbb{R}_+^2)$, Z_t can be written as a semimartingale of the form

$$\langle Z_t, f\rangle \overset{\text{def}}{=} \int_{\mathbb{R}_+^2} f(\mathbf{x}) Z_t(d\mathbf{x}) = \langle Z_0, f\rangle + \int_0^t \langle Z_s, \mathcal{Q}f\rangle \, ds + \mathscr{M}_t^f, \tag{1.2}$$

where $\mathscr{M}_t^f$ is a square-integrable martingale, and the infinitesimal generator $\mathcal{Q}$ is given for any $f \in C_b^{1,1}(\mathbb{R}_+^2)$ by

$$\mathcal{Q}f(a,y) = \lambda y \left(\partial_a + \partial_y\right) f(a,y) + \lambda y B(a) \left(2\int_0^1 f(0,\rho y) F(\rho) \mathrm{d}\rho - f(a,y)\right), \tag{1.3}$$

where F is a probability kernel supported in $[0,1]$, describing a self-similar division, i.e., whose law depends only on the proportion between the size of the mother and its daughter, and not on the absolute size of the mother.

Statistical inference of division rates has been extensively explored in other related models and through complementary approaches (see, for instance, Doumic and Hoffmann's review chapter on the subject [46]). Noteworthy works include Osella et al. [117], Doumic et al. [47], Hoffmann and Olivier [78], and Van Heerden et al. [141]. In these studies, division rates are inferred from *single-cell* observations of MM using non-parametric estimators. Regarding the estimation of B in our case, as pointed out by [46], the adder hypothesis reduces the size-and-age structured model to a simple renewal model, to which classical survival analysis techniques can be applied (see, for example, the book by [135]). For instance, if we have an i.i.d. sample $(A_i)_{i\in[\![1,N]\!]}$ with survival function $1-S$, we can define the classical non-parametric estimator

$$\hat{B}(a) = \frac{\sum_{i=1}^N K_h(a-A_i)}{\sum_{i=1}^N \mathbb{1}_{A_i \le a}},$$

where $K_h = K(a/h)/h$, with K being a suitable kernel (e.g., Gaussian) and $h > 0$ being a given bandwidth. Proposition 4.1 by Doumic and Hoffmann [46] shows that if B is a α-Hölder continuous function, the optimal value of h yields a convergence rate of order $N^{-\alpha/(2\alpha+1)}$ of $\hat{B}$ towards B. In our case, we seek a statistical framework that not only allows the estimation of B from the data, but which is also capable of quantifying the effect of continuous covariates (fluorescence intensity of the SOS response) and qualitative covariates (culture medium), that will be added in the second part of the chapter. Similarly, we aim for a framework that facilitates the prediction (extrapolation) of the division rate, which can be reused for simulations based on the fitted model. These reasons naturally led us to a parametric statistical framework. From a biological perspective, this approach enables us to provide quantitative and biologically interpretable results when comparing different experimental setups. Furthermore, we provide numerical evidence that, for the proposed model, maximum likelihood maximization is numerically tractable. This may also allow relevant extensions within our parametric framework, such as the inclusion of random effects (*frailty* models [79]), which we discuss in the chapter's conclusion.

Finally, the richness of data acquired in El Karoui's laboratory (both in MM and in population, for the same strains and under the same conditions) allows us to quantify the difference between population and single-cell data. Thus, under a stationarity assumption, demonstrated in Chapter 3, we compare single-cell data with population data acquired in the absence of stress. We highlight a systematic shift that may be due to an exogenous effect limiting the growth of E. coli in MM compared to population measurements.

Secondly, we study the growth dynamics under the action of stress. We couple this model with a stochastic diffusion model representing the intensity of the stress response (SOS response) as a continuous variable $(X_t)_{t\geq 0}$ evolving over time. In particular, we consider an Ornstein-Uhlenbeck model

$$\begin{cases} dX_t &= -\theta_{c(t)}\left(\mu_{c(t)} - X_t\right)dt + \zeta^2_{c(t)}dB_t \\ c(t) &= \mathbb{1}_{[\tau_0,\tau_1[}(t) \end{cases}$$

where $[\tau_0, \tau_1[$ is the interval of antibiotic treatment, the parameters $\{\theta_i, \mu_i, \zeta_i^2\}_{i\in\{0,1\}}$ model the action of the antibiotic on the SOS response dynamics, and B_t is a standard Brownian motion. Motivated by the experimental measurements of X_t by fluorescence marking, we construct a new branching model describing the effect of this variable on the growth and division dynamics modelled in the first place. In this regard, we consider division rates of the form $B(a, x)$ depending on the added size and the value $X_t = x$ at the time of division.

Moreover, the observations show the presence of asymmetric divisions, dependent on the size y of the mother, which we model with a kernel $k(y, \cdot)$ that is no longer self-similar. Indeed, when *E. coli* becomes long, an intracellular regulatory system acts to define the position of cell division, which is not necessarily at the middle of the cell but can also occur peripherally. In light of the data, we propose to model $k(y, \cdot)$ as a uniform mixture of $N(y)$ Beta distributions, where $N(y) \in \mathbb{N}$ represents the number of positions where division could occur in a bacterium of size y. It is thus written as

$$k(y, \rho) = \frac{1}{N(y)} \sum_{n=1}^{N(y)} F_n^{N(y)}(\rho),$$

where for any $N > 1$, $\{F_n^N, n \in [\![1, N]\!]\}$ is a family of N Beta distribution densities, and their parameters are estimated by maximum likelihood from the data. Thus, the new process is generated at any time $t \geq 0$ by the non-homogeneous generator

$$\begin{aligned} \tilde{\mathcal{Q}}_{(t)} f(a, y, x) = &- \theta_{c(t)}(\mu_{c(t)} - x)\partial_x f(a, y, x) + \frac{\zeta^2_{c(t)}}{2}\partial_{xx} f(a, y, x) \\ &+ \lambda y \left(\partial_a + \partial_y\right) f(a, y, x) + \lambda y B(a, x) \left(\int_0^1 f(0, \rho y, x) k(y, \rho) \mathrm{d}\rho - f(a, y, x) \right). \end{aligned}$$

In particular, we use a flexible parametric model based on the generalised Gamma distribution [131], allowing the generation of functions $B(a, x)$ with very broad biological properties and interpretations. This will allow us to quantify the perturbative effect of the stress response on the size control mechanisms in *E. coli*. Moreover, we highlight that the heterogeneity of the SOS response can bias the observed adder division rate. This explains the

apparent emergence of a *loss of control* regime, where the division rate would decrease for longer bacteria.

1.2.2 Chapter 3: Exponential ergodicity of a general model structured in size and age

The work of this chapter was published in the form of an article in *Acta Applicandae Mathematicae* [103].

The key assumption of stationarity, crucial for comparing individual and population measures, is demonstrated in the third chapter. This is done for a more general version of the piecewise deterministic size-and age-structured model introduced in Chapter 2. We study the long-term behaviour of the transition semigroup $M_t : C_b^{1,1}(\mathbb{R}_+^2) \to C_b^{1,1}(\mathbb{R}_+^2)$ associated with the process Z_t defined by

$$M_t f(a,y) \overset{\text{def}}{=} \mathbb{E}^{a,y}\left[\langle Z_t, f\rangle\right] = f(a,y) + \int_0^t M_s\left(\mathcal{Q}f\right)(a,y)\,ds$$

using the probabilistic method known as *Harris' theorem* [71, 69, 10, 14]. This method follows the theory initiated by Doeblin [40] and widely developed and popularised by Meyn and Tweedie [112]. To achieve this, we first establish estimates concerning the eigenelements of the infinitesimal generator $\mathcal{Q}$ using analytical methods based on the Krein-Rutman theorem, following ideas developed notably by B. Perthame [119] for transport equations.

We consider a more general model than the adder, characterised by a new generator $\mathcal{Q}$ defined for any $f \in C_b^{1,1}(\mathbb{R}_+^2)$ by

$$\mathcal{Q}f(a,y) = g(a,y)^\top \nabla f(a,y) + \beta(a,y)\left(\int_0^\infty f(0,z)k(a,y,z)\,dz - f(a,y)\right),$$

where $g(a,y) = (g_1(a,y), g_2(a,y))$ contains the aging rate $g_1(a,y)$ and the elongation rate $g_2(a,y)$ of an individual of age a and size y, $\beta(a,y)$ is the division rate of an individual of age a and size y, and $k(a,y,z)$ is a density kernel describing the sizes z of the offspring of an individual of age a and size y at the time of its division. Thus, special cases include the classic adder model, given by $g_1(a,y) = g_2(a,y) = \lambda y$ and $k(a,y,z) = k(y,z) = \frac{2}{y}F\left(z/y\right)$, and the adder model with asymmetric division, where the kernel k is given by (1.4).

We use the version of the ergodic theorem of Harris formulated under the name of the *Uniform V-Ergodicity Theorem* by Meyn and Tweedie [111] as follows:

Theorem 1.2.1 (Theorem 6.1 of [111]). *Let $(X_t)_t$ be a right-continuous Markov process taking values in a locally compact Polish space E equipped with its Borel $\mathcal{B}(E)$, and let $\mathcal{A}$ be the infinitesimal generator of X. Let P_t be the associated transition semigroup. If the following two conditions are satisfied:*

(H1) ***Minorization condition (also known as the Doeblin or small set condition for compact sets of** E**).** *Any compact set in E is small for a skeleton of X, i.e., for any compact set $\mathscr{K} \subset E$, there exists a discrete probability measure $\mu = (\mu_n)_{n\in\mathbb{N}}$ on $\mathbb{N}$ and a $\Delta > 0$*

such that there exists a non-trivial measure ν (which may depend on Δ and μ) on $\mathcal{B}(E)$ such that for all $\mathbf{x} \in \mathscr{K}$, the lower bound holds:

$$\langle \mu, \delta_{\mathbf{x}} P_{\cdot} f \rangle = \sum_{n \in \mathbb{N}} \mu_n P_{n\Delta} f(\mathbf{x}) \geq \langle \nu, f \rangle .$$

(H2) ***Foster-Lyapunov condition***

There exists a coercive function V, i.e., $V(\mathbf{x}) \to +\infty$ as $||\mathbf{x}|| \to +\infty$, such that $V(\mathbf{x}) \geq 1$ for all $\mathbf{x}$, and constants $c > 0$, $d < \infty$ such that

$$\mathcal{A}V(\mathbf{x}) \leq -cV(\mathbf{x}) + d \quad \forall \mathbf{x} \in E,$$

Then, there exists a unique non-trivial probability measure π and constants $C, \omega > 0$ such that for all $\mathbf{x} \in E$ and $t \geq 0$

$$||\delta_{\mathbf{x}} P_t - \pi||_V \leq CV(\mathbf{x}) \exp(-\omega t), \tag{1.4}$$

where $||\cdot||_V$ is a norm defined by

$$||\mu||_V := \sup_{g : ||g|| \leq V} |\langle \mu, g \rangle|$$

In particular, $||\mu||_1 = ||\mu||_{TV}$ is the total variation norm.

However, the semigroup generated by $\mathcal{Q}$ is not necessarily conservative. Although Bansaye et al. recently established in [10] a result extending the Harris theorem to non-conservative semigroups, it turns out that the conditions known as *mass ratio control* (assumptions (A3) and (A4) *ibidem*) are quite challenging to demonstrate in the case of two continuous dimensions (size and age). These conditions are related to the irreducibility of the process and are associated with the existence of a coupling time from which trajectories arising from any initial condition mix (see, for example, the discussion in [34]). The difficulty in our case is to construct such trajectories because the deterministic flow determined by g can only explore $\mathbb{R}^2_+$ through one-dimensional trajectories. Moreover, the transitions are non-local and degenerate: although the sizes of daughter cells admit a density $k(a, y, \cdot)$, the age of newborn cells is deterministically set to 0. The *small set* condition established by (H1) allows us to overcome this difficulty because, instead of requiring a uniform coupling time for any initial condition, it allows us to take a time average with respect to the discrete sampling law μ. Readers familiar with other now more classical versions of the Harris theorem can refer to the discussion in Chapter 3, where we comment on these equivalent versions.

So, to apply this theorem, we must first construct a good conservative semigroup, which then allows us to deduce the ergodic behaviour of M_t. To do this, we first show that under the assumptions 3.3.3, there exists a unique eigenfunction $h : \mathbb{R}^2 \to \mathbb{R}_+$ and eigenvalue $\Lambda > 0$ satisfying the eigenvalue problem

$$\mathcal{Q}h = \Lambda h. \tag{1.5}$$

This allows us to construct an auxiliary process with generator

$$\mathcal{A}f(a,y) = g(a,y)^\top \nabla f(a,y) + \beta(a,y)\left(\int_0^\infty (f(0,z) - f(a,y))\,\frac{h(0,z)}{h(a,y)}k(a,y,z)\mathrm{d}z\right)$$

whose associated semigroup P_t is Markovian and conservative ($P_t 1 \equiv 1$) and can thus be studied using the techniques of Meyn and Tweedie. Then, we recover the semigroup associated with the original process via an *h-transform of Doob*:

$$M_t f(a,y) = e^{\Lambda t} h(a,y) P_t\left(\frac{f}{h}\right)(a,y).$$

This finally allows us to obtain the main result of the chapter:

Theorem 1.2.2 (Exponential Ergodicity)**.** *Under Assumptions 3.3.3 and if condition (H2) is satisfied for a coercive function $V : \mathbb{R}_+^2 \to \mathbb{R}_+$, then there exists a unique probability measure π and constants $C, \omega > 0$ such that for any initial condition $\mu_0 \in \mathcal{M}_p(\mathbb{R}_+^2)$*

$$||e^{-\Lambda t}\mu_0 M_t - \langle \mu_0, h\rangle \pi||_V \leq C \langle \mu_0, V\rangle e^{-\omega t}. \tag{1.6}$$

The proof ideas are as follows:

1. **Existence of h**

   a) We begin by reducing the problem (1.5) to a scalar problem using the renewal property in a. In Lemma 4.4.2, we show that (Λ, h) is a solution to (1.5) (and a certain boundary condition) with $\Lambda > 0$ and $h \in W^{1,\infty}_{loc}(\mathbb{R}_+^2)$ if and only if

   $$h(a,y) = \int_0^\infty h(0,z) K_\Lambda(a,y,z)\mathrm{d}z$$

   for a certain kernel $K_\Lambda : \mathbb{R}_+^3 \to \mathbb{R}_+$ whose spectral properties determine those of $\mathcal{Q}$. We then consider the operator $\mathcal{G}_\lambda$ defined for any $f \in C^1(\mathbb{R}_+)$ by

   $$\mathcal{G}_\lambda f(y) = \int_0^\infty f(z) K_\lambda(0,y,z)dz \quad \forall y > 0. \tag{1.7}$$

   b) We then demonstrate the existence of $\Lambda > 0$ and $h \in W^{1,\infty}_{loc}(\mathbb{R}_+^2)$ solutions to (1.5), adapting a classical scheme built upon the Krein-Rutman theorem, as follows:

      i. We construct a truncated version of $\mathcal{G}_\lambda$ that is compact. We then apply the Krein-Rutman theorem to show that for any $\lambda \geq 0$, the truncated operator has a unique eigenvalue $\mu_\lambda \geq 0$ and eigenfunction $h_\lambda \geq 0$, up to normalisation.

ii. We show that there exists a unique $\lambda_0 > 0$ such that $\mu_{\lambda_0} = 1$. Moreover, we demonstrate that the value of λ_0 is uniformly bounded for any truncation of $\mathcal{G}_\lambda$.

iii. We take the limit and show that the limit eigenpairs $(\lambda_0, h_{\lambda_0})$ of the family of compact truncations of $\mathcal{G}_\lambda$ are indeed solutions to the eigenvalue problem.

2. **Proof of the Doeblin condition (H1)**

   Conditioning on the division times, we express the action of the semigroup P_t as the *mild* solution to a recursive equation (Duhamel's formula (3.39)). Then, for any measurable and bounded function f, we can lower bound $P_t f(a, y)$ by iteratively applying the formula and retaining the terms that we can control under the assumptions 3.3.3. The proof essentially involves estimating lower bounds for these terms along trajectories originating from a given compact set.

We conclude the chapter with the application to the adder model where $\mathcal{Q}$ is given by (1.3), for which we demonstrate exponential convergence to its stationary measure. In particular, for the adder model with exponential growth, the eigenelements are explicit: $h(a, y) = y$ and $\Lambda = \lambda$ (the elongation rate), and the Lyapunov condition (H2) is satisfied by $V(a, y) = y^{-1} + y$. The general result also extends to cases where growth is not exponential or divisions are not symmetric. This set of results provides answers to open questions posed by the analysis of Gabriel and Martin [62].

1.2.3 Chapter 4 : *Trade-offs* in a bacterial proliferation model under stress

In the fourth chapter, we aim to incorporate a key element into the analysis deliberately omitted in our earlier chapters: the presence of *cell death*. Even at assumed sub-lethal doses of ciprofloxacin, a non-negligible number of bacteria completely arrest their growth and division. However, the induction of the SOS response is expected to play a protective role. Indeed, our analysis of the data reveals that the SOS response is not only heterogeneous among individual cells but also fluctuates significantly during the life of a bacterium, giving rise to a phenomenon known as *phenotypic plasticity*. At certain times, randomly but depending on the environment and the intensity of stress, *E. coli* can transition from its normal state of apparent SOS response inactivity to a state of high activity. Thus, in the presence of antibiotics, bimodal distributions in the SOS response level are observed. Subsequently, after one or more divisions, the progeny of high SOS bacteria are capable of returning to the normal state.

In order to improve the phenomenological and quantitative understanding of the evolutionary significance of this plasticity strategy in response to stress, we formulate a minimal stochastic model that preserves the main elements of the phenomenon. Thus, we maintain an age structure, while the variability in the SOS response is summarised in two discrete traits. We consider vulnerable cells (type $i = 0$), susceptible to death at the time of their division with a probability $p \in (0, 1)$, and tolerant cells (type $i = 1$), whose division times are much longer. The division times of both phenotypes are characterised by their division

rates $\beta_0(a)$ and $\beta_1(a)$. Vulnerable cells can become tolerant at a rate $\alpha > 0$. In turn, tolerant cells can only revert to being vulnerable after their division, which happens with a recovery probability $\gamma \in (0,1)$. We formalise this dynamics with a measure-valued stochastic process Z_t supported on $\mathbb{R}_+ \times \{0,1\}$ such that

$$Z_t(da, di) = Z_t(da, \{0\})\delta_0(di) + Z_t(da, \{1\})\delta_1(di)$$

and which, for any $f \in C^{1,\cdot}(\mathbb{R}_+ \times \{0,1\})$ and $t \geq 0$, has the semimartingale decomposition

$$\begin{aligned} &\int (f(a,0)Z_t(da,\{0\}) + f(a,1)Z_t(da,\{1\})) \\ &= \int (f(a,0)Z_0(da,\{0\}) + f(a,1)Z_0(da,\{1\})) \\ &\quad + \int_0^t \int (\mathcal{Q}f(a,0)Z_s(da,\{0\}) + \mathcal{Q}f(a,1)Z_s(da,\{1\}))ds + \mathcal{M}_t^f \end{aligned} \tag{1.8}$$

where $\mathcal{M}_t^f$ is a square-integrable martingale, and the generator $\mathcal{Q}$ is defined by

$$\begin{aligned} \mathcal{Q}f(a,i) = \partial_a f(a,i) &+ (1-i)\alpha(f(a,1) - f(a,0)) - \beta_i(a)f(a,i) \\ &+ 2(1-i)(1-p)\beta_i(a)f(0,0) + 2i\beta_i(a)(\gamma f(0,0) + (1-\gamma)f(0,1)) \end{aligned} \tag{1.9}$$

We are interested in the long-term behaviour of Z_t. Firstly, we highlight an explicit trade-off between the phenotypic switching rate and the probability of recreating vulnerable individuals, which depends on the stress level p. If we denote $\lambda_{\alpha,\gamma}$ the exponential growth rate of the population and $\pi_i^{\alpha,\gamma}$ the extinction probability of the population from an individual cell of age 0 and type i, we show

Théorème 5.3.6 and 5.4.5. *Under assumptions 4.2.1, we have*

$$\lambda_{\alpha,\gamma} > 0 \iff \pi_0^{\alpha,\gamma}, \pi_1^{\alpha,\gamma} < 1 \iff \left\{p \leq \frac{1}{2}\right\} \cup \left\{p > \frac{1}{2} \text{ and } \gamma < \frac{1}{2}\left(1 + \frac{q}{(2p-1)(1-q)}\right)\right\}.$$

where $q = \int_0^{+\infty} \alpha \exp\left(-\int_0^a (\alpha + \beta_0(s))\mathrm{d}s\right) \mathrm{d}a$ *is the probability that a type 0 cell switches to type 1 before dividing.*

Next, we analyse the sensitivities of $\lambda_{\alpha,\gamma}$ and $\pi_i^{\alpha,\gamma}$ to variations in α and γ. In contrast to the results of Campillo et al. [27], who also investigate the links between the two fitness measures but for a single-type model structured in size, we show that the presence of phenotypic plasticity can break the expected monotonicity between variations in the Malthusian parameter and the probability of population establishment. Indeed, we demonstrate that variations in α and γ that decrease the probability of population establishment can increase the overall population growth rate. This is the main result as follows:

Théorème 5.5.6. *Under assumptions 4.2.1 and 4.2.4, for any* $\alpha \geq 0$,

$$\partial_\gamma \pi_0^{\alpha,\gamma}, \partial_\gamma \pi_1^{\alpha,\gamma} > 0$$

However, for any $\alpha \geq 0$, *there exists a critical value* $\bar{p} \leq 1/2$ *such that for any* $\gamma \in (0,1)$

$$\partial_\gamma \lambda_{\alpha,\gamma} > 0 \iff p < \bar{p},$$
$$\partial_\gamma \lambda_{\alpha,\gamma} < 0 \iff p > \bar{p}.$$

This result indicates that only the "extreme strategies" of phenotypic plasticity ($\gamma = 0$ or $\gamma = 1$) are optimal in the Darwinian sense of maximising $\lambda_{\alpha,\gamma}$. In conclusion, we show that the interest in non-trivial plasticity strategies emerges when the environment (i.e., the death probability p) is allowed to fluctuate over time. To do this, we consider the case where the death probability is a continuous and T-periodic function of time, denoted as $p(t)$. Thus, we extend our previous results using Floquet theory [32]. Although we cannot explicitly exhibit the trade-off as in the case of constant p, we show that the sign of the derivative $\partial_\gamma \lambda_{\alpha,\gamma}$ can change non-trivially depending on the values of $p(t)$. In particular, we numerically illustrate that, depending on the period T, the optimal value of $\lambda_{\alpha,\gamma}$ is achieved inside the parameter space, i.e., for $\gamma \in (0,1)$ and $\alpha > 0$.

Interestingly, we can compare our mathematical results to previous experimental work that attempted to measure the fitness of populations of *E. coli* by manipulating the rates of induction and repression of the SOS response to DNA damage through genetic modifications [92]. This enables the authors to infer a fitness landscape, providing the value of λ as a function of the genetic modifications made. Thus, if we associate our switch parameter α with their parameter for inducing the SOS response (which transitions vulnerable cells to tolerant cells) and our recovery parameter γ with their parameter for repressing the SOS response (allowing a return to the normal state when DNA damage has been repaired), we can compare our predictions of $\lambda_{\alpha,\gamma}$ with their fitness landscapes. We discuss some qualitative behaviours that our mathematical results can help elucidate.

1.2.4 Chapter 5: Regime shift in the propagation speed of a size-structured population of Myxobacteria

The work of this chapter was initiated during the summer school CEMRACS 2022 at CIRM (Marseille), in collaboration with Vincent Calvez, Adil El Abdouni, Maxime Estavoyer, Florence Hubert, Julien Olivier, and Magali Tournus.

The fifth chapter focuses on the spatial propagation phenomenon of a population of bacteria structured in size and spatial position. Although this time it involves *Myxococcus xanthus*, a terrestrial bacterium that preys on *E. coli* and exhibits behaviour quite different from its prey, the study aims to analyse the effect of the underlying size structure on the population's macroscopic behaviour. This time, the growth rate is not examined as an indicator of the population's fitness, but rather the speed of its spatial propagation. In the presence of prey, *M. xanthus* moves collectively through propagation fronts composed of clusters of bacteria of various sizes, ranging from isolated bacteria to several thousand bacteria biochemically glued together. Interestingly, this clustering has a synergistic effect, and the spatial diffusion coefficient of the clusters is higher than that of isolated bacteria.

We consider a minimal reaction-diffusion model with a highly simplified size structure, consisting of clusters of only 1 or 2 bacteria. For $i \in \{1, 2\}$, let $p_i(x, t)$ denote the density of clusters with i bacteria at spatial position $x \in \mathbb{R}$ at time $t \geq 0$. We also denote $p = p_1 + 2p_2$ as the density of the total number of bacteria. We consider the large population scale, assuming all cells are well mixed, so that p_1 and p_2 are solutions of the reaction-diffusion system:

$$\partial_t p_1 = \theta_1 \Delta p_1 - \tau_1 p_1^2 + 2\tau_2 p_2 + \alpha p_1 \left(1 - \frac{p}{K}\right), \tag{5.1}$$

$$\partial_t p_2 = \theta_2 \Delta p_2 + \frac{\tau_1}{2} p_1^2 - \tau_2 p_2, \tag{5.2}$$

The first term in (5.1) and (5.2) is a diffusion term, describing the random spatial movement of isolated bacteria and pairs of bacteria. We assume $\theta_2 > \theta_1$, i.e., clusters diffuse more rapidly than isolated bacteria. The nonlinear term $\tau_1 p_1^2$ represents the coagulation of 2 isolated bacteria becoming 1 cluster of 2 bacteria at rate $\tau_1 > 0$. Similarly, the term $\tau_2 p_2$ corresponds to the fragmentation of 1 cluster of 2 bacteria becoming 2 individual bacteria at rate $\tau_2 > 0$. We assume that only isolated bacteria can divide. Furthermore, we assume that this growth is logistic, with a growth rate $\alpha > 0$ and carrying capacity $K > 0$. Thus, the system (5.1)-(5.2) is an extension of the Fisher-KPP Equation [54, 90]. In particular, Fisher-KPP can be obtained by setting $\tau_2 = 0$, which decouples the two equations.

We numerically explore the long-term behaviour of the model based on the values of the coagulation rates τ_1 and fragmentation τ_2 of clusters, as well as the ratio between the diffusion coefficients of clusters θ_2/θ_1. Numerical simulations of this system allow us to conclude the existence of wave solutions for all positive parameter values. Furthermore, we observe two distinct regimes separated by a constant threshold θ^* for the ratio θ_2/θ_1.

When $\theta_2/\theta_1 < \theta^*$, the propagation front consists of so-called "pulled" waves. This implies that the propagation speed equals the Fisher-KPP model speed. In this case, population spread is limited by the motility of isolated bacteria, so the clustering effect does not significantly affect the speed. However, when $\theta_2/\theta_1 > \theta^*$, the propagation front consists of so-called "pushed" waves. In this case, the propagation speed is strictly greater than the Fisher-KPP speed, thanks to the non-negligible effect of nonlinearity introduced by the coagulation term. In other words, we conclude that when the motility of clusters is sufficiently high compared to the motility of isolated bacteria, the collective behaviour of *M. xanthus* allows the entire population to spread more rapidly than in the asocial case.

We also observe that θ^* is independent of the coagulation and fragmentation rates. In particular, we can reduce the system to the case $\tau_1, \tau_2 \to +\infty$, yielding a scalar equation that we study numerically, providing some heuristics for its analytical study.

Then, we turn our attention to a more general model with a continuous size structure, related to the structured population models formulated in the previous chapters. We extend the system (5.1)-(5.2) to a general model of Diffusion-Growth-Fragmentation-Coagulation described by (5.3)-(5.5) below, where $\rho(t, x, z)$ is the density of the number of clusters of size $z \in [0, z_{max}]$ at spatial position $x \in \mathbb{R}$ and time $t \geq 0$. We model ρ as the solution to the

following integro-differential system:

$$\partial_t \rho(t,x,z) = \partial_{xx}\left[\theta(z)\rho(t,x,z)\right] - \partial_z\left[v(z,m)\rho(t,x,z)\right] + \mathcal{F}[\rho](t,x,z) + \mathcal{G}[\rho](t,x,z), \tag{5.3}$$

where $m(t,x) = \int_0^{z_{\max}} z'\rho(t,x,z')\ dz'$ is the local density of the number of bacteria, $v(z,m) \geq 0$ is the growth rate of clusters of size z when the local number of surrounding bacteria is m, $\mathcal{F}$ is the fragmentation operator defined by

$$\mathcal{F}[\rho](t,x,z) = 2\int_z^{z_{\max}} \beta(z')k(z',z)\rho(t,x,z')\ dz' - \beta(z)\rho(t,x,z), \tag{5.4}$$

and $\mathcal{G}$ is the coagulation operator defined by

$$\begin{aligned}\mathcal{G}[\rho](t,x,z) = \frac{1}{2}\int_0^z \gamma(z-z',z')\rho(t,x,z-z')\rho(t,x,z')\ dz' \\ - \rho(t,x,z)\int_0^{z_{\max}-z} \gamma(z',z)\rho(t,x,z')dz'.\end{aligned} \tag{5.5}$$

The existence of propagation fronts in models of structured populations has been studied in various particular cases [49, 21, 2, 67]. The numerical investigation of the case with a coagulation operator is novel. Thus, our numerical experiments show that the solution of the integro-differential system also admits wave-like solutions. Moreover, as for the 2-type model, we observe the existence of a threshold for the diffusion coefficient beyond which the velocity is greater than the Fisher-KPP velocity.

We conclude the chapter with numerical experiments of an extension of the 2-type model where prey is added to the environment. Upon contact with their prey, bacteria can switch to a feeding state, where they consume the prey while ceasing to diffuse. The idea is to capture, at least qualitatively, the front advancement data of *M. xanthus* on a *E. coli* droplet (prey), where the deceleration of the front upon contact with *E. coli* is observed. Our simulations show qualitative agreement with biological experiments, validating our highly simplified model. Thus, we conclude that the sociability and strong diffusion of *M. xanthus* clusters play a crucial role in the speed of predation and spatial propagation of the population.

1.2.5 General conclusion and perspectives

The specific discussion of these results is provided at the end of each chapter. We take the opportunity to provide here a synoptic conclusion in light of these four parts, as well as some perspectives opened up by this work.

From a biological perspective, the results of this thesis mathematically and numerically illustrate the positive effect that cellular heterogeneity can have on various measures of the fitness of a bacterial population, despite the seemingly negative effects it may have at the microscopic level. Thus, the decrease in the division rate induced by the SOS response highlighted by statistical inference in Chapter 2 would, however, ensure better Malthusian

yield if longer cells become tolerant at the same time, as shown by the results of Chapter 4. Similarly, the results of Chapter 5 show that the accelerated diffusion of cell clusters can speed up the propagation velocity of the overall population, even if only isolated cells are capable of feeding and reproducing.

However, it is evident that these effects are often subject to trade-offs involving the risk associated with heterogeneity strategies, such as the probability of death (p) for rapidly dividing cells in Chapter 4. These trade-offs yield interesting results and suggest evidence of the evolutionary advantage of the emergence of such strategies. For instance, the emergence of filamentation in *E. coli* can be partly explained by the joint adaptation of the rates of induction and repression of the SOS response (α, γ) and the division rates (β_0, β_1) in a fluctuating environment.

Moreover, the mathematical results from Chapter 4 suggest that certain modifications of the SOS response, such as those induced by certain antibiotic molecules, can decrease the probability of microcolony establishment but increase the asymptotic growth rate of the population. This raises serious methodological questions when comparing experimental results where the outcome of interest is colony survival, versus others, where the focus is on the population growth rate. Furthermore, these differences stem from underlying and often overlooked heterogeneity. Thus, modelling approaches that explicitly consider heterogeneity in antibiotic treatment and allow for the comparison of single-cell and population data, as presented in Chapter 2, become crucial.

Yet, we observe the presence of additional heterogeneity, not entirely captured by the SOS intensity level. It would be very interesting to model this additional heterogeneity with a mixed-effects approach. Recent advances in this theory, adapting it to stochastic flows on one side and cell lineages on the other, could be employed in our case. Thus, our model could serve as a starting point with versatile laws and tractable likelihoods.

From the perspective of mathematical tools, we provide our major contribution in Chapter 3. The chosen probabilistic approach allows us to overcome issues related to the lack of compactness that arise in estimating hypocoercivity bounds in more analytical approaches. This enables us to present new results that, even for the original adder case, were not accessible previously. Similarly, we contribute with some original ideas for constructing the eigenfunctions of the associated operator $\mathcal{Q}$ (in the absence of assumptions of self-similarity for the fragmentation kernel, for example) and for the trajectory construction of the Doeblin condition that may be applicable in other contexts.

In conclusion, the question of cellular heterogeneity has been treated here in a fundamentally phenomenological manner: the mechanisms behind intracellular variability have been reduced to division rates, cell types, and continuous traits, whose biomolecular interpretation is rather diffuse. Although this already allows us to link dynamics at the individual cell level with population-level dynamics, an interesting perspective is to obtain cellular heterogeneity as a result of metabolic heterogeneity. This would allow us to connect biomolecular dynamics to population dynamics. The metabolic regulation of cell size control (to explain the adder model, in particular) is an active area of research in biology, but the impact of these mechanisms on population growth is far from clear. Thus, the question of size control and bacterial heterogeneity constitutes an ideal application field for methods at the interface of analysis and probability. Moreover, the advancement of experimental techniques

and the richness of data enable the confrontation of theoretical results with empirical results on a level comparable to that of physics, as well as inquiries into long-term trends and evolutionary adaptations. Many biologists and physicists agree that the development of microbiology over the last 80 years is comparable to that of astronomy and physics at the dawn of the 17th century [84]. Similarly, the need for suitable mathematical tools is expected to increase, highlighting the value of rigorous and robust approaches that help unravel the inherent multiscale complexity of these phenomena.

Chapter 2

Modelling and Calibration of the adder model from single-cell data under DNA stress

2.1 Introduction

The development of high-throughput single-cell imaging techniques, such as the mother machine (MM) [142, 116] or the dynamic cytometer [72], designed to track multiple single bacteria over several generations, have allowed a better grasp on the emergence mechanisms of long-term population trends at the individual scale. In particular, a strong interest has been given to bacterial size regulation and its effects on population-level growth. The modelling, analysis and statistical calibration of this dynamics, both from phenomenological and coarse-grained mechanistic approaches, has since attracted the attention of an increasing number of biologists, physicists and mathematicians [46, 47, 4].

A prototypical case of study is the steady-state growth of *E. coli* bacteria during the exponential phase. Whilst recent experiments have brought some consensus to the exponential character of cellular elongation [65], the comprehension of the control of cell division is still far from being well understood. A number of variables and key checkpoint events have been proposed as candidates for drivers of cell division (see the reviews [110, 126] and the references therein). Nonetheless, the simple "adder model", in which individuals cells divide after adding a *constant* amount of volume tightly controlled and non correlated to the cell initial size, has been shown to provide an excellent fit to the size distributions of *E. coli* under diverse experimental settings [133], in contrast to purely age-structured ("timer") or purely volume-structured ("sizer") models. Recent works have contributed to the exploration of the underlying molecular origins of the adder model, and suggest it as an emergent property of the still unclear coordination of DNA replication, RNA/protein allocation and protein accumulation [85, 126].

The goodness of fit of the adder with respect to other size control models has been shown by correlation-based graphic tests [133] and using non-parametric estimators based on the steady-state solution of the associated PDE (see Doumic and Hoffmann [46] and the

references therein). The main assumption of this last approach is the stationarity of the cell size distribution, which allows to consider the observations as independent and identically distributed realisations of the stationary measure associated to the model. Moreover, the resolution of the associated inverse problem has been shown to be generally quite difficult [*ibidem*].

On the other hand, heterogeneous single-cell data motivates the construction of individual-based models evolving in time. In general, the formalisation of these processes as measure-valued stochastic processes, as introduced by [57], allows to rigorously link individual dynamics to macroscopic observables via limit theorems, under the assumption of a large population [57, 53]. Non-parametric estimators of the division rate based on this stochastic approach have been proposed for other models of structured branching populations, for example with age structure in [68, 78], and with a general Markovian (not necessarily piece-wise deterministic) structure by [77].

As in the previous case, the main assumption is the ergodicity of the relying process. Of course, this assumption is no longer valid under out-of-equilibrium dynamics, such as during the adaptation to antibiotics, which corresponds to the data we will analyse, acquired by James Broughton and Meriem El Karoui at the University of Edinburgh, and that will be described in detail in the following paragraphs. Based on these observations, we introduce in Section 2.2 a statistical framework based on an individual-based stochastic process adapted to two datasets we have, which are introduced in Section 2.3. First, we consider a control dataset of healthy bacteria, which we model using the classical adder model. Second, we consider bacteria under the effect on the antibiotic ciprofloxacin.

Starting in Section 2.4, we will consider control datasets of wild-type strains of *E. coli* growing in three different media, which from the poorest to the richest are: glycerol (*gly*), glucose (*glu*) and glucose with amino-acids (*gluaa*). The same strains and conditions are used to make macroscopic cultures on an agar pad and to cultivate individual cells in the MM. These observations are obtained after carefully leading bacterial to steady-state growth conditions (see [82] for the details of the experimental setting). This justifies the assumption of ergodicity, proven rigorously in a more general model in [103], and allows us to ultimately compare the macroscopic distributions with the distributions predicted by the microscopic acquisitions, which we do in Section 2.5

Then, from Sections 3.6 to 3.9 we will consider the case where 3ng/ml of ciprofloxacin (*cip*) are added for 12 hours mid-experiment. We aim to quantify the effects of this environmental shift under the three media considered, relatively to the baseline parameters calibrated for the unperturbed model. In that regard, we propose a parametric extension to the adder model of [85] to filamentous *E. coli*, by including the effects of growth and stress level as covariates of the baseline adder division rate.

Indeed, although previous experiments have suggested that the adder model is robust under diverse kinds of growth inhibitions [129], some types of stress can be multifactorial, which may lead to perturbations of the adder model. Particularly, antibiotic molecules causing DNA damage, such as ciprofloxacin (*cip*), are known to have a substantial impact on the growth dynamics of *E. coli* [115]. Under this type of damage, bacteria induce a stress response mechanism called the **SOS response** [145, 102], which induces the delay or arrest of cell division. This produces the emergence of "filamentous" bacteria several times longer

than normal strains in the same medium [144], as shown by Fig. 1.1 further below.

At the same time, the intensity of the SOS response exhibits high heterogeneity among individuals, even in isogenic populations under the same concentration of antibiotic [82]. Interestingly, once the stress is removed, filamentous bacteria are able to resume proliferation through a series of asymmetrical divisions [121, 144, 30]. Moreover, their divisions fulfill, in average, the adder hypothesis [144, 121]. However, it is not clear how robust the adder model is under such a heterogeneous response, and how fast it is able to restore size homeostasis when the antibiotic is added and removed from the media.

In Section 3.6 we analyse the experimental results acquired by J. Broughton. The dose of 3ng/ml of cip triggers a mild induction of the SOS response. The intensity of the SOS response is quantified experimentally in each cell by the fluorescence-per-area of the GFP-marked SOS reporter P_{sulA}-mGFP, which serves as proxy for the concentration of the promoter P_{sulA} in the cell. It shows the great heterogeneity, time-wise and cell-wise, of our SOS reporter, and propose an Ornstein-Uhlenbeck process to model their stochastic time dynamics. Then, we model the effects of the SOS response on the adder mechanism. We show again that, even at the same level of SOS induction, there is great variability on the distribution of the added sizes at division. Thus, we introduce a probabilistic model giving the distribution of the added size conditionally to the SOS level. We use in particular a Generalised Gamma distribution [131] that allows to model the *geometrical* change of the division rate induced by the SOS response and show its consequences. Finally, we model the effect of the SOS level on the division position along the cell to account for the observed asymmetrical divisions of filamentous bacteria.

Based on this parametrisation, in Section 3.7 we calibrate the proposed model by Maximum Likelihood Estimation (MLE). The estimated parameters are then used to simulate the model and to compare it with the original single-cell data as validation. In this section we also give some biological implications of our results, finishing with some concluding remarks in Section 3.9. At that moment we take the opportunity to comment a crucial observation that we purposely disregard in this first model: the presence of cellular death, both size-induced and SOS-induced.

2.2 The individual-based population model

We consider a stochastic formulation which accounts for the individual variability within the population. To that extent, each individual cell i is characterised by a three-dimensional vector $\boldsymbol{\xi}_i(t) = (a_i(t), y_i(t), x_i(t))$ consisting of:

- $a_i(t)$ is the **added size** from its birth to current time t,
- $y_i(t)$ is the **current size** at time t,
- $x_i(t)$ is the **SOS level** at time t.

In a first analysis, we will study the case of an unperturbed population, where the stress level is assumed to be at its baseline, say $x \equiv 0$, for all individuals, so it does not affect the dynamics.

We call $\mathcal{X} = \{(a, y) \in \mathbb{R}^2 : 0 < a < y, y > 0\}$ the state space of all possible sizes. Then, following the approach introduced by [57] and later extended to age-structured populations [53], we formalise the population dynamics as a measure-valued stochastic process Z_t, which for every instant $t > 0$ gives the composition of the current population. It consists of a discrete measure over the state space $\mathcal{X}$ in which each individual cell is represented by a point mass on $\mathcal{X}$, as illustrated by Fig. 2.1:

$$Z_t = \sum_{i=0}^{N_t - 1} \delta_{\boldsymbol{\xi}_i(t)} \tag{2.1}$$

where $N_t = \int_{\mathcal{X}} Z_t(\mathrm{d}x)$ is the population size at time t, and each cell i is characterised by the vector $\boldsymbol{\xi}_i(t) = (a_i(t), y_i(t))$. The formal construction and well-posedness of such process is discussed in Appendix A.

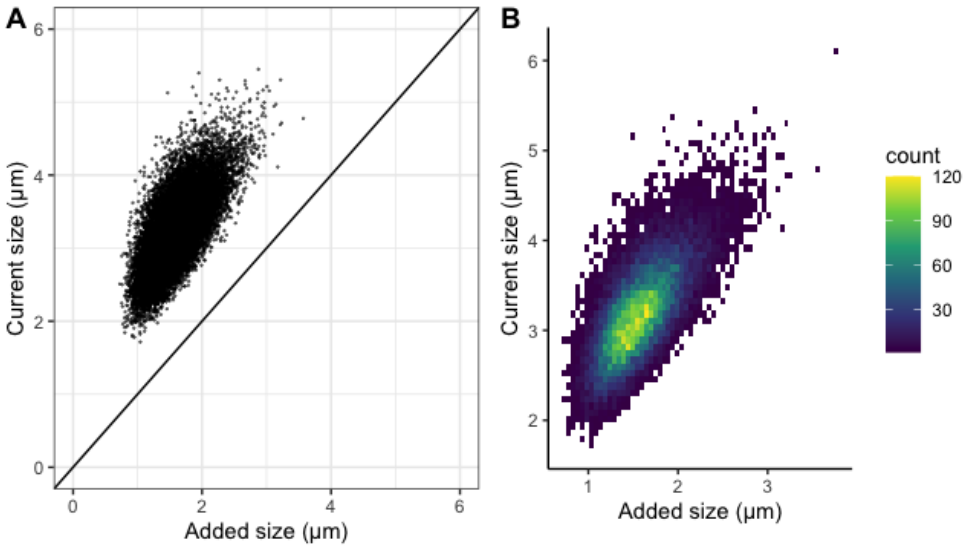

Figure 2.1: A possible realisation of the process Z_t at a certain time $t > 0$ with a total of $N_t = 20000$ cells. **A.** Each dot corresponds to a single cell whose coordinates in the plane code for its added size and current size (a, y). **B.** The integral $\int_{\mathcal{X}} Z_t(da, dy) = N_t$ gives the total number of individuals.

We assume that each cell in the population behaves independently. The population then evolves in the continuous time through two fundamental dynamics: growth and division. Whilst growth is assumed to be deterministic, the division mechanism will account for the observed stochasticity.

1. **Growth:** Each cell i of size y_i grows exponentially [65] at elongation rate $\lambda > 0$ which we assume to be the same for the whole population:

$$\frac{dy_i(t)}{dt} = \lambda y_i(t).$$

Thereby, the size $y(t)$ and added size $a(t)$ at time $t \geq 0$ of a bacterium which had size $y(s)$ and added size $a(s)$ at time $s < t$ are given by the following deterministic

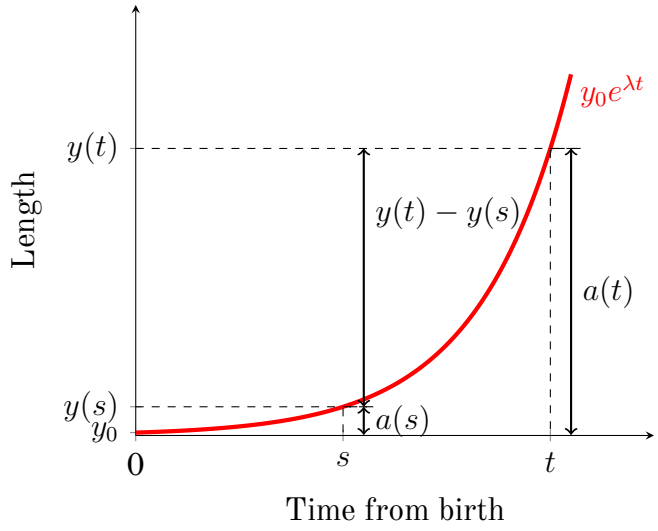

Figure 2.2: Variables modelling the deterministic growth between division

equations (see Fig. 2.2):

$$y(t) = y(s)\exp(\lambda(t-s)) \tag{2.2}$$
$$a(t) = a(s) + y(s)\exp(\lambda(t-s)) - y(s) \tag{2.3}$$

2. **Division:** Cells divide independently, according to the adder model [133, 62]: a bacterium of birth size y_0 will divide at a random size $y_0 + A_{div}$ where the added size A_{div} is independent from y_0, distributed according to

$$S(a) = \mathbb{P}(\text{Added size at division} \geq a) = \exp\left(-\int_0^a B(\alpha)d\alpha\right). \tag{2.4}$$

S is called the survival function, since $S(a)$ equals the probability of still having not divided at an added size a. Thereby, function B can be understood as a *division rate per added length*, with units length^{-1}. The probability density function associated to the added size is then

$$f_A(a) = -S'(a) = B(a)S(a). \tag{2.5}$$

This formalisation corresponds to meaningful biological assumptions. It implies that in order to decide the division time, cells do not sense time or their absolute size, but rather the mass they have acquired since birth. Moreover, this formulation assures that the added size is independent from the birth size, assuring also the lack of correlation between added and birth sizes as reported in earlier observations [133, 85].

Finally, when a cell of size y divides, it is replaced by two cells of sizes ρy and $(1-\rho)y$, where $\rho \in (0,1)$ is a random variable with probability distribution F.

The model is summarised in Fig. 2.3

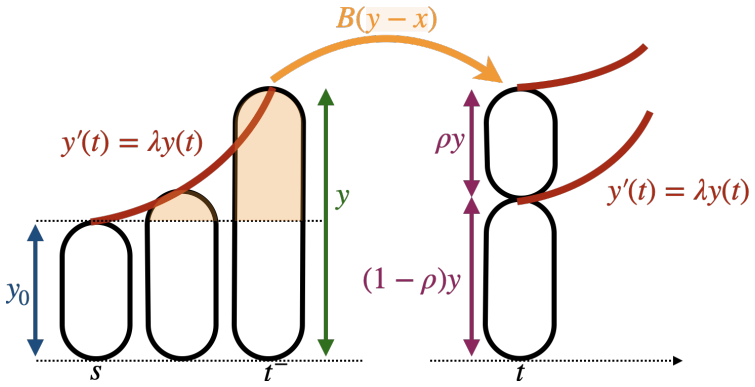

Figure 2.3: Summary of the adder model. The division occurs at rate $B(a)$, where $a = y - x$ is the added size from birth.

2.3 Model of growth in mother machine

2.3.1 Indexation by vertical position

In order to describe the population growth inside a MM tube, we associate to each individual i living at time t the vertical position $h_i(t) > 0$ on the MM tube, see Fig. 2.4. We call $\tilde{Z}_t$ the extended measure-valued process with spatially positioned individuals:

$$\tilde{Z}_t = \sum_{i=0}^{N_t-1} \delta_{(\boldsymbol{\xi}_i(t), h_i(t))},$$

whose first coordinates $\boldsymbol{\xi}_i(t) = (a_i(t), y_i(t), x_i(t))$ are a copy of Z_t and such that $h_i(t)$ follows the following additional dynamics:

3. **Spatial configuration:** When a cell of size y and vertical position h divides, its replaced by two newborn cells of size ρy and $(1-\rho)y$ as explained above, and which respective vertical positions are h and $h - \rho y$. Between divisions the position growths exponentially at elongation rate λ : $h'(t) = \lambda h(t)$. See Fig. 2.4.

Then we order the individuals in $\tilde{Z}_t$ from lowest to highest in the h coordinate. This indexation is represented in Fig. 2.4. Following [57], this indexation can be formalised using the coordinate projection described in Definition A.1.2 in the Appendix. In particular, let us set $\mathscr{O}_0 : \mathcal{M}_p(\mathcal{X} \times \mathbb{R} \times \mathbb{R}_+) \to \mathcal{X} \times \mathbb{R} \times \mathbb{R}_+$ the projection

$$\mathscr{O}_0 \left(\sum_{i=0}^{N_t-1} \delta_{(a_i(t), y_i(t), x_i(t), h_i(t))} \right) = (a_0(t), y_0(t), x_0(t), h_0(t))$$

giving the first element in the order given by the h coordinate. Therefore, the tracked lineage of the cell trapped at the bottom of the tube (see Fig. 1.1) is given for all $t \geq 0$ by the individual indexed 0 in $\tilde{Z}_t$. This lineage is given by $\mathscr{O}_0(\tilde{Z}_t)$. When there is no possible ambiguity, we will simply write $\mathbf{O}_t := \mathscr{O}_0(\tilde{Z}_t)$, and coordinate by coordinate $\mathbf{O}_t = (A_t, Y_t, X_t, H_t)$.

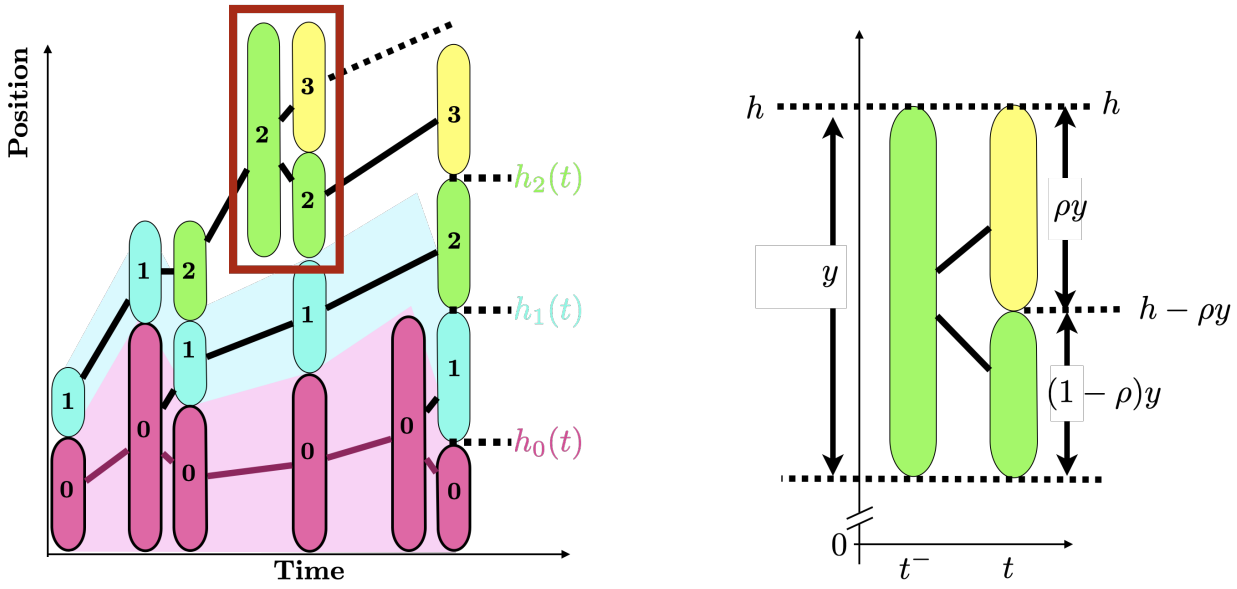

Figure 2.4: Indexation by vertical position in the MM.

Now, consider a time grid of N time points $\{n\Delta t, n \in [\![0, N]\!]\}$, with an acquisition time Δt. We model the MM observations as a discrete sample of J independent realisations (one for each MM tube) written

$$(\mathbf{O}^j_{n\Delta t})^{j=1,\dots,J}_{n=0,\dots,N}.$$

2.3.2 Censored data in a finite depth mother machine

If the mother machine is supposed infinitely long, this scheme is equivalent to choose one daughter at random at each division event. This is called *forward sampling* in the biophysics literature [136]. If the mother machine is supposed to have a finite depth $L > 0$, cells that reach $h = L$ are eliminated. This induces the presence of *right censoring*: division events such that the division size is greater than L cannot be observed. This is, conditionally to an initial size Y_0, the added size at division A^L_{div} that can be observed in a finite MM of length L is given by

$$A^L_{div} = A_{div} \wedge C,$$

where $C = L - Y_0$ is the *censoring added size* imposed by the MM depth. Under the adder assumption the distribution of the added size at division A_{div} does not depend on Y_0, so A_{div} and C are independent. The censoring is said to be *non informative* in this case [135]. We introduce the censoring indicator $\Delta = \mathbb{1}_{A_{div} \leq C}$, and, as in classical survival analysis, we suppose that we dispose of joint observations (A^L_{div}, Δ). Suppose that g_{Y_0} and G_{Y_0} are the probability density function and cumulative distribution function of the birth size Y_0. Thanks to the independence of the censoring, the joint distribution of (A^L_{div}, Δ) is given for

all measurable bounded function $h : \mathbb{R}_+ \times \{0,1\} \to \mathbb{R}_+$ by

$$\begin{aligned}\mathbb{E}\left[h\left(A^L_{div}, \Delta\right)\right] &= \mathbb{E}\left[h\left(A^L_{div}, 1\right) \mathbb{1}_{A_{div}=A^L_{div}, C\geq A_{div}}\right] + \mathbb{E}\left[h\left(A^L_{div}, 0\right) \mathbb{1}_{A_{div}>A^L_{div}, C=A^L_{div}}\right] \\ &= \sum_{\delta\in\{0,1\}} \int_0^{+\infty} h(a,\delta) \left(f_A(a)(1-G_{Y_0}(L-a))\right)^{\delta} \left(S(a) g_{Y_0}(L-a)\right)^{1-\delta} \mathrm{d}a,\end{aligned}$$

In practice, the birth size is observed, so the joint likelihood of (A^L_{div}, Δ) is simply reduced (up to a normalisation constant) to

$$p((a,\delta)) \propto f_A(a)^{\delta} S(a)^{1-\delta}. \tag{2.6}$$

Censoring events ($\Delta = 0$) occur fairly rarely in the control dataset. However, since we will work under conditions that induce filamentation, it becomes biologically relevant to accurately account for this bias. Right censoring of this kind is a classical problem in the literature of survival analysis. In particular, we use the `R` package `flexsurvreg` [81] that allows to easily integrate the censoring status of the observations.

2.4 Inference of the model parameters from individual cells at stationarity

2.4.1 Estimation of the adder division rate function B

To estimate the adder division rate B we consider only the observations of cells at division (or censoring time, if the observation is right-censored):

$$(\mathbf{O}^j_{T^j_n \wedge C^j_n})^{j=1,\dots,J}_{n\in\mathbb{N}},$$

where T^j_n is the time of the n-th division or censoring event observed in the j-th lineage. In general this information is poorer than the previous scheme. However, in the case of the adder model, since the added size is independent from the initial size, one has that the joint sample of added sizes at division $\left(A^L\right)^j_{T_n}$ and censor status $(\Delta)^j_{T_n}$ are independent and identically distributed random variables of joint density p given by (2.6). In this case, the estimation is the same as for a classical renewal model, which can be done by the classical approaches of parametric and non-parametric survival analysis [135, 46].

Function B is a hazard rate on length units, for which several classical parametric hazard models might be suitable. The simplest one is the exponential model: if B is assumed to be equal to a constant, then Eq. (2.4) implies that the distribution of the added sizes at division follows an exponential law. Other more realistic models are the Gamma distribution, the Lognormal distribution and the Weibull and Gompertz models which are extensively used in hazard rates estimation. The selection of the most suitable model can be performed using the Bayesian Information Criterion (BIC), among other statistics.

Generally speaking, to build an estimator $\hat{B}$ of B we use the empirical distributions obtained from the mother machine. Call $\hat{f}_A$ the Maximum Likelihood Estimator of the distribution of added sizes obtained by fitting the chosen model to the mother machine data (using the joint likelihood (2.6) to include eventual censorship). Then, from (2.5), we use the point-wise estimator

$$\hat{B}(a) = \frac{\hat{f}_A(a)}{\hat{S}(a)} \tag{2.7}$$

where $\hat{S}$ is obtained by integration of $\hat{f}_A$.

Table 2.1 shows that the BIC supports systematically the selection of the lognormal model. The quantile-quantile plots of Fig 2.5 reflect the same conclusion. Nonetheless, important deviations from the predicted quantiles are observed in the tail of the distribution.

Model	Glycerol medium	Glucose medium	Glucose + aa medium
Weibull	3959.145	1689.818	15339.65
Gamma	2323.495	1376.991	14113.94
Lognormal	2224.319	1313.494	14083.10

Table 2.1: BIC scores for the fitted models in each medium.

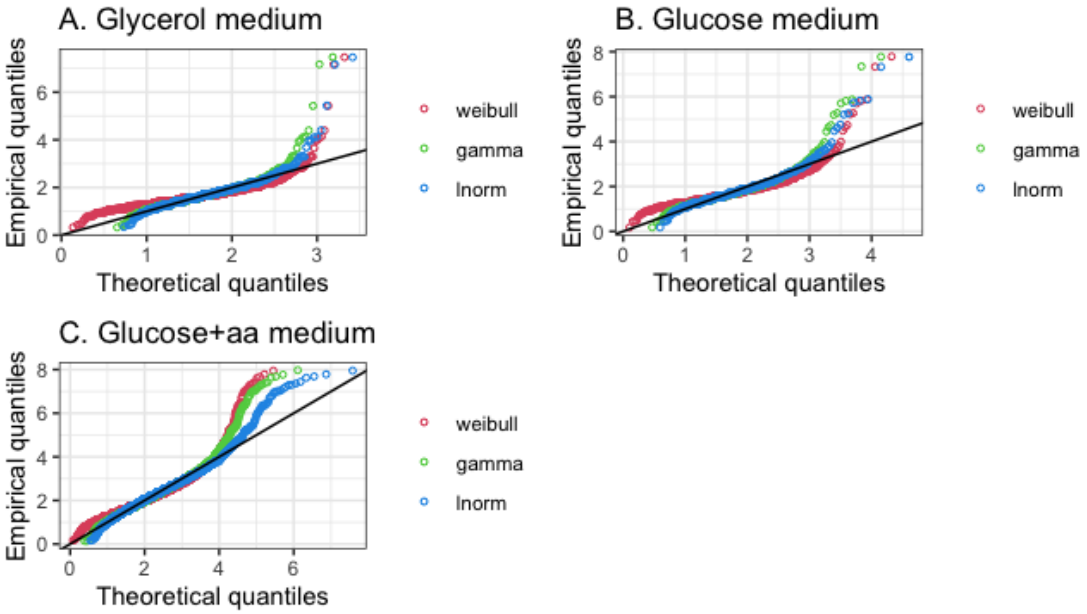

Figure 2.5: Q-Q plots of the fitted distributions to the added sizes in each medium. Each graph compares the predicted quantiles and the observed ones. It confirms the best fit of the lognormal distribution. However, systematic underestimations are observed in the tails of the distribution.

We recall that the lognormal distribution is parametrised by two quantities: the mean log-added size μ and the standard deviation of the log-added size σ. If ϕ is the standard

Medium	μ ($\log \mu$m)	σ ($\log \mu$m)
Glycerol	0.4606340 ± 0.0071999	0.2123930 ± 0.0050906
Glucose	0.5034900 ± 0.0212816	0.3156287 ± 0.0150477
Glucose + aa	0.7063365 ± 0.0084250	0.3483618 ± 0.0059572

Table 2.2: 95% CI of the lognormal distribution parameters for the fitted distributions in each medium.

Normal PDF and Φ its CDF, we have that

$$S(a) = \mathbb{P}(\log(\text{Added size}) \geq \log(a)) = 1 - \Phi\left(\frac{\log a - \mu}{\sigma}\right).$$

Therefore the parametric estimator $\hat{B}$ has the form

$$\hat{B}(a) = \frac{\phi\left(\frac{\log(a)-\hat{\mu}}{\hat{\sigma}}\right)}{\hat{\sigma}a \cdot \left(1 - \Phi\left(\frac{\log a-\hat{\mu}}{\hat{\sigma}}\right)\right)} \tag{2.8}$$

The estimated parameters and 95% confidence intervals are given in Table 2.2 for the three different media. The respective resulting $\hat{B}$ functions along with their 95% confidence intervals are given in Fig. 2.6. We are able to infer some quantitative effects of the environmental richness on the adder mechanism. For example, Fig. 2.6 shows that the adder division rate is twice as big in glycerol than in glucose, for example, which means that in average, after adding the same amount of size, cells in glucose are two times more likely to divide than in glycerol.

2.4.2 Estimation of the division ratio distribution F

The mother machine device allows to identify the progenitor cell for each followed individual. In particular, this allows to compute the ratio between the birth size of each cell and the division size of its mother. In the mother machine experiments, only one daughter cell is followed after the division. This induces a spurious bias in the empirical distribution of ratios which is then non necessarily symmetrical. Since this should not be observed in a population dynamic where both daughter cells are preserved, we complete the dataset by adding the complementary ratios, such that the sample is centred around 1/2.

We compute this ratio for every cell in each medium and we fit a Beta distribution $\hat{F}$ as a suitable estimator of the ratio distribution. The estimated parameters along with their 95% confidence intervals are given in Table 2.3 for the three different media. We see in particular that the estimates for both parameters of the Beta distribution have almost the same value, which comes from the symmetry of the distribution. The bigger the value of α and β the more concentrated the distribution, which can be observed in Fig. 2.7. We see that the distribution is wider in richer media. This could mean that the position of the division septum is less exact in fast growing bacteria.

Finally, using the estimated $\hat{B}$ and $\hat{F}$, we can simulate the process Z_t for different initial conditions. The stochastic simulation consists on a Gillespie algorithm which exploits

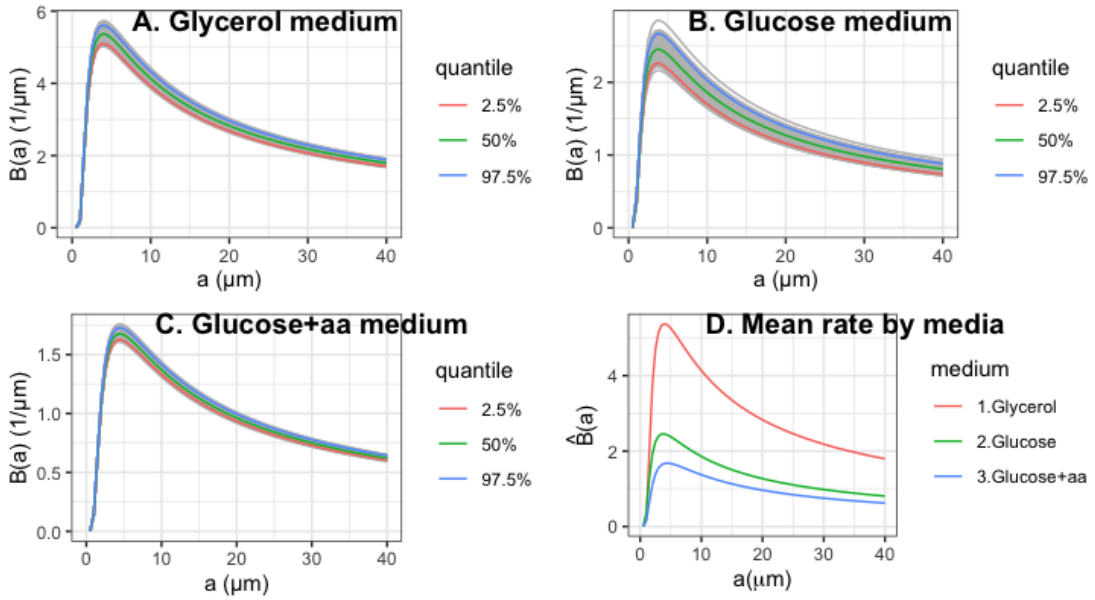

Figure 2.6: Estimated values of $\hat{B}$ (Eq. (2.8)) for the three different media according to the parameters of Table 2.2. Grey curves correspond to random realisations of B with parameters sampled from the asymptotic distribution of each parameter estimator. The median curve and the borders of the 95% confidence interval are coloured.

Medium	α (First shape parameter)	β (Second shape parameter)
Glycerol	20.541535 ± 0.6927115	20.541012 ± 0.6926937
Glucose	8.946326 ± 0.5966249	8.946660 ± 0.5966478
Glucose+aa	5.961458 ± 0.1415771	5.961717 ± 0.1415835

Table 2.3: 95% confidence intervals of the Beta distribution parameters for the fitted distributions of the mother-to-daughter-size ratios in each medium.

the fact that the proposed B function is bounded to perform an efficient rejection sampling technique. The result is a simulated population process $\hat{Z}_t$ which can be compared to macroscopic population data. Fig. 2.8 summarises the core of the method.

2.5 Comparison to population "snapshot" data

As we have proven in [103] (see also Chapter 3 herein), in expectation, the process Z_t converges exponentially fast in weighted total-variation norm (V-uniform convergence) towards its steady-state distribution π^*. This is, for all test function g we have

$$\mathbb{E}\left[\sum_{i=1}^{N_t} g\left(\mathbf{X}_i(t)\right)\right] \underset{t\to+\infty}{\sim} \frac{e^{\lambda t}\sum_{i=1}^{N_0} y_i(0)}{\langle \mathbf{y}\rangle} \int_{\mathcal{X}} g(\mathbf{x})\pi^*(\mathbf{x})\mathrm{d}\mathbf{x} + O(e^{-\omega t}), \tag{2.9}$$

where the elongation rate λ is also the population growth rate (Malthusian parameter), the total mass $\sum_{i=1}^{N_t} y_i(t)$ propagates the effect of the initial condition and the steady-state mean

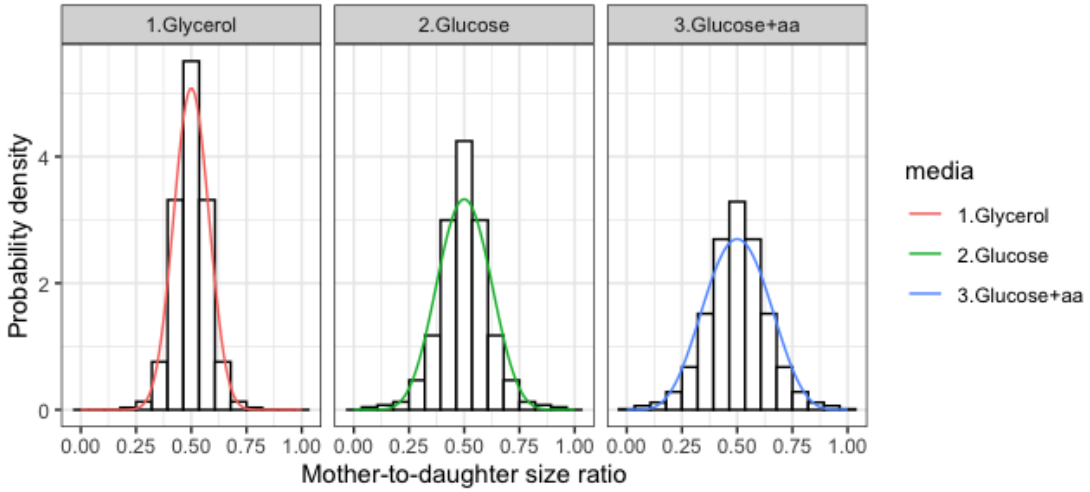

Figure 2.7: Estimated densities $\hat{F}$ for the three different media according to the parameters of Table 2.3

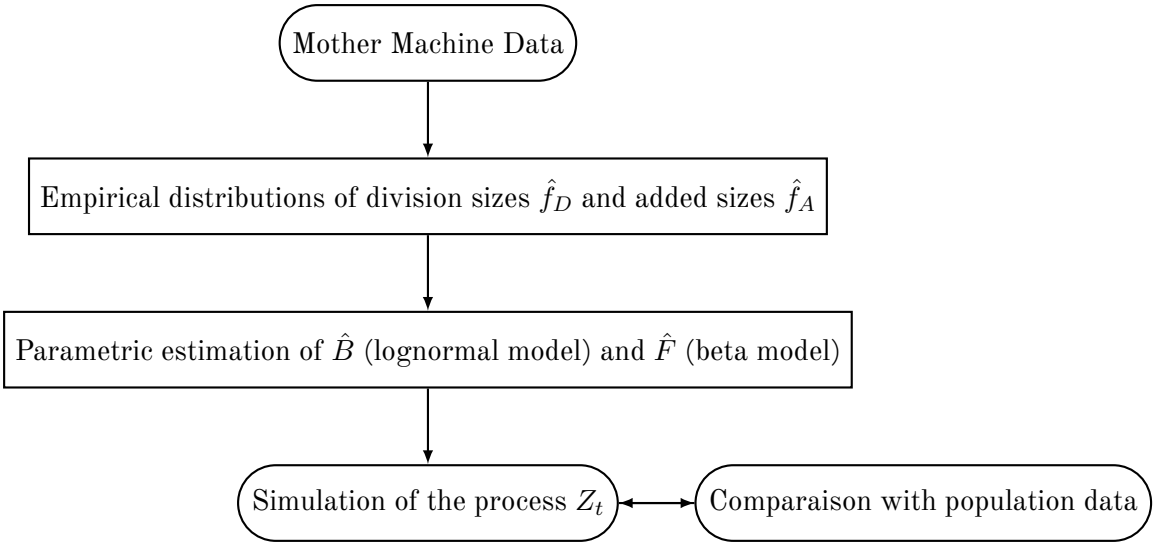

Figure 2.8: From microscopic observations to the macroscopic characterization of the growing population. Schematic representation of the proposed parametric framework.

size $\langle \mathbf{y} \rangle = \iint y\pi^*(a,y)\mathrm{d}a\mathrm{d}y$ acts as a normalisation constant. The constant $\omega > 0$ quantifies the speed of convergence. Moroever, π^* is given by [70]:

$$\pi^*(a,y) = \frac{\exp\left(-\int_0^a B(\alpha)d\alpha\right)}{y^2}\mathfrak{f}_0(y-a), \tag{2.10}$$

where $\mathfrak{f}_0$ is the unique solution to the fixed point problem

$$\mathfrak{f}_0(x) = 2\mathcal{T}[f](x) = 2\int_0^1 \mathfrak{f}_0 \star f_A\left(\frac{x}{\rho}\right) F(\rho)d\rho, \tag{2.11}$$

where $\star$ denotes the convolution product. The unique solution $\mathfrak{f}_0$ to Eq. (2.11) can be obtained numerically, using an iterative power method. This is, from any function q_0 over $\mathbb{R}_+$, the successive iterations

$$q_{k+1} = \mathcal{T}[q_k] \ , \ k > 0$$

give approximated solutions with $q_k \to \mathfrak{f}_0$ as $k \to \infty$. [62] show the theoretical properties of this fixed point problem assuring the convergence of this method to $\mathfrak{f}_0$. Then, using the estimates of B and F obtained from the MM data we can obtain the predicted steady-state distribution as presented in Fig. 2.9.

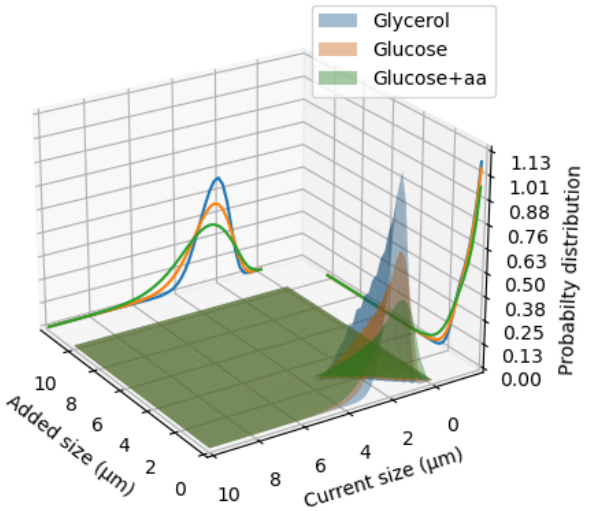

Figure 2.9: Plot of π^* given by Eq. (2.10) with B and F as given by the parametric estimators fitted for each medium. Projected onto each plane the marginal distributions of a and y are also shown.

We are particularly interested in the marginal steady-state distribution of sizes p, which is the sole observable distribution in the snapshot data. From Eq. (2.10) we have that

$$p(y) = \int_0^y \pi^*(a, y)da = \frac{1}{y^2}\int_0^y S(a)\mathfrak{f}_0(y-a)da = \frac{\mathfrak{f}_0 \star S(y)}{y^2}$$

In particular, the mean cell size is given by

$$\langle \mathbf{y} \rangle = \int_0^\infty \frac{\mathfrak{f}_0 \star S(y)}{y} dy$$

and its variance by

$$\mathbf{s}^2 = \int_0^\infty \left(\frac{y - \langle \mathbf{y} \rangle}{y}\right)^2 \mathfrak{f}_0 \star S(y)dy.$$

We call $\hat{p}(y)$ the predicted values of $p(y)$ using the estimates for B and F fitted to the mother machine data in each medium. Figure 2.10 and Table 2.4 compare the values of $\hat{p}$ with the empirical distributions of sizes observed in population growth experiments with the same media.

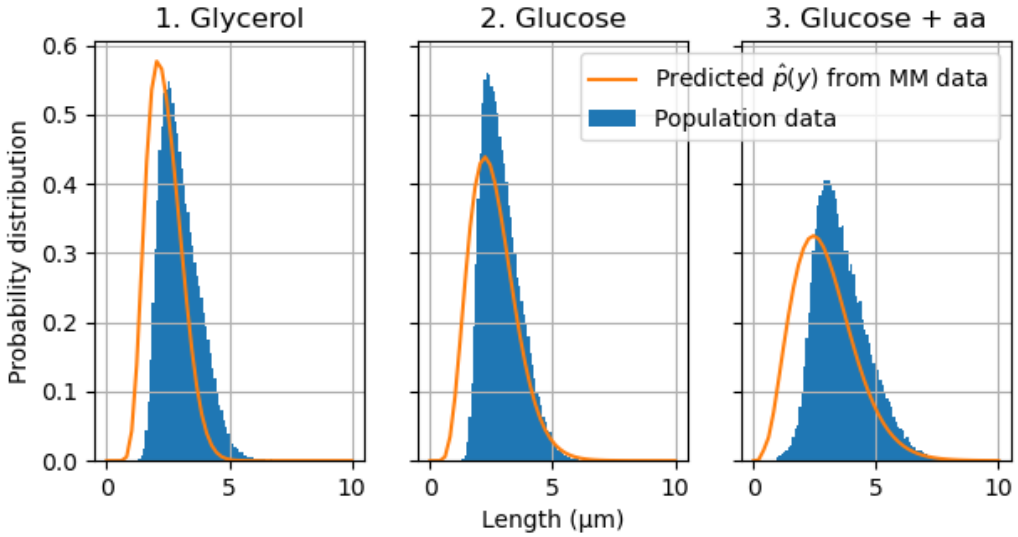

Figure 2.10: Comparison of the predicted steady-state size distributions and the size measurements in the agarose pads.

	Glycerol	Glucose	Glucose + aa
Predicted mean size $\widehat{\langle \mathbf{y} \rangle}$ (μm)	2.3696	2.5913	2.9172
Observed mean size (μm)	3.0188	2.9154	3.6144
Predicted size standard deviation $\widehat{\mathbf{s}}$ (μm)	0.6846	0.9432	1.2679
Observed size standard deviation (μm)	0.8963	0.8082	1.1423

Table 2.4: Comparison of the predicted steady-state size distributions and the size measurements in the agarose pads.

We recall that the population data and the estimated $\hat{p}$ came from completely independent experiments (no fitting parameter). Thus, the similarity between the shapes of the distributions is rather surprising. This could imply that the macroscopic dynamics is driven by similar division rates and mother-daughter size ratio as observed in the MM. In particular, while the dispersion is well approximated, there is a systematic shift to the left in all distributions. This might indicate an exogenous effect that affects systematically all the cells, producing smaller cells in the mother machine than in the population. This could by explained by the physical constraints that the mother machine device imposes on the bacteria.

2.6 Modelling the single-cell response under dynamic DNA damage

2.6.1 Adder statistics under DNA damage

As we can see in Fig. 2.11, the presence of ciprofloxacin affects substantially the size control dynamics considered in the previous paragraphs. The first two sample lineages #467 and #7405 show that despite cip-induced filamentation, bacteria are able to divide during the antibiotic treatment and to keep dividing after the stress is removed. On the contrary, the sample lineage #8158 shows that, even after some successful divisions, certain bacteria seem to *die* (stop growing and dividing, *stricto sensu*). In the following lines we aim to model the effect of ciprofloxacin-induced DNA damage in the division dynamics previously modelled using the adder. To that extent, in all our data analysis and further modelling we will disregard these *dying* individuals, which we suppose will never divide.

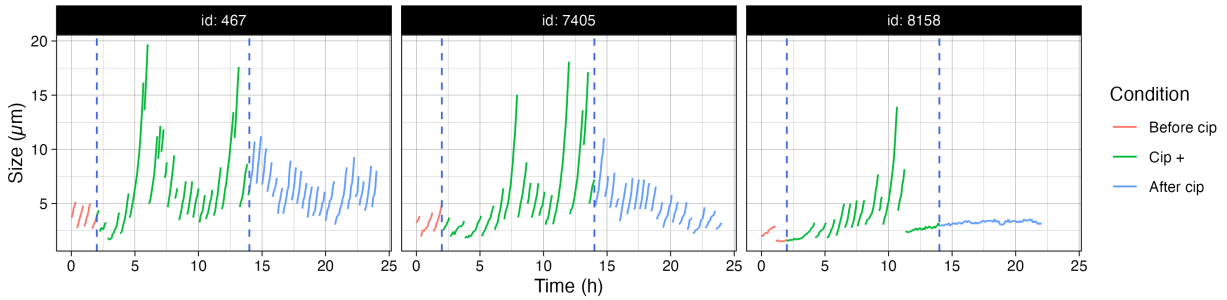

Figure 2.11: Sample of 3 cell size lineages Y_t in glucose-aminoacids medium. Data acquired by J. Broughton. Cells are exposed to cip during $4 \leq t < 14$ (Cip +), indicated between dashed lines. In $0 \leq t < 4$ (Before cip) and $14 \leq t < T = 25$ (After cip) there is no antibiotic.

Let us first focus on the distribution of the added size at division A_{div} when the cip-induced DNA damage is present. As shown by Fig. 2.12A, despite the presence of antibiotic in the media, the adder mechanism is kept in average. Indeed, we see that for all media and conditions, the median added size (circles) is independent from birth size, in coherence to the adder model and previous observations under different kind of damage [144, 121]. At the same time however, the distributions of the added size are wider under ciprofloxacin than under control, indicating a perturbation of the adder model in higher moments of the added size distribution. This is confirmed by Fig.2.12B, that shows that the standard deviation of the added size is positively correlated with birth size, specially in rich media, breaking the independence property of the adder model considered so far. Indeed, Fig.2.12C shows that the coefficient of variation (CV, defined as the quotient between the standard deviation and the mean of the distribution) of the added size distributions increases with the level of SOS induction measured at division, for all three media. Fig 2.12D quantifies the effect of the SOS level on the added size CV and shows what seems to be a linear trend with respect to the logarithm of PsulA fluorescence, with medium-dependent slopes.

The effect of SOS induction on the adder variability is specially visible in fast growing medium and under the presence of ciprofloxacin, but it is also present in the control ex-

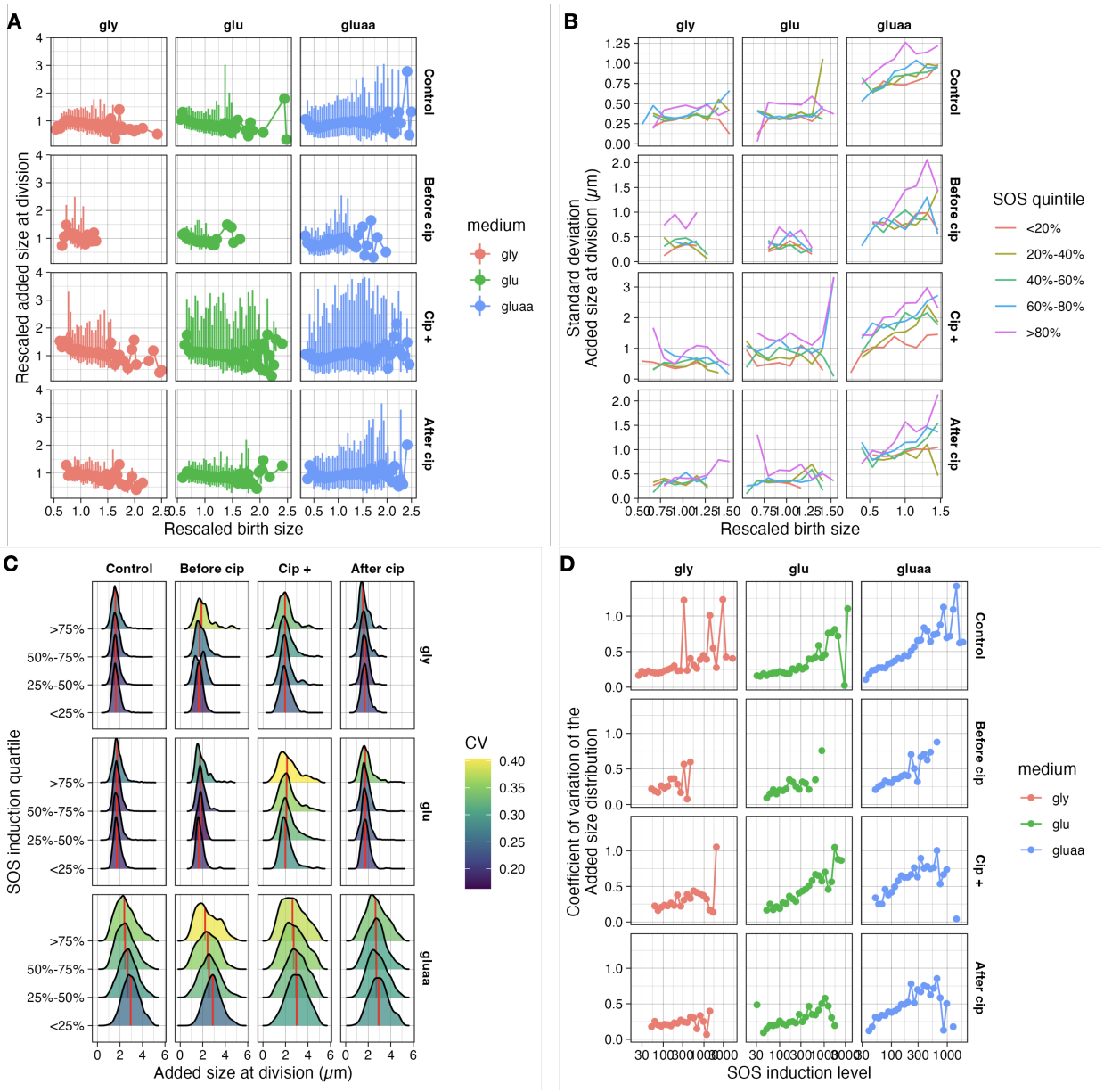

Figure 2.12: The adder is increasingly perturbed by the level of SOS induction. Descriptive statistics of the data acquired by J. Broughton. **A**. Rescaled added size at division (added size divided by the mean value by media) as function of the birth size (also rescaled by its mean by media). Circles indicate median values and lines correspond to the interquartile range. **B**. Standard deviation of the added size as function of the rescaled birth size, grouped by quintiles of SOS level observed at division. **C**. Added size distributions (kernel density estimates) grouped by quartile of SOS level at division in the vertical axis. The mean of the distribution is indicated by a red vertical line. The densities are coloured idepending on their coefficient of variation (CV). **D** CV of added size distribution in function of the level of SOS induction at division.

periments. This made us wonder whether the decreasing ("loss of control") regime of the division rate suggested by the Lognormal fit of Section 2.4 and reported by Osella et al. [117] was linked to the level of SOS induction. To address this question we will introduce in Section 2.6.3 a more flexible model that, conditionally to the SOS level, includes the Lognormal distribution, but also distributions with non vanishing division rates. Before introducing the coupled SOS-adder model, we establish below a model for the dynamics of the SOS response.

2.6.2 Dynamics of the SOS response

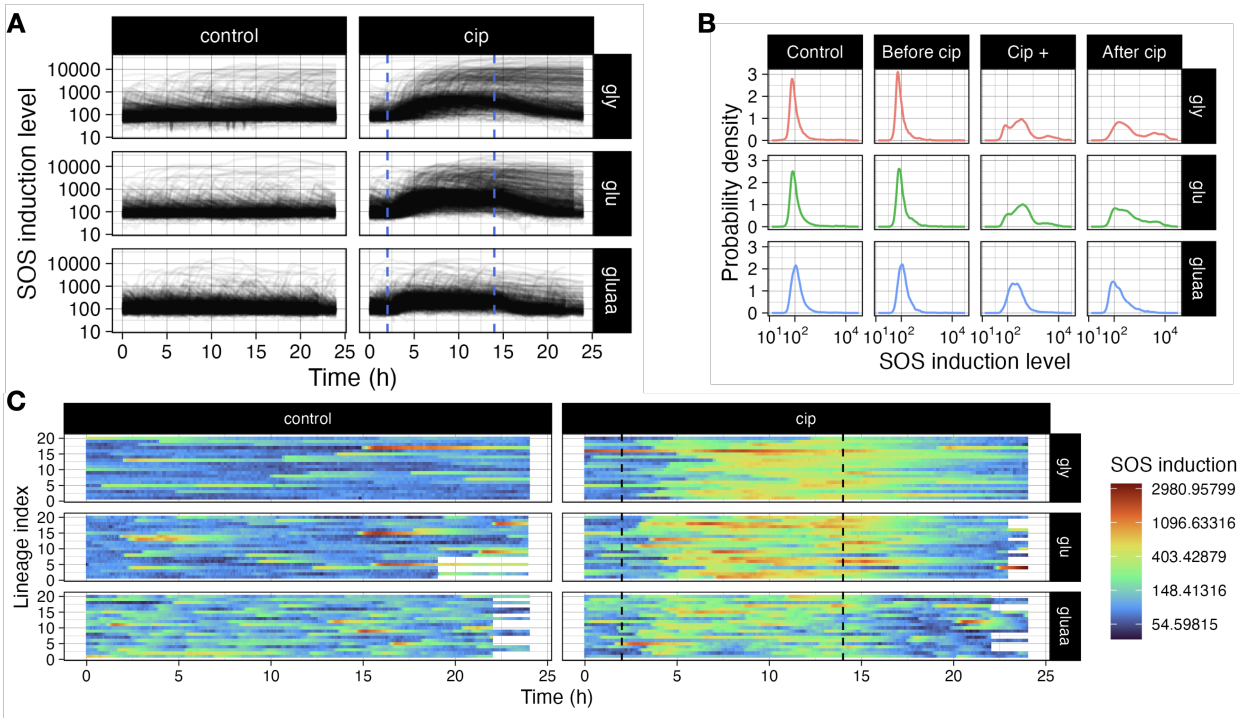

Figure 2.13: Single-cell trajectories of SOS induction in MM lineages. Experimental data acquired by J. Broughton. **A** SOS induction (PsulA-mGFP fluorescence) of the acquired MM lineages under different media, without any antibiotic (left) and under 3 ng/ml cip (right). The antibiotic is administrated during $t \in [2, 14]$ marked by dashed lines. **B.** Density estimates of the distribution of the SOS induction level in the control dataset and during the different phases of the antibiotic treatment. **C.** Random subsample of 20 MM lineages, coloured by the level of SOS induction.

We recall that we have access to time series of the fluorescence-per-area of a GFP-marked SOS transcriptional reporter, PsulA [82]. The observations summarised in Fig. 2.13 show the important heterogeneity, both time-wise and cell-wise, of the SOS fluorescence signal. Fig. 2.13A shows that the dynamics are modulated by the presence or absence of ciprofloxacin. However, the intensity of the response is far from being homogeneous among the individual bacteria. Fig. 2.13B shows broad distributions of the SOS response, especially under the effect ciprofloxacin. Moreover, Fig. 2.13C shows that the

SOS response is not coordinated either. During the antibiotic treatment, but even in control conditions, the times of strong SOS induction arrive rather stochastically across the different lineages. Thus, two crucial differences with respect to the classical adder studied is that the SOS response (and hence the perturbation it has on the adder mechanics observed in Fig. 2.12)) is dynamic and random. Based these observations we introduce now a time-continuous stochastic model of the SOS response.

Precedent simulation studies that have looked at the expression levels of several proteins participating in the SOS response, have shown that the SOS regulatory network can be accurately modelled by low-dimensional chemical reaction models [58, 128, 132]. These models are typically characterised by negativetely autoregulated motifs, as shown in Fig. 2.14, where a stressor u produces some damage z, which triggers a response x that, in turn, repairs the damage z.

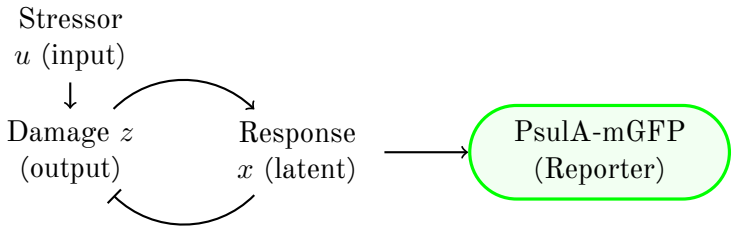

Figure 2.14: Scheme summarising the negative autoregulation models of the SOS response of [132] (from where the Figure was adapted). Arrows marked $\rightarrow$ represent positive regulation (v.g. synthesis or disinhibition), while $\dashv$ represents negative regulation (repression or inhibition). The fluorescent SOS transcriptional reporter PsulA-mGFP that we use as measure of the SOS activity (variable trait x) appears highlighted.

To account for this dynamic feedback, the authors in [132] propose a simple deterministic model they name integral feedback model (IF). Let u, x, z three real-valued functions of time representing at all time $t \geq 0$, the stressor signal $u(t)$ (ciprofloxacin in our case), the stress response $x(t)$ (the SOS response) and the amount of damage $z(t)$ induced by the stress (DNA breaks), which are solution to the ODE

$$\begin{cases} z(t) = u(t) - x(t) \\ x'(t) = \theta z(t) \end{cases} . \tag{IF}$$

This supposes that the amount of damage $z(t)$ is the result of the difference between the value of the stressor signal $u(t)$ (damage induction) and the stress response $x(t)$ (damage repair). At the same time, the stress response $x(t)$ senses the damage, and its intensity increases linearly with the level of damage $z(t)$ with a proportionality factor equal to $\theta > 0$. The parameter θ thus represents the rate of reactivity of the stress response with respect to the perceived damage.

Now, substituting the first equation on the latter, the equation for $x(t)$, reduces to the autonomous equation

$$x'(t) = \theta(u(t) - x(t)).$$

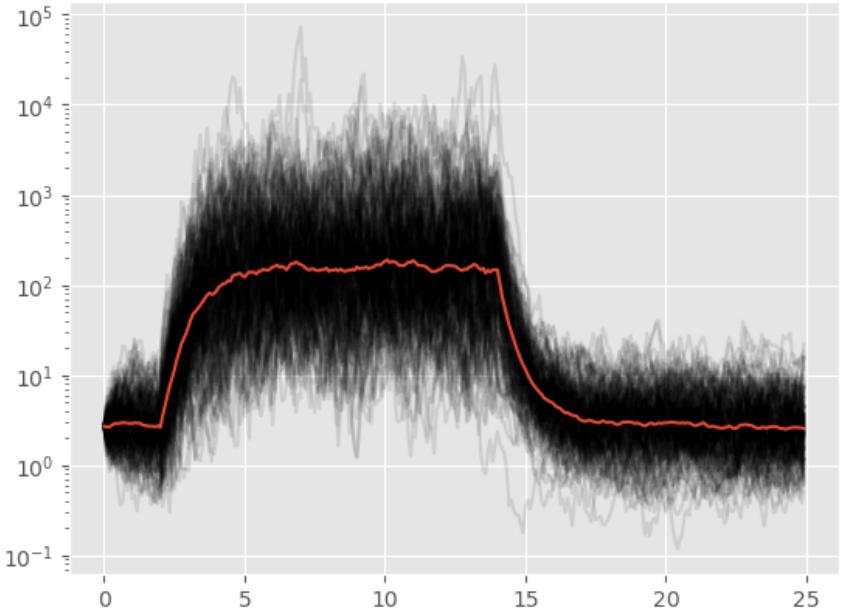

Figure 2.15: Simulated trajectories of the SOS level X_t according to Eq. (2.12) with $\theta_0 = \mu_0 = \zeta_0 = 1$ and $\mu_1 = 5$, $\theta_1 = 1$, $\zeta_1 = 2$.

However, we have seen that the SOS response is not coordinated, and varies significantly both among individuals and in time. Thus, to incorporate this dymamic variability, we generalise the deterministic (IF) model to the solution of a stochastic differential equation (SDE). We propose to model the dynamics of the SOS signal (measured as log-fluorescence by unit of volume, in the scale presented in Fig. 2.13) as a real-valued diffusion process $(X_t)_{t\geq 0}$ solution to the Orstein-Uhlenbeck SDE

$$\mathrm{d}X_t = \theta_{c(t)}(\mu_{c(t)} - X_t)\mathrm{d}t + \zeta_{c(t)}\mathrm{d}B_t \tag{2.12}$$

where B_t is a standard Brownian motion, $c(t) = \mathbb{1}_{t\in[2,14[}$ equals 1 whenever the antibiotic is present in the medium and 0 otherwise, and θ_i, μ_i, ζ_i, $i \in \{0, 1\}$ are some non-negative constants. In particular, these parameters can be interpreted as follows:

- μ_i is the basal SOS expression level under stress $i \in \{0, 1\}$.
- $\theta_i > 0$ measures the strength at which the SOS expression reverts to its basal level after periods of under or over-expression. It is related to the molecular rates of induction and repression of the SOS response.
- $\zeta_i^2 > 0$ is the variance with which the log-fluorescence level fluctuates around the average value, accounting for various potential sources of stochasticity in the signal.

Fig. 2.15 shows an example of a simulation of Eq. (2.12). Interestingly, notice how the inflexion of the observed SOS level at the regime changes (Fig. 2.13A) can be well recovered by the Ornstein-Uhlenbeck model.

2.6.3 Coupling the adder and SOS dynamics

Using the Ornstein-Uhlenbeck model for the SOS dynamics, we propose now a phenomenological model describing how the SOS induction affects the adder division rate. Later in this section, we will model in a similar way, the effect of SOS induction on the mother-to-daughter size ratio distribution F.

We recall that divisions occur at random times, driven by an instantaneous division rate $\beta \geq 0$ that depends on the current cell trait $\boldsymbol{\xi}_t = (a_t, y_t, X_t)$ such that

$$\mathbb{P}(\text{Division time} \in [t + \mathrm{d}t[\,|\text{Division time} \geq t, \boldsymbol{\xi}_t) = \beta(\boldsymbol{\xi}_t)\mathrm{d}t + o(\mathrm{d}t). \tag{2.13}$$

Within the framework of the adder model, β is written as

$$\beta(a, y, x) = \lambda y B(a, x), \tag{2.14}$$

where B is the adder division rate and λ is the elongation rate. Under the adder hypothesis, the function B considered in Section 3.4 depended only on a. Our observations discussed above, lead us to propose rates B that depend also on the value of the SOS level x.

Notice that in general this will result in the lost of the adder property. Indeed, let $\mathbf{x}_0 = (0, y_0, x_0)$ the initial vector trait for a newborn individual of birth size y_0 and SOS level at birth x_0. Then, for every measurable bounded function $h : \mathbb{R}_+ \to \mathbb{R}$, doing the change of variables $t \mapsto a := y(t) - y_0$ we obtain

$$\begin{aligned}\mathbb{E}_{\mathbf{x}_0}[h(A_{div})] &= \mathbb{E}_{\mathbf{x}_0} \int_0^{+\infty} h\left(y(t) - y_0\right) \beta\left(y(t) - y_0, y(t), X_t\right) e^{-\int_0^t \beta(y(\tau)-y_0, y(\tau), X_\tau)\mathrm{d}\tau} \mathrm{d}t \\ &= \int_0^{+\infty} h\left(a\right) \mathbb{E}_{x_0}\left[B\left(a, X_{\tau(a)}\right) \exp\left(-\int_0^a B\left(s, X_{\tau(s)}\right) \mathrm{d}s\right)\right] \mathrm{d}a,\end{aligned}$$

where the expectation is taken over the Ornstein-Uhlenbeck process X and $\tau(a) = \lambda^{-1} \log(1 + y_0^{-1} a)$ is the time needed to reach an added size a given the birth size y_0. Therefore, the distribution of A_{div} depends on general on the initial size y_0.

Henceforth, in agreement with the observations presented in Fig. 2.12, we consider that the SOS induction might perturb the adder mechanism, so that the probability law of the added size at division can ultimately depend on the initial size of the cell. In general, we will consider B of the parametric form

$$B(a, x) = \frac{f(a|x)}{\int_a^{+\infty} f(u|x)\mathrm{d}u} \tag{2.15}$$

where $f(a|x)$ is a probability density function on the a variable that depends on some parameters which are function of x. In particular, if the SOS response is constant, we recover

$$\mathbb{P}(\text{Division added size} \in [a + \mathrm{d}a[\,|X \equiv x) = f(a|x)da,$$

independently on the initial size, which is in accordance to the adder hypothesis. Recall however that, when X_t evolves through time, it is not longer true that $f(\cdot|x)$ corresponds

to the conditional distribution of the added size at division when the SOS induction level at that time equals x, as we discussed in the paragraph above.

To contrast with the results without antibiotic perturbation, we will consider the case when $f(\cdot|x)$ corresponds to a Generalised Gamma distribution [131, 120], which includes the three cases tested in Section 2.4.1 at the cost of an additional parameter. This distribution is parameterised by 3 parameters $(m, s, q) \in \mathbb{R}*\times\mathbb{R}_+\times\mathbb{R}$ and can be characterised as follows. Let R be a Gamma random variable of parameters $(1/q^2, 1)$ and let $W = \log(q^2 R)/q$. Then the probability law of $A = \exp(m + sW)$ is called GenGamma(m, s, q). This means that A follows a log linear model [120]:

$$A \sim \text{GenGamma}(m, s, q) \iff \log A = m + sW. \tag{2.16}$$

Thus, the parameter m plays the role of a scale parameter and it is related to the log-scaled mean, while the parameters s an q determine the shape of the distribution (see Fig. 2.16). We consider the case $q > -1/(2s)$, which is necessary and sufficient to have finite variance, see [131].

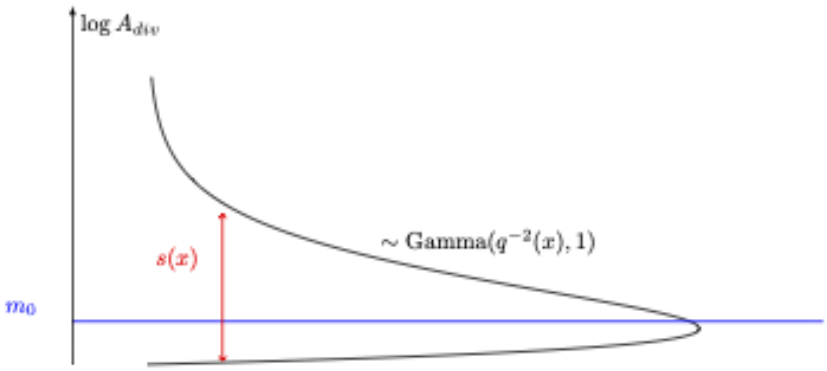

Figure 2.16: Generalised Gamma model for the effect of the SOS response on the added size distribution. Scheme of the generalised gamma model for A_{div} given by (2.16). The scale parameter m_0 is fixed and the shape parameters $s(x)$ and $q(x)$ are SOS dependent.

Interestingly, Cox et al. [37] show that different values of s and q can generate very flexible rate functions (Fig. 2.17). Indeed, the Gamma distribution of mean e^m and CV s is obtained doing $q = s$. The Lognormal distribution, of log mean m and log standard deviation s is obtained by doing $q = 0$. This flexibility will be important to account for the SOS-induced filamentation, as our results will show further below.

Thus, based on the empirical observations summarised in Fig. 2.12, we aim to model the dependence of the SOS intensity x on the parameters $m(x)$, $s(x)$ and $q(x)$ of $f(\cdot|x)$. First, as shown by Fig. 2.12A and C we will make the assumption that, conditionally to a constant SOS response, the median added size (in log scale) does not depend on the intensity of the response. This means that we fix a medium-dependent constant $m(x) = m_0$ for all $x \in \mathbb{R}$.

Second, we make the following assumptions concerning the effect of SOS induction on the shape of the added size distribution. Motivated by the linear trends observed in Fig.

2.12D, we make the strong assumption that both $q(x)$ and $s(x)$ are affine functions of the SOS level x. This is, we introduce two parameters $q_1 \in \mathbb{R}$ and $s_1 > 0$ such that

$$q(x) = q_0 + q_1 x,$$
$$s(x) = s_0 + s_1 x,$$

where the intercepts q_0 and s_0, obtained in total absence of SOS response, can be obtained from the previously analysed control dataset, and will be supposed known. Then, starting from a certain (s_0, q_0), depending on the values of q_1 and s_1, the value of x can change the shape of the division rate as shown by the example at the left panel of Fig. 2.17.

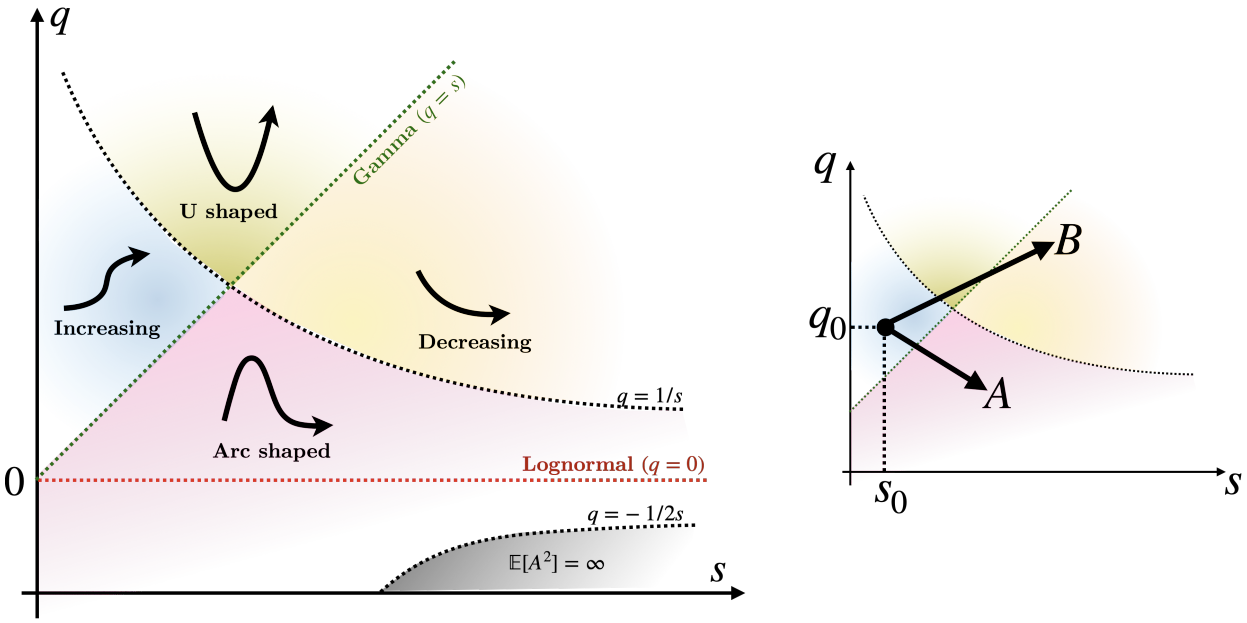

Figure 2.17: Adapted from [37]. See Fig. 1 therein to see a more detailed version. At the left panel, scheme representing the 4 possible shapes of the division rate B that can be obtained with a GenGamma(m, s, q) model at fixed $m > 0$. At the right panel, starting from (s_0, q_0) giving a monotonically increasing division rate, and depending on the values of q_1 and s_1, an increased level of SOS response might lead to an arc shaped lognormal-like division rate (A), or to a monotonically decreasing division rate (B).

2.6.4 Effect of SOS induction on the mother-to-daughter size ratio distribution

As before, we let $\rho \in [0, 1]$ the ratio between the observed size of the followed mother after and before division and we write $k(y, \rho)$ the probability density that a mother of size y produces a daughter of size ρy. In Fig. 2.18A we present the empirical distribution of ρ observed throughout the experiment in the three different media. We see that the number of possible septa (position where the division occurs) increases with the mother size. Similar observations have been reported in similar experimental settings. [144] observed

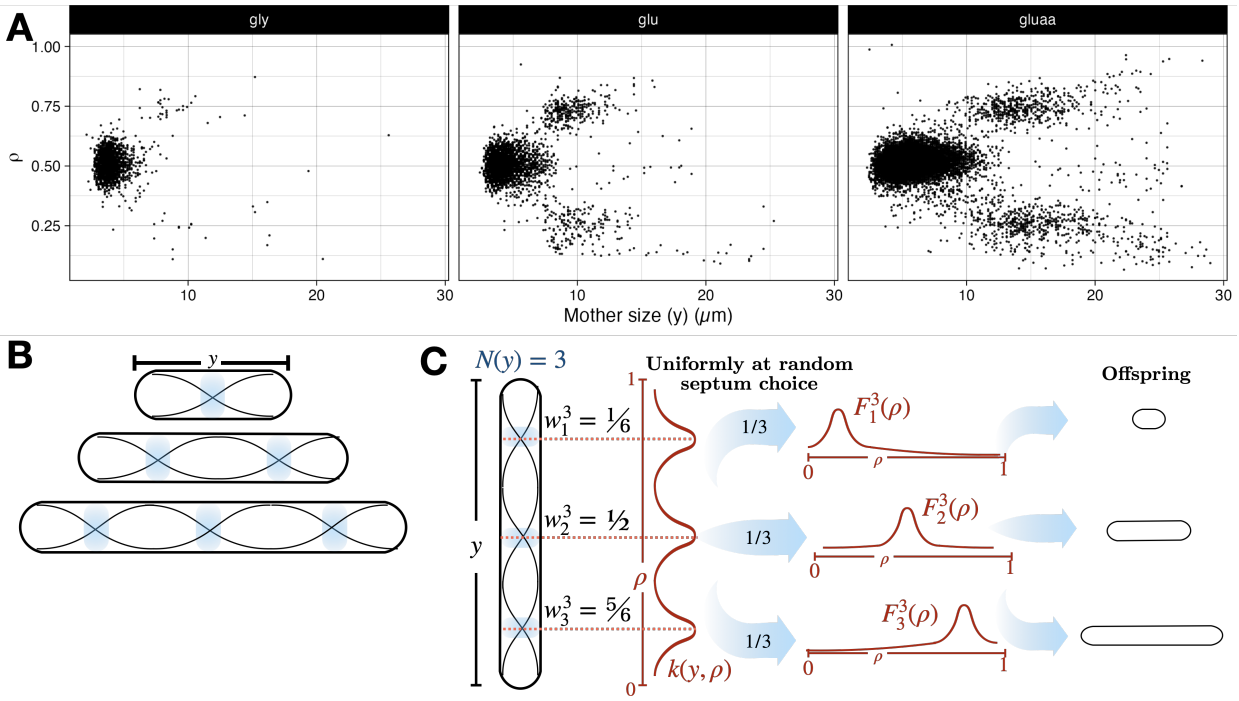

Figure 2.18: Size-dependent cell division of filamentous *E. coli*.- A. Empirical distribution of ρ as function of the mother size y extracted from single lineages in MM. Data acquired by J. Broughton. **B.** Scheme of the Min system. The reaction-diffusion dynamics of the Min proteins (vector function U in the cartoon), produce standing waves at whose nodes division proteins accumulate. **C.** Scheme of the proposed Beta mixture model. Example with $N(y) = 3$.

very similar distributions when looking at the distribution of ρ after switching from stress medium (1μM tetracycline, another antibiotic) to non-stress medium, in in a microfluidic chamber (different experimental setting than ours).

Moreover, previous studies have shown that the number of septa is tightly controlled by a system of proteins called the Min system [107], that diffuse inside the cells. It has been shown experimentally and by PDE simulations that the spatial reaction-diffusion dynamics of these Min proteins lead to standing waves inside E. coli [107]. Remarkably, division proteins accumulate in the nodes of these standing waves [107]. Thus, division septa can originate at these positions. Since the vibration mode depends on the length y of the cell, so does the number of nodes, and thus, of possible septum positions (see te cartoon of Fig. 2.18B). This introduces a size-dependence on the division kernel that was absent in the previous model. In particular we loose the property of *self-similarity*: the division place does not only depend on the mother-to-daughter size ratio, but also on the absolute size of the mother. This important generalisation will be taken into account in the analysis carried out in Chapter 3 and [103], where an application of the main result shows that a steady-state distribution of sizes still exists, and that any population of cells converge at exponential speed towards it.

In particular, the experimental results and PDE simulations of a reaction-diffusion model of the Min system carried out by Wehrens et al. [144] show that the nodes appear near very

precise positions. This is, they show that both the empirical and simulated distributions of ρ, reaches their maximum at constant positions $(w_n^N)_{n\in[\![1,N]\!]} \in]0,1[$ determined by the total number N of nodes and given explicitly by

$$w_n^N = \frac{2n-1}{2N}. \tag{2.17}$$

Based on these previous findings and our own observations, we propose a parametric model for $k(y,\rho)$. First, we call $N(y)$ the number of possible septa, which is function of the mother size y. In particular, we suppose that there is a critical size parameter y^* that determines the number of possible septa by the rule

$$N(y) = \left[\frac{y}{2y^*}\right] + 1, \tag{2.18}$$

where $[u]$ is the integer part of u. This means that if the mother size is below $2y^*$ there is only one possible septum ($N=1$), if the mother size is between $2y^*$ and $4y^*$, then there are two possible septa ($N=2$), etc. As such, y^* can be thought as related to the characteristic wavelengths of the standing waves produced by the Min system.

Additionally, we suppose that, conditionally to the mother size y, the division can occur at each possible septum with equal probability, this is, each possible site can be chosen uniformly with probability $1/N(y)$. Therefore, we suppose that k is of the form

$$k(y,\rho) = \frac{1}{N(y)} \sum_{n=1}^{N(y)} F_n^{N(y)}(\rho), \tag{2.19}$$

where, for all fixed N and n, $F_n^N(\rho)$ is the probability density of producing a daughter of size ρ times the size of the mother, when the division happens at the n-th septum among the N possible ones.

Finally, we suppose that cells have no particular orientation. For example, if $N=3$, the first and the third septa cannot be distinguished. In general, this imposes that our densities F have to verify, for all $n \leq N/2$ and all $\rho \in [0,1]$ a symmetry condition written

$$F_n^N(\rho) = F_{N+1-n}^N(1-\rho).$$

To contrast with the distributions fitted in Section 2.4, we will suppose in particular that F_n^N is the probability density function of the Beta distribution of parameters (α_n^N, β_n^N). This is

$$F_n^N(\rho) = \frac{\Gamma(\alpha_n^N + \beta_n^N)}{\Gamma(\alpha_n^N)\Gamma(\beta_n^N)} \rho^{\alpha_n^N - 1}(1-\rho)^{\beta_n^N - 1}. \tag{2.20}$$

The findings of Wehrens et al. suggest to take, for all $N > 1, n \in [\![1,N]\!]$, w_n^N as the mode of the distribution F_n^N, this is, such that $w_n^N = \text{argmax}_{0\leq\rho\leq 1} F_n^N(\rho)$ (i.e. as the *peak* of the observed distribution). Since for $\alpha_n^N > 1$ and $\beta_n^N > 1$ the mode is given by $\frac{\alpha_n^N - 1}{\alpha_n^N + \beta_n^N - 2}$ (otherwise equal to 0 and 1, and therefore not of our interest), we want

$$w_n^N = \frac{\alpha_n^N - 1}{\alpha_n^N + \beta_n^N - 2}.$$

Let the denominator be called $v_n^N := \alpha_n^N + \beta_n^N - 2 > 0$. Then we can write

$$\begin{aligned}\alpha_n^N &= 1 + v_n^N w_n^N, \\ \beta_n^N &= 1 + v_n^N \left(1 - w_n^N\right).\end{aligned}$$

The value of v_n^N is related to the variance as follows

$$\mathrm{Var}_{\rho\sim\mathrm{Beta}(\alpha_n^N,\beta_n^N)}(\rho) = \frac{\alpha_n^N \beta_n^N}{(\alpha_n^N + \beta_n^N + 1)(\alpha_n^N + \beta_n^N)^2} = \frac{1 + v_n^N + (v_n^N)^2(w_n^N - (w_n^N)^2)}{(v_n^N + 3)(v_n^N + 2)^2},$$

which is a decreasing function of v_n^N. As such, v_n^N measures the "concentration" (as contrary to dispersion) of the distribution of ρ. We make the biological assumption that the concentration of division proteins around the chosen septum is independent of the length of the cell and the total number of possible septa. This translate as setting for all $N \geq 1$, $n \in [\![1, N]\!]$, $v_n^N = v > 0$ constant, depending only on the culture medium.

Therefore, using the parametrisation, the kernel k depends only on two parameters (for each medium): the critical size y^* which defines the number of possible septa, and the constant v which determines the dispersion of the Beta distributions around them. Fig. 2.18C summarises this model.

2.6.5 Summary of the model for the coupled SOS-adder dynamics

To model the coupling between the SOS dynamics and the adder control we have done the following assumptions:

1. **SOS stochastic dynamics.** The SOS response intensity X_t is an Ornstein-Uhlenbeck process given by SDE (2.12). The drift and diffusion parameters are functions of a deterministic stress signal $c(t) = \mathbb{1}_{[}\tau_0, \tau_1[(t)$, equal to 1 during the antibiotic treatment (for all t such that $2 = \tau_0 \leq t < \tau_1 = 14$), and equal to 0 otherwise. For each value of $c \in \{0, 1\}$ the process is driven by 3 parameters: the long-term mean $\mu_i > 0$, a drift term $\theta_i > 0$ and a variance term $\zeta_i^2 > 0$. We call $\eta_X := (\mu_0, \theta_0, \zeta_0^2, \mu_1, \theta_1, \zeta_1^2)$ the vector of these parameters.

2. **Decision of the division instant.** The division is supposed to be triggered by the added size since birth $a(t)$ (adder model) and the level of SOS intensity X_t. This is described by a division rate $\beta(a, y, X) = \lambda y B(a, X)$, where λ is the elongation rate, supposed to be the same constant for all cells. Given x, $B(\cdot, x)$ is supposed to be the rate function (given by (2.15), for a density function f) of a Generalised Gamma distribution of parameters $(m_0, s(x), q(x))$. This means that under constant SOS expression $(X_t)_t \equiv x$,

$$\begin{cases} \log A_{div} = m_0 + \dfrac{s(x)}{q(x)} \log\left(q^2(x) R\right) \\ R \sim \mathrm{Gamma}(q^{-2}(x), 1) \\ s(x) = s_0 + s_1 x \ , \ q(x) = q_0 + q_1 x \end{cases}$$

The intercepts s_0 and q_0 are to be obtained from the control dataset. The unknown parameters $s_1 > 0$ and $q_1 \in \mathbb{R}$ measure the additional linear effect of the SOS level x on the dispersion of the distribution around m_0 (Fig. 2.16). We call $\eta_\beta := (s_1, q_1)$ the vector of these parameters.

3. **Offspring production.** When a cell of size y divides, it produces two daughters of sizes ρy and $(1-\rho)y$, only one of whom is followed. The value of ρ is generated by the probability kernel $k(y, \cdot)$ given by a mixture model of Beta distributions (2.19)-(2.20). The mixture depends on an unknown critical size y^* and a concentration parameter v, both depending only on the culture medium. We call $\eta_k = (y^*, v)$ the vector of these parameters.

The biological regulatory effects conveyed by this model are summarised in Fig. 2.19. The SOS level is supposed to be immediately autoregulated by the Ornstein-Uhlenbeck equation (2.12). The Generalised Gamma model chosen for the adder division rate imposes a non-trivial negative regulation (if $s_1 > 0$) consistent with SOS-induced division arrest, by increasing the tail of the distribution of added sizes. In turn, the division rate controls the size homeostasis in agreement with the adder model. In particular, in presence of filamentation, the birth size, which depends on the septum relative position, is controlled by the mother division size, as imposed by (2.19).

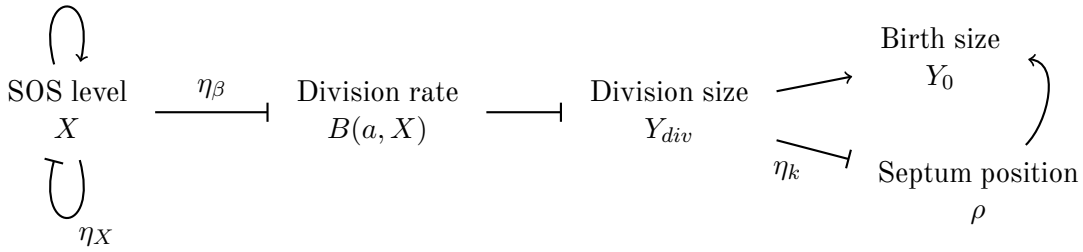

Figure 2.19: Summary of the regulatory effects of SOS induction on the adder mechanism proposed by our model. Arrows marked $\rightarrow$ represent positive regulation ($A \rightarrow B$ if B increases with A), while $\dashv$ represents negative regulation ($A \dashv B$ if B decreases as A increases). Over the arrows the concerned parameters of the model.

2.7 Parameter estimation of the coupled SOS-adder dynamics using cell lineages

As introduced in Section 2.3, we model our observations as a discrete sample of I independent realisations during time $t \in [0, T]$, with $T = N\Delta t$. This is, we consider a sample

$$\left(O^i_{n\Delta t}\right)^{i=1,\dots,I}_{n=0,\dots,N} = \left(A^i_{n\Delta t}, Y^i_{n\Delta t}, X^i_{n\Delta t}\right)^{i=1,\dots,I}_{n=0,\dots,N}$$

To model this discrete-time process we define first $p(a, y, x)$ as the probability to divide in the following Δt interval starting with state (a, y, x). Then, for all n we let U^i_n be a Bernoulli

random variable of parameter $p(A_n^i, Y_n^i, X_n^i)$, this is, which is equal to 1 if the lineage i divides in the interval $[n\Delta t, (n+1)\Delta t[$, and 0 otherwise. Since the intervals of time when a a division occurs are observed, U_n is also an observed variable, available from the mother machine data.

In general, $p(a, y, x)$ is given by

$$p(a,y,x) = \mathbb{E}_x\left[\int_0^{\Delta t} \beta(a + y(e^{\lambda t}-1), ye^{\lambda t}, X_t)\exp\left(-\int_0^t \beta(a+y(e^{\lambda s}-1), ye^{\lambda s}, X_s)\mathrm{d}s\right)\mathrm{d}t\right]$$

However, since Δt is small enough, we do the first-order approximation

$$p(a, y, x) \approx \beta(a, y, x)\Delta t.$$

Thus, given (A_0^i, Y_0^i, X_0^i) we can generate (A_n^i, Y_n^i, X_n^i) by the following hierarchical model (since they are i.i.d. samples, we forget the $i \in \{1, ..., I\}$ corresponding to each independent lineage):

$$\text{Draw independently } \begin{cases} U_n \sim & \text{Bernoulli}(p(A_n, Y_n, X_n)) \\ \rho_n \sim & k(Y_n e^{\lambda\Delta t}, \cdot) \\ W_n \sim & \mathcal{N}(0,1) \end{cases} \tag{2.21}$$

$$c_n = \mathbb{1}_{2<n\Delta t\leq 14} \tag{2.22}$$

$$X_{n+1} = X_n e^{-\theta_{c_n}\Delta t} + \mu_{c_n}\left(1 - e^{-\theta_{c_n}\Delta t}\right) + \zeta_{c_n}\sqrt{\frac{1-e^{-2\theta_{c_n}\Delta t}}{2\theta_{c_n}}}W_n \tag{2.23}$$

$$Y_{n+1} = U_n\rho_n Y_n e^{\lambda\Delta t} + (1-U_n)Y_n e^{\lambda\Delta t} \tag{2.24}$$

$$A_{n+1} = (1-U_n)(A_n + Y_{n+1} - Y_n) \tag{2.25}$$

Eq. (2.25) resets the added size at 0 at each division (i.e., when $U_n = 1$), and otherwise adds the increment of size $Y_{n+1} - Y_n$, with Y_{n+1} given by Eq. (2.24). When a division occurs the size is multiplied by the daughter-to-mother size ratio ρ_n distributed according the size-dependent probability kernel $k(y, \cdot)$ defined in (2.19). Eq. (2.23) corresponds to the explicit solution of the Ornstein-Uhlenbeck Equation (2.12).

2.7.1 Likelihood of the observations

Let $\eta = (\eta_X, \eta_\beta, \eta_k)$ the vector of parameters considered. From the previous set of equations, the likelihood of the observations under the considered parametric model is given by

$$\begin{aligned}\mathcal{L}((A_n^i, Y_n^i, X_n^i, U_n^i)|\eta) &:= \prod_{i\geq 1, n\geq 1} \mathbb{P}((A_n^i, Y_n^i, X_n^i, U_n^i), (A_{n+1}^i, Y_{n+1}^i, X_{n+1}^i, U_{n+1}^i)|\eta) \\ &= \prod_{i\geq 1, n\geq 1} \mathfrak{g}\left(X_{n+1}^i \middle| X_n e^{-\theta_{c_n}\Delta t} + \mu_{c_n}\left(1-e^{-\theta_{c_n}\Delta t}\right)\ ;\ \frac{\zeta_{c_n}^2(1-e^{-2\theta_{c_n}\Delta t})}{2\theta_{c_n}}\right) \\ &\quad \times k(Y_n^i e^{\lambda\Delta t}, Y_{n+1}^i|\eta)^{U_n^i} \\ &\quad \times \left(p(A_n^i, Y_n^i, X_n^i|\eta)\right)^{U_n^i}\left(1 - p(A_n^i, Y_n^i, X_n^i|\eta)\right)^{1-U_n^i}\end{aligned} \tag{2.26}$$

where $\mathfrak{g}(\cdot|\mu;\sigma^2)$ is the Gaussian probability distribution function of mean μ and variance σ^2 and k is given by Eq. (2.19), parameterised by y^* and c. The division probability p, which depends on β, is parameterised by v_1. In particular the contributions of the parameters related to k, to β, and to the Ornstein-Uhlenbeck are all independent. This is, the log-likelihood of the observations can be written as

$$\begin{aligned}\log \mathcal{L}((A_n^i, Y_n^i, X_n^i, U_n^i)|\eta) =& \ell_1((Y_n^i, U_n^i)|\eta_k) \\ &+ \ell_2((A_n^i, Y_n^i, X_n^i, U_n^i)|\eta_\beta) \\ &+ \ell_3((X_n^i)|\eta_X) \\ &+ \text{constant independent from } \eta\end{aligned}$$

where the log-likelihood of the septum position observations are given by

$$\ell_1((Y_n^i, U_n^i)|\eta_k) = \sum_{i=1}^{I} \sum_{M=1}^{+\infty} \sum_{\substack{n\in[\![0,N]\!]: \\ Y_{n-1}^i \le 2My^*, \\ Y_{n-1}^i > 2(M-1)y^*}} U_n^i \log\left(\sum_{m=1}^{M} \frac{1}{M} F_m^M\left(\frac{Y_n^i}{Y_{n-1}^i e^{\lambda\Delta t}}\middle| v\right)\right), \tag{2.27}$$

the log-likelihood of the division times observations is independently given by

$$\begin{aligned}\ell_2((A_n^i, Y_n^i, X_n^i, U_n^i)|\eta_\beta) = \sum_{i=1}^{I} \Bigg(&\sum_{n=1}^{N} U_n^i \log\left(\beta(A_n^i, Y_n^i, X_n^i|\eta_\beta)\Delta t\right) \\ &+ \sum_{n=1}^{N} (1-U_n^i)\log\left(1-\beta(A_n^i, Y_n^i, X_n^i|\eta_\beta)\Delta t\right)\Bigg)\end{aligned} \tag{2.28}$$

and the log-likelihood of the SOS dynamic observations is independently given by

$$\ell_3((X_n^i)|\eta_X) = \sum_{i=1}^{I}\sum_{n=0}^{N-1} \log\mathfrak{g}\left(X_{n+1}^i \middle| X_n e^{-\theta_{c_n}\Delta t} + \mu_{c_n}\left(1-e^{-\theta_{c_n}\Delta t}\right), \frac{\zeta_{c_n}^2(1-e^{-2\theta_{c_n}\Delta t})}{2\theta_{c_n}}\right) \tag{2.29}$$

We see that the likelihoods of the model can be computed explicitly, and we show below some first numerical results concerning their computation.

2.7.2 Estimation of SOS dynamics parameters η_X

One of the remarkable properties of the Ornstein-Uhlenbeck process is that the three parameters (θ, μ, ζ) possess explicit Maximum Likelihood Estimators (MLE) [64, 134]. Thus, using the data from the time interval $t \in]2, 14]$, in which the cells are under the effect of the antibiotic, we infer the values of of $(\theta_1, \mu_1, \zeta_1)$. Using the remaining time (pre and post exposure), we infer the values of $(\theta_0, \mu_0, \zeta_0)$. The results are summarised in Table 2.5. The estimated parameters show that the presence of ciprofloxacin produces a shift in the mean value μ of the SOS signal of 10-100 times the basal fluorescence (the values in the table are

in log-scale), without significantly varying the regulation parameter θ. This could represent that ciprofloxacin leads to an increased production of the fluorescent marker PsulA, without altering the average response rates of the SOS regulatory circuit of itself. This is, without affecting the turning off of the SOS response once the damage is repaired, for example. At the same time however, the noise of the SOS intensity, conveyed by ζ, is systematically superior under the effect of ciprofloxacin, which could indicate the presence of other perturbations. Nonetheless, the small variations of these parameters points towards a certain robustness of the SOS response facing the damage caused by ciprofloxacin. Concerning the variations under different media, we see that the SOS dynamic response is noisier under fast growing conditions, however it is more tightly controlled by larger values of θ. In particular, this means that the steady-state of SOS intensity is reached faster in fast growing media. On the other hand, the mean SOS expression seems relatively constant across the different media.

Medium	**SOS diffusion parameters**					
	θ_c		μ_c		ζ_c^2	
	Cip$-$ ($c=0$)	Cip$+$ ($c=1$)	Cip$-$	Cip$+$	Cip$-$	Cip$+$
gly	0.217	0.233	4.57	6.01	0.0702	0.103
glu	0.319	0.223	4.60	6.12	0.1074	0.117
gluaa	0.423	0.351	4.53	5.46	0.1439	0.161

Table 2.5: Maximum Likelihood Estimators of the parameters driving the Ornstein-Uhlenbeck Equation (2.12) for the three differente media, and under the presence or not of ciprofloxacin.

2.7.3 Estimated parameters for the division: adder rate (η_β) and septum positioning (η_k)

Contrary to the Ornstein-Uhlenbeck process, the likelihoods ℓ_1 and ℓ_2 do not allow to obtain the MLE in close forms. However, ℓ_1 and ℓ_2 are both numerically tractable and our computations show that they are convex (see Fig. 2.20), so that the numerical maximisation can be done by classical approaches.

Fig. 2.20A gives the value of ℓ_1 as functions of y^* and v. We see that the log-likelihood has convex contour levels, and a unique global maximum. The MLE of y^* and v are tabulated in Table 2.6. The MLE of y^* is approximately given by the mean division size observed in the control dataset (3.25 μm in *gly*, 3.53 μmm in *glu*, and 4.89 μm in *gluaa*). This comforts the interpretation of y^* as a characteristic length. The smallest concentration parameter v is estimated in the the richest medium, *gluaa*. This confirms the trend observed in the control dataset (Fig. 2.7), where the septum position seemed to be less precise in fast growing media.

Similarly, we can compute the value of ℓ_2 (2.28). Fig. 2.20B shows the log-likelihood as function of the SOS-induced linear factors s_1 and q_1 multiplying the dispersion parameters of the Generalised Gamma model (2). The intercepts s_0 and q_0 were inferred as the MLE of a Generalised Gamma fitted directly to the added size distributions of the 10% of cells

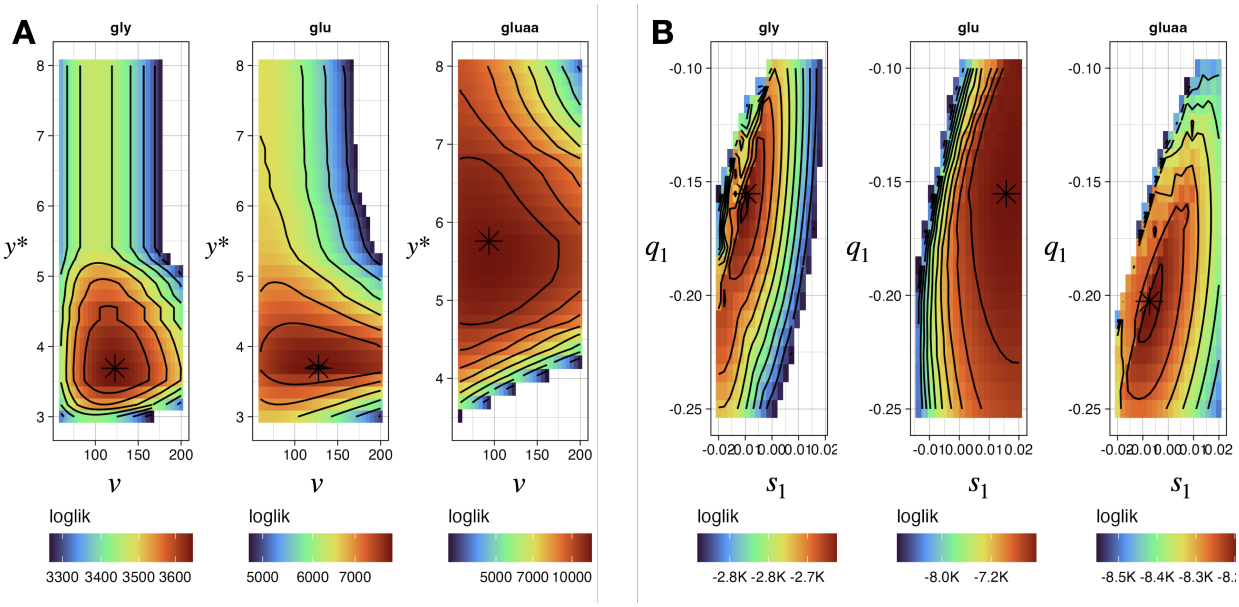

Figure 2.20: Log-likelihoods of the parameters of the SOS perturbed adder model. The MLE are marked $*$. **A.** Log-likelihood ℓ_1 (2.27) of the division size observations as function of the critical mother length y^* and the concentration parameter v of the Beta mixture (2.19)-(2.20). **B.** Log-likelihood ℓ_2 (2.28) of the added sizes at division as function of s_1 and q_1.

Medium	**Division parameters**					
	Adder rate β				Septum kernel k	
	s_0†	s_1	q_0†	q_1	y^* (μm)	v
gly	0.4207	-0.009473	0.7832	-0.1552	3.6896	122.758
glu	0.3019	0.01579	0.5559	-0.1552	3.6896	127.586
gluaa	0.6626	-0.007368	0.6963	-0.2026	5.7586	93.7931

Table 2.6: Maximum Likelihood Estimators of the parameters driving division (the adder division rate B and the mother-to-daughter ratio kernel k) for the three differente media. Parameters marked by † are inferred by fitting a Generalised Gamma distribution directly to the added size distributions of the first SOS decile of control cells.

with lowest SOS signal at division of the control dataset. The numerical computations show that ℓ_2 also has convex contours and a unique global maximum. All the inferred parameters are tabulated in Table 2.6. In all three media the multiplicative noise effect conveyed by s_1 is much less significant than the shape change effect conveyed by q_1. Moreover, q_1 increases with the richness of the medium. This confirms that the perturbative effect of the SOS response on the adder control is stronger in fast growing conditions, supporting the experimental observations of Fig. 2.12.

To see more clearly the effects of s_1 and q_1 in the division dynamics we calculate the division rates $B(\cdot, x)$ predicted by the MLE for different values of x in all three media, presented in Fig. 2.21. First, the expected result that the division rate is lower in richer media, as found previously in Fig. 2.6, holds still. There is, however, a notorious effect of the SOS level. In all three media, increasing the SOS level leads to lower division rates, perfectly compatible to the fact that the SOS response induces the delay of division. Relatively to each medium, the strength of this inhibition seems to be stronger in poorer media, where the division rates in absence of stress are generally stronger. In other words, it seems that the adder size control is more sensible to stress in poorer conditions. This comforts the results of [82], that the fraction of cells with high SOS level is larger in slow growth conditions. Not only the value of the division rate is changed, but also its shape. At low SOS level, in all three media, the most likely division rate is a increasing function. Indeed, the intercept parameters s_0 and q_0 (see Table 2.6) are all three in the "increasing" region of the parameter space represented in Fig. 2.17. At first glance, this seems to contradict the selection of a lognormal distribution in Section 2.4, and the decreasing division rate for longer cells found by Osella et al. [117]. However, as x increases the division rate changes its shape, and tends in all three media towards an arc-shaped "lognormal-like" distribution, similarly to the path A followed at the right panel of Fig. 2.17. The apparent contradiction emerges from the fact that, both our first analysis and Osella's et al., measure the division rate as function solely of the added size (the absolute size in Osella's et al.). Yet, by doing so, we are implicitly marginalising over all the unknown individual variables that might have an effect. This is similar to the problem of *random effects* in the Mixed Effect Models literature [97]. Indeed, if starting from $B(a, x)$ we wanted to obtain a *real adder* division rate $\bar{B}(a)$, function of a only, we can compute, from (2.15),

$$\bar{B}(a) = \frac{\mathrm{d}}{\mathrm{d}a}\left(-\log \bar{S}(a)\right),$$

where $\bar{S}$ is the *population survival function* given by

$$\bar{S}(a) = \mathbb{P}\left(A_{div} \geq a\right) = \mathbb{E}\left[\exp\left(-\int_0^a B(a, X_{\tau(a)})\right)\mathrm{d}a\right],$$

where the expectation is taken over the Ornstein-Uhlenbeck process X and $\tau(a) = \lambda^{-1}\log(1+y_0^{-1}a)$ is the time needed to reach an added size a given the birth size y_0. Hence, under suitable integrability assumptions for $\bar{S}$ we can differentiate under the expectation sign and

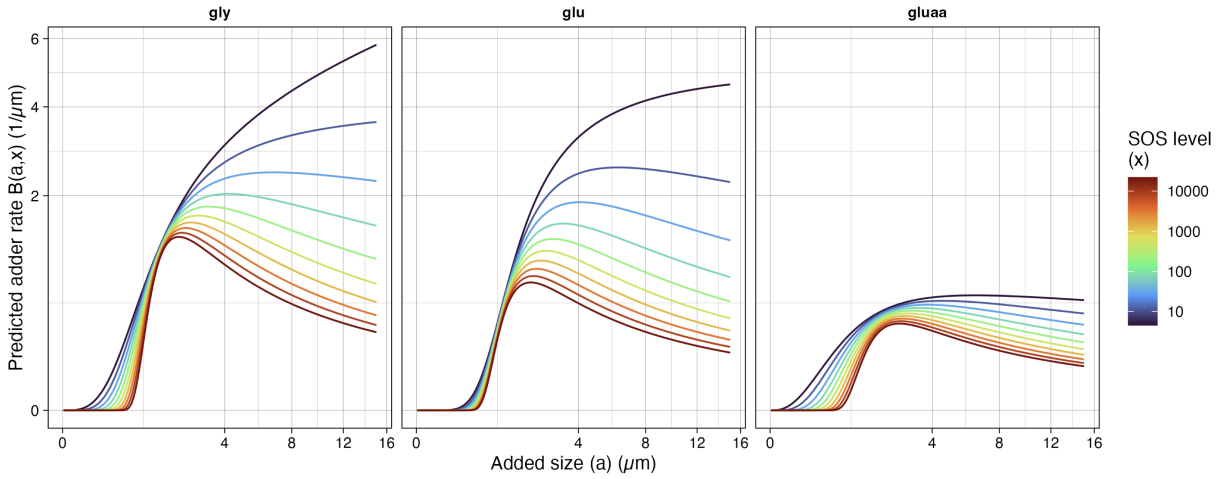

Figure 2.21: Predicted adder division rate $B(a, X)$ by MLE.

then

$$\bar{B}(a) = \frac{\mathbb{E}\left[B(a, X_{\tau(a)})e^{-\int_0^a B(s,X_{\tau(s)})\mathrm{d}s}\right]}{\mathbb{E}\left[-\int_0^a B(s, X_{\tau(s)})\mathrm{d}s\right]} = \mathbb{E}\left[B(a, X_{\tau(a)})\middle| A_{div} \geq a\right] \neq \mathbb{E}\left[B(a, X_{\tau(a)})\right]. \tag{2.30}$$

This relation puts in evidence a bias on $\bar{B}(a)$. Only the individuals that have yet not divided at added size a contribute to the value of $\bar{B}(a)$. Therefore, if only cells with very high SOS intensity x survive until longer added sizes, and the conditional division rate $B(a, x)$ is lower for high x, then the marginal rate $\bar{B}(a)$ will be lower for larger a, producing an "effective catastrophe" region in $\bar{B}$, even if $B(a, x)$ were not decreasing themselves. In our case, if the stress is low enough, division rates are monotonically increasing (as one naively might expect for a homeostatic system: the more size that has been added, the more likely should the cell divide). And, if the stress is high enough they tend towards a characteristic arc-shaped division rate. In other words, our findings suggest that it is the stressed bacteria that might inadvertently produce an apparent depression of the division rate when measuring it with population-level statistics.

2.8 Simulation results with the fitted parameters

Finally, using the MLE of η, we simulated single-cell lineages that we compared to the MM original data. The results of the simulations of $I = 10^4$ independent lineages are given in Fig. 2.23.

Concerning the SOS dynamics, the predictions of Eq. (2.12) using the parameters η_X given by Table 2.5 are shown in Fig. 2.22. Panel A of the figure shows the predicted mean SOS intensity in time (dashed line) and compares it to the empirical mean (solid line). We see an excellent qualitative agreement between the two curves. We notice however a systematic shift of the prediction towards the right. This could represent a delay in the SOS

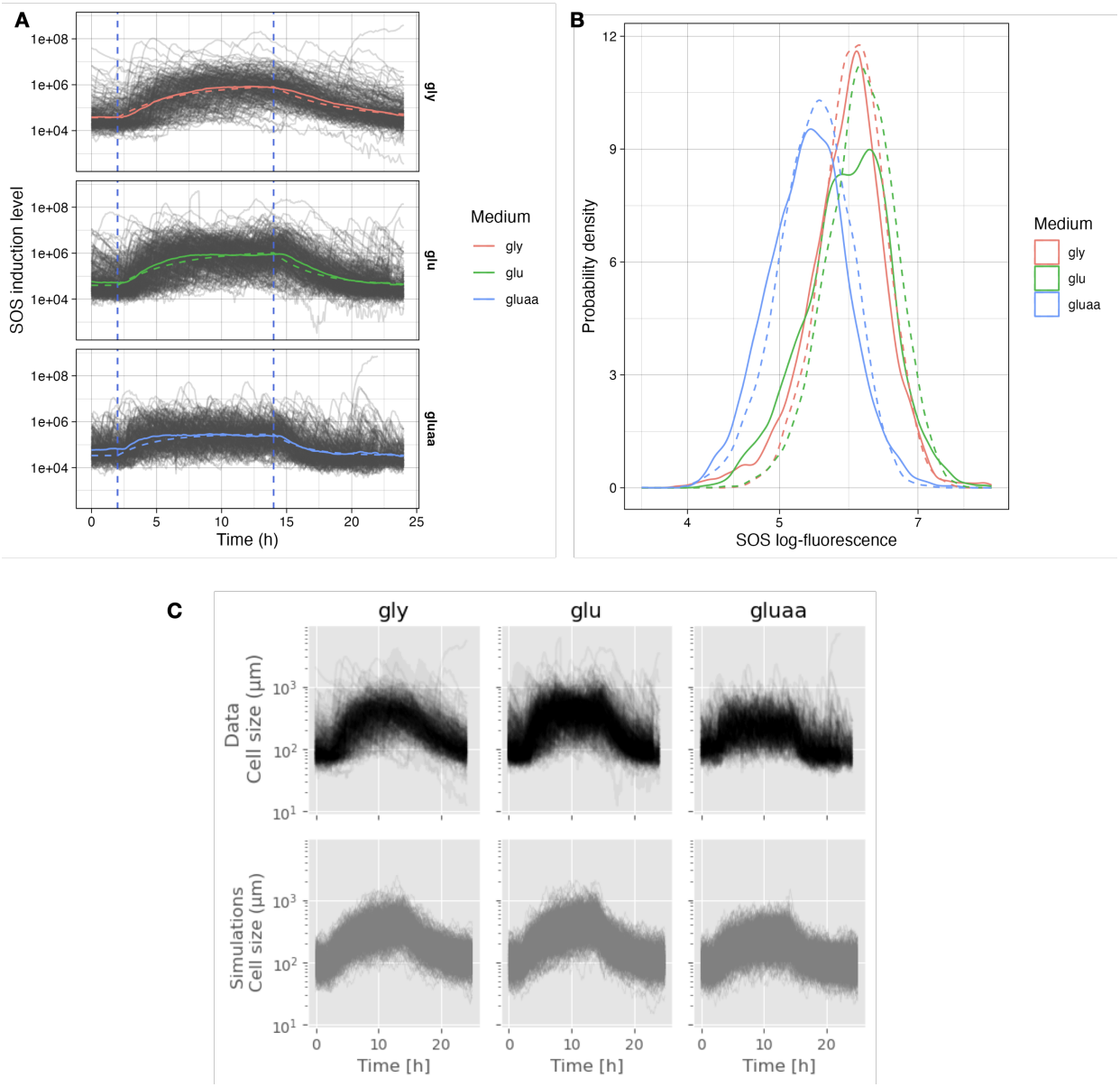

Figure 2.22: Fitting results of the SOS dynamics using the Ornstein-Uhlenbeck model (2.12)**: dynamic and stationary. A.** In solid lines, empirical mean of the SOS intensity calculated from the grey trajectories in the background. Only lineages with observed divisions were retained. In dashed lines, the mean SOS intensity predicted by Eq. (2.12) using the parameters summarised in Table 2.5. **B.** In solid lines, empirical steady-state distribution of the SOS intensity under ciprofloxacin, obtained from the data observed between $t = 10$ and $t = 14$ (last 4 hours of cip treatment, 8 hours after initial dose). In dashed lines, stationary distribution expected from the Eq. (2.12) using the parameters summarised in Table 2.5. **C.** Comparison of the empirical fluorescennse observations (first row) and the simulated trajectories of (2.12) using the MLE.

response that is not captured by the Ornstein-Uhlenbeck process, which models a rather instantaneous regulation. However, these fast regulation dynamics seem to recover well the dynamic transition at times $t = 2$ and $t = 14$. In particular, the Ornstein-Uhlenbeck model recovers very accurately the shape of the inflexion observed at this regime change. We see also that, as already discussed above and as is shown by the values of θ in Table 2.5, the steady-state is reached faster in fast-growing media.

Panel B of Fig. 2.22 shows the empirical (solid line) and predicted (dashed line) steady-state distributions of SOS intensity under the effect of ciprofloxacin. Indeed, the Ornstein-Uhlenbeck process (2.12) is stationary, and its stationary distribution is explicit: a Gaussian of mean μ and variance $\zeta^2/(2\theta)$. We see also an excellent qualitative agreement in the steady-state distribution, particularly around the mean value, except for glucose medium, whose distribution is wider than the predicted Gaussian. In general, the observed distributions are more skewed to the left. This can be explained by the fact that the Ornstein-Uhlnebeck process imposes a symmetrical noise around the mean value, while the observations show that cells, even under ciprofloxacin, tend to concentrate below the expected value. At the same time, but more rarely, some lineages can induce very strongly the SOS response, which also widen the distribution towards the right.

Concerning the division dynamics, Fig. 2.23A shows that the asymmetric division statistics are well recovered by our Beta mixture model. Although the transition boundaries determined by y^* are less marked in the empirical observations, suggesting some non captured individual heterogeneity. Finally, Fig. 2.23B-D shows the joint distributions of size and SOS response averaged in time. The bulk of the distribution seems well recovered, particularly during the presumed stationary reached after 12 hours of antibiotic treatment (Panel D). However, some rare events associated to *excessive* filamentation seem not be captured by the model. This also might indicate the presence of individual heterogeneity in the parameters of the division rate, that cannot be explained only by the SOS measurements.

2.9 Concluding remarks

2.9.1 Some perspectives

We have proposed a parametric model of the perturbative effects of ciprofloxacin-induced SOS response over the adder model of size control in *E. coli*. Our findings coincide with the previous observations that the adder model is robust to various growth inhibitions [129]. In contrast, we have found that the SOS response, which is known to have multifactorial physiological effects, induces a loss of size control, translated in broader distributions of the added size at division, while keeping the median relatively constant. In terms of the division rate, we have shown, using a parametric Generalised Gamma model, that the adder division rate function B is reduced by the SOS response in a medium-dependent way. In particular, the previously observed *catastrophe* or decreasing regions in the division rate can be explained quantitatively by the contribution of high SOS individuals in division arrest. We have seen however that the experimental heterogeneity of the joint SOS and size distributions is still more important than our model predicts. In this sense, one interest-

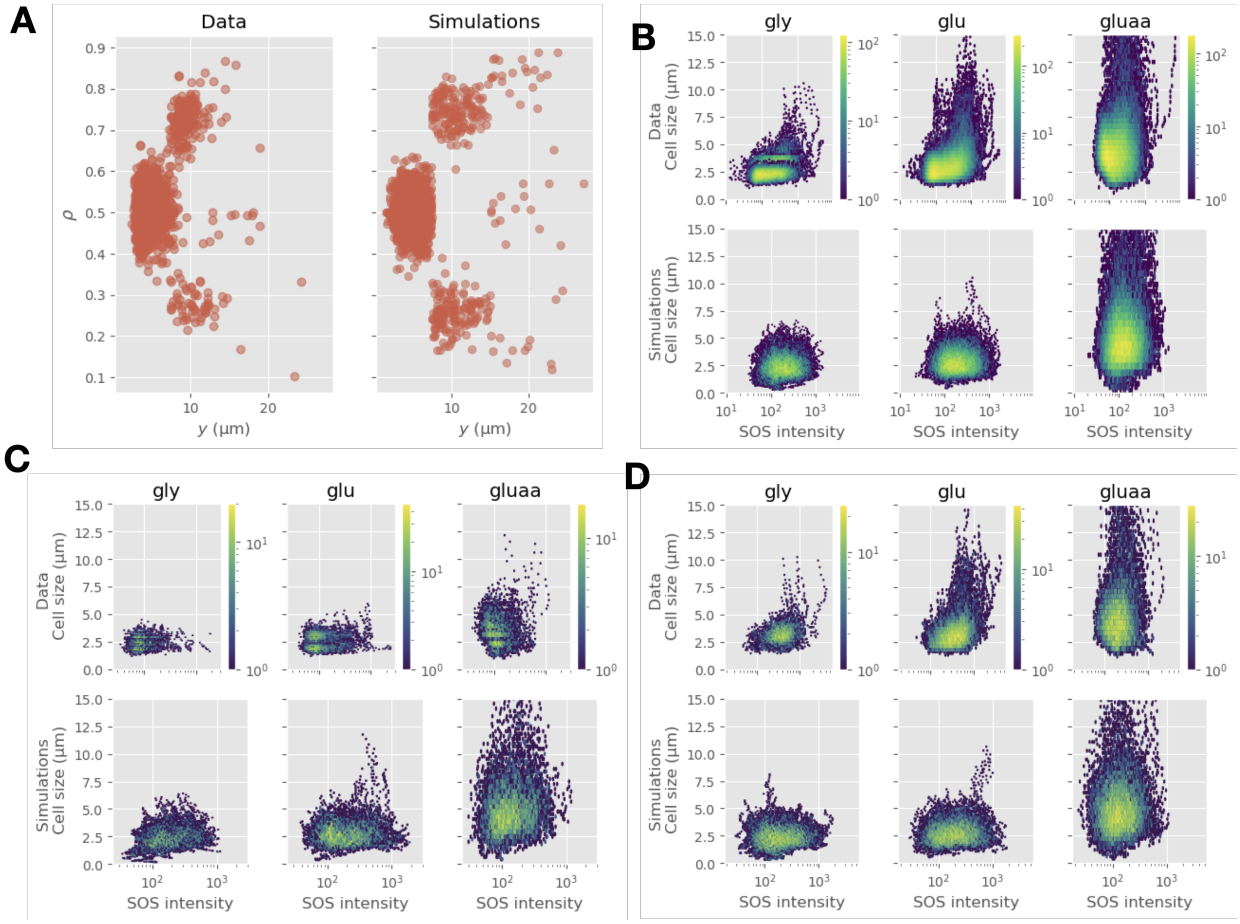

Figure 2.23: **A.** Data and simulations of $\rho \sim k(\cdot|y)$ (septum position given the mother size) for $I = 100$ independent lineages and the MLE as parameters (glucose+aa medium, where a larger number of possible septa can be observed). **B-D.** Data and simulations of the joint distributions of the SOS level at division and the division size. **B** is the time average over the whole experiment, **C** is during the first 2 hours, and **D** during the last 4 hours of cip exposure ($10 \leq t < 14$).

ing axis of future work might be the extension of our model to include *mixed effects* [97], this is, to allow individual heterogeneity in the parameters of the probability distributions of the model. For instance, this could enable having a Generalised Gamma model at the population level (the *fixed effects*) consistent with the idea that the adder is robust *in average*, but with some parameters that can have some variability among the individuals (the *random effects*). Further, this could also enable to statistically test the heterogeneity of the population. Mixed Effects Models are extensively used to model individual-based responses in pharmacokinetics, for example, where the evolution of the drug in time is driven by a deterministic ODE. The extensions required to adapt the method to a stochastic diffusion process, as our Ornstein-Uhlenbeck model, which is moreover coupled to the also stochastic process of cell division, are not trivial, see for example [41].

Chapter 3

V-uniform ergodicity of a general adder proliferation model

This chapter is based on the article "Exponential Ergodicity of a Degenerate Age-Size Piecewise Deterministic Process", published in *Acta Applicandae Mathematicae* [103].

Abstract. We study the long-time behaviour of a non conservative piecewise deterministic measure-valued Markov process modelling the proliferation of an age-and-size structured population, which generalises the "adder" model of bacterial growth. Firstly, we prove the existence of eigenelements of the associated infinitesimal generator, which are used to bring ourselves back to the study of a conservative Markov process using a Doob h-transform. Finally, we obtain the exponential ergodicity of the process via drift-minorisation arguments. Specifically, we show the "petiteness" of the compact sets of the state space. This permits to circumvent the difficulties encountered when trying to construct mixing trajectories at a fixed uniform time on an unbounded two-dimensional space with only advection and degenerate jump terms.

3.1 Introduction

The need to include age as a structuring variable in the description of population dynamics has come to be a useful strategy for modellers searching to account for non-Markovian behaviours in a Markovian setting. In particular, in the context of biological applications, the arising of high-throughput single-cell techniques has allowed microbiologists to follow heterogenous populations of isolated bacteria (where the structure is given by their length, biological markers or any other observable) through time. Thereby, this also grants access to the age structure and has put in evidence the non-trivial dependence of age and other observables at the individual and population scales. The most recent models of bacterial

growing include then some sort of age variable, which might not correspond exactly with the *chronological age*, but which might rather evolve in time as a function of the individual traits. For example, in the *adder model* of bacterial growth discussed in Example 3.1.1 below, the *age* corresponds to the length added from the birth of the individual, so it grows along with the size variable, but resets at 0 at each reproduction event. This *age* variable still obeys a renewal equation, which justifies nonetheless its name. In this regard, an important biological and mathematical question concerns the long-time behaviour of such dynamics: whether a certain steady-state distribution exists and the convergence rate towards it. Biologically, it allows to explain the observation of homeostatic behaviours in experimental timescales. Mathematically, it corresponds to the non trivial task of extending classical stability results to a broader class of stochastic models, by studying the spectral and ergodic properties of a certain family of operators.

In this spirit, we study the long-time behaviour of a stochastic process modelling non-conservative population dynamics which are formalised as a measure-valued process $(Z_t)_{t\geq 0}$ with values in the point measures over $\mathbb{R}_+^2$, $\mathcal{M}_p(\mathbb{R}_+^2)$, which represents the age and size of the individuals. For every instant $t > 0$ we can write

$$Z_t = \sum_{i \leq \langle Z_t, 1\rangle} \delta_{\mathbf{x}_i}, \tag{3.1}$$

where $\mathbf{x}_i = (a_i, y_i)$ denotes the vector trait of individual i, consisting in its age a_i and size y_i. We assume that each cell in the population behaves independently. The population then evolves in the continuous time through two fundamental dynamics: growth and division. Whilst growth is assumed to be deterministic, the division mechanism will account for the observed stochasticity. We present below informally the main characteristics of these two ingredients, which are formalised in Section 3.3:

- **Growth and ageing:** Between reproduction events, the variable $\mathbf{x}$ evolves following the deterministic ODE
$$\mathbf{x}'(t) = g(\mathbf{x}(t)).$$
The function $g : \mathbb{R}_+^2 \to \mathbb{R}_+^2$ represents the growth rate of the size and age coordinates. We denote $\mathbf{x} \mapsto \varphi^t(\mathbf{x})$ the deterministic flow induced by the ODE with initial condition $\mathbf{x}$ (see Lemma 3.3.1 for the details), this is, the age and size at time t of an individual of age and size $\mathbf{x}$ at time 0. For example, if a coincides with the chronological age, and y grows exponentially at rate λ, we will have $g(a, y) = (1, \lambda y)$ and $\varphi^t(a, y) = (a + t, ye^{\lambda t})$. More interestingly, age and size can evolve in a dependent way. It is the case in Example 3.1.1 discussed further below: the *adder model* of bacterial growth. There, the age corresponds to the size added since the last division, so that age and size grow at the same rate. Therefore, if y grows exponentially at rate λ, we have $g(a, y) = (\lambda y, \lambda y)$ and $\varphi^t(a, y) = (a + ye^{\lambda t} - y, ye^{\lambda t})$.

- **Reproduction:** Individuals divide independently. An individual of birth state $\mathbf{x} = (a_0, y_0)$ at time t_0 will reproduce at a random time $t_0 + T$, where T is distributed

according to

$$\mathbb{P}_{\mathbf{x}}\left(T \geq t\right) = \exp\left(-\int_0^t \beta(\varphi^s(\mathbf{x}))ds\right).$$

The function $\beta : \mathbb{R}_+^2 \to \mathbb{R}_+$ is called the reproduction rate. The value of $\beta(a, y)$ gives the infinitesimal probability by unit of time for an individual of age a and size y to reproduce. Then, when an individual of state $\mathbf{x}$ reproduces, it gives birth to new individuals of age 0 and random size Z, that depends on the value of $\mathbf{x}$. The probability distribution of Z conditional to $\mathbf{x}$ is characterised by the transition kernel $k : \mathbb{R}_+^2 \to \mathbb{R}_+$, which is a positive integrable function. Thus, the number of new individuals of size z produced by an individual of state $\mathbf{x}$ is proportional to $k(\mathbf{x}, z)dz$. In particular, the value of the integral $\int_0^{+\infty} k(\mathbf{x}, z)dz$ gives the total offspring produced by that individual. The age variable, on the other hand, resets at 0 at each jump. This means that the transition kernel over $\mathbb{R}_+^2$ is degenerate, of the form $\mathbf{x} \mapsto \delta_0(da) \otimes k(\mathbf{x}, z)dz$.

Following the approach introduced by [57, 140], by using a pathwise representation of Z_t with respect to a Poisson point measure, we can prove that for every $f \in C_b^{1,1}(\mathbb{R}_+^2)$, Z_t decomposes as a semi-martingale of the form

$$\langle Z_t, f\rangle \stackrel{\text{def}}{=} \int_{\mathbb{R}_+^2} f(\mathbf{x})Z_t(d\mathbf{x}) = \langle Z_0, f\rangle + \int_0^t \langle Z_s, \mathcal{Q}f\rangle\, ds + \mathscr{M}_t^f, \tag{3.2}$$

where $\mathscr{M}_t^f$ is a squared-integrable martingale, and $\mathcal{Q}$ is given for every $f \in C_b^{1,1}(\mathbb{R}_+^2)$ by

$$\mathcal{Q}f(\mathbf{x}) = g(\mathbf{x})^\top \nabla f(\mathbf{x}) + \beta(\mathbf{x})\left(\int_0^\infty f(0, z)k(\mathbf{x}, z)dz - f(\mathbf{x})\right) \quad \forall \mathbf{x} \in \mathbb{R}_+^2 \tag{3.3}$$

In the following, we consider the extended version of the generator $\mathcal{Q}$ (see for example Section 20.3.2 of [112]), associated to a domain $D(\mathcal{Q})$ in which the integral term is well defined. We recall that a function f is said to be in the domain of the extended generator of $\mathcal{Q}$ if there exists a measurable function u such that

$$\left(\langle Z_t, f\rangle - \langle Z_0, f\rangle - \int_0^t \langle Z_s, u\rangle\, ds\right)_t$$

is a local martingale. In that case we will write $\mathcal{Q}f = u$. This is a natural definition since our starting point is the decomposition (A.48).

Example 3.1.1 (The adder model)**.** In the particular case of the bacterial proliferation model that interests us, and that will be studied in Section 3.6, we consider the dynamics of an age-size-structured population of *E. coli* bacteria as a measure-valued process with values in $\mathcal{M}_p(\mathcal{X})$, the point measures over the state space $\mathcal{X} = \{(a, y) \in \mathbb{R}_+^2 : 0 < a < y, y > 0\}$, where a represents the added size and y the current size of each cell. This is, the age of a cell is given by the difference between its current size and its initial size. Therefore, the variable a is not a chronological age, and has actually

length units. However, it is indeed a variable that increases with time and is reset to zero after reproduction events. The importance of considering the added size as a structural variable to accurately model the growing dynamics of *E. coli* has been strongly suggested in the recent years by experimental works and statistical analysis in unperturbed conditions [133, 44], but also in the case where the growth is perturbed by anti-DNA antibiotics (unpublished work by J. Broughton, M. El Karoui, S. Méléard and the author). The dynamics are driven by the generator

$$\begin{aligned}\mathcal{Q}f(a,y) =& \lambda y\left(\partial_a + \partial_y\right) f(a,y) \\ &+ \lambda y B(a)\left(2\int_0^1 f(0,\rho y)F(\rho)d\rho - f(a,y)\right) - d_0 f(a,y). \end{aligned} \tag{3.4}$$

In our previous notation this translates as $g(a,y) = (\lambda y, \lambda y)$, $\beta(a,y) = \lambda y B(a)$, and $k((a,y),z) = 2\frac{1}{y}F\left(\frac{z}{y}\right)\mathbb{1}_{z\leq y}$, where F has support in $[0,1]$. The growth dynamics correspond to an exponential elongation at constant rate $\lambda > 0$. The second term in $\mathcal{Q}$ represents the divisions, which occur at rate $\lambda y B(a)$ where B is a hazard function such that for every individual,

$$\mathbb{P}\left(\text{Added size at division} \geq a\right) = \exp\left(-\int_0^a B(s)ds\right).$$

Hence, the jump term reads as follows: a cell of size y and added size a divides at rate $\lambda y B(a)$, and is replaced by two cells of added size 0 and sizes ρy and $(1-\rho)y$ respectively, where ρ is randomly distributed following the density F. The third term represents deaths at a constant rate $d_0 > 0$.

In the following we will study the much general model generated by (4.19).

Our goal is to obtain the long-time behaviour of the first-moment semigroup $M_t f(\mathbf{x}) := \mathbb{E}\left[\delta_{\mathbf{x}}\right]\langle Z_t, f\rangle$, which describes the expected behaviour of the population. In particular, we prove a **Malthusian behaviour**:

$$M_t f(\mathbf{x}) = h(\mathbf{x})e^{\lambda t}\langle \pi, f\rangle + O\left(e^{(\lambda-\omega)t}\right), \tag{3.5}$$

which shows the convergence of $e^{-\lambda t}M_t$ towards a unique stationary measure π at an exponential rate. The parameter $\lambda > 0$ is called the Malthus parameter and represents the growth rate of the population, so that $e^{-\lambda t}$ allows to rescale the mean population size as $t \to +\infty$. The function h propagates the effect of the initial structure of the population. The constant ω indicates the convergence rate towards π.

Different methods have been developed during the recent years to prove this behaviour: spectral methods, as reviewed in [114] (see for example [122] for an application to a close model); others based on the study of the associated semigroup by Harris' theorem as proposed in some general frameworks by [10, 31, 11] with recent applications in the models considered by [20, 138, 35]. We will follow the latter methods, using the criteria established by Meyn and Tweedie [111], namely: a petite-set condition (H1) and the existence of a Lyapunov function (H2), as given in Theorem 3.2.1. This methods present an alternative

to PDE techniques, where criteria based on the probabilistic control of moments replace the harder to obtain Poincaré-type inequalities.

We explore two directions left open in the previous applications, which represent also the sources of our major technical issues: first, the bi-dimensionality of the dynamics, and second, the degeneracy of the transition kernel. Indeed, the underlying stochastic process consists on unidimensional trajectories over a two-dimensional space. Hence, to uniformly bound in probability the region explored by these trajectories with respect to a non-degenerate measure is not trivial. Similar difficulties have been found for other two-dimensional models such as [56, 139, 36]. Here, we propose to construct explicit trajectories and to average them in time with respect to a nice sampling measure. The inclusion of time sampling allows to compensate the lack of stochasticity of the degenerate jump-transport dynamics on an unbounded state space. Indeed, it is not trivial to find a fixed time $t_0 > 0$ such that the trajectories originated from any initial state mix uniformly on the support of some non-trivial measure of the unbounded two-dimensional space $\mathcal{X}$. However, if we authorise the time t_0 to be sampled from some probability distribution, chances are the uniform exploration of the space will be easier to prove, as we show indeed later. More technically, the utilisation of a petite-set condition instead of a small-sets one is key to obtain the convergence in this setting.

Moreover, compared to the previous works mentioned above, the probabilistic framework brings naturally to work with the operator $\mathcal{Q}$ instead of its dual, as in the more classical PDE settings. Thus, this work lies also in the framework of measure solutions as rigorously developed for example in [61] for the one-dimensional conservative case. Moreover, only the existence of eigenelements for $\mathcal{Q}$ is needed to be able to compute the Doob h-transform and use Harris' theorem. Then, the existence of the *direct* eigenfunction associated to the classical PDE is a consequence of our main result. Our method is then in the spirit of [31], where the authors could exploit known results of existence of the dual eigenelements in the one-dimensional case provided by [9, 43]. In our case, we will have to adapt the latter to the two-dimensional degenerate case studied here.

In particular, we will apply our method to determine the exponential convergence towards a stable size distribution in a bacterial proliferation model called the *adder* model [133, 100, 70, 62]. Individual cells are structured by their added size a which renews to 0 at each division, and their size y which evolves deterministically at exponential rate. The existence of a steady-state distribution and its form was already known since [70], however the exponential convergence could not be obtained using entropy methods by [62]. Since the eigenelements of the generator are known in this case, by the direct application of Theorem 3.2.1, our method permits to obtain the exponential convergence while evading technical issues linked to the lack of compactness of the model, which make a classic treatment by PDE and hypocoercivity methods harder to prove and less general.

Finally, it is worth noticing that other models share similar dynamics with the ones generated by (4.19). In an unrelated context, but fairly similar setting, Piecewise Deterministic Markov Processes (PDMP) have been recently used to sample target distributions in the framework of Markov Chain Monte Carlo (MCMC) methods, as described for example in [52]. There, an important task is to show good convergence rates of the MC-PDMP towards the target stationary distribution. Methods relying on drift-minorisation conditions,

similar to conditions (H1) and (H2) of Theorem 3.2.1, have been proven useful in that context [16, 38, 60], where issues related to dimensionality and degeneracy might also be encountered. Notice however that the processes considered in all these contexts are always conservative.

Other biological models can also be generated by similar semigroups, so their spectral and ergodic properties might be deduced from our results. For example, the non-trivial uniform bound estimate for the population growth rate established in Step 5 of the Proof of Proposition 3.4.1 relies mainly in the assumption that the newborn sizes are almost surely smaller than the parent size, without any additional requirements for the form of the kernel k. In particular, we do not require conservation of mass $y = \int k((a,y),z)dz$, as in classical size-structured models [43]. Therefore, the same arguments can be used in general age-trait models that authorise only negative jumps for the trait coordinate. Biologically, this could account for a trait evolving deterministically, and which is almost surely eroded or corrupted at each reproduction event. This is the case, for example, in some telomere-shortening models [22]. In particular, Assumptions 3.6.1 give necessary conditions such that the growth rate g compensates the *fragmentation* events arriving at each reproduction, in order to preserve ergodicity.

3.2 Malthusian behaviour

We are interested in the average dynamics as given by first-moment semigroup M_t defined for every test function $f \in \mathcal{C}_b^{1,1}(\mathbb{R}_+^2)$ by:

$$M_t f(\mathbf{x}) := \mathbb{E}\left[\langle Z_t, f\rangle \,|Z_0 = \delta_{\mathbf{x}}\right] \quad \forall \mathbf{x} \in \mathbb{R}_+^2 \tag{3.6}$$

Using Markov's property it's easy to see that M_t verifies the semigroup property. However it is not a Markovian semigroup since it does not necessarily preserve mass (we say it is non conservative). Moreover, using the semi-martingale decomposition (A.48), we verify that M_t is the semigroup associated to the extended generator $\mathcal{Q}$. This is, for every test function $f \in C^{1,1}(\mathcal{X})$, it is the weak solution of Kolmogorov's equations

$$\partial_t M_t f = M_t \mathcal{Q} f = \mathcal{Q} M_t f. \tag{3.7}$$

Moreover, for any finite measure μ we define the dual semigroup as the measure νM_t given by:

$$(\nu M_t) f := \nu(M_t f) = \int_{\mathcal{X}} M_t f(\mathbf{x}) \nu(d\mathbf{x})$$

So by definition we have $(\mu M_t) f = \mu(M_t f)$ which we write as $\mu M_t f$.

Our main result states the Malthusian behaviour of the semigroup by means of Harris' Ergodic Theorem as stated in Theorem 6.1 of [111], which we recall below in Theorem 3.2.1.

Theorem 3.2.1 (V-uniform Ergodic Theorem (also known as Harris' Ergodic Theorem) (Theorem 6.1 of [111])). *Let $(X_t)_t$ be a right-continuous Markov process with values in*

some locally compact separable metric space E equipped with its Borelian set $\mathcal{B}(E)$, and let $\mathcal{A}$ be the infinitesimal generator of X. We call P_t the associated transition semigroup. If the two following conditions are verified:

(H1) ***Minorisation condition for compact sets.***

All compact sets of E are petite for a skeleton chain of X. This is, for every compact set $\mathscr{K} \subset E$ there's a probability mass distribution $\mu = (\mu_n)_{n\in\mathbb{N}}$ over $\mathbb{N}$ and some $\Delta > 0$ such that there exists a non-trivial measure ν (which might depend on Δ and μ) over $\mathcal{B}(E)$ that for every $\mathbf{x} \in \mathscr{K}$ gives the following lower bound:

$$\langle \mu, \delta_{\mathbf{x}} P_{\cdot} f\rangle = \sum_{n\in\mathbb{N}} \mu_n P_{n\Delta} f(\mathbf{x}) \geq \langle \nu, f\rangle .$$

(H2) ***Foster-Lyapunov drift condition.***

There exists a coercive function V, meaning that $V(\mathbf{x}) \to +\infty$ as $||\mathbf{x}|| \to +\infty$, such that $V(\mathbf{x}) \geq 1$ for all $\mathbf{x}$, and there exist some $c > 0$, $d < \infty$ such that

$$\mathcal{A}V(\mathbf{x}) \leq -cV(\mathbf{x}) + d \quad \forall \mathbf{x} \in E,$$

Then, there exist a unique non-trivial probability measure π and $C, \omega > 0$ such that for every $\mathbf{x} \in E$ and $t \geq 0$

$$||\delta_{\mathbf{x}} P_t - \pi||_V \leq CV(\mathbf{x}) \exp(-\omega t), \tag{3.8}$$

where the V-norm defined by

$$||\mu||_V := \sup_{g:||g||\leq V} |\langle \mu, g\rangle|$$

is an extension of the total variation norm. In particular $||\mu||_1 = ||\mu||_{TV}$.

Remark 3.2.2. The reader familiar with other versions of V-uniform ergodicity theorems, such as Theorem 20.3.2 of [112], the results of [48], or more the more recently derived version of [69] might find that conditions (H1) and (H2) are written in a slightly exotic way, even thought they are extracted without much modification from source [111]. We address briefly these potential concerns. First, it is worth noticing that petiteness condition (H1) is stressed for a skeleton chain on the process and not for the continuous-time process. This allows to circumvent issues related to periodicity. A classical pathological example is the clock process, defined by the deterministic semigroup $P_t f(x) = f(x\mathrm{e}^{2\pi i t})$, for $x \in \mathbb{S}_1 = \{z \in \mathbb{C} : |z| = 1\}$, $t \geq 0$. It consists on periodic orbits along $\mathbb{S}_1$. Since even irrational skeleton chains are not mixing, it is not possible to establish a uniform minorisation condition valid for all starting points of any fixed compact set $\mathscr{K}$ of $\mathbb{S}_1$. Condition (H1) is therefore not verified by the clock process. Notice, however, that for the uniform sampling measure $\mu(dt) = \mathbb{1}_{[0,1]}(t)dt$, the continuous-time semigroup P_t does verify Doeblin condition $\langle \mu, \delta_x P_{\cdot}\rangle \geq \nu$, for all $x \in \mathbb{S}_1$, with ν the uniform measure over $\mathbb{S}_1$. Thus the importance of testing petiteness for the skeleton chains.

Second, condition (H2) is usually stated with an indicator function over some petite set C, this is, as

$$\mathcal{A}V \leq -cV + b\mathbb{1}_C, \tag{V4}$$

called drift condition (V4) in [112] and many later works. Indeed, from Section 5 of [48], it can be shown that if the function V is *unbounded off petite sets*, i.e., if for every $n \in \mathbb{N}$, the set $\{\mathbf{x} \in \mathcal{X} : V(\mathbf{x}) \leq n\}$ is either empty or petite, condition (V4) is equivalent to (H2). In our case, since V is coercive and that by (H1), all compact sets are petite for some skeleton chain, we have that V is unbounded off petite sets for that skeleton chain, and therefore an equivalent discrete-time version of (V4) is verified for the skeleton (condition $(\mathscr{D}_T)$ of [48], p. 1679). Theorem 5.1 of [48] shows finally that $(\mathscr{D}_T)$ and (V4) (called $(\tilde{\mathscr{D}})$ therein) are actually equivalent.

Notice that we need a Markovian (conservative) semigroup. To overcome this problem, similarly as in [31], we perform a so-called Doob h-transform, to obtain a conservative semigroup P_t with the dynamics of M_t. To do so, we require first to have some pair (λ, h) such that $\mathcal{Q}h = \lambda h$ and $h > 0$. Then, using such pair we define

$$P_t f(\mathbf{x}) := \frac{M_t(hf)(\mathbf{x})}{e^{\lambda t} h(\mathbf{x})}. \tag{3.9}$$

Then we can come back the ergodic behaviour of $(M_t)_{t\geq 0}$ by looking at the limit of $M_t f = e^{\Lambda t} h P_t (f/h)$. In particular, the generator associated with P_t is given explicitly by Eq. (3.10).

Proposition 3.2.3. *Suppose the existence of a pair (λ, h), $\lambda > 0$, $h > 0$ such that $\mathcal{Q}h = \lambda h$. Then, P_t defined by Eq. (3.9) is a positive Markovian semigroup whose infinitesimal generator is given for $f \in C_b^{1,1}(\mathbb{R}^2_+)$ by*

$$\mathcal{A}f(\mathbf{x}) = g(\mathbf{x})^\top \nabla f(\mathbf{x}) + \beta(\mathbf{x}) \left(\int_0^\infty [f(0,z) - f(\mathbf{x})] \frac{h(0,z)}{h(\mathbf{x})} k(\mathbf{x}, z) dz \right) \quad \forall \mathbf{x} \in \mathbb{R}^2_+ \tag{3.10}$$

Proof. By definition and evaluating at $t = 0$ we have:

$$\begin{aligned} \mathcal{A}f(\mathbf{x}) &= \frac{\partial}{\partial t} P_t f \Big|_{t=0} (\mathbf{x}) \\ &= \frac{M_t \mathcal{Q}(hf)}{e^{\lambda t} h} - \frac{\lambda M_t(hf)}{e^{\lambda t} h} \Big|_{t=0} (\mathbf{x}) \\ &= \frac{\mathcal{Q}(hf)(\mathbf{x})}{h(\mathbf{x})} - \lambda f(\mathbf{x}) \end{aligned}$$

Then, using the value of $\mathcal{Q}$ applied to hf and that $\mathcal{Q}h = \lambda h$ we get

$$\begin{aligned}
\frac{\mathcal{Q}(hf)(\mathbf{x})}{h(\mathbf{x})} &= \frac{f(\mathbf{x})}{h(\mathbf{x})} g(\mathbf{x})^\top \nabla h(\mathbf{x}) + g(\mathbf{x})^\top \nabla f(\mathbf{x}) + \beta(\mathbf{x}) \left(\int_0^\infty h(0,z) f(0,z) \frac{k(\mathbf{x},z)}{h(\mathbf{x})} dz - f(\mathbf{x}) \right) \\
&= \frac{f(\mathbf{x})}{h(\mathbf{x})} \left(g(\mathbf{x})^\top \nabla h(\mathbf{x}) - \beta(\mathbf{x}) h(\mathbf{x}) \right) + g(\mathbf{x})^\top \nabla f(\mathbf{x}) \\
&\quad + \beta(\mathbf{x}) \int_0^\infty h(0,z) f(0,z) \frac{k(\mathbf{x},z)}{h(\mathbf{x})} dz \\
&= \frac{f(\mathbf{x})}{h(\mathbf{x})} \left(\lambda h(\mathbf{x}) - \beta(\mathbf{x}) \int_0^\infty h(0,z) k(\mathbf{x},z) \right) + g(\mathbf{x})^\top \nabla f(\mathbf{x}) \\
&\quad + \beta(\mathbf{x}) \int_0^\infty h(0,z) f(0,z) \frac{k(\mathbf{x},z)}{h(\mathbf{x})} dz \\
&= \lambda f(\mathbf{x}) + g(\mathbf{x})^\top \nabla f(\mathbf{x}) + \beta(\mathbf{x}) \int_0^\infty \left[f(0,z) - f(\mathbf{x}) \right] \frac{h(0,z)}{h(\mathbf{x})} k(\mathbf{x},z) dz
\end{aligned}$$

Finally, subtracting $\lambda f(\mathbf{x})$ we obtain the form of generator $\mathcal{A}$. □

Hence, the work is structured as follows: first, in Section 3 we prove the existence of a pair (λ, h) which solves the eigenvalue problem $\mathcal{Q}h = \lambda h$ under the Assumptions 3.3.3. The same set of assumptions allows us to prove the Doeblin condition (H1) in Section 4. We do not provide a general Foster-Lyapunov condition (H2), suitable for our general case. However, we show its existence in our application to a growth-fragmentation model in Section 5. This last model has already been studied since the works of [70], and the exponential convergence has been recently shown in [62] using Generalized Relative Entropy techniques. Here, we show that the knowledge of the eigenelements (λ, h) for the generator allows to provide a simpler proof of convergence using Harris' theorem. Indeed, the arguments presented in Section 3.4 can be avoided when the existence of eigenelements is known apriori, which might be the case in several practical applications. Nonetheless, our general method allows us to give an answer to one of the perspectives listed by [62], who couldn't generalise their argument in the case of a general drift function g. Thus, our main result reads as follows:

Theorem 3.2.4 (Exponential ergodicity). *Under Assumptions 3.3.3 and if the Lyapunov-Foster condition (H2) of Theorem 3.2.1 is verified for some coercive function $V : \mathbb{R}_+^2 \to \mathbb{R}_+$, there is a unique probability measure π such that there exist constants $C, \omega, \Lambda > 0$ which verify for every initial condition $\mu_0 \in \mathcal{M}_p(\mathbb{R}_+^2)$*

$$||e^{-\Lambda t} \mu_0 M_t - \langle \mu_0, h \rangle \pi||_V \leq C \langle \mu_0, V \rangle e^{-\omega t}. \tag{3.11}$$

Moreover, π is absolutely continuous with respect to the Lebesgue measure.

3.3 Preliminary definitions and assumptions

We begin by recalling some useful properties of the deterministic flow, which are classical results for an autonomous system of first order ODE (refer for example to Theorem D.1 of [98]):

Lemma 3.3.1 (Flow properties and notations.). *Let $\mathbf{x} \in \mathbb{R}^2_+$. Consider $g = (g_1, g_2) \in C^1(\mathbb{R}^2_+)$ and suppose that $g_1 > 0$. The autonomous first-order system of Ordinary Differential Equations (ODE)*

$$\begin{aligned} \frac{d\mathbf{u}(t)}{dt} &= g\left(\mathbf{u}(t)\right) \ , \ t \in \mathbb{R} \\ \mathbf{u}(0) &= \mathbf{x} \end{aligned} \tag{3.12}$$

defines a unique flow $\varphi^t : \mathcal{X} \ni \mathbf{x} \mapsto \varphi^t(\mathbf{x}) \in \mathcal{X}$ which is the solution $\mathbf{u}(t)$ of (3.12) at time t with initial condition $\mathbf{x} \in \mathcal{X}$ where $\mathcal{X} = \bigcup_{y \geq 0} \Gamma^+_{(0,y)}$ where $\Gamma^+_{\mathbf{x}}$ will be defined below. We write $\varphi^t = (\varphi^t_1, \varphi^t_2)$ for the marginal flows of the age and size. We define then $\Gamma^+_{\mathbf{x}} = \{\varphi^t(\mathbf{x}), t \geq 0\}$ and $\Gamma^-_{\mathbf{x}} = \{\varphi^t(\mathbf{x}), t \leq 0\}$ and call $\Gamma_{\mathbf{x}} = \Gamma^+_{\mathbf{x}} \cup \Gamma^-_{\mathbf{x}}$ the unique orbit passing through $\mathbf{x}$. Moreover:

1. *The flow is a group in the time variable: $\varphi^t \varphi^s = \varphi^{t+s} = \varphi^s \varphi^t$, $\varphi^0 = \mathrm{Id}$, and has inverse $(\varphi^t)^{-1} = \varphi^{-t}$, which is the solution to the ODE $\mathbf{u}'(t) = -g\left(\mathbf{u}(t)\right)$.*

2. *The flow depends smoothly on the initial conditions: $\forall t \in \mathbb{R}$, $\varphi^t \in C^1(\mathbb{R}^2_+)$. We call $\mathcal{D}\varphi^t(\mathbf{x})$ the Jacobian matrix of the flow with respect to the initial condition.*

3. *For all fixed $\mathbf{x} = (a_0, y_0) \in \mathcal{X}$, if $g_1 > 0$, then there is a unique function $Y_{\mathbf{x}} : \mathbb{R}_+ \to \mathbb{R}_+$ such that for all $(a, y) \in \Gamma_{\mathbf{x}}$, we have $Y_{\mathbf{x}}(a) = y$. This represents the size at a given age of an individual with initial condition $\mathbf{x}$. In other words, for all $t \geq 0$,*

$$\varphi^t\left(\mathbf{x}\right) = \left(a(t), Y_{\mathbf{x}}(a(t))\right).$$

Moreover, $Y_{\mathbf{x}} \in C^1(\mathbb{R}_+)$ and it is solution of the first order one-dimensional ODE

$$Y'_{\mathbf{x}}(a) = \frac{g_2(a, Y_{\mathbf{x}}(a))}{g_1(a, Y_{\mathbf{x}}(a))} \quad ; \quad Y_{\mathbf{x}}(a_0) = y_0$$

Analogously, one defines its inverse function $A_{\mathbf{x}}(y)$ which gives the age at size y for an individual with initial condition $\mathbf{x}$, and hence verifies

$$\varphi^t\left(\mathbf{x}\right) = \left(A_{\mathbf{x}}(y(t)), y(t)\right), \quad t \geq 0.$$

4. *For all fixed $\mathbf{x} \in \mathcal{X}$, we write $\phi_{\mathbf{x}}(t) := \varphi^t(\mathbf{x})$ as a function of time (from $\mathbb{R}$ to $\mathbb{R}^2_+$). Then, the inverse function $\phi^{-1}_{\mathbf{x}} : \Gamma_{\mathbf{x}} \to \mathbb{R}$ such that $\phi^{-1}_{\mathbf{x}}(\phi_{\mathbf{x}}(t)) = t$ is well defined. For every $\mathbf{x}_0 \in \mathcal{X}$ and $\mathbf{x}_1 \in \Gamma_{\mathbf{x}_0}$ we read $\phi^{-1}_{\mathbf{x}_0}(\mathbf{x}_1)$ as the time needed along $\Gamma_{\mathbf{x}_0}$ to go from $\mathbf{x}_0$ to $\mathbf{x}_1$. Moreover if we write $\mathbf{x}_0 = (a_0, y_0)$, $\mathbf{x}_1 = (a_1, y_1)$, this quantity is given by*

$$\phi^{-1}_{\mathbf{x}_0}(\mathbf{x}_1) = \int_{a_0}^{a_1} \frac{1}{g_1\left(a, Y_{\mathbf{x}_0}(a)\right)} da = \int_{y_0}^{y_1} \frac{1}{g_2\left(A_{\mathbf{x}_0}(y), y\right)} dy.$$

Importantly, for the set of assumptions given below, we have $0 < \phi_{\mathbf{x}_0}^{-1}(\mathbf{x}_1) < \infty$ *for all* $\mathbf{x}_0 \in \mathcal{X} \setminus \{0\}$ *and* $\mathbf{x}_1 \in \Gamma_{\mathbf{x}_0}$.

Let us also consider the following probability space which well be useful to compute and interpret some of the estimates which will be obtained below.

Definition 3.3.2. Consider a probability space $(\mathbb{R}_+, \mathcal{B}(\mathbb{R}_+), \mathbb{P}_{\mathbf{x}})$ in which the random couple $(T, Z) \in \mathbb{R}_+ \times \mathbb{R}_+$ gives the first jump time T and size Z after this first jump of a trajectory beginning at $\mathbf{x} \in \mathcal{X}$. Hence, for all $\mathbf{x} \in \mathcal{X}$, the couple (T, Z) has joint probability density

$$p_{\mathbf{x}}(t, z) = \frac{1}{C_{\mathbf{x}}} k(\varphi^t(\mathbf{x}), z)\psi(t|\mathbf{x}),$$

where the normalisation constant is given by

$$C_{\mathbf{x}} = \int_0^\infty \int_0^\infty k(\varphi^t(\mathbf{x}), z')\psi(t|\mathbf{x})dtdz',$$

which is the mean number of offspring produced by an individual of initial configuration $\mathbf{x}$ after its first jump, and

$$\psi(t|\mathbf{x}) = \beta(\varphi^t(\mathbf{x})) \exp\left(-\int_0^t \beta\left(\varphi^s(\mathbf{x})\right) ds\right)$$

is the marginal probability density of the time of the first jump, conditionally to the initial configuration $\mathbf{x}$, and which is well defined for the set of assumptions given below. We write $\mathbb{E}_{\mathbf{x}}$ the associated expectation. Fig. 3.1 summarises the definitions introduced in this section.

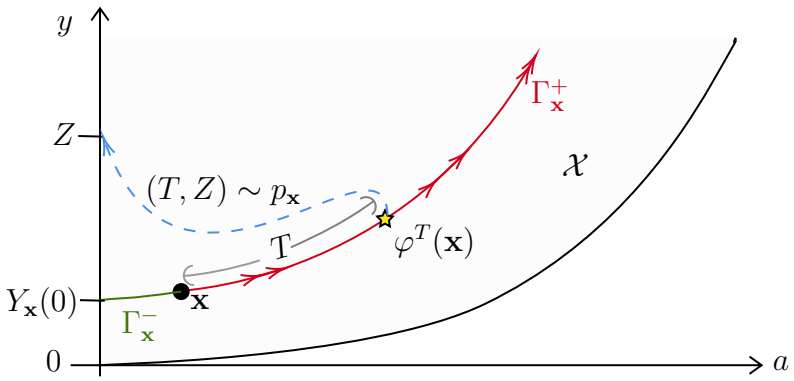

Figure 3.1: Flow notations introduced in Lemma 3.3.1 and the probabilistic definition of the random couple (T, Z) introduced in Definition 3.3.2.

Now, let us consider the following set of assumptions, whose biological meaning and implications are commented below.

Assumptions 3.3.3. Assume that we have

(i) *Smooth and uniformly controlled flow:* $g = (g_1, g_2) \in C^1(\mathbb{R}^2_+)$, $g_1 > 0$ and there are some constants $c_0, c_1, c_2 > 0$ such that for all $(a, y) \in \mathbb{R}^2_+$

$$g_1(a,y) \geq c_0\, a, \quad g_1(a,y) \leq c_1(1+a), \quad g_2(a,y) \leq c_1(1+y),$$
$$|\partial_a g_i(a,y)| \leq c_2(1+a+y), \quad |\partial_y g_i(a,y)| \leq c_2(1+a+y).$$

and for all $y > 0$, $a \geq 0$, we have $g_2(a,y) \leq g_2(0,y)$.

(ii) *Regular reproduction rate:* $\beta \in C(\mathbb{R}^2_+, \mathbb{R}_+)$, and $B = \beta/g_1 \in C(\mathbb{R}^2_+)$, such that there are constants $a^*, \beta_-, \beta_+ > 0$ s.t. for all $a > a^* y \geq 0$, $\beta_- < B(a,y) < \beta_+$, and $B(a,y) = 0$ for all $a \leq a^*$.

(iii) *Regular transition kernel:* For all $z \geq 0$, $\mathbf{x} \mapsto k(\mathbf{x}, z)$ is a continuous function on $\mathbb{R}^2_+$, and for all $\mathbf{x} \in \mathbb{R}^2_+$, $z \mapsto k(\mathbf{x}, z)$ is a continuous function on $\mathbb{R}_+$. The total offspring of individuals of trait $\mathbf{x}$ is $||k(\mathbf{x}, \cdot)||_1 := \int_0^{+\infty} k(\mathbf{x}, z)dz$ with $1 < ||k(\mathbf{x}, \cdot)||_1 \leq \bar{K}$ for all $\mathbf{x} \in \mathbb{R}^2_+$. In particular, we consider two distinct cases:

a) *Fragmentation kernel:* For all $a \geq 0$, supp $k(a, y, \cdot) \subseteq (0, y)$.

b) *Compactly supported mutational kernel:* It exists a compact set $S \subset \mathbb{R}_+$ such that for all $a \geq 0$, supp $k(a, y, \cdot) \subseteq S$, and some interval $I \subset \mathbb{R}_+$ and $\epsilon_0 > 0$ such that for all $y \in S$ and $z \in S \cap \mathbb{B}_{\epsilon_0}(y)$, the open ball of radius ϵ_0 around y, we have $I \subset \{a > 0 : \beta(a,y)k(a,y,z) > 0\}$.

(iv) *Lower bounded transition kernel:* For all fixed value of $z > 0$, there exists some non-empty open interval $D(z)$ with length bounded between δ_- and δ_+, both independent of z, and a positive value $\varepsilon(z)$ such that for all $\mathbf{x} \in \mathbb{R}^2_+$, $k(\mathbf{x}, z) > \varepsilon(z)\mathbb{1}_{D(z)}(\mathbf{x})$.

We comment on the meaning of these assumptions. Assumption 3.3.3-(i) ensures that the size and age do not explode in finite time. The control on the derivatives will also allow to control the influence of the initial conditions on the flow (Lemma 3.1.2). Assumption 3.3.3-(ii) allows to write the division rate as $\beta(\mathbf{x}) = g_1(\mathbf{x})B(\mathbf{x})$ where function B should be interpreted as an "*age hazard rate*", a generalisation of the adder division rate introduced in Example 3.1.1. Thus, we allow ourselves to have unbounded division rates, provided that the *age hazard rate* B is bounded, which will allow to control nonetheless the law of ages at division. Biologically this has been interpreted as individuals not perceiving actual time, but rather their own biological age, upon which the division event is decided [133]. The parameter a^* is the minimal division age. It imposes that it is not possible to divide immediately after birth. For ages bigger than a^*, the bounds on B allow to stochastically bound the age at division between two exponential random variables of rate parameter β_- and β_+. Assumption 3.3.3-(iii) imposes inexact cell divisions which always give a bounded number of individuals, but almost surely more than 1, which sets us in the supercritical case. The two considered cases bring together a broad family of transition kernels used in similar models. In particular the assumptions concerning the mutational kernel are inspired from [122]. Importantly, the compactness is needed to prove the existence of the eigenelements of $\mathcal{Q}$ but not for the Doeblin minorisation, which holds in more general cases. In this

line, Assumption 3.3.3-(iv) is key to obtain the Doeblin minorisation condition and generalises similar requirements needed in the one-dimensional case, such as Eq. (8) of [31] for auto-similar fragmentation kernels, and Eq. (10) of [34], or Assumption (A4) of [122] for general non-local mutation-type kernels. Finally, a major difference with respect to classical size-structured models, is that we do not require conservation of mass during reproduction events.

3.4 Existence of the eigenelements of $\mathcal{Q}$

Now, in order to bring ourselves to the conservative setting, we begin by showing the existence of some pair of eigenelements for $\mathcal{Q}$.

Proposition 3.4.1 (Existence of eigenelements)**.** *Under Assumptions 3.3.3, there exist a positive constant $\lambda > 0$ and a positive function $h \in W^{1,\infty}_{loc}(\mathcal{X})$ such that*

$$\mathcal{Q}h = \lambda h.$$

To do so, we can reformulate the eigenvalue problem as a one-dimensional fixed point problem. This is a classical strategy and other applications in two-dimensional spaces can be found for example in [42, 73, 62]. In particular, we follow closely the arguments of [42] which corresponds to the case $g_1 \equiv 1$ with a fragmentation kernel and with additional confinement assumption in the drift term which would allow us to work in a compact interval in one of the two dimensions. We generalise this approach here.

Lemma 3.4.2 (Reformulation as a renewal equation)**.** *Any pair (λ, h) such that $\lambda > 0$ and $h \in W^{1,\infty}_{loc}(\mathcal{X})$ is solution almost everywhere to $\mathcal{Q}h = \lambda h$ and verifies*

$$\lim_{t\to+\infty} h(\varphi^t(\mathbf{x}))\exp\left(-\int_0^t \beta\left(\varphi^s(\mathbf{x})\right)ds - \lambda t\right) = 0 \tag{3.13}$$

if and only if it verifies the renewal formula

$$h(\mathbf{x}) = \int_0^\infty h(0,z)K_\lambda(\mathbf{x},z)dz, \tag{3.14}$$

where

$$K_\lambda(\mathbf{x},z) = C_{\mathbf{x}}\int_0^\infty e^{-\lambda t}\, p_{\mathbf{x}}(t,z)dt \tag{3.15}$$

Remark 3.4.3. Using Definition 3.3.2 we can then write Eq. (3.14) as

$$h(\mathbf{x}) = C_{\mathbf{x}}\,\mathbb{E}_{\mathbf{x}}[h(0,Z)e^{-\lambda T}]. \tag{3.16}$$

Proof of Lemma 3.4.2. We proceed by the method of integration along characteristics. First of all, take $h \in W^{1,\infty}_{\mathrm{loc}}(\mathcal{X})$ and fix some $\mathbf{x} \in \mathcal{X}$ and $\lambda \geq 0$. We study $\mathcal{R}^{h,\lambda}_{\mathbf{x}} : \mathbb{R}_+ \to \mathbb{R}$ defined by

$$\mathcal{R}^{h,\lambda}_{\mathbf{x}}(t) := h(\varphi^t(\mathbf{x})) \exp\left(- \int_0^t \beta\left(\varphi^s(\mathbf{x})\right) ds - \lambda t \right), \quad t \geq 0.$$

It is clear that $\mathcal{R}^{h,\lambda}_{\mathbf{x}}$ is in $L^1_{\mathrm{loc}}(\mathbb{R}_+)$. We show now that it is weakly differentiable. At least formally, we have that

$$\begin{aligned} &\frac{\partial}{\partial t}\mathcal{R}^{h,\lambda}_{\mathbf{x}}(t) \\ &= \left(\nabla h(\varphi^t(\mathbf{x}))^\top g(\varphi^t(\mathbf{x})) - (\beta(\varphi^t(\mathbf{x})) + \lambda) h(\varphi^t(\mathbf{x}))\right) \exp\left(- \int_0^t \beta\left(\varphi^s(\mathbf{x})\right) ds - \lambda t \right), \end{aligned} \tag{3.17}$$

which is well defined and in $L^1_{\mathrm{loc}}(\mathbb{R}_+)$ since $h \in W^{1,\infty}_{\mathrm{loc}}(\mathcal{X})$, and g and β are also locally bounded from Assumptions 3.3.3. Therefore $\mathcal{R}^{h,\lambda}_{\mathbf{x}} \in W^{1,\infty}_{\mathrm{loc}}(\mathbb{R}_+)$. Now, using the definition of $\mathcal{Q}$ we get whenever $h \in D(\mathcal{Q})$,

$$\begin{aligned} &\frac{\partial}{\partial t}\mathcal{R}^{h,\lambda}_{\mathbf{x}}(t) \\ &= \left(\mathcal{Q}h(\varphi^t(\mathbf{x})) - \lambda h(\varphi^t(\mathbf{x})) - \beta(\varphi^t(\mathbf{x})) \int_0^\infty h(0,z) k(\varphi^t(\mathbf{x}), z) dz \right) e^{-\int_0^t \beta(\varphi^s(\mathbf{x}))ds - \lambda t}. \end{aligned}$$

• $\underline{\mathcal{Q}h = \lambda h \cap (3.13) \implies (3.14)}$: Now, suppose that (λ, h) is solution a.e. to $\mathcal{Q}h = \lambda h$. Then, for almost every t

$$\begin{aligned} \frac{\partial}{\partial t}\mathcal{R}^{h,\lambda}_{\mathbf{x}}(t) &= -\beta(\varphi^t(\mathbf{x})) e^{-\int_0^t \beta(\varphi^s(\mathbf{x}))ds - \lambda t} \int_0^\infty h(0,z) k(\varphi^t(\mathbf{x}), z) dz \\ &= -C_{\mathbf{x}} e^{-\lambda t} \int_0^\infty h(0,z) p_{\mathbf{x}}(t,z) dz, \end{aligned} \tag{3.18}$$

which is well defined and integrable over $(0, +\infty)$ by Assumptions 3.3.3, and since the eigenfunction h must be in the domain of the extended generator, so the integral term is well defined. Now, suppose that Eq. (3.13) is also verified. Then, integrating Eq. (3.18) in $(0, +\infty)$ and using the decay condition Eq. (3.13) results into

$$h(\mathbf{x}) = \int_0^{+\infty} C_{\mathbf{x}} e^{-\lambda t} \int_0^\infty h(0,z) p_{\mathbf{x}}(t,z) dz \, dt$$

which, by Fubini, gives exactly Eq. (3.14).

• (3.14) $\implies$ $\mathcal{Q}h = \lambda h \cap$ (3.13) : Finally, suppose that we have Eq. (3.14). Then we have:

$$\begin{aligned}
h(\varphi^t(\mathbf{x})) &= \int_0^\infty h(0,z)K_\lambda(\varphi^t(\mathbf{x}),z)dz \\
&= \int_0^\infty \int_0^\infty h(0,z)k(\varphi^{t+s}(\mathbf{x}),z)\beta(\varphi^{t+s}(\mathbf{x}))\exp\left(-\int_t^{t+s}\beta\left(\varphi^u(\mathbf{x})\right)du - \lambda s\right)dsdz \\
&= \left(\int_0^\infty \int_0^\infty h(0,z)k(\varphi^s(\mathbf{x}),z)\beta(\varphi^s(\mathbf{x}))\exp\left(-\int_0^s\beta\left(\varphi^u(\mathbf{x})\right)du - \lambda s\right)dsdz\right. \\
&\quad \left. - \int_0^\infty \int_0^t h(0,z)k(\varphi^s(\mathbf{x}),z)\beta(\varphi^s(\mathbf{x}))\exp\left(-\int_0^s\beta\left(\varphi^u(\mathbf{x})\right)du - \lambda s\right)dsdz\right) \\
&\quad \times \exp\left(\int_0^t \beta\left(\varphi^u(\mathbf{x})\right)du + \lambda t\right)
\end{aligned}$$

Therefore, using Eq. (3.14) again to replace the double integrals of the RHS we obtain:

$$\begin{aligned}
\mathcal{R}_{\mathbf{x}}^{h,\lambda}(t) &= h(\varphi^t(\mathbf{x}))\exp\left(-\int_0^t \beta\left(\varphi^s(\mathbf{x})\right)ds - \lambda t\right) \\
&= h(\mathbf{x}) - \int_0^\infty \int_0^t h(0,z)k(\varphi^s(\mathbf{x}),z)\psi(s|\mathbf{x})e^{-\lambda s}dsdz
\end{aligned} \tag{3.19}$$

As $t \to +\infty$, the improper integral in the RHS of Eq. (3.19) converges towards

$$\lim_{t\to+\infty}\int_0^\infty \int_0^t h(0,z)k(\varphi^s(\mathbf{x}),z)\psi(s|\mathbf{x})e^{-\lambda s}dsdz = \int_0^\infty h(0,z)K_\lambda(\mathbf{x},z)dz = h(\mathbf{x}),$$

from which we obtain Eq. (3.13). Moreover, supposing that $h \in W^{1,\infty}_{\text{loc}}(\mathcal{X})$, from the previous analysis, we have that $\mathcal{R}_{\mathbf{x}}^{h,\lambda} \in W^{1,\infty}_{\text{loc}}(\mathbb{R}_+)$, so by differentiation of Eq. (3.19) we obtain almost everywhere,

$$\frac{\partial}{\partial t}\mathcal{R}_{\mathbf{x}}^{h,\lambda}(t) = -\int_0^\infty h(0,z)k(\varphi^t(\mathbf{x}),z)\psi(t|\mathbf{x})e^{-\lambda t}dz$$

Hence, a comparison with Eq. (3.17) gives that $h \in D(\mathcal{Q})$, and for all $\mathbf{x} \in \mathcal{X}$ and $t > 0$ we have almost everywhere $\mathcal{Q}h(\varphi^t(\mathbf{x})) - \lambda h(\varphi^t(\mathbf{x})) = 0$, or equivalently, $Qh = \lambda h$ almost everywhere in $\mathcal{X}$. □

Remark 3.4.4. In particular the function $\eta(y) := h(0,y)$ defined for all $y \geq 0$ is solution to the fixed point problem

$$\eta(y) = \int_0^\infty \eta(z)K_\lambda(0,y,z)dz. \tag{3.20}$$

Therefore we will consider the operator G_λ defined for $f \in C^1(\mathbb{R}_+)$ by

$$\mathcal{G}_\lambda f(y) = \int_0^\infty f(z)K_\lambda(0,y,z)dz \quad \forall y > 0. \tag{3.21}$$

We also introduce the operator $\mathcal{J}_\lambda : \mathcal{M}(\mathbb{R}_+) \to \mathcal{M}(\mathbb{R}_+)$ which for any Radon measure ν supported in $\mathbb{R}_+$ gives

$$\mathcal{J}_\lambda \nu = \left(\int_0^\infty K_\lambda(0, z, y)\nu(dz) \right) dy \tag{3.22}$$

and verifies the duality property below:

Proposition 3.4.5. *For every $\lambda \geq 0$, $\mathcal{J}_\lambda$ is the adjoint operator of $\mathcal{G}_\lambda$.*

Proof. Let $f \in C(\mathbb{R}_+^2)$ and $\nu \in \mathcal{M}(\mathbb{R}_+^2)$. By Fubini's Theorem,

$$\begin{aligned} \langle \nu, \mathcal{G}_\lambda f \rangle &= \int_0^\infty \left(\int_0^\infty f(z) K_\lambda(0, y, z) dz \right) \nu(dy) \\ &= \int_0^\infty f(z) \left(\int_0^\infty K_\lambda(0, y, z)\nu(dy) \right) dz = \langle \mathcal{J}_\lambda \nu, f \rangle . \end{aligned}$$

□

Remark 3.4.6. From Eq. (3.16), we can write

$$\mathcal{G}_\lambda f(y) = C_{(0,y)}\, \mathbb{E}_{(0,y)}[f(Z)e^{-\lambda T}].$$

where again $C_{(0,y)} = ||K_0(0, y, \cdot)||_1$ is the mean number of offspring produced by an individual of initial size y after its first jump.

Proof of Proposition 3.4.1. We aim to prove that there is a unique $\lambda > 0$ for which the operator $\mathcal{G}_\lambda$ admits a unique fixed point $h(0, \cdot)$. The pair (λ, h) is then solution to the eigenproblem $\mathcal{Q}h = \lambda h$. This will be proven by means of Krein-Rutman's theorem. In order to be able to apply this theorem we need to work with a strictly positive compact operator. For the compactly supported mutational kernel it is immediately the case, however it is not the case for G_λ with a fragmentation kernel. Thus, we shall follow a standard approximation scheme for the proof which is structured as follows:

1. We define a truncated version of $\mathcal{G}_\lambda$ which by Arzéla-Ascoli's theorem we prove to be a positive compact operator in the Banach space of continuous functions.
2. We apply Krein-Rutman theorem to prove that for each $\lambda \geq 0$ the truncated operator admits a unique eigenvalue $\mu_\lambda \geq 0$ and suitably normalised eigenfunction $h_\lambda \geq 0$.
3. We prove that there exists a unique $\lambda_0 > 0$ such that $\mu_{\lambda_0} = 1$
4. We prove that the value of λ_0 is uniformly bounded for all the members of the family of truncated operators.
5. We pass to the limit and show that the limit eigenelements $(\lambda_0, h_{\lambda_0})$ of the family of truncated operators are indeed solution to the fixed point problem.

Note that the proof is also valid for the compact mutational kernel which verifies Assumption 3.3.3-(iii)-(b), but in that case neither the truncation nor the uniform estimates are needed.

Step 1 : Construction of the truncated operator.
For each $R > 0$ let $\mathcal{G}_\lambda^R : C^1([0,R]) \to C^1([0,R])$ defined for all $\lambda > 0$, for $f \in C^1([0,R])$ by

$$\mathcal{G}_\lambda^R f(y) = \int_0^R f(z) K_\lambda^R(0,y,z)dz \quad \forall y \in (0,R) \tag{3.23}$$

with

$$K_\lambda^R(0,y,z) = \int_0^\infty \left(k(\varphi^t(0,y),z) + \frac{1}{R}\int_R^\infty k(\varphi^t(0,y),\zeta)d\zeta \right) \psi(t|(0,y))e^{-\lambda t}dt$$

We require to add the uniform correction $z \mapsto \frac{1}{R}\int_R^\infty k(\varphi^t(0,y),\zeta)d\zeta$ in order to endorse the strict positivity of the operator. Indeed, for all $y \in [0,R]$, from Fubini's theorem, Assumption 3.3.3-(iii) and Jensen's inequality we obtain

$$\begin{aligned}\int_0^R K_\lambda^R(0,y,z)dz &= \int_0^\infty \left(\int_0^\infty k(\varphi^t(0,y),z)dz \right) \psi(t|(0,y))e^{-\lambda t}dt \\ &> \int_0^\infty e^{-\lambda t}\psi(t|(0,y))dt \\ &\geq \exp\left(-\lambda \mathbb{E}\left[(0,y)\right] T\right).\end{aligned}$$

Moreover, Assumption 3.3-(ii) gives that

$$0 < \mathbb{E}\left[\phi_{(0,y)}^{-1}\left(\mathbf{A}_-, Y_{(0,y)}(\mathbf{A}_-)\right)\right] \leq \mathbb{E}\left[(0,y)\right] T \leq \mathbb{E}\left[\phi_{(0,y)}^{-1}\left(\mathbf{A}_+, Y_{(0,y)}(\mathbf{A}_+)\right)\right] < +\infty$$

where $\mathbf{A}_-$ (respectively $\mathbf{A}_+$) follows an Exponential distribution of parameter β_- (respectively β_+). Therefore for all positive $f \in C^1([0,R])$, $G_\lambda^R f > 0$.
Moreover, if in analogy with Definition 3.3.2, we define for all $R > 0$ the random couple $(T_R, Z_R) \in \mathbb{R}_+ \times [0,R]$ such that under $\mathbb{P}_{(0,y)}$ they have joint probability density

$$p_{(0,y)}^R(t,z) = \frac{1}{C_{(0,y)}}\left(k(\varphi^t(0,y),z) + \frac{\mathbb{1}_{z\leq R}}{R}\int_R^\infty k(\varphi^t(0,y),\zeta)d\zeta \right)\psi(t|(0,y)),$$

then we can write

$$\mathcal{G}_\lambda^R f(y) = C_{(0,y)}\, \mathbb{E}_{(0,y)}[f(Z_R)e^{-\lambda T_R}\mathbb{1}_{Z_R\leq R}]. \tag{3.24}$$

Step 2 : Existence of the eigenelements of $\mathcal{G}_\lambda^R$.
We begin by proving that for all $\varepsilon > 0, \lambda \geq 0$ and $R > 0$, $\mathcal{G}_\lambda^R$ is compact. We show that for every sequence $(f_n)_n$ in the unit ball of $C([0,R])$ there exists a subsequence of $\left(\mathcal{G}_\lambda^R f_n\right)_n$ which converges in $C([0,R])$ equipped with the uniform norm.

i. **Uniform bound:** For all $y \in (0,R)$, f in the unit ball of $C[0,R]$ we have from Eq. (3.24):

$$\mathcal{G}_\lambda^R f(y) \leq C_{(0,y)}||f||_\infty \leq \bar{K}$$

ii. **Equicontinuity:** Since $g_1 \in C^1(\mathbb{R}_+^2)$ and is strictly positive, and k is continuous in the first two variables, we have that for every $\lambda \geq 0$, $(y,z) \in [0,R]\times[0,R] \mapsto K_\lambda(0,y,z)$ is an uniformly continuous function on $[0,R]\times[0,R]$. Therefore for all $\lambda \geq 0$ and $\varepsilon > 0$ there exists $\delta > 0$ such that if $|y_1 - y_2| + |z_1 - z_2| < \delta$ for $y_1, y_2, z_1, z_2 \in [0,R]$, then $|K_\lambda(0,y_1,z_1) - K_\lambda(0,y_2,z_2)| < \varepsilon/R$. Hence, for all f in the unit ball, $y_1, y_2 \in [0,R]$ such that $|y_1 - y_2| < \delta$ we have:

$$\left|\mathcal{G}_\lambda^R f(y_1) - \mathcal{G}_\lambda^R f(y_2)\right| \leq \int_0^R |f(z)||K_\lambda(0,y_1,z) - K_\lambda(0,y_2,z)|dz < \varepsilon$$

independently on y_1, y_2.

Finally, by Ascoli's criterium, there exists a convergent subsequence of $\left(\mathcal{G}_\lambda^R f_n\right)_n$ and so the operator $\mathcal{G}_\lambda^R$ is strictly positive and compact for the uniform topology of $C([0,R])$. Therefore, by Krein-Rutman theorem [119] there exists a unique triplet of a positive real value $\mu_\lambda^R > 0$, function $\eta_\lambda^R > 0$ continuous on $[0,R]$, and a positive Radon measure ν_λ^R supported on $[0,R]$ such that

$$\mathcal{G}_\lambda^R \eta_\lambda^R = \mu_\lambda^R \eta_\lambda^R \tag{3.25}$$

$$\mathcal{J}_\lambda^R \nu_\lambda^R = \mu_\lambda^R \nu_\lambda^R \ , \ \nu_\lambda^R([0,R]) = 1 \tag{3.26}$$

$$\left\langle \nu_\lambda^R, \eta_\lambda^R \right\rangle_R = 1, \tag{3.27}$$

where we denote $\langle \nu, f \rangle_R = \int_0^R f(y)\nu(dy)$.

Step 3 : Existence and uniqueness of $\lambda_0 > 0$ such that $\mu_{\lambda_0}^R = 1$
We show that the mapping $\lambda \mapsto \mu_\lambda^R$ is a continuous strictly decreasing function which goes through the value of 1 at some point. First, note that from Equations (3.25) and (3.27), we have

$$\left\langle \nu_\lambda^R, \mathcal{G}_\lambda^R \eta_\lambda^R \right\rangle_R = \mu_\lambda^R \tag{3.28}$$

We prove that $\lambda \mapsto \left\langle \nu_\lambda^R, \mathcal{G}_\lambda^R \eta_\lambda^R \right\rangle_R$ is differentiable continuous and decreasing. Let us consider the derivatives in the sense of distributions $\partial_\lambda \nu_\lambda^R$ and $\partial_\lambda \eta_\lambda^R$. We show below that $\lambda \mapsto \left\langle \nu_\lambda^R, \mathcal{G}_\lambda^R \eta_\lambda^R \right\rangle_R$ is actually strongly differentiable with respect to λ as it has the same regularity as $\lambda \mapsto \mathcal{G}_\lambda^R f$. First, by dominated convergence, differentiating under the integral sign on Eq. (3.24) gives for every $f \in C^1([0,R])$,

$$\left(\partial_\lambda \mathcal{G}_\lambda^R\right) f(y) = -C_{(0,y)}\, \mathbb{E}_{(0,y)}[f(Z_R) T_R e^{-\lambda T_R} \mathbb{1}_{Z_R \leq R}]. \tag{3.29}$$

Then, by differentiating under the duality brackets, and using the duality between $\mathcal{G}$ and $\mathcal{J}$ with (3.25) and (3.26), we obtain

$$\begin{aligned}
\partial_\lambda \mu_\lambda^R &= \left\langle \partial_\lambda \nu_\lambda^R, \mathcal{G}_\lambda^R \eta_\lambda^R \right\rangle + \left\langle \nu_\lambda^R, \mathcal{G}_\lambda^R \left(\partial_\lambda \eta_\lambda^R\right) \right\rangle + \left\langle \nu_\lambda^R, \left(\partial_\lambda \mathcal{G}_\lambda^R\right) \eta_\lambda^R \right\rangle \\
&= \left\langle \partial_\lambda \nu_\lambda^R, \mathcal{G}_\lambda^R \eta_\lambda^R \right\rangle + \left\langle \mathcal{J}_\lambda^R \nu_\lambda^R, \partial_\lambda \eta_\lambda^R \right\rangle + \left\langle \nu_\lambda^R, \left(\partial_\lambda \mathcal{G}_\lambda^R\right) \eta_\lambda^R \right\rangle \\
&= \mu_\lambda^R \left(\left\langle \partial_\lambda \nu_\lambda^R, \eta_\lambda^R \right\rangle + \left\langle \nu_\lambda^R, \partial_\lambda \eta_\lambda^R \right\rangle \right) + \left\langle \nu_\lambda^R, \left(\partial_\lambda \mathcal{G}_\lambda^R\right) \eta_\lambda^R \right\rangle \\
&= \mu_\lambda^R \partial_\lambda \left\langle \nu_\lambda^R, \eta_\lambda^R \right\rangle + \left\langle \nu_\lambda^R, \left(\partial_\lambda \mathcal{G}_\lambda^R\right) \eta_\lambda^R \right\rangle
\end{aligned}$$

Eq. (3.27) gives $\partial_\lambda \langle \nu_\lambda^R, \eta_\lambda^R \rangle = 0$, and therefore $\partial_\lambda \mu_\lambda^R = \langle \nu_\lambda^R, (\partial_\lambda \mathcal{G}_\lambda^R)\, \eta_\lambda^R \rangle$, i.e.,

$$\partial_\lambda \mu_\lambda^R = -\int_0^R C_{(0,y)}\, \mathbb{E}_{(0,y)} \left[\eta_\lambda^R(Z_R) T_R e^{-\lambda T_R} \mathbb{1}_{Z_R \leq R} \right] \nu_\lambda^R(dy) \tag{3.30}$$

Since all the integrands are non-negative we have $\partial_\lambda \mu_\lambda^R < 0$. So $\lambda \mapsto \mu_\lambda^R$ is a continuous strictly-decreasing function. Moreover, doing $\lambda = 0$, integrating Eq. (3.26), using Fubini's theorem to integrate first in the z variable, and using Assumption 3.3.3-(iii), we obtain

$$\begin{aligned}
\mu_0^R &= \int_0^R \mathcal{J}_0^R \nu_0^R(dz) \\
&= \int_0^R \int_0^R \int_0^\infty \left(k(\varphi^t(0,y),z) + \frac{\int_R^\infty k(\varphi^t(0,y),\zeta)d\zeta}{R} \right) \psi(t|(0,y))dt\, \nu_0^R(dy)\, dz \\
&= \int_0^R \int_0^\infty \left(\int_0^\infty k(\varphi^t(0,y),z)dz \right) \psi(t|(0,y))dt\, \nu_0^R(dy) > 1
\end{aligned}$$

On the other hand, doing $\lambda \to \infty$, passing to the limit under the expecation of Eq. (3.24) we get for every $f \in C([0,R])$, $\mathcal{G}_\lambda^R f \to 0$ uniformly as $\lambda \to \infty$. In particular, by the equicontinuity of $\mathcal{G}_\lambda^R$, for every $\delta \in (0,2)$, there must be λ_* large enough such that for every $f \in C([0,R])$, $\mathcal{G}_\lambda^R f \leq \delta$ for all $\lambda \geq \lambda_*$ and hereby, $\mu_\lambda^R \leq \delta$ for all $\lambda \geq \lambda_*$. Therefore $\mu_\lambda^R \to 0$ as $\lambda \to \infty$. In consequence, there must be a unique $\lambda_0 > 0$ such that $\mu_{\lambda_0}^R = 1$. We then define λ_R as the only $\lambda_0 > 0$ such that $\mu_{\lambda_0}^R = 1$ and denote $\eta_R = \eta_{\lambda_R}^R$ the respective eigenfunction. Next, we construct a sequence of h_R from η_R which are to converge to the solution of the intial eigenproblem and we show that we can establish an uniform bound over λ_R.

Step 4 : Construction of h_R.
We extend the definition of K_λ to all $(a,y) \in \mathcal{X}$, $z \in [0,R]$. Define

$$K_\lambda^R(a,y,z) := \int_0^\infty \left(k(\varphi^t(a,y),z) + \frac{\int_R^\infty k(\varphi^t(0,y),\zeta)d\zeta}{R} \right) \psi(t|(a,y))e^{-\lambda t}dt,$$

and let

$$h_R(a,y) := \int_0^R \eta_R(z) K_{\lambda_R}^R(a,y,z)dz. \tag{3.31}$$

Hence, taking $a = 0$, since η_R solves Eq. (3.25) for $\mu_\lambda^R = 1$, we have that:

$$h_R(0,y) = \int_0^R \eta_R(z) K_{\lambda_R}^R(0,y,z)dz = \mathcal{G}_{\lambda_R}^R \eta_R(y) = \eta_R(y),$$

and therefore h_R verifies

$$\begin{cases} h_R(\mathbf{x}) = \int_0^R h_R(0,z) K_{\lambda_R}^R(\mathbf{x},z)dz = C_{\mathbf{x}}\, \mathbb{E}_{\mathbf{x}} \left[\eta_R(Z_R) e^{-\lambda_R T_R} \mathbb{1}_{Z_R \leq R} \right] & \forall \mathbf{x} \in \mathcal{X} \\ h_R(0,y) = \eta_R(y) \quad \forall y \in (0,R) \end{cases} \tag{3.32}$$

where $C_{\mathbf{x}} = ||K_0(\mathbf{x}, \cdot)||_{L_1(\mathbb{R}_+)}$. Then, we can repeat the steps of the proof of Lemma 3.4.2 to show that the truncated renewal equation (3.32) (which is the truncated version of Eq. (3.14)) is equivalent to have the boundary condition

$$\lim_{t\to+\infty} h_R(\varphi^t(\mathbf{x})) \exp\left(-\int_0^t \beta(\varphi^s(\mathbf{x}))ds - \lambda_R t\right) = 0 \tag{3.33}$$

and to have that h_R is solution to the truncated eigenvalue problem

$$\mathcal{Q}_R h_R(a, y) = \lambda_R \, h_R(a, y)$$

where

$$\begin{aligned}\mathcal{Q}_R h(a, y) = {} & g(a, y)^\top \nabla h(a, y) \\ & + \beta(a, y) \left(\int_0^R h(0, z) \left(k(a, y, z) + \frac{\int_R^\infty k(a, y, \zeta) d\zeta}{R} \right) dz - h(a, y) \right).\end{aligned}$$

Hence, developing $\mathcal{Q}_R h_R(0, y)$ one obtains

$$\begin{aligned}\mathcal{Q}_R h_R(0, y) = {} & g_1(0, y)\partial_a h_R(0, y) + g_2(0, y)\partial_y h_R(0, y) \\ & + \beta(0, y) \left(\int_0^R h_R(0, z) \left(k(a, y, z) + \frac{\int_R^\infty k(a, y, \zeta) d\zeta}{R} \right) dz - h_R(a, y) \right).\end{aligned}$$

Therefore $\eta_R = h_R(0, \cdot)$ is solution to

$$\begin{aligned}\lambda_R \eta_R(y) = {} & g_2(0, y)\eta_R'(y) - \beta(0, y)\eta_R(y) \\ & + \beta(0, y) \int_0^R \eta_R(z) \left(k(0, y, z) + \frac{\int_R^\infty k(a, y, \zeta) d\zeta}{R} + g_1(0, y)\partial_a K_{\lambda_R}^R(0, y, z) \right) dz\end{aligned} \tag{3.34}$$

In our case, Assumption 3.3.3-(ii) which imposes $\beta(0, y) = 0$ for every initial size y simplifies this last equation into

$$g_2(0, y)\eta_R'(y) - \lambda_R \, \eta_R(y) = 0$$

Therefore for all $R > 1$, if we impose the normalisation condition $\eta_R(1) = 1$, we have

$$\eta_R(y) = \exp\left(\lambda_R \int_1^y \frac{1}{g_2(0, z)} dz \right), \; y \in [0, R] \tag{3.35}$$

Finally, coming back to (3.24) and (3.25), we have for all $y \in (0, R)$,

$$\begin{aligned}& \eta_R(y) = C_{(0,y)} \, \mathbb{E}_{(0,y)}[\eta_R(Z_R) e^{-\lambda T_R} \mathbb{1}_{Z_R \le R}] \\ \iff & 1 = C_{(0,y)} \, \mathbb{E}_{(0,y)} \left[\frac{\eta_R(Z_R)}{\eta_R(y)} e^{-\lambda T_R} \mathbb{1}_{Z_R \le R} \right] \\ \iff & 1 = C_{(0,y)} \, \mathbb{E}_{(0,y)} \left[\exp\left(\lambda_R \left(\int_y^{Z_R} \frac{1}{g_2(0, z)} dz - T_R \right) \right) \right]\end{aligned}$$

In particular the last equation characterises λ_R as the unique $\lambda > 0$ such that for all $y \in (0, R)$, the following Euler-Lotka-type equation is verified

$$1 = C_{(0,y)}\mathbb{E}_{(0,y)}\left[\exp\left(\lambda\left(\int_y^{Z_R}\frac{1}{g_2(0,z)}dz - T_R\right)\right)\right]. \tag{3.36}$$

Step 5 : Uniform bound for λ_R (Fragmentation case)
Suppose that for all $a \geq 0$, supp $k(a, y, \cdot) \subseteq (0, y)$. This is, the newborns sizes are almost surely smaller than the parent size. Hence, for all initial size y we have

$$\mathbb{P}_{(0,y)}\left(T_R > \int_y^{Z_R}\frac{1}{g_2(A_{0,y}(z), z)}dz\right) = 1. \tag{3.37}$$

Indeed, from Lemma 3.3.1-(4.) we have that $\phi_{0,y}^{-1}(A_{0,y}(z), z) = \int_y^z \frac{1}{g_2(A_{0,y}(z),z)}dz$ is the time needed to go from size y to z following the deterministic flow only, and it has to be smaller than the division time at which the trajectory jumps to z. Then, thanks to Assumption 3.3.3-(i) which gives $g_2(0, y) \geq g_2(a, y)$, we have also that

$$\mathbb{P}_{(0,y)}\left(T_R > \int_y^{Z_R}\frac{1}{g_2(0,z)}dz\right) = 1.$$

Therefore for all $\lambda > 0$

$$\exp\left(\lambda\left(\int_y^{Z_R}\frac{1}{g_2(0,z)}dz - T_R\right)\right) \leq 1 \in L^1(\mathbb{R}_+^2, p_{(0,y)}dtdz), \quad \mathbb{P}_{(0,y)}\text{-a.s.}, \tag{3.38}$$

and by dominated convergence if λ_R converges to $+\infty$ as $R \to \infty$, then

$$\mathbb{E}_{(0,y)}\left[\exp\left(\lambda_R\left(\int_y^{Z_R}\frac{1}{g_2(0,z)}dz - T_R\right)\right)\right] \to 0$$

which contradicts Eq. (3.36). So there must exist $\bar{\Lambda} > 0$ such that for all $R > 1$, $\lambda_R < \bar{\Lambda}$. Moreover, analogous to Step 3, if we differentiate Eq. (3.28) in the sense of distributions with respect to R, we obtain

$$\partial_R \mu_\lambda^R = \left\langle \nu_\lambda^R, \left(\partial_R \mathcal{G}_\lambda^R\right)\eta_\lambda^R\right\rangle.$$

Again, the definition $\mathcal{G}_\lambda^R$ gives us that this derivative can be computed in the strong sense.

Indeed, for any positive continuous function $f : [0, R] \to \mathbb{R}_+$ we have

$$\begin{aligned}
&\partial_R \mathcal{G}_\lambda^R f(y) \\
&= \frac{\partial}{\partial R} \int_0^R f(z) \int_0^\infty \left(k(\varphi^t(0,y), z) + \frac{\int_R^\infty k(\varphi^t(0,y), \zeta) d\zeta}{R} \right) \psi(t|(0,y)) e^{-\lambda t} dt dz \\
&= f(R) \left(\int_0^\infty \left(k(\varphi^t(0,y), R) + \frac{\int_R^\infty k(\varphi^t(0,y), \zeta) d\zeta}{R} \right) \psi(t|(0,y)) e^{-\lambda t} dt \right) \\
&\quad - \int_0^R f(z) \int_0^\infty \frac{1}{R} \left(k(\varphi^t(0,y), R) + \frac{\int_R^\infty k(\varphi^t(0,y), \zeta) d\zeta}{R} \right) \psi(t|(0,y)) e^{-\lambda t} dt dz \\
&= \left(\int_0^R \frac{f(R) - f(z)}{R} dz \right) \\
&\quad \times \left(\int_0^\infty \left(k(\varphi^t(0,y), R) + \frac{\int_R^\infty k(\varphi^t(0,y), \zeta) d\zeta}{R} \right) \psi(t|(0,y)) e^{-\lambda t} dt \right),
\end{aligned}$$

which is positive whenever f is an increasing function. Since Eq. (3.35) gives that for every fixed λ, $\eta_\lambda^R(y)$ is increasing in y, then $\left(\partial_R \mathcal{G}_\lambda^R\right) \eta_\lambda^R > 0$ and therefore $\partial_R \mu_\lambda^R > 0$. In particular, the sequence of λ_R, which is defined as the values of λ such that $\mu_\lambda^R = 1$, is then also increasing in R.

Step 6 : Identification of the limit

Step 5 gives that $(\lambda_R)_R$ is an increasing bounded sequence as $R \to \infty$, so with a limit written $\lambda > 0$. Moreover, for each λ_R exists a unique h_R associated, defined by Eq. (3.31). The family of h_R is equibounded and equicontinuous thanks to Eq. (3.33), Eq. (3.35) and the bound on λ_R. Note indeed that Eq. (3.35) depends on R only through λ_R. We can therefore extract a subsequence converging to some (λ, h) as $R \to \infty$. We must now check that (λ, h) is a good pair of eigenelements, which we do by dominated convergence. In Step 4 we have constructed h_R such that it is solution to Equations (3.32) and (3.33) which we repeat below to justify each limit.

$$\begin{cases}
h_R(\mathbf{x}) = C_\mathbf{x}\, \mathbb{E}_\mathbf{x} \left[\eta_R(Z_R) e^{-\lambda_R T_R} \mathbb{1}_{Z_R \leq R} \right] & \forall \mathbf{x} \in \mathcal{X} \\
h_R(0,y) = \eta_R(y) & \forall y \in (0,R) \\
h_R(\varphi^t(\mathbf{x})) \underset{t\to\infty}{\sim} \exp\left(\int_0^t \beta(\varphi^s(\mathbf{x})) ds + \lambda_R t \right)
\end{cases}$$

The normalisation constant $C_\mathbf{x}$ is already the one required in the limit case. For the expectation term, recalling from Eq. (3.35) that

$$\frac{\eta_R(y_2)}{\eta_R(y_1)} = \exp\left(\lambda_R \int_{y_1}^{y_2} \frac{1}{g_2(0,z)} dz \right)$$

and using Eq. (3.38) in Step 5, we deduce that for all $y \in (0, R)$,

$$\eta_R(Z_R) e^{-\lambda_R T_R} \leq \eta_R(y) \quad \mathbb{P}_{(0,y)}\text{-a.s.}$$

Therefore for all $R > 1$,

$$\mathbb{E}_{(a,y)}\left[\eta_R(Z_R)e^{-\lambda_R T_R}\mathbb{1}_{Z_R\leq R}\right] \leq \eta_R(y) < +\infty$$

and we can pass to the limit under the expectations and conclude that the limit h and λ verify the renewal formula

$$h(\mathbf{x}) = C_{\mathbf{x}}\,\mathbb{E}_{\mathbf{x}}\left[h(0,Z)e^{-\lambda T}\right] \quad \forall \mathbf{x}\in\mathcal{X}$$

which is Eq. (3.16) and is equivalent to Eq. (3.14). Thus, by Lemma 4.2 the couple (λ, h) is almost everywhere solution to $\mathcal{Q}h = \lambda h$.

□

Remark 3.4.7. The assumption $\beta(0,\cdot)\equiv 0$ is crucial for the characterisation of h in Step 4 of the proof of Proposition 3.4.1. The case $\beta(0,x) > 0$ could possibly be treated, but it would require additional assumptions in order to have $a \mapsto K_\lambda^R(a,x,z) \in W^{1,1}_{loc}(\mathbb{R}_+)$ and to then control the age derivatives of the kernel K_λ^R. Then, Eq. (3.34) would be a scalar transport equation for h_λ^R, which thereby admits an elliptic maximum principle. Nonetheless, the assumption $\beta(0,\cdot)\equiv 0$, while being perfectly biologically meaningful, allows us to avoid this technicalities.

3.5 Petiteness of compact sets for sampled chains

We want to prove the following Doeblin petite-set condition for all the compact sets of $\mathcal{X}$.

Proposition 3.5.1. *Let P_t be the Markov process characterised by the infinitesimal generator $\mathcal{A}$ defined by Eq. (3.10). If Assumptions 3.3.3 are verified, then every compact $\mathscr{K}\subset\mathbb{R}_+^2$ is a petite-set for some skeleton chain of P_t. This is, there is a non-trivial discrete sampling measure μ over $\mathbb{R}_+$ and a non-trivial measure ν over $\mathbb{R}_+^2$ such that*

$$\langle \mu, \delta_{\mathbf{x}} P.f\rangle = \int_0^\infty P_t f(\mathbf{x})\mu(dt) \geq \langle \nu, f\rangle \quad \forall \mathbf{x}\in\mathscr{K}$$

Before the proof we will introduce some useful lemmas. First, we recall Duhamel formula (3.39), which describes the trajectories driven by the semigroup P_t and allows us to extend the definition of the semigroup as the mild solution of an iterative evolution equation.

Lemma 3.5.2 (Duhamel formula)**.** *For all $\mathbf{x}\in\mathcal{X}$, $f\in C_b^{1,1}(\mathcal{X})$, P_t is the mild solution to*

$$\begin{aligned} P_t f(\mathbf{x}) =& f\left(\varphi^t(\mathbf{x})\right)\exp\left(-\int_0^t \beta\left(\varphi^s(\mathbf{x})\right)ds\right) \\ &+ \int_0^t \psi(s|\mathbf{x})\int_0^\infty P_{t-s}f(0,z)\frac{h(0,z)k\left(\varphi^s(\mathbf{x}),z\right)}{\int_0^\infty h(0,z')k\left(\varphi^s(\mathbf{x}),z'\right)dz'}dzds, \end{aligned} \tag{3.39}$$

Proof. A classical probabilistic proof consists in writing $P_t f(\mathbf{x})$ conditionally to the occurrence of the first jump. It is also possible to prove it by means of a variation of parameters method, as in Corollary 1.7 from [51], for example. Here we provide the probabilistic proof. Let X a Markov process whose law is given by generator $\mathcal{A}$ defined in Eq. (3.10). Recall from definition 3.3.2 the random variables T and Z which represent the time of the first jump and the new size after the first jump. Note however that the transition kernel of the Markovian generator $\mathcal{A}$ has been rescaled, so that the joint law of (T, Z) under $\mathbb{P}_{\mathbf{x}}$ is from now on given by the density function

$$p_{\mathbf{x}}(t,z) = \psi(t|\mathbf{x}) \cdot \frac{\beta(\mathbf{x})\frac{h(0,z)}{h(\mathbf{x})}k(\varphi^t(\mathbf{x}),z)}{\int_0^\infty \beta(\mathbf{x})\frac{h(0,z')}{h(\mathbf{x})}k(\varphi^t(\mathbf{x}),z')dz'} = \psi(t|\mathbf{x}) \cdot \frac{h(0,z)k\left(\varphi^s(\mathbf{x}),z\right)}{\int_0^\infty h(0,z')k\left(\varphi^s(\mathbf{x}),z'\right)dz'}$$

where the probability density of the transition $\mathbf{x} \mapsto (0,z)$ is computed as the ratio between the transition rate of $\mathbf{x} \mapsto (0,z)$ and the total transition rate, as described by the generator $\mathcal{A}$. Hence, by conditioning on T under $\mathbb{P}_{\mathbf{x}}$ and using the strong Markov property of X, we have:

$$\begin{aligned}
P_t f(\mathbf{x}) = \mathbb{E}\left[\mathbf{x}\right] f(X_t) =& \mathbb{E}\left[\mathbf{x}\right] f(X_t)\mathbb{1}_{T>t} + \mathbb{E}\left[\mathbf{x}\right] f(X_t)\mathbb{1}_{T\leq t} \\
=& \mathbb{E}\left[\mathbf{x}\right] f(X_t)|T>t\mathbb{P}_{\mathbf{x}}(T>t) + \mathbb{E}\left[\mathbf{x}\right]\mathbb{E}\left[\mathbf{x}\right] f\left(X_t\right)|T\mathbb{1}_{T\leq t} \\
=& \mathbb{E}\left[\mathbf{x}\right] f(X_t)|T>t\mathbb{P}_{\mathbf{x}}(T>t) + \mathbb{E}\left[\mathbf{x}\right]\mathbb{E}\left[(0,Z)\right] f(X_{t-T})\mathbb{1}_{T\leq t} \\
=& f\left(\varphi^t(\mathbf{x})\right)\exp\left(-\int_0^t \beta\left(\varphi^s\left(\mathbf{x}\right)\right)ds\right) \\
&+ \int_0^t \psi(s|\mathbf{x})\int_0^\infty P_{t-s}f(0,z)\frac{h(0,z)k\left(\varphi^s(\mathbf{x}),z\right)}{\int_0^\infty h(0,z')k\left(\varphi^s(\mathbf{x}),z'\right)dz'}dzds.
\end{aligned}$$

□

We can give now the proof of Proposition 3.5.1:

Proof of Proposition 3.5.1. Let $\mathbf{x} \in \mathscr{K}$ compact such that $\mathscr{K} \subset [\underline{a},\bar{a}] \times [\underline{y},\bar{y}]$. We iterate once Duhamel's formula (3.39), using the positivity of P_t:

$$\begin{aligned}
P_t f(\mathbf{x}) =& f\left(\varphi^t(\mathbf{x})\right)\exp\left(-\int_0^t \beta\left(\varphi^s\left(\mathbf{x}\right)\right)ds\right) \\
&+ \int_0^t \psi(s|\mathbf{x})\int_0^\infty \frac{h(0,z)k\left(\varphi^s(\mathbf{x}),z\right)}{\int_0^\infty h(0,z')k\left(\varphi^s(\mathbf{x}),z'\right)dz'}\Bigg\{ \\
&\quad f\left(\varphi^{t-s}(0,z)\right)\exp\left(-\int_0^{t-s} \beta\left(\varphi^s\left((0,z)\right)\right)ds\right) \\
&\quad + \int_0^{t-s} \psi(u|\mathbf{x})\int_0^\infty P_{t-s-u}f(0,\xi)\frac{h(0,\xi)k\left(\varphi^u(0,z),\xi\right)}{\int_0^\infty h(0,\xi')k\left(\varphi^u(0,z),\xi'\right)d\xi'}d\xi du\Bigg\}dzds \\
\geq& \int_0^t \psi(s|\mathbf{x})\int_0^\infty f\left(\varphi^{t-s}\left(0,z\right)\right)\exp\left(-\int_0^{t-s} \beta\left(\varphi^s\left((0,z)\right)\right)ds\right) \\
&\quad \frac{h(0,z)k\left(\varphi^s(\mathbf{x}),z\right)}{\int_0^\infty h(0,z')k\left(\varphi^s(\mathbf{x}),z'\right)dz'}dzds
\end{aligned} \tag{3.40}$$

To obtain the desired result we aim to solve two crucial steps:

i. First, to prove the existence of some C^1-diffeomorphism which could allow us to change variables inside the latter integral as to obtain a measure over $\mathcal{X}$.

ii. Second, to bound from below the resulting integral uniformly for every $\mathbf{x} \in \mathscr{K}$, using its compactness.

Fix some final time $t \geq 0$, and define $\gamma_t : \mathcal{X} \to \mathcal{X}$ as

$$\gamma_t(s, z) := \varphi^{t-s}(0, z).$$

We show first that it's a differentiable function. Fix s, z and suppose

$$(a, y) = \gamma_t(s, z).$$

Then the function u defined as $u(s) = \gamma_t(s, z)$ is the unique solution to the Initial Value Problem

$$\begin{cases} u'(s) &= -g(u(s)), \ s \leq t \\ u(0) &= (a, y) \end{cases}$$

Thus, $\partial_s \gamma_t(s, z) = -g(u(s))$. Moreover, by Lemma 3.3.1, the smoothness of the vector field g and the fact that the ODE system is autonomous gives the smoothness of the flow with respect to the initial condition. Thus, the Jacobian matrix of γ_t equals for all $s \leq t$ and $z > 0$:

$$\mathcal{D}\gamma_t(s, z) = \left[-g\left(\varphi^{t-s}(0, z)\right) \qquad \partial_z \varphi^{t-s}(0, z)\right], \tag{3.41}$$

where, from Lemma 3.3.1-2, the derivative of the flow with respect to the initial size is given by

$$\partial_z \varphi^t(0, z) = \exp\left(\int_0^t \mathcal{D}g\left(\varphi^s(0, z)\right) ds\right) \begin{pmatrix} 0 \\ 1 \end{pmatrix}.$$

where we recall that $\mathcal{D}g$ stands for the Jacobian matrix of g and $\exp(\cdot)$ is an exponential matrix. Moreover, let $r \mapsto Y_{(a,y)}(r)$ be the unique orbit of the vector field g passing trough the point (a, y). Its is straightforward that $z = Y_{(a,y)}(0)$, so that the inverse of γ_t is given for all $(a, y) \in \mathbb{R}^2_+$ by

$$\gamma_t^{-1}(a, y) = \left(t - \phi^{-1}_{0, Y_{(a,y)}(0)}(a, y)\ ,\ Y_{(a,y)}(0)\right).$$

Fig. 3.2 summarises graphically the change of variables and the definition of γ_t^{-1}. Given $a, y, \mathbf{x}$ and t, the inversion of γ consists in determinating the value of ordinate z when the integral curve flowing towards (a, y) hits the y-axis and the time $t - s$ required to go from this point to (a, y). Since $Y_{(a,y)}$ (green line) is known, the inversion is direct. We conclude

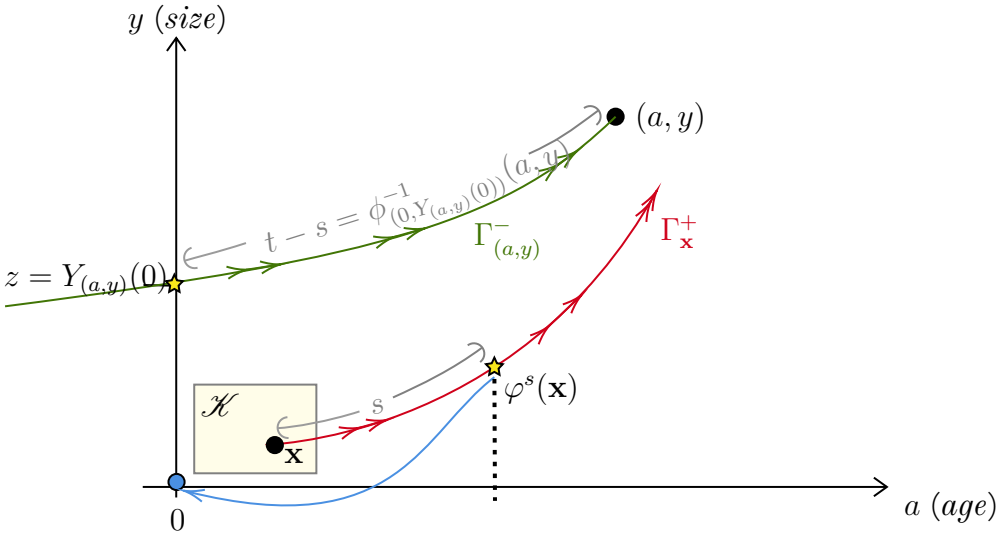

Figure 3.2: Graphical description of the change of variables defined by γ_t

that γ_t is a C^1-diffeomorphism and then performing the change of variables $(a, y) = \gamma_t(s, z)$ in the RHS of Eq. (3.40) gives

$$P_t f(\mathbf{x}) \geq \int_{\mathbb{R}_+^2} f(a,y) \Bigg\{ \psi\left(t - \phi^{-1}_{0,Y_{(a,y)}(0)}(a,y)|\mathbf{x}\right) \exp\left(-\int_0^{\phi^{-1}_{0,Y_{(a,y)}(0)}(a,y)} \beta\left(\varphi^s\left((0,Y_{(a,y)}(0)\right)\right)\right) ds\right) \frac{h(0,Y_{(a,y)}(0))k\left(\varphi^{t-\phi^{-1}_{0,Y_{(a,y)}(0)}(a,y)}(\mathbf{x}), Y_{(a,y)}(0)\right)}{\int_0^\infty h(0,z)k\left(\varphi^{t-\phi^{-1}_{0,Y_{(a,y)}(0)}(a,y)}(\mathbf{x}), z\right) dz} \frac{1}{\left|\det \mathcal{D}\gamma_t\left(\gamma_t^{-1}(a,y)\right)\right|} \mathbb{1}_{\phi^{-1}_{0,Y_{(a,y)}(0)}(a,y) \leq t} \Bigg\} da\, dy. \tag{3.42}$$

Now, using Assumptions 3.3.3, we can bound the functions and the Jacobian found in the obtained integral. First, since $g \geq 0$, note that $||\varphi^t(\mathbf{x})|| \geq ||\varphi^s(\mathbf{x})||$ for all $t > s$. Second, $\beta_- g_1(\mathbf{x}) \leq \beta(\mathbf{x}) \leq \beta_+ g_1(\mathbf{x})$. And third, by the definition of the flow, $\int_0^t g_1\left(\varphi^s\left(\mathbf{x}\right)\right) = \varphi_1^t(\mathbf{x})$ which equals the age at time t of an individual with trait $\mathbf{x}$ at time 0. Then, recalling that $\mathscr{K} \subset [\underline{a}, \bar{a}] \times [\underline{y}, \bar{y}]$, for all $t > 0$ we obtain the following bounds:

i. For all $(a_0, y_0) \in \mathscr{K}$, using the superior bounds on g_1 from Assumptions 3.3.3-i. we have

$$\varphi_1^t(a_0,y_0) = a_0 + \int_0^t g_1(\varphi^s(a_0,y_0))ds \leq a_0 + \int_0^t c_1(1 + \varphi_1^s(a_0,y_0))ds$$

Hence, by Gronwall inequality

$$\varphi_1^t(a_0, y_0) \leq (a_0 + c_1 t)\, e^{c_1 t} \leq (\bar{a} + c_1 t)\, e^{c_1 t}$$

Analogously, using the lower bounds on g_1 from Assumptions 3.3.3-i., we obtain

$$\varphi_1^t(a_0, y_0) \geq a_0 e^{c_0 t} \geq \underline{a} e^{c_0 t}$$

ii. From the previous result, for all $\mathbf{x} \in \mathscr{K}$

$$\exp\left(-\int_0^t \beta\left(\varphi^s\left(\mathbf{x}\right)\right) ds\right) \geq \exp\left(-\beta_+ \int_0^t g_1(\varphi^s(\mathbf{x}))ds\right) = e^{-\beta_+ \varphi_1^t(\mathbf{x})}$$
$$\geq e^{-\beta_+(\bar{a}+c_1 t)e^{c_1 t}},$$

iii. Analogously

$$\beta(\varphi^t(\mathbf{x})) \geq \beta_- g_1(\varphi^t(\mathbf{x})) \geq \beta_- c_0 \varphi_1^t(\mathbf{x}) \geq \beta_- c_0 \underline{a} e^{c_0 t}.$$

Therefore there are some constants $A_0, B_0 > 0$ such that

$$\psi\left(t - s|\mathbf{x}\right) \geq A_0 \exp\left(-B_0(1 + t - s)e^{c_1(t-s)}\right) \tag{3.43}$$

iv. Moreover, recall that the eigenfunction h is solution to Eq. (3.14). Then, by Fubini's Theorem, for all $\mathbf{x} \in \mathscr{K}$,

$$h(\mathbf{x}) = \int_0^\infty \left(\int_0^\infty h(0, z) k\left(\varphi^t(\mathbf{x}), z\right) dz\right) \psi(t|\mathbf{x}) e^{-\lambda t} dt.$$

Thus, in particular, the integrability gives us that

$$\left(\int_0^\infty h(0, z) k\left(\varphi^t(\mathbf{x}), z\right) dz\right) \frac{\psi(t|\mathbf{x})e^{-\lambda t}}{h(\mathbf{x})} \to 0 \quad \text{as } t \to +\infty.$$

Therefore, there exist some constants $C_1, C_2 > 0$ such that for all $\mathbf{x} \in \mathscr{K}$ there is some time $T(\mathbf{x}) > 0$ such that for all $t > 0$ we have

$$\left(\int_0^\infty h(0, z) k\left(\varphi^t(\mathbf{x}), z\right) dz\right) \frac{\psi(t|\mathbf{x})e^{-\lambda t}}{h(\mathbf{x})} \leq C_1 \mathbb{1}_{t \geq T(\mathbf{x})} + C_2 \mathbb{1}_{t < T(\mathbf{x})}$$

where

$$\sup_{\mathbf{x} \in \mathscr{K}} \sup_{t < T(\mathbf{x})} \left(\int_0^\infty h(0, z) k\left(\varphi^t(\mathbf{x}), z\right) dz\right) \frac{\psi(t|\mathbf{x})e^{-\lambda t}}{h(\mathbf{x})} \leq C_2,$$

since the suprema are taken in a compact set and for a continuous locally bounded function. Then, taking $C_0 = \max\{C_1, C_2\}$ we have

$$\frac{1}{\int_0^\infty h(0, z) k\left(\varphi^t(\mathbf{x}), z\right) dz} \geq \frac{\psi(t|\mathbf{x})e^{-\lambda t}}{C_0 h(\mathbf{x})}$$

where $\psi(t|\mathbf{x})$ can again be bounded by below using Eq. (3.43). Moreover, the continuity of h implies that h is locally bounded and hence, for all $\mathbf{x} \in \mathscr{K}$, $h(\mathbf{x}) \leq H_0 < \infty$. Hence we obtain finally

$$\frac{1}{\int_0^\infty h(0,z)k\left(\varphi^t(\mathbf{x}),z\right)dz} \geq \frac{A_0}{C_0 H_0}\exp\left(-B_0(1+t)e^{c_1 t} - \lambda t\right) \tag{3.44}$$

Note that these three estimates give bounds which are dependent only on t.

v. From (3.41), for all $s \leq t$ and $z > 0$, the Jacobian determinant equals

$$\det \mathcal{D}\gamma_t(s,z) = ||g\left(\varphi^{t-s}(0,z)\right)||\,||\nabla_z \varphi^{t-s}(0,z)||\sin\theta(s,t,z) \tag{3.45}$$

where $\theta(s,t,z)$ is the angle between $g\left(\varphi^{t-s}(0,z)\right)$ and $\nabla_z\varphi^{t-s}(0,z)$. Hence, from Lemma 3.3.1.2, we get

$$\left|\det \mathcal{D}\gamma_t\left(s,z\right)\right| \leq ||g\left(\varphi^{t-s}(0,z)\right)||\;\left|\left|\left|\mathcal{D}\varphi^{t-s}\left(0,z\right)\right|\right|\right|,$$

where $|||\cdot|||$ is the matrix norm induced by $||\cdot||$, and therefore

$$\begin{aligned}\left|\det \mathcal{D}\gamma_t\left(\gamma_t^{-1}(a,y)\right)\right| &\leq ||g(a,y)||\left|\left|\left|\mathcal{D}\varphi^{\phi^{-1}_{0,Y_{(a,y)}(0)}(a,y)}\left(0,Y_{(a,y)}(0)\right)\right|\right|\right| \\ &=: ||g\left(a,y\right)||E_0(a,y)\end{aligned} \tag{3.46}$$

Note that this bound depends only on (a,y) and neither on $\mathbf{x}$ or t.

Hence, coming back to Eq. (3.42) and applying the bounds (3.43), (3.44) and (3.44) to the integrands, we obtain

$$\begin{aligned}P_t f(\mathbf{x}) \geq \int_{\mathbb{R}_+^2} f(a,y)\Bigg\{ &\frac{A_0^2}{C_0 H_0}\exp\left(-2B_0(1+t)e^{c_1 t} - \lambda t\right) \\ &\exp\left(-\int_0^{\phi^{-1}_{0,Y_{(a,y)}(0)}(a,y)} \beta\left(\varphi^s\left(0,Y_{(a,y)}(0)\right)\right)ds\right) \\ &h(0,Y_{(a,y)}(0))k\left(\varphi^{t-\phi^{-1}_{0,Y_{(a,y)}(0)}(a,y)}(\mathbf{x}),Y_{(a,y)}(0)\right) \\ &\frac{1}{||g\left(a,y\right)||E_0(a,y)}\mathbb{1}_{\phi^{-1}_{0,Y_{(a,y)}(0)}(a,y)\leq t}\Bigg\}\,da\,dy.\end{aligned} \tag{3.47}$$

Now, we make use of the petite-set condition which allows us to average the value of $P_t f(\mathbf{x})$ against a discrete sampling measure $\mu(dt)$ over a Δ-skeleton. This is, consider some $\Delta > 0$, which will be fixed later on, and a measure μ over $\{j\Delta : j \in \mathbb{N}\}$, characterised by a sequence $(\mu_j)_{j\in\mathbb{N}}$ with $\sum \mu_j = 1$ and $\mu_j > 0$ for all $j \in \mathbb{N}$. We have

$$\begin{aligned}\langle \mu, \delta_{\mathbf{x}} P.f\rangle \geq \sum_{j=0}^\infty \mu_j \int_{\mathcal{X}} f(a,y)\; &k\left(\varphi^{j\Delta-\phi^{-1}_{0,Y_{(a,y)}(0)}(a,y)}(\mathbf{x}),Y_{(a,y)}(0)\right) \\ &\zeta(a,y)e^{-\tilde{\beta}j\Delta e^{j\Delta}}\mathbb{1}_{\phi^{-1}_{0,Y_{(a,y)}(0)}(a,y)\leq j\Delta}\,da\,dy,\end{aligned}$$

where the the function $\zeta(a,y)$ is constructed by regrouping all the terms which depend only on (a,y) (and neither on $\mathbf{x}$ or t), and the constant $\tilde{\beta}>0$ is obtained after selecting only the dominant term inside the exponential. Now, it remains to loose the dependency on $\mathbf{x}$ using that $\mathbf{x}\in\mathscr{K}$ to find a uniform lower bound for the whole compact. By Assumption 3.3.3-(iv), we have that for all z, exists $D(z)\subset\mathbb{R}_+$ such that $k(\varphi^s(\mathbf{x}),z)>\varepsilon(z)\mathbb{1}_{D(z)}(\varphi^s(\mathbf{x}))$. Then, let

$$\mathcal{T}(\mathbf{x},z):=\{s>0:\varphi^s(\mathbf{x})\in D(z)\},$$

then

$$k(\varphi^s(\mathbf{x}),z)>\varepsilon(z)\mathbb{1}_{\mathcal{T}(\mathbf{x},z)}(s).$$

Now, let $\Delta=\inf_{z>0}\operatorname{diam}(D(z))>\delta_->0$. Then, for all $\mathbf{x}\in\mathscr{K}$ and $z>0$ there exists $n=n(\mathbf{x},z)\in\mathbb{N}$ such that $n\Delta\in\mathcal{T}(\mathbf{x},z)$. Then for all $\mathbf{x}\in\mathscr{K}$ and $z>0$,

$$\sum_{j=0}^{\infty}\mathbb{1}_{j\Delta\in\mathcal{T}(\mathbf{x},z)}\geq 1.$$

Moreover, since for all $z>0$, $\operatorname{diam}(D(z))<\delta_+$, there exists some j big enough such that the trajectory leaves $D(z)$. In particular, the compactness of $\mathscr{K}$ implies that it exists j^* such that for all $\mathbf{x}\in\mathscr{K}$

$$\mathbb{1}_{j\Delta\in\mathcal{T}(\mathbf{x},z)}=0\ \ \forall j\geq j^*.$$

Therefore for any sampling measure $(\mu_j)_j$ we have

$$\sum_{j=0}^{\infty}\mu_j\mathbb{1}_{j\Delta\in\mathcal{T}(\mathbf{x},z)}\geq\min_{j\leq j^*}\mu_j,$$

and finally for all fixed $\tau>0$,

$$\begin{aligned}\sum_{j=0}^{\infty}\mu_j e^{-\tilde{\beta}j\Delta e^{j\Delta}}k\left(\varphi^{j\Delta-\tau}(\mathbf{x}),z\right)\mathbb{1}_{\tau\leq j\Delta}&\geq\sum_{j=0}^{\infty}\mu_j e^{-\tilde{\beta}j\Delta e^{j\Delta}}\epsilon(z)\mathbb{1}_{j\Delta-\tau\in\mathcal{T}(\mathbf{x},z)}\\&\geq\epsilon(z)\min_{j\leq j^*}\mu_j\ \min_{j\leq j^*}e^{-\tilde{\beta}j\Delta e^{j\Delta}}\end{aligned}$$

from what we can conclude that

$$\langle\mu,\delta_{\mathbf{x}}P.f\rangle\geq\int_{\mathcal{X}}f(a,y)\nu(a,y)dady$$

with

$$\nu(a,y)=\zeta(a,y)\epsilon\left(Y_{(a,y)}(0)\right)e^{-\tilde{\beta}j^*e^{\Delta j^*\Delta}}\min_{j\leq j^*}\mu_j$$

□

Finally, the proof of the main theorem 3.2.4 is a direct application of Harris Theorem 3.2.1.

3.6 Application: Steady-state size distribution of the adder model of bacterial proliferation

We recall the generator of the adder model of *E. coli* growth introduced in Example 3.1.1:

$$\begin{aligned}\mathcal{Q}f(a,y) =& \lambda y\left(\partial_a + \partial_y\right) f(a,y) \\ &+ \lambda y B(a)\left(2\int_0^1 f(0,\rho y)F(\rho)d\rho - f(a,y)\right) - d_0 f(a,y).\end{aligned}$$

We assume that:

Assumptions 3.6.1. Suppose

(A1) There exist $0 < \underline{b} \leq \bar{b} < \infty$ such that for all $a \geq 0$, $\underline{b} < B(a) < \bar{b}$.

(A2) F is a continuous positive function in $[0,1]$, with connected support. We call for all $k \geq 0$,

$$m_k = \int_0^1 \rho^k F(\rho)d\rho$$

and suppose that $m_0 = 1$, $m_1 = 1/2$ and $m_2 < +\infty$. Note that, since $\rho \in (0,1)$ almost surely, then for all $k > 0$ we have $m_k \leq m_1 = 1/2$.

(A3) $\lambda > d_0$.

Remark 3.6.2 (Doob h-transform.)**.** In this case, it is straightforward to verify that $h(a,y) = y$ is an eigenfunction of $\mathcal{Q}$ associated to eigenvalue $\Lambda = \lambda - d_0$. In particular, from Eq. (3.10) the Doob h-transformed semigroup P_t is generated by the conservative infinitesimal generator

$$\mathcal{A}f(a,y) = \lambda y\left(\partial_a + \partial_y\right) f(a,y) + 2\lambda y B(a)\int_0^1 \left(f(0,\rho y) - f(a,y)\right)\rho F(\rho)d\rho. \tag{3.48}$$

Indeed, the rescaled kernel gives

$$\frac{h(0,z)}{h(a,y)}k(a,y,z) = 2\frac{z}{y}\cdot\frac{1}{y}F\left(\frac{z}{y}\right)\mathbb{1}_{z\leq y},$$

which under the change of variables $z \mapsto \rho = z/y$ gives the probability density $\rho \mapsto 2\rho F(\rho)$ supported in $[0,1]$, which is indeed a probability by Assumption (A2).

Then, we have the following result of exponential convergence, that completes the analysis started by [62] from an operator theory approach, where exponential convergence could not be obtained from the estimates of relative entropy.

Theorem 3.6.3. *Under Assumptions (A1)-(A3), there is a unique probability measure π^* such that there exist constants $C, \omega > 0$ which verify Eq. (3.11) with $\Lambda = \lambda - d_0$, $h(a,y) = y$ and $V(a,y) = y^{-1} + y$. Moreover π^* admits a density given explicitly by*

$$\pi^*(a,y) = \frac{\exp\left(-\int_0^a B(\alpha)d\alpha\right)}{y^2}\eta^*(y-a),$$

where η^* is the unique solution to the fixed point problem

$$\eta^*(y) = 2\int_0^1 \left\{ \int_0^{\frac{x}{\rho}} \psi\left(\frac{y}{\rho} - z\right)\eta^*(z)\,dz \right\} F(\rho)d\rho,$$

where $\psi(a) = B(a)\exp\left(-\int_0^a B(\alpha)d\alpha\right)$.

Proof. 1. **Minorisation condition.** It is a direct application of Proposition 3.5.1, since the same hypothesis in Assumptions 3.3.3 are verified by Assumptions 3.6.1. Assumption 3.6.1-(v) requires some attention. Indeed, since F is bounded and with connected support, $k(a,y,z) = \frac{1}{y}F\left(\frac{z}{y}\right)\mathbb{1}_{z\leq y}$ can be lower bounded in the form $k(a,y,z) > \varepsilon(z)\mathbb{1}_{y\in D(z)}$, with $\varepsilon(z)$ of order $1/z$, as represents the example of Fig. 3.3.

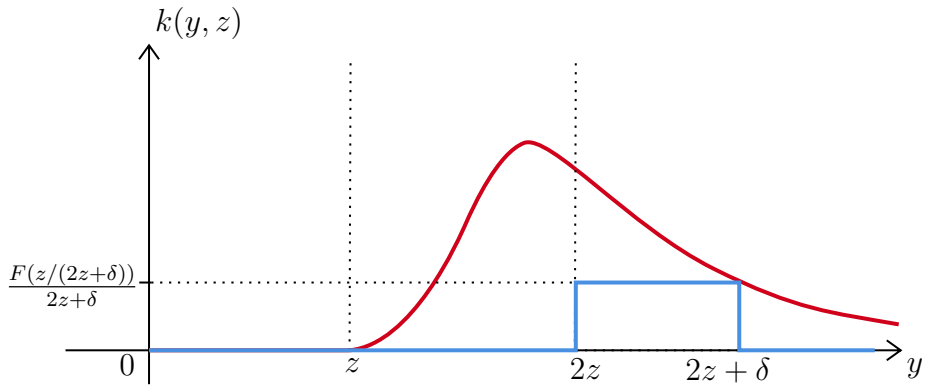

Figure 3.3: Example of minorisation for $k(a,y,z) = \frac{1}{y}F\left(\frac{z}{y}\right)\mathbb{1}_{z\leq y}$ and F given by the probability density function of a Beta distribution. Then we have $k(a,y,z) > \varepsilon(z)\mathbb{1}_{y\in D(z)}$ as required by Assumption 3.3.3-(v), with $|D(z)| = \delta$ for all z.

In general, we have for all $\delta > 0$:

$$k(a,y,z) > \min_{z'\in[2z,2z+\delta]} \frac{F(z/z')}{z'}\,\mathbb{1}_{y\in[2z,2z+\delta]}$$

and we verify then Assumption 3.3.3-(v) with $\varepsilon(z) = \min_{z'\in[2z,2z+\delta]} \frac{F(z/z')}{z'}$ and $D(z) = [2z, 2z+\delta]$ for a chosen $\delta > 0$.

Fig. 3.4 shows the characteristics curves $y - a =$ constant, and the shadowed region corresponds the space that is a priori reachable from the initial point along trajectories with exactly one jump before time t. It is the version of Fig. 3.2 in this specific case.

Moreover, given an initial point (A in Fig. 3.2) and total trajectory time, this reachable region is compact, which also simplifies some minorisations.

Finally, depending on the choice of the compact set $\mathscr{K} \subset [\underline{a}, \bar{a}] \times [\underline{y}, \bar{y}]$ and of δ (which gives also the discretisation timeStep of the δ-skeleton), the value of the minorant measure ν can be computed explicitly by numerical approximations, as given in Fig. 3.5 for different forms of F.

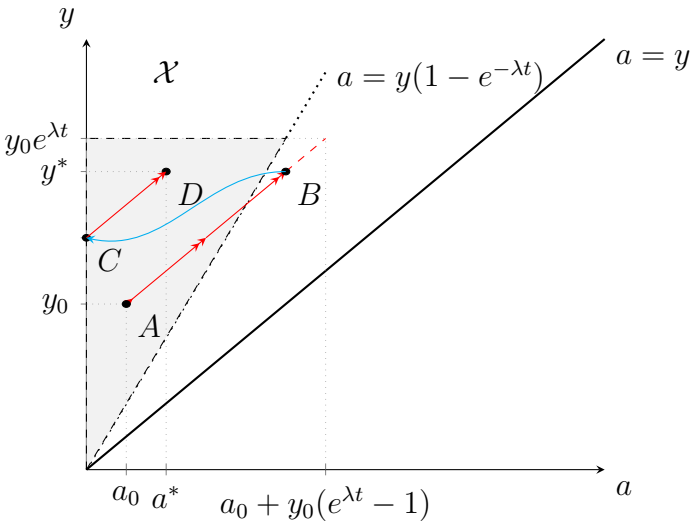

Figure 3.4: Ideal trajectory from initial point $A = (a_0, y_0)$ to point $D = (a^*, y^*)$ in time t. The individual spends a time $t - s$ growing from A to B. Then, it divides and renews at point C. Finally, it grows the remaining time s until point D.

2. **Lyapunov-Foster condition.** Consider the generator $\mathcal{A}$ defined by Eq. (3.48). Let $V(a, y) = y^{-1} + y$ with. It is clear that $V(a, y) \to \infty$ as $|(a, y)| \to \infty$. Let $v(a, y) = y^k$, then

$$\begin{aligned}\mathcal{A}v(a, y) &= \lambda y^k + 2\lambda y B(a) \int_0^1 \left(\rho^k y^k - y^k\right) \rho F(\rho) d\rho \\ &= \left(k\lambda + 2\left(m_{k+1} - \frac{1}{2}\right)\lambda y B(a)\right) v(a, y)\end{aligned}$$

So, for $V(a, y) = y^{-1} + y$, we obtain

$$\mathcal{A}V(a, y) = -\lambda V(a, y) + \Delta(a, y),$$

where

$$\Delta(a, y) := 2\lambda y + 2\lambda B(a)\left(\left(\frac{1}{2} + \left(m_2 - \frac{1}{2}\right) y^2\right)\right).$$

We already have $-\lambda < 0$ in the first term of the RHS. It remains to prove that $\Delta(a, y)$ defined in the RHS above, is bounded. Indeed, notice that

$$\Delta(a, y) \leq 2\lambda\left(\bar{b}\left(m_2 - \frac{1}{2}\right) y^2 + y + \frac{\bar{b}}{2}\right)$$

which is quadratic in y with a negative quadratic coefficient since $m_2 - 1/2 \leq 0$. Thus

$$\mathcal{A}(a,y) \leq \lambda \left(\bar{b} + \frac{1}{\bar{b}(1-2m_2)} \right) =: d \in \mathbb{R}_+ \tag{3.49}$$

So finally we obtain that for every $(a,y) \in \mathbb{R}_+^2$

$$\mathcal{A}V(a,y) \leq -\lambda V(a,y) + d$$

3. **Application of V-uniform Ergodic Theorem** Using Theorem 3.2.1 we conclude the existence of some $C, \omega > 0$ such that for every $\mathbf{x} \in \mathcal{X}$ and $t \geq 0$

$$||\delta_{\mathbf{x}} P_t - \pi||_V \leq CV(\mathbf{x}) \exp(-\omega t) \tag{3.50}$$

Now, using that by construction, $M_t f = e^{\Lambda t} h P_t (f/h)$, we obtain that for all $\mathbf{x} \in \mathcal{X}$,

$$||e^{-\Lambda t} \delta_{\mathbf{x}} M_t - h(\mathbf{x})\pi^*||_V \leq CV(\mathbf{x}) e^{-\omega t} \tag{3.51}$$

where for every $A \in \mathcal{B}(\mathbb{R}_+^2 \setminus \{0\})$,

$$\pi^*(A) = \int_A \frac{\pi(d\mathbf{x})}{h(\mathbf{x})}$$

Moreover, we know that $h(a,y) = y$. On the other hand, π is the unique solution to $\pi P_t = \pi$, or equivalently, to the dual eigenvalue problem associated to the conservative problem $\pi \mathcal{A} = 0$. From (3.10) we obtain from the latter that π is then the measure solution to the following PDE in the sense of distributions

$$\begin{cases} (\partial_a + \partial_y)(\lambda y \pi(a,y)) - \lambda y B(a) \pi(a,y) = 0 \\ \pi(0,y) = 2 \displaystyle\int_0^1 \int_0^\infty B(a) \frac{F(\rho)}{\rho} \pi\left(a, \frac{y}{\rho}\right) da d\rho \\ \displaystyle\int_0^\infty \int_0^y \pi(a,y) da dy = 1 \end{cases} \tag{3.52}$$

We solve it by the method of characteristics. From the first equation of (3.52), π solves the ODE

$$\begin{cases} \frac{d}{da}\pi(a,y(a)) = -\left(B(a) + \frac{1}{y(a)}\right) \pi(a,y(a)) \\ \pi(0,y(0)) = 2\int_0^1 \int_0^\infty B(a) \frac{F(\rho)}{\rho} \pi\left(a, \frac{y(0)-a}{\rho}\right) da d\rho \end{cases}$$

where the associated characteristics are of the form $y(a) = a + (y(0) - a(0))$. Then, the solution π of (3.52) is given by

$$\pi(a,y) = \frac{\exp\left(-\int_0^a B(\alpha) d\alpha\right)}{y} \eta^*(y-a),$$

where the definition of η^* is inherited from the initial condition of the ODE:

$$\pi(0, y(0)) = \frac{\eta^*(y-a)}{y-a} = 2\int_0^1 \int_0^\infty B(a)\frac{F(\rho)}{\rho}\pi\left(a, \frac{y(0)-a}{\rho}\right) dad\rho.$$

Note that the RHS still depends implicitly on π. Hence, η^* is solution to the fixed point problem

$$\begin{aligned}\eta^*(x) &= 2\int_0^1 \int_0^\infty B(a)F(\rho)\exp\left(-\int_0^a B(\alpha)d\alpha\right)\eta^*\left(\frac{x}{\rho}-a\right) dad\rho \\ &= 2\int_0^1 \int_0^{\frac{x}{\rho}} F(\rho)\psi\left(\frac{x}{\rho}-a\right)\eta^*(a)\, dad\rho,\end{aligned}$$

where

$$\psi(a) = B(a)\exp\left(-\int_0^a B(\alpha)d\alpha\right)$$

is the probability density function of the added size at division. The existence of a formal solution to this problem is then a by-product of the existence of π, here provided by Harris' Theorem.

Thus finally, the stationary profile of M_t is given by

$$\pi^*(a, y) = \frac{\exp\left(-\int_0^a B(\alpha)d\alpha\right)}{y^2}\eta^*(y-a)$$

□

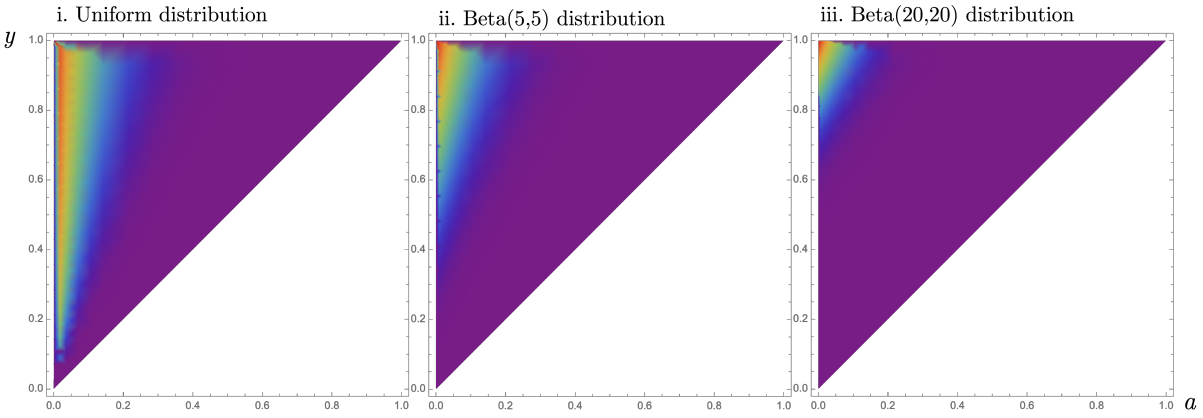

Figure 3.5: Minorant measure ν for F given by *i.* the uniform distribution, *ii.* a Beta(5,5) distribution and *iii.* a Beta(20,20) distribution. The values were obtained from numerical approximation. Only F changes between the three cases.

Remark 3.6.4. The stability of this model has already been studied in the early works of [70] for an application to plant physiology, and more recently by [62] where the exponential ergodicity could not be obtained using General Relative Entropy techniques. In our case however, the direct application of Theorem 3.2.1, since the eigenelements of $\mathcal{Q}$ are known, allows to prove this result. More generally, when the drift term $g(a, y)$ is not necessarily given by the exponential elongation, the previous section allows to prove the existence of the suitable eigenelements. This was left as an open question by the works of [62].

Remark 3.6.5. The proof presented above does not work for singular divisions as given, in lieu of a density F, by ρ distributed according to $\delta_{1/2}(d\rho)$ as in a perfectly symmetric mitosis. Indeed, the change of variables is no longer possible since z would be constant. Moreover, if we try to pursue the method and average in time, one can check that the obtained ν would be the trivial measure for some large enough compacts. Such a limitation is not really surprising, since the authors of [45] have already shown that if the elongation rate λ is constant for the whole population (as in our case), and the divisions are perfectly symmetrical, then we do not have convergence, and a periodic behaviour is observed.

Remark 3.6.6. Figure 3.5 shows the shape of ν for different forms of the density F. As F concentrates we can observe the increasing degeneracy of ν.

Remark 3.6.7. Here, the existence of η^* is a by-product of the existence and uniqueness of π provided by Harris' Theorem. In contrast, in the works of [62], the existence of the stationary measure depended on the existence of a unique solution to the fixed point problem. Thus, the authors had to show compactness properties of the operator associated to the fixed point problem, which our approach evades. Moreover, our approach allows more general forms for F, which [62] requires to be of compact support strictly included in $]0, 1[$.

3.7 Conclusions

The present article studies spectral and ergodic properties of the first-moment semigroup of an age-size piecewise deterministic measure-valued process. The specificities discussed here are two-fold.

First, we have that the process is non-conservative, and that the eigenelements are in general unkwnon. This is addressed by following a classical truncation scheme in order to apply Krein-Rutman's theorem. The key is to use the renewal property brought by the age structure that allows to reduce the dimension of the problem. Second, we have some sort of degeneracy arising from the age-coordinate jumps (reset at 0 at each reproduction event), along with a pure advection term between jumps, that makes it non-trivial to show mixing trajectories that explore the two-dimensional unbounded domain $\mathcal{X}$ independently with respect to the initial state. This is addressed by proving a minorisation condition for petite sets. This condition is seemingly weaker than more usual small set conditions, since it allows to average the action of the semigroup with respect to a suitable discrete sampling measure in time, instead of fixing a uniform mixing time. However, as the works of Meyn

and Tweedie show, petiteness and smallness are intimately related, and if a discrete-time chain is irreducible and aperiodic, then every petite set is indeed small (Theorem 5.5.7. of [112]). Despite this equivalence, as clearly shown in our setting, petiteness properties are much easier to verify, even in degenerate cases. This appears as one of Meyn and Tweedie's theory main points (see Commentary 5.6 of [112], for example), and the implications are strong when petiteness can be checked for all compact sets. Similar strategies could turn out to be useful when trajectorial coupling conditions or "*mass-ratio control*" conditions as the ones discussed by [34] prove hard to verify. Finally, it is worth noticing that a similar approach can be followed in a PDE framework by constructing "*controllabilty sets*", in the sense discussed in P.L. Lions' lectures [101], which play a role equivalent to petite sets in that theory.

As commented in the Introduction, PDMP evolving at higher dimensions could be of particular interest for sampling complex target distributions in recent MCMC methods, as in the models studied by [38, 16, 60]. Concerning the extension of the minorisation condition to higher dimensions, this does not seems to be much of an issue. The bound relies on the Duhamel representation (3.39) of the semigroup P_t which would be identical in a higher dimensional case. Therefore, if $\gamma_t(s, \mathbf{z}) := \varphi^{t-s}(0, \mathbf{z})$ is still a C^1-diffeomorphism on $\mathcal{X} \subset \mathbb{R}_+^{n+1}$, and suitable assumptions are made to bound uniformly from below the integrals, the extension of the presented method should be possible.

Finally, as pointed out by one of the reviewers, it could be also interesting to prove Large Deviations Asymptotics, by employing the theory presented by [91], which extends the approach presented here to a *multiplicative* ergodic theory. Such estimates are also interesting from biological points of view, where the Large Deviations rate function can be used to obtain variational representations of the Malthusian parameter, as shown for example in [7]. This could be the subject of future works.

Chapter 4

Phenotypic plasticity trade-offs in an age-structured model of bacterial growth under stress

4.1 Introduction

Under the presence of antibiotics and other stress factors, bacteria can exhibit a dynamic and heterogeneous expression of stress-response genes. In the case of *Escherichia coli* growing under a sublethal concentration of an antibiotic targeting chromosome integrity such as ciprofloxacin, the detection of DNA breaks in the cell chromosome triggers the initiation of a DNA damage response called SOS response [145, 102, 115]. The intensity of this response depends on the amount of damage, but it also exhibits high heterogeneity among individuals, even in a isogenic population, because of the stochastic expression of several factors [83, 3, 82]. Observations at single-cell level of this stress response have shown that the heterogeneity of the SOS response is strongly dependent on the growth conditions [82]. Moreover, for each individual cell, the SOS response can fluctuate substantially in time, often as a sequence of pulses, transitioning from periods of apparent SOS inactivity to periods of strong SOS response [83, 125, 58, 96, 74, 93, 128]. A distinct signature of this strong expression is the highly perturbed division dynamics, caused by the SOS-dependent expression of a cell division inhibitor, which induces in turn interdivision times which are much longer than in non SOS inducing cells. At the same time however, cell growth is not repressed by the SOS response, leading to the production of cells several times longer than the normally observed ones, a phenomenon known as filamentation. Importantly, SOS inducing cells are able to produce non SOS inducing offspring, which results in a subset of cells that divide normally and could be able to rapidly take over the population once the stress is stopped [144, 121, 86]. Interestingly, similar phenotypic variability has also been shown in others stress response systems, with important consequences for the survival of the population [125]. Collectively, these observations suggest strong links between single-cell phenotypic heterogeneity and population level stress survival, which might be a key to

explain antibiotic tolerance [3, 8, 23, 1].

Nonetheless, at least theoretically, the unconstrained heterogenenous expression of stress strategies might lead to poor population-level performance, especially if the intensity of the stress response is anti-correlated to the mechanisms that usually contribute to the population fitness, such as fast division (inhibited by the SOS response) and volume increase (inhibited by other general stress responses). Furthermore, the protein expression of stress response genes has been shown to be generally within the noisiest in *E. coli*'s proteome [130].

Here, to shed some conceptual and quantitative light into this puzzle, we propose a minimal model that preserves the main elements that characterise the stress response described above. First, we consider two discrete phenotypes: vulnerable (type $i = 0$) and tolerant (type $i = 1$). Vulnerable cells can die with probability $p \in [0, 1]$ at each division. Second, we consider an age-structured population, in order to account for the random amount of time that cells might spend in each state, as well as for the competition between division and switching that is at heart of the trade-off between population growth and phenotypic plasticity. On that account, cells of type 0 switch their type to type 1 at constant rate $\alpha > 0$. Third and finally, we consider that tolerant cells are able to stochastically *recover*, in the sense that they can regenerate offspring of the vulnerable phenotype with a certain probability γ at each division.

Several models have been studied in the context of other somehow similar *bet-hedging* phenomena. After the model and data presented in [8], were the authors introduced a bi-type model of normal and persistent cells, [95, 104, 99, 94] studied further generalisations in fluctuating and random environment, under responsive and stochastic strategies. More recently, [18, 17] studied bi-type non-structured populations of *active* and *dormant* cells in a discrete-time setting, and analysed the effect of different switching strategies in a randomly varying environment. In this work we generalise these fundamental ideas to the case of stress response and give a detailed study of the fitness sensibility with respect to the parameters, from both a probabilistic and deterministic approach.

Sections 4.2 to 4.6 give the main results of the paper and discuss their biological implications, whilst we postpone all the proofs and technical details to Sections 4.9 to 4.12. In Section 4.2 we describe the model in detail and formalise it as a measure-valued random process, from which we derive in Section 4.3 the extinction probability of a population initiated by a single cell in an environment with a constant stress signal. Moreover, we obtain an explicit condition linking the model parameters and under which this population establishes with positive probability. We relate this result with the capacity of *evolutionary rescue* [12, 29] of phenotype switching populations.

Later, in Section 4.4 we show that under the survival condition, we can observe a Malthusian behaviour for the first-moment semigroup of the stochastic process, characterised by an exponential population growth rate $\lambda > 0$ and a stationary distribution of types and ages. Moreover, we show that there is a equivalence relation between the criterion for the establishment of the population obtained by stochastic and deterministic approaches, which is in general not trivial for infinite-dimensional branching processes. Indeed, the measure of *fitness* obtained from each approach, corresponds to different biological realities [109, 50, 39]: in the microscopic case it corresponds to the probability that the branching

process initiated by a single individual survives forever, while in the macroscopic case it is the asymptotic rate of exponential growth of the population. Our results extend the parallel results of [26, 27] in a mono-type growth-fragmentation-death case. However, in contrast with [27] we show that the extinction probability and the Malthusian parameter do not always vary in the same direction with respect to variations in the parameter space. In particular, if the stress is low enough ($p < \bar{p}$ for some critical value $\bar{p} < 1/2$), increasing γ will lead to a decreased survival probability of the population, but at the same time, to a higher population growth rate. Our proofs show that the lost of the classical monotonic behaviour arises from the crucial Assumption 4.2.4 that vulnerable individuals divide stochastically faster than tolerant individuals. In the context of a size-structured cell growth model, [25] have also shown similar loss of monotonicity, also in contrast to what was expected from simpler cases. The work is also similar in spirit to [35], where the authors studied the variation of the Malthusian parameter with respect to an asymmetry factor in a size-structured bi-type model with asymmetric divisions and growth in constant environment.

The results show that the *optimal parameters* in the sense of any of the two notions of fitness can only correspond to extreme strategies: indeed, an optimal population under high stress ($p > \bar{p}$) is expected to bet all on type 1, and to favour a recovery probability $\gamma = 0$, since any creation of cells of type 0 is detrimental for the population fitness. Under a low stress ($p \leq \bar{p}$) an optimal population is expected to bet all on type 0 and to favour $\gamma = 1$. The real interest of non-trivial switching strategies will appear when the environment (i.e., the stress parameter p) fluctuates in time. In Section 4.6, using Floquet's theory [33, 32] we extend our results to the case where we consider a T-periodic signal $p(t)$. Although in that case our results cannot be equally quantitative, we show that the variation of the fitness with respect to the model parameters is now non-trivial and its sign depends on the weighted time-average of the difference between the *reproductive value* [55] of each type within a period length, with weights given by the mean division rate of the subpopulation of type 1 at each instant. We then conclude with an outlook on the consequences for general stress-response strategies and in particular for the case of the SOS response, for which experimental estimations of the *fitness landscape* induced by varying some cell physiological parameters are available [92].

4.2 Description of the individual-based model

4.2.1 Mechanisms of reproduction, phenotypic switching and death

Each individual cell is characterised by their age $a \geq 0$ and a type $i \in \{0, 1\}$. The type $i = 0$ stands for the *vulnerable cells* which are prone to death but are rather fast-dividing. The type $i = 1$ are the *tolerant cells* which are supposed transiently protected from the stress while being compelled to divide after much longer times. The inclusion of age as a variable is two-fold. Firstly, we want to account for memory-effects for both normally dividing and slowly dividing cells. Indeed, the distributions of division times, even in the absence of antibiotic and under ideal conditions, are not exponential and are much better explained by probability laws with memory, that need the inclusion of an age-like structure

in the construction of the model [47]. Secondly, we can use the age as a proxy of other cellular characteristics. For example, in the case of SOS inducing cells, filamentous cells would correspond ideally to rather old individuals of type 1. Thus, we suppose that for each individual cell, the division mechanism is triggered by its age in a phenotype-dependent way. In particular, we suppose that the distribution of the interdivision times of cells of type i are driven by an age-dependent division rate β_i in the sense that for all individuals we have

$$\mathbb{P}\left(\text{Divide at age } < a + \Delta a \middle| \text{Type } = i, \text{Age } \geq a\right) = \beta_i(a) \cdot o(\Delta a)$$

We suppose that the transition between types is determined by the genotype which is common to the whole population. Specifically, we suppose that for all the individuals of the population, the switch between type 0 and 1 occurs after a random exponential time with rate parameter $\alpha \geq 0$. In particular, this means that the $0 \to 1$ switch is memoryless and can take place at any moment of the cell cycle, independently of the age of the individual. Importantly, the switch and division dynamics are supposed independent, so it is possible for a cell of type 0 to never switch, if its division time (determined by the value of β_0 at its current age) occurs before the intended switching time (determined by α). On the other hand, we suppose that during the lifetime of a cell of type 1, switching back from type 1 to type 0 is impossible. However, we also say that when a cell of type 1 divides, its offspring can become of type 0 as consequence of a successful DNA repair induced by the burst of SOS response which characterises the cells of type 1. In other words, when tolerant cells divide, their strong DNA repairing abilities, prevent their daughters from dying at birth, but maybe not for their next division. Indeed, in that case, we suppose that each daughter can be born with type 0 with probability $\gamma \in [0, 1]$. The daughter will keep type 1 with probability $1 - \gamma$. We can think of γ as a measure of the DNA repair efficiency from one generation to the next one, and as for α, we assume its value is encoded by the genotype which is common to the whole population, so its value is the same for all individuals.

Finally, we suppose that the presence of antibiotic impacts the survival of vulnerable cells only. Concretely, if a cell of type 0 initiates division, due to the antibiotic presence, it might die instead of dividing with probability $p \in [0, 1]$, which translates the environmental concentration of antibiotic. Otherwise, with probability $1 - p$, it will produce two new identical cells. Although there is no biological reason for death to happen at division, it seems a reasonable approximation to account in a minimal and very simple way the fact that the considered stress targets only proliferating bacteria.

Table 4.1 summarises all these parameters and Fig 4.1 represents the described dynamics.

Parameter	**Definition**
$\beta_i(a) \in \mathbb{R}_+$	Division rate at age a and type i
$\alpha \in \mathbb{R}_+$	Switching rate from type 0 to 1 (phenotypic plasticity)
$p \in [0, 1]$	Probability of death at division for cells of type 0 (environmental effect)
$\gamma \in [0, 1]$	Probability that a type 1 divides and produces a type 0 (DNA repair effect)

Table 4.1: Summary of the model parameters.

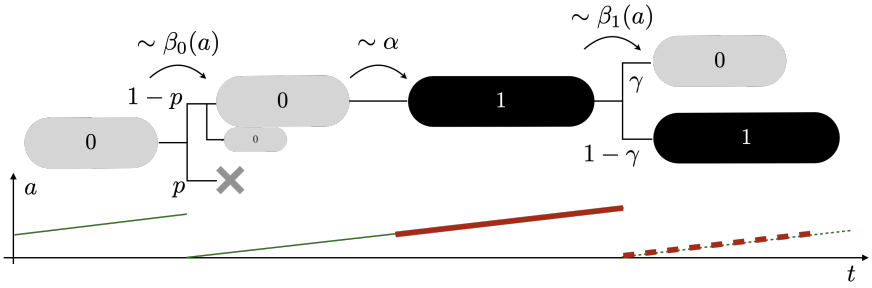

Figure 4.1: Schematic representation of the model.

4.2.2 The stochastic process Z_t

Following the approach introduced by [57, 140], we represent the population as a measure-valued stochastic process $(Z_t)_{t\geq 0}$ which at each time $t \geq 0$ can be written as a point measure

$$Z_t = \sum_{k=1}^{N_t} \delta_{(A_k(t), I_k(t))} \tag{4.1}$$

where $N_t = \langle Z_t, 1\rangle$ is the total number of cells alive at time t, and $(A_k(t), I_k(t)) \in \mathbb{R}_+ \times \{0,1\}$ for $k \in \{1, ..., N_t\}$ is the age and phenotype at time t of cell number k, for any fixed arbitrary order (e.g. numbered using Neveu's notation, or by lexicographical order). In Section 4.8 we define rigorously the paths of Z_t as solution of a Stochastic Differential Equation which describes the desired dynamics conditionally to a given initial population.

We will work under the following set of assumptions.

Assumptions 4.2.1.

(A1) Division times are almost surely finite: For all $i \in \{0,1\}$,

$$\int_0^{+\infty} \beta_i(a)da = +\infty.$$

(A2) Division rates are uniformly bounded: $\exists\, \bar{b} > 0$ such that $\forall i \in \{0,1\}\,, a \geq 0,\ \beta_i(a) \leq \bar{b}$.

(A3) Division rates are uniformly bounded by below from a certain age: $\exists\ a_0 > 0, \underline{b} > 0$ such that $\beta_0(a) \geq \underline{b}$ whenever $a \geq a_0$.

Under assumption (A1) we define the survival probabilities for an individual of type 0 or 1 to do not experience any event between ages s and t, given that it has already survived until age s:

$$\psi_0(s,t) = \exp\left(-\int_s^t (\alpha + \beta_0(u))du\right), \tag{4.2}$$

$$\psi_1(s,t) = \exp\left(-\int_s^t \beta_1(u)du\right), \tag{4.3}$$

and we define the $\star$ composition between the two survival functions as

$$\psi_0 \star \psi_1(s,t) = \int_s^t \psi_0(s,u)\psi_1(u,t)du. \tag{4.4}$$

In particular $\alpha\psi_0 \star \psi_1(s,t)$ represents the probability for an individual of type 0 at initial age s, to switch to type 1 at some point between ages s and t and survive the remaining time until it has reached age t, given that it has already survived until age s.

We provide now some useful definitions that will be used in the next paragraphs.

Definition 4.2.2.
1. For any finite positive point measure μ, set $\mathbb{P}_\mu$ the probability under the initial condition $Z_0 = \mu$, and $\mathbb{E}_\mu$ the respective expectation.
2. Let T_1 be the first jump of Z.
3. Let (I_1, I_2) be the types of the two daughters obtained after the first jump, if it was a division.

Lemma 4.2.3 stated below characterises the probability laws of these random variables, and will be very useful to compute the probability that a population initiated by a single bacterium goes extinct.

Lemma 4.2.3. *Under Assumptions 4.2.1,*

1. *The probability that one cell of initial state (a,i) dies before time $t_0 \geq 0$, instead of dividing or switching before that, is*

$$\mathbb{P}_{\delta_{(a,i)}}\left(Z_{T_1} = 0, T_1 \leq t_0\right) = \mathbb{1}_{i=0}\, p \int_0^{t_0} \beta_i(a+t) \exp\left(-\int_0^t \beta_i(a+u)du - \alpha t\right) dt. \tag{4.5}$$

2. *For any bounded measurable function $h : \mathbb{R}_+ \to \mathbb{R}$, the conditional law of the switching time is characterised by*

$$\mathbb{E}_{\delta_{(a,0)}}\left[h(T_1)\mathbb{1}_{Z_{T_1}=\delta_{(a+T_1,1)},T_1\leq t_0}\right] = \int_0^{t_0} h(t)\, \alpha \exp\left(-\int_0^t \beta_0(a+u)du - \alpha t\right) dt. \tag{4.6}$$

3. *For any bounded measurable function $h : \{0,1\} \times \{0,1\} \to \mathbb{R}$, the conditional law of the daughter types after division is characterised by*

$$\begin{aligned}\mathbb{E}_{\delta_{(a,i)}}&\left[h(I_1,I_2)\mathbb{1}_{Z_{T_1}=\delta_{(0,I_1)}+\delta_{(0,I_2)},T_1\leq t_0}\right] = \\ &\int_0^{t_0} \beta_i(a+t)\exp\left(-\int_0^t \beta_i(a+u)du - (1-i)\alpha t\right) dt \left\{\mathbb{1}_{i=0}\,(1-p)h(0,0)\right. \\ &\left. + \mathbb{1}_{i=1}\Big(\gamma^2 h(0,0) + (1-\gamma)^2 h(1,1) + \gamma(1-\gamma)(h(0,1)+h(1,0))\Big)\right\}\end{aligned} \tag{4.7}$$

Proof. By the construction introduced in Definition 4.8.1, if the initial population consists on only one individual, $Z_0 = \delta_{(a,i)}$, then T_1 is the first jump time of the process

$$J_t = \int_0^t \int_{\{1\}\times\mathbb{R}_+\times[0,1]^2} \mathbb{1}_{\{z\leq\alpha(1-i)+\beta_i(a+u)\}}\mathcal{N}(du, di, dz, d\omega),$$

which, by definition of $\mathcal{N}$, is a non-homogeneous Poisson process whose time-dependent rate is then given by $t \mapsto ((1-i)\alpha + \beta_i(a+t))$. Therefore T_1 has the probability distribution

$$\mathbb{P}_{\delta_{(a,i)}}(T_1 > t) = \mathbb{P}_{\delta_{(a,i)}}(J_t = 0) = \exp\left(-\int_0^t ((1-i)\alpha + \beta_i(a+u))\, du\right). \tag{4.8}$$

From Assumptions 4.2.1 (A1) we can then deduce that $\mathbb{P}_{\delta_{(a,i)}}(T_1 < +\infty) = 1$. Moreover, by differentiation we get that T_1 admits the probability density function

$$\mathbb{P}_{\delta_{(a,i)}}(T_1 \in [t+dt[) = ((1-i)\alpha + \beta_i(a+t)) \exp\left(-\int_0^t ((1-i)\alpha + \beta_i(a+u))\, du\right) dt. \tag{4.9}$$

Now, the value of the process Z_t at time $t = T_1$, i.e. just after the first jump, is given by

$$Z_{T_1} = \begin{cases} 0 & \text{(death) with probability } \dfrac{(1-i)p\beta_i(a+T_1)}{(1-i)\alpha + \beta_i(a+T_1)} \\ \delta_{(0,I_1)} + \delta_{(0,I_2)} & \text{(division) with probability } \dfrac{((1-i)(1-p)+i)\beta_i(a+T_1)}{(1-i)\alpha + \beta_i(a+T_1)} \\ \delta_{(T_1,1)} & \text{(switch) with probability } \dfrac{(1-i)\alpha}{(1-i)\alpha + \beta_i(a+T_1)} \end{cases}. \tag{4.10}$$

The equations of Lemma 4.2.3 are obtained by computing joint probabilities and expectations using the marginal probability density of T_1, obtained from (4.9), and the conditional probability of Z_{T_1} given T_1, (4.10). For example, we have

$$\begin{aligned}
\mathbb{P}_{\delta_{(a,i)}}(Z_{T_1} = 0, T_1 \leq t_0) &= \mathbb{E}_{\delta_{(a,i)}}[\mathbb{P}(Z_{T_1} = 0|T_1)\mathbb{1}_{T_1\leq t_0}] \\
&= \mathbb{E}_{\delta_{(a,i)}}\left[\frac{(1-i)p\beta_i(a+T_1)}{(1-i)\alpha + \beta_i(a+T_1)}\mathbb{1}_{T_1\leq t_0}\right] \\
&= \mathbb{1}_{i=0}\int_0^{t_0} \frac{p\beta_i(a+t)}{\alpha+\beta_i(a+t)}(\alpha+\beta_i(a+t))\exp\left(-\int_0^t (\alpha+\beta_i(a+u))\, du\right) dt.
\end{aligned}$$

We obtain analogously the conditional law of the switching time. For the conditional law of the daughter types, we have also to notice that, if $i = 0$, then $I_1 = I_2 = 0$, and that, if $i = 1$, then I_1 and I_2 are independent Bernoulli random variables of parameter $1-\gamma$. □

We are interested by the case motivated in Section 1, in which individuals of type 1, while tolerant, divide slower than individuals of type 0. We will only use this assumption to study the sensitivity of the population fitness with respect to the model parameters, starting in Section 4.5.

Assumptions 4.2.4.

(B1) Let T_{div} be the time of division of a non-switching cell, this is,

$$\mathbb{P}_{\delta_{(0,i)}}\left(T_{div} \geq a\right) = \exp\left(-\int_0^a \beta_i(s)ds\right).$$

We suppose that the type 0 division time is stochastically dominated (in first order) by the type 1 division time:

$$\mathbb{P}_{\delta_{(0,0)}}\left(T_{div} \geq a\right) < \mathbb{P}_{\delta_{(0,1)}}\left(T_{div} \geq a\right).$$

Remark 4.2.5. For individuals of type 0, $T_1 = \min\left(T_{div},\ T_{switch}\right)$, where T_{switch} is a Exponential random variable of parameter α. Therefore, for all $\alpha \geq 0$, the first event time T_1 is stochastically larger for individuals of type 1 than for individuals of type 0, which implies $\psi_0(0,a) < \psi_1(0,a)$. Moreover, for all non-decreasing function g we we have $\mathbb{E}_{\delta_{(0,0)}}\left[g(T_1)\right] < \mathbb{E}_{\delta_{(0,1)}}\left[g(T_1)\right]$.

4.3 Conditions for microscopic establishment

We give now conditions for the parameters α, γ such that for two given division rates β_0, β_1 and death probability p, the population initiated by a single initial cell establishes indefinitely. We begin by computing the probability that the population initiated by a single cell goes extinct.

Definition 4.3.1. Let $\pi_i(a,i)$ be the extinction probability of a population initiated by a single cell of type $i \in \{0,1\}$ and age $a \geq 0$. This is

$$\pi_i(a,i) := \mathbb{P}_{\delta_{(a,i)}}\left(\exists t > 0 : N_t = 0\right). \tag{4.11}$$

Set $\pi_i = \pi(0,i)$ the extinction probability associated with a single initial cell of age 0.

We will focus now in what happens when the initial cell has age 0. We will see, nevertheless, that the extinction probabilities of a population issued from a single cell of any initial age $a > 0$ can be obtained explicitly from the two extinction probabilities π_0 and π_1.

Theorem 4.3.2. *Let T_1 be the time of the first jump event. For all $a \geq 0$, let q_a the probability that an individual of type 0 switches before dividing, conditionally to have already survived until age a:*

$$q_a = \mathbb{P}_{\delta_{(0,0)}}\left(Z_{T_1} = \delta_{(T_1,1)} | T_1 \geq a\right) = \mathbb{P}_{\delta_{(0,a)}}\left(Z_{T_1} = \delta_{(T_1,1)}\right) = \int_0^{+\infty} \alpha\psi_0(a,t)dt$$

and let in particular

$$q = q_0 = \mathbb{P}_{\delta_{(0,0)}}\left(Z_{T_1} = \delta_{(T_1,1)}\right) = \int_0^{+\infty} \alpha\psi_0(0,t)dt. \tag{4.12}$$

The vector of extinction probabilities (π_0, π_1) *is the smallest solution on* $[0,1]$ *of the quadratic system*

$$\begin{cases} \pi_0 = (1-q)p + (1-q)(1-p)\pi_0^2 + q\pi_1, & \text{(4.13a)} \\ \pi_1 = (\gamma\pi_0 + (1-\gamma)\pi_1)^2, & \text{(4.13b)} \end{cases}$$

in the sense that for any other admissible solution $\tilde{\pi}$*, we have* $\pi_i \leq \tilde{\pi}_i$ *for both* $i \in \{0,1\}$*. Moreover, for any* $a \geq 0$ *we can obtain* $\pi(a,i)$ *as explicit functions of* π_0 *and* π_1 *(which justifies our analysis focused in the initial condition* $\mathbf{0}$*), as given by*

$$\pi(a,0) = (1-q_a)p + (1-q_a)(1-p)\pi_0^2 + q_a\pi_1 \quad \text{(4.14)}$$
$$\pi(a,1) = \pi_1. \quad \text{(4.15)}$$

The proof of this theorem is postponed in section 4.10.

Remark 4.3.3. Since cells of type 1 do not die in their generation, the division rate β_1 does not play any role in the extinction probability.

Remark 4.3.4. Thanks to the integrability assumption (A1), we can differentiate the integral (4.12) to obtain $\partial_\alpha q|_{\alpha=0} = \mathbb{E}_{\delta_{(0,0)}}[T_{\text{div}}]$, where T_{div} is the division time of cells of type 0 (which depends only on β_0). Therefore, at least for small values of α, the sensitivity of q with respect to α is proportional to the mean division time of vulnerable cells. We give a more practical example below.

Example 4.3.1 (Gamma distributed inter-division times)**.** Suppose that β_0 is such that for some $a_0, b_0 > 0$, we can write for all $t \geq 0$

$$\beta_0(t)\exp\left(-\int_0^t \beta_0(u)du\right) = \frac{b_0^{a_0}}{\Gamma(a_0)}t^{a_0-1}e^{-b_0 t}.$$

Then, the inter-division times are Gamma random variables of shape parameter a_0 and rate parameter b_0. This has been shown to be a good parametric model to explain the distributions of division ages [66]. An integration by parts of (4.12) shows that under this assumption,

$$q = 1 - \left(1 + \frac{\alpha}{b_0}\right)^{-a_0}.$$

The general shape for q as function of α is given in Fig. 4.2. Calibrating the values of a_0 and b_0 can modify the sensibility of q with respect to α. In particular, choosing $a_0 = 1$ reduces to the memoryless case $\beta_0 \equiv b_0$, where age does not affect the division times, which are then identically distributed exponential random variables of rate parameter b_0. More in general, notice that the derivative at the origin of q with respect to α is equal to a_0/b_0, which is the expected division time in the Gamma case.

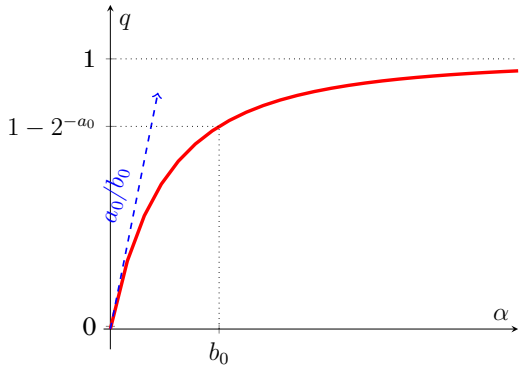

Figure 4.2: Form of q as function of α in the case of division times following a Gamma distribution of parameters (a_0, b_0) (Example 4.3.1). Note that q is always an increasing function of α. As the parameter a_0 increases and b_0 decreases, the curve $q(\alpha)$ approaches faster its asymptotic value of 1, as we can see in the derivative at 0, which equals a_0/b_0.

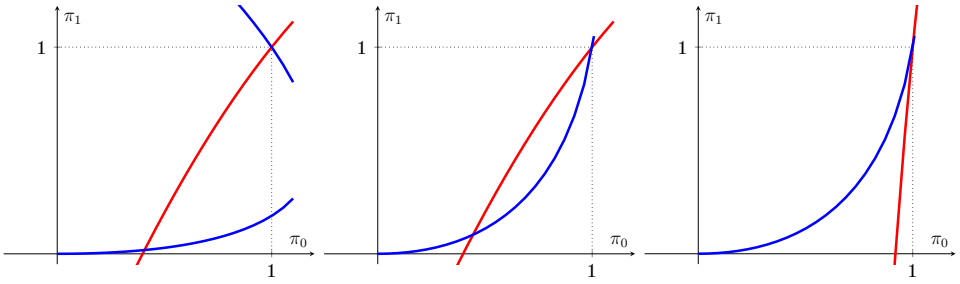

Figure 4.3: Parabolic curves defined by (4.13a) (red) and (4.13b) (blue) for $p = 0.6$. In the first case we have $\gamma = 0.3 < 1/2$ and $q = 0.4$. In the second case we have $\gamma = 0.6 > 1/2$ and $q = 0.4$. In the third case we have $\gamma = 0.6$ and $q = 0.02$, so the condition (4.16) is violated and the only intersection in the unit square is (1,1).

In particular, we can characterise explicitly the subcritical region in which extinction happens almost surely as a function of γ, p and the probability q introduced above. The proof of Theorem 4.3.5 is postponed in Section 4.10.

Theorem 4.3.5. *The population initiated by a single cell of age 0 survives with positive probability if and only if*

$$\left\{p \leq \frac{1}{2}\right\} \text{ or } \left\{p > \frac{1}{2} \text{ and } \gamma < \frac{1}{2}\left(1 + \frac{q}{(2p-1)(1-q)}\right)\right\}. \tag{4.16}$$

In the interesting case $p > 1/2$ in which the vulnerable subpopulation would not be able to survive on its own, the expression above evinces a trade-off between the repair dynamics (conveyed by γ), and the ratio between the effect of the phenotypic plasticity (conveyed by the *odds* of switching before dividing: $q/(1-q)$), and the strength of the environmental effect (conveyed by the expected number of (net) lost individuals after each non-persister division: $1 - 2(1-p) = 1 - 2p$). On the other hand, we see that in order to ensure survival with positive probability, the production of cells of type 0 (or equivalently, the efficiency of the

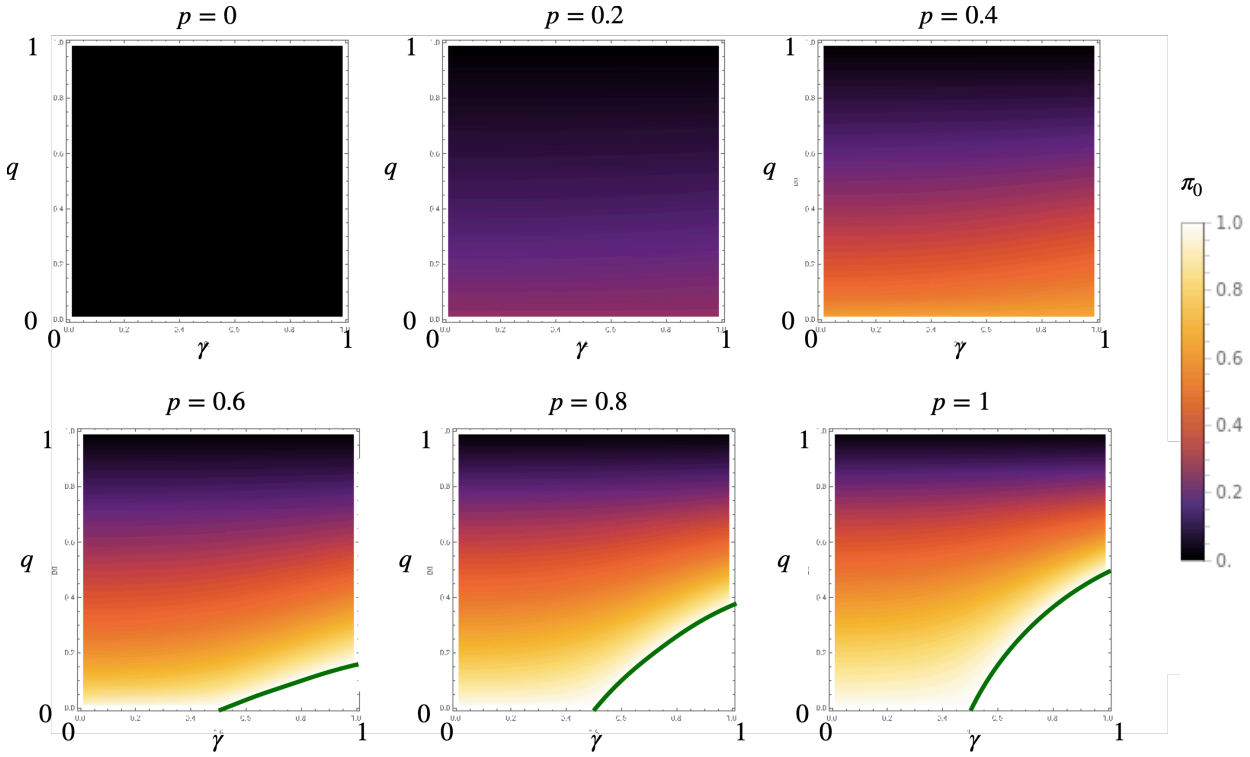

Figure 4.4: Value of the extinction probability of a population initiated by a single non-persistant cell (π_0), numerically computed as the minimal solution to the system (4.13a)-(4.13b) for different values of the environmental variable p (along the plots), γ (x axis) and q (y axis). For the scenarios where $p > 1/2$, the green line represents the critical case of equality for Condition (4.16).

repair dynamics) is limited by the mortality of type 0 in a way that is inversely proportional to the expected number of cell lost at each division. However, this upper bound can be relaxed by an augmentation of the odds of switching before dividing.

Fig. 4.4 shows numerical solutions of this system. We can observe that as expected in this setting, the extinction probabilities decrease as α increases (which makes q increase for fixed β_0), since type 1 is not submitted to death. Nonetheless, the probability γ to produce type 0 progeny might introduce a significant risk of extinction, particularly when p is large. However, this risk can be reduced by increasing q, i.e., by increasing the value of α relatively to β_0. Moreover, a pair of γ and q which can produce a persistent population with positive probability at low p, can lead to extinction if the environment changes to a larger value of p. In that context, having a bigger switch rate is of interest for the persistence of the population, in order to escape from the risk region. This is specially true when the division of tolerant cells produce more frequently vulnerable daughters, which are easily prone to death.

Corollary 4.3.6. *Let $p > 1/2$. Then the extinction probability of the population is at most $\frac{1}{2}(1 - \log 2)$, a value which is attained in the extreme case $p = 1$ where individuals of type 0 die almost surely at each division attempt.*

Proof. The proof consists simply in calculating the area of the extinction region delimited

by the complement of condition (4.16). Indeed, the probability that the population traits belong to this region (so that the establishment probability is 0) is equal to

$$\iint_{[0,1]^2} \mathbb{1}_{\left\{\gamma > \frac{1}{2}\left(1+\frac{q}{(2p-1)(1-q)}\right)\right\}} dq d\gamma = \int_0^{\frac{2p-1}{2p}} dq \int_{\frac{1}{2}\left(1+\frac{q}{(2p-1)(1-q)}\right)}^1 d\gamma$$
$$= \frac{1}{2}\left(p^2 + \frac{1}{2p-1}\log\left(1 - \frac{p(2p-1)}{2}\right)\right).$$

We can see easily that it is an increasing function of p for $p > 1/2$ and thus its maximum its attained for $p = 1$ which gives the value $\frac{1}{2}(1 - \log 2)$. □

Remark 4.3.7. A maximum *evolutionary risk* of $\frac{1}{2}(1-\log 2) \approx 15.34\%$ might seem not very restrictive. However, one could argue that keeping a high value of q, i.e. a high phenotypic plasticity, could be associated with a high energetic cost and other constraints not included in our model, which would enlarge the zone of non viability.

Remark 4.3.8. Note that the previous computation can also be interesting in an evolutionary framework, since it gives a measure of the capacity of random evolutionary rescue. If a mutant cell appears with $p > 1/2$ and new characteristics (γ', q') that are independently and uniformly distributed on the square $[0, 1]$, the survival probability of its subpopulation will be at least $\frac{1}{2}(1 + \log 2)$ and minimum for $p = 1$.

4.4 Long-time behaviour of the population and links with the microscopic establishment condition

In the following we establish some fundamental links between necessary and sufficient conditions for the establishment of a population issued from a single cell from both a probabilistic approach based on the trajectories of Z_t, and for a deterministic approach based on the long-time behaviour of the semigroup M_t, which describes the expected value of the population dynamics, as defined below. Dichotomy properties linking the survival probability with the behaviour of M_t have been studied in size-structured models by [27]. Numerical studies have been performed in the same spirit by [59]. We show in particular that under the survival conditions there is a positive Malthusian parameter $\lambda > 0$ such that the rescaled dynamics $e^{-\lambda t}M_t$ converge to a non-zero stationary measure, and that this convergence is at exponential rate.

Definition 4.4.1 (First-moment semigroup and vector representations)**.** Let us define over the space of bounded Borel functions $\mathcal{B}_b(\mathbb{R}_+ \times \{0, 1\})$, the first-moment semigroup $M_t : \mathcal{B}_b(\mathbb{R}_+ \times \{0, 1\}) \to \mathcal{B}_b(\mathbb{R}_+ \times \{0, 1\})$ by

$$M_t f(a, i) = \mathbb{E}_{\delta_{(a,i)}}\left[\langle Z_t, f\rangle\right], \ \forall (a, i) \in \mathbb{R}_+ \times \{0, 1\} \tag{4.17}$$

and for all signed Borel measure $\mu \in \mathcal{M}(\mathbb{R}_+ \times \{0, 1\})$ we define $\mu M_t \in \mathcal{M}(\mathbb{R}_+ \times \{0, 1\})$ as the measure which, for all $f \in \mathcal{B}_b(\mathbb{R}_+ \times \{0, 1\})$, verifies the duality relation

$$\langle \mu M_t, f\rangle = \langle \mu, M_t f\rangle = \int_{\mathbb{R}_+ \times \{0,1\}} M_t f(a, i)\mu(da, di). \tag{4.18}$$

We give also a vector representation, which will be useful in the sequel. Let us write $\mathbf{f} = (f(\cdot,0), f(\cdot,1)) \in (\mathcal{B}_b(\mathbb{R}_+))^2$ and define for all $a \geq 0$ the matrix semigroup $\mathbf{M}_t : (\mathcal{B}_b(\mathbb{R}_+))^2 \to (\mathcal{B}_b(\mathbb{R}_+))^2$ as

$$\mathbf{M}_t\mathbf{f}(a) = (M_t f(a,0),\ M_t f(a,1)) \in \mathbb{R}^2.$$

Analogously, for all Borel set A of $\mathbb{R}_+$, we let $\boldsymbol{\mu}(A) = (\mu(A\times\{0\}),\ \mu(A\times\{1\})) \in (\mathcal{M}(\mathbb{R}_+))^2$ and define

$$\boldsymbol{\mu}\mathbf{M}_t(A) = (\mu M_t(A\times\{0\}),\ \mu M_t(A\times\{1\})) \in \mathbb{R}^2.$$

Taking expectations in the the semi-martingale decomposition (4.41) associated with Z_t, we easily show that the infinitesimal generator $\mathcal{Q}$ associated to $\mathbf{M}_t$ such that for all $a \geq 0$

$$\frac{d}{dt}\mathbf{M}_t\mathbf{f}(a) = \mathbf{M}_t\left(\mathcal{Q}\mathbf{f}\right)(a) = \mathcal{Q}\left(\mathbf{M}_t\mathbf{f}\right)(a)$$

is given by

$$\mathcal{Q}\mathbf{f}(a) = \mathbf{f}'(a) - \mathbf{D}(a)\mathbf{f}(a) + 2\mathbf{B}(a)\mathbf{f}(0) \tag{4.19}$$

where $\mathbf{f}'(a) := (\partial_a f(a,0), \partial_a f(a,1))$ and

$$\mathbf{B}(a) = \begin{bmatrix} (1-p)\beta_0(a) & 0 \\ \gamma\beta_1(a) & (1-\gamma)\beta_1(a) \end{bmatrix} \text{ and } \mathbf{D}(a) = \begin{bmatrix} \alpha+\beta_0(a) & -\alpha \\ 0 & \beta_1(a) \end{bmatrix}. \tag{4.20}$$

An useful alternative approach is the following representation of $\mathbf{M}_t\mathbf{f}$ as the mild solution to a renewal equation:

Proposition 4.4.2 (Forward Equation)**.** *For all test function $\mathbf{f} \in (\mathcal{B}_b(\mathbb{R}_+))^2$ in the form introduced above, the right action of the semigroup $\mathbf{M}_t\mathbf{f}$ is solution to the renewal equation, for all $a \geq 0$*

$$\mathbf{M}_t\mathbf{f}(a) = \mathbf{\Psi}(a, a+t)\mathbf{f}(a+t) + 2\int_0^t \mathbf{K}(a, a+s)\mathbf{M}_{t-s}\mathbf{f}(0)ds, \tag{4.21}$$

where the matrix $\mathbf{\Psi}(s,t)$ is given by

$$\mathbf{\Psi}(s,t) = \begin{bmatrix} \psi_0(s,t) & \alpha\psi_0 \star \psi_1(s,t) \\ 0 & \psi_1(s,t) \end{bmatrix} \tag{4.22}$$

and the kernel $\mathbf{K}$ is given by

$$\mathbf{K}(s,t) = \begin{bmatrix} (1-p)\beta_0(t)\psi_0(s,t) + \gamma\alpha\beta_1(t)\psi_0\star\psi_1(s,t) & (1-\gamma)\alpha\beta_1(t)\psi_0\star\psi_1(s,t) \\ \gamma\beta_1(t)\psi_1(s,t) & (1-\gamma)\beta_1(t)\psi_1(s,t) \end{bmatrix}. \tag{4.23}$$

Recall that ψ_0 and ψ_1 have been defined respectively in (2) and (3). The first column of the matrix kernel $\mathbf{K}$ corresponds to the possible outcomes for individuals of type 0, which can persist with probability $(1-p)$ or switch at rate α and then give offspring of type 0 or 1 with probabilities γ and $1-\gamma$ respectively. The second column corresponds to the individuals of type 1, whose contributions are pondered by γ or $1-\gamma$ as recalled above.

Remark 4.4.3. In particular, by setting $a = 0$, $t \mapsto \mathbf{M}_t\mathbf{f}(0)$ is the unique fixed point of

$$\mathbf{M}_t\mathbf{f}(0) = \mathbf{\Psi}(0,t)\mathbf{f}(t) + 2\int_0^t \mathbf{K}(0,s)\mathbf{M}_{t-s}\mathbf{f}(0)ds, \tag{4.24}$$

and we can then obtain $\mathbf{M}_t\mathbf{f}(a)$ for all $a \geq 0$ injecting this fixed point into the integral term of (4.21).

The proof of Proposition 4.4.2 is postponed in Section 4.11.

Analogously, the left action of the semigroup can be identified to the measure solution to the following PDE.

Proposition 4.4.4 (Multitype renewal PDE)**.** *For all initial vector measure $\boldsymbol{\mu} \in (\mathcal{M}(\mathbb{R}_+))^2$, the vector measure $\boldsymbol{\mu}\mathbf{M}_t$ is equal to the measure-valued solution $\mathbf{n}(t,\cdot)$ of the multitype McKendrick–von Foerster Equation*

$$\begin{cases} \partial_t \mathbf{n}(t,a) &= -\partial_a \mathbf{n}(t,a) - \mathbf{D}^\top(a)\mathbf{n}(t,a) \\ \mathbf{n}(t,0) &= 2\int_0^{+\infty} \mathbf{B}^\top(a)\mathbf{n}(t,da) \\ \mathbf{n}(0,\cdot) &= \boldsymbol{\mu} \end{cases} \tag{4.25}$$

with $\mathbf{B}^\top$ and $\mathbf{D}^\top$ the transposed matrices of the ones defined by (4.20).

Moreover, if $\boldsymbol{\mu}$ are absolutely continuous with respect to the Lebesgue measure, then $\boldsymbol{\mu}\mathbf{M}_t$ is a strong solution to (4.25).

Then, solving (4.25) by variation of parameters we have that the vector measure $\boldsymbol{\mu}\mathbf{M}_t$ admits, for any test function $f \in \mathcal{B}_b(\mathbb{R}_+)$, the representation

$$\langle \boldsymbol{\mu}\mathbf{M}_t, f\rangle = \int_0^t f(a)\mathbf{\Psi}^\top(0,a)\boldsymbol{\eta}(t-a)da + \int_t^{+\infty} f(a)\mathbf{\Psi}^\top(a-t,a)\boldsymbol{\mu}(a-t)da. \tag{4.26}$$

The function $\mathbf{\Psi}(s,t)$ appears in this new context as the fundamental matrix solution to the ODE

$$\begin{cases} \partial_t \mathbf{\Psi}^\top(s,t) = -\mathbf{D}^\top(t)\mathbf{\Psi}^\top(s,t), \quad t > s & \text{(4.27a)} \\ \mathbf{\Psi}(s,s) = \mathbf{I} & \text{(4.27b)} \end{cases}$$

with $\mathbf{I}$ the 2×2 identity matrix, and $\boldsymbol{\eta}$ is defined by the boundary condition of (4.25), giving

$$\boldsymbol{\eta}(t) = 2\int_0^t \mathbf{B}^\top(a)\mathbf{\Psi}(0,a)\boldsymbol{\eta}(t-a)da + 2\int_t^{+\infty} \mathbf{B}^\top(a)\mathbf{\Psi}(a-t,a)\boldsymbol{\mu}(a-t)da. \tag{4.28}$$

In particular, for an initial condition $\boldsymbol{\mu} = (c_0\delta_0, c_1\delta_0)$ consisting on c_0 initial individuals of type 0 with age 0, and c_1 initial individuals of type 1 with age 0, we have that $\boldsymbol{\eta}$ is solution to the linear Volterra equation of the second kind

$$\boldsymbol{\eta}(t) = g(t) + 2\int_0^t \mathbf{K}^\top(0,a)\boldsymbol{\eta}(t-a)da. \tag{4.29}$$

since indeed $\mathbf{B}^\top(a)\mathbf{\Psi}(0,a) = \mathbf{K}^\top(0,a)$ for $\mathbf{K}$ introduced in (4.23). Meanwhile, the inhomogeneous term is given by

$$g(t) = 2\mathbf{B}^\top(t)\mathbf{\Psi}(0,t)\begin{pmatrix} c_0 \\ c_1 \end{pmatrix} = 2\mathbf{K}^\top(0,t)\mathbf{c} \tag{4.30}$$

We can interpret $\boldsymbol{\eta}(t)$ as the instantaneous number of offspring produced at time t. The term $g(t)$ gives the contribution of the initial individuals that have survived for the whole interval $[0,t]$ before dividing. The integral term counts the contributions of the individuals of age $a \in [0,t]$, this is, that were born $t-a$ ago.

We are interested in the long-time behaviour of the semigroup $\mathbf{M}_t$ in the case when we have survival of the population, using some classical ideas from the spectral theory of C_0-semigroups, adapting the approach followed by [143] to age-structured population dynamics, and more recently applied by [108] to study the equilibrium of a birth-death model of ageing, also formulated as an individual-based stochastic model. To this end, we set ourselves on the Banach space $(L^1(\mathbb{R}_+))^2$ equipped with the norm $||\mathbf{f}||_1 = \int_0^{+\infty} |f(a,0)| + |f(a,1)|da$. We also write $||\cdot||_1$ for vectors and matrices, meaning, as usually: $||\mathbf{x}||_1 = \sum_i |x_i|$, and $||\mathbf{A}||_1 = \max_j \sum_i |A_{ij}|$. We then consider $\mathbf{M}_t : (L^1(\mathbb{R}_+))^2 \to (L^1(\mathbb{R}_+))^2$, which is the mild solution of (4.21) on $(L^1(\mathbb{R}_+))^2$. The existence of such semigroup is a direct consequence of the well-possedness of the measure-valued process Z_t and the control of its first moment as stated in Prop. 4.8.2. Our main convergence result is then the following:

Theorem 4.4.5. *Under Assumptions 4.2.1 and if the survival conditions established by (4.16) are verified, there is a unique triplet of a positive function $\mathbf{h} \in (L^1(\mathbb{R}_+))^2$, a positive Radon measure $\boldsymbol{\nu} \in (\mathcal{M}(\mathbb{R}_+))^2$, normalised such that $\langle \boldsymbol{\nu}, 1\rangle = 1$ and $\langle \boldsymbol{\nu}, \mathbf{h}\rangle = 1$, and a positive constant $\lambda > 0$ such that for all $\mathbf{f} \in (L^1(\mathbb{R}_+))^2$*

$$||e^{-\lambda t}\mathbf{M}_t\mathbf{f} - \langle \boldsymbol{\nu}, \mathbf{f}\rangle \mathbf{h}||_1 \leq ce^{(\omega-\lambda)t}||\mathbf{f} - \langle \boldsymbol{\nu}, \mathbf{f}\rangle \mathbf{h}||_1. \tag{4.31}$$

The positive number λ is called the Malthusian parameter or the population fitness and is the largest real root of the characteristic equation

$$\det\left(\mathbf{F}(\lambda) - \mathbf{I}\right) = 0, \tag{4.32}$$

where

$$\mathbf{F}(\lambda) := 2\int_0^{+\infty} e^{-\lambda a}\mathbf{K}(0,a)da.$$

Moreover, both coordinates of $\boldsymbol{\nu}$ admit a density with respect to the Lebesgue measure.

An important role is played by the matrix

$$\mathbf{K}_\infty := \mathbf{F}(0) = 2\int_0^{+\infty} \mathbf{K}(0,a)da,$$

whose spectral properties determine the long-time behaviour of $\mathbf{M}_t$. Lemmas 4.4.6 and 4.4.7 will be useful to prove Theorem 4.4.5 in Section 4.11. Furthermore, they show how the conditions for survival with positive probability derived in Theorem 4.3.5 and the existence of a positive eigenvalue $\lambda > 0$ are linked through the spectral properties of $\mathbf{K}_\infty$.

Lemma 4.4.6. *The survival condition* (4.16) *is equivalent to have to* $\rho(\mathbf{K}_\infty) > 1$

Lemma 4.4.7. *Under Assumptions 4.2.1, there is a unique* $\lambda > 0$ *such that* $\rho(\mathbf{F}(\lambda)) = 1$ *(in particular,* λ *is solution to the characteristic equation* (4.32)*) if and only if the survival conditions established by* (4.16) *are verified.*

We conclude this section by noticing an useful bound for the value of λ, which is natural to obtain when the division rates are uniformly bounded.

Remark 4.4.8. We have $\lambda \leq \bar{b}$, with $\bar{b}$ the bound on the division rate of Assumption (A1) of 4.2.1.

4.5 Sensitivity of the population fitness with respect to phenotypic switching strategies

In the following we denote by $\mathcal{Q}_{\alpha,\gamma}$ the generator (4.19) and $(\lambda_{\alpha,\gamma}, \boldsymbol{\nu}_{\alpha,\gamma}, \mathbf{h}_{\alpha,\gamma})$ the triplet of elements verifying Theorem 4.4.5 for a given pair of parameters (α, γ) in the survival region defined by Proposition 4.3.5. First, we show that the eigenfunction $(\alpha, \gamma) \in \mathbb{R}_+ \times [0,1] \mapsto \mathbf{h}_{\alpha,\gamma} \in (L^1(\mathbb{R}_+))^2$ is indeed continuous in α and γ. This will allow us to study the variations of the Malthusian parameter with respect to α and γ.

The proofs of next lemmas and propositions are postponed in Section 4.11.

Lemma 4.5.1. *Under Assumptions 4.2.1 and if* $\beta_0, \beta_1 \in C(\mathbb{R}_+)$*, then* $\mathbf{h} \in C^1(\mathbb{R}_+,\ \mathbb{R}_+^2)$.

Lemma 4.5.2. *Under Assumptions 4.2.1, for all fixed* $a \geq 0$*, the map* $(\alpha, \gamma) \mapsto \mathbf{h}_{\alpha,\gamma}(a)$ *is continuous for the uniform norm.*

Proposition 4.5.3 characterises the partial variations of the population growth rate $\lambda_{\alpha,\gamma}$ with respect to α and γ.

Proposition 4.5.3. *For fixed* (α, γ) *and* $(\lambda_{\alpha,\gamma}, \boldsymbol{\nu}_{\alpha,\gamma}, \mathbf{h}_{\alpha,\gamma})$ *the triplet of eigenelements associated to* $\mathcal{Q}_{\alpha,\gamma}$ *we have that both* $\alpha \mapsto \lambda_{\alpha,\gamma}$ *and* $\gamma \mapsto \lambda_{\alpha,\gamma}$ *are continuously differentiable functions such that*

$$\partial_\alpha \lambda_{\alpha,\gamma} = \int_0^{+\infty} \left(h_{\alpha,\gamma}(a,1) - h_{\alpha,\gamma}(a,0)\right) \nu_{\alpha,\gamma}(da,0), \tag{4.33}$$

$$\partial_\gamma \lambda_{\alpha,\gamma} = 2\left(h_{\alpha,\gamma}(0,0) - h_{\alpha,\gamma}(0,1)\right) \int_0^{+\infty} \beta_1(a) \nu_{\alpha,\gamma}(da,1). \tag{4.34}$$

Let us recall that the eigenfunction $\mathbf{h}$ corresponds to Fisher's reproductive value [55]: $h(a,i)$ is a measure of the contribution of an individual of age a and type i to the future growth of the population. Indeed, the longtime behaviour of the expected total number of individuals issued from an individual of age a and type i is $M_t 1(a,i)$ and by Theorem 4.4.5 is given by $e^{\lambda t} h(a,i)$. Thus, Equations (4.33) and (4.34) show that the value of the fitness

response to variations in α and γ depends on the difference in the reproductive values of type 1 an type 0.

In particular, in the case of the variations with respect to parameter γ, we see that the sign of $\partial_\gamma \lambda_{\alpha,\gamma}$ depends only on the sign of the difference between the newborn's reproductive values of type 0 and type 1, which are given by the vector $\mathbf{h}_{\alpha,\gamma}(0)$. Moreover, Proposition 4.5.4 below shows that increasing the probability γ is beneficial for the growth of the population if and only if the population growth rate is already larger than the population growth rate associated with the subpopulation of type 1. Then, exploiting the equivalency of Lemma 4.4.6, we can link the variations of the Malthusian parameter with the variations of the establishment probability . This will allow to show that increasing γ is detrimental from a Malthusian point of view only if the death probability p is greater than some critical value $\bar{p}$, i.e. if the environmental stress is high enough. In contrast, increasing γ is always detrimental from the point of view of the establishment probability. This is also shown by the numerical simulations presented in Fig. 4.7. We will see later that it is not true in the more general case where the environment changes in time.

Proposition 4.5.4. *For (α, γ) in the survival region defined by Proposition 4.3.5, we have the following implicit equivalence*

$$\begin{aligned} \partial_\gamma \lambda_{\alpha,\gamma} > 0 &\iff \lambda_{\alpha,\gamma} > \lambda_1^* \\ \partial_\gamma \lambda_{\alpha,\gamma} < 0 &\iff \lambda_{\alpha,\gamma} < \lambda_1^* \end{aligned}$$

where λ_1^* is the population growth rate of subpopulation 1 alone, i.e., the unique solution to

$$1 = 2\int_0^{+\infty} e^{-\lambda_1^* a}\beta_1(a)\psi_1(0,a)da.$$

Corollary 4.5.5. *If $\lambda_{\alpha,\gamma=0} > \lambda_1^*$ then for all $\gamma \in [0,1[$, $\partial_\gamma \lambda_{\alpha,\gamma} > 0$.*

Proof. Let us recall that we denote $\xi_i(\lambda) = \mathbb{E}_{\delta_{(0,i)}}\left[e^{-\lambda T_{div}}\right]$ the Laplace transform associated to the division times of type $i \in \{0,1\}$. In the case $\gamma = 0$, the matrix $\mathbf{F}(\lambda)$ becomes triangular, and thus the characteristic equation

$$\det\left(\mathbf{I} - \mathbf{F}(\lambda_{\alpha,\gamma})\right) = 0$$

reduces to

$$\left(2(1-p)\xi_0(\alpha+\lambda) - 1\right)\left(2\xi_1(\lambda) - 1\right) = 0,$$

which admits as solutions λ_1^* and some $\tilde{\lambda}_0 \in \mathbb{R}$ such that

$$2(1-p)\xi_0(\alpha+\tilde{\lambda}_0) - 1 = 0,$$

represented in Fig. 4.5. By Theorem 4.4.5, the fitness $\lambda_{\alpha,\gamma=0}$ corresponds then to the maximum value between λ_1^* and $\tilde{\lambda}_0$. If $\lambda_1^* < \tilde{\lambda}_0$ (or equivalently, $\lambda_{\alpha,\gamma=0} > \lambda_1^*$) , by Proposition 4.5.4, $\partial_\gamma \lambda_{\alpha,\gamma}|_{\gamma=0} > 0$. And then, by the continuity of $\gamma \mapsto \partial_\lambda \lambda_{\alpha,\gamma}$, which follows easily from the continuity properties exhibited in the proof of Proposition 4.5.3, $\partial_\gamma \lambda_{\alpha,\gamma} > 0$ for all $\gamma \in [0,1[$. □

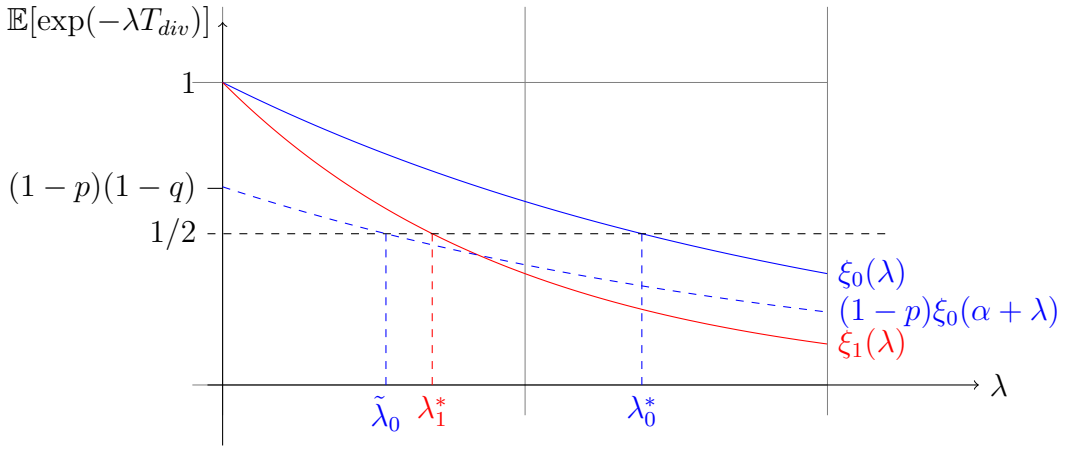

Figure 4.5: Laplace transform of division times in the case $\gamma = 0$. If $(1-p)(1-q)$ is small enough (for example, if $p > 1/2$ or $q > 1/2$, but also in more general cases, as represented in the figure), then $\lambda_1^* > \tilde{\lambda}_0$ and the largest solution to the characteristic equation is the type 1 growth rate λ_1^*. On the other hand, if p and q are sufficiently small, then the population growth rate might be larger than λ_1^*, and then by Corollary 4.5.5, $\partial_\gamma \lambda_{\alpha,\gamma} > 0$ for all $\gamma \in [0,1[$.

Notice however that if $\lambda_1^* \geq \tilde{\lambda}_0$, then $\lambda_{\alpha,\gamma} = \lambda_1^*$ and thus by Proposition 4.5.4, $\partial_\gamma \lambda_{\alpha,\gamma}|_{\gamma=0} = 0$. Therefore, we cannot conclude about the sign of $\partial_\gamma \lambda_{\alpha,\gamma}$ for $\gamma \in (0,1)$. This is the case represented in Fig. 4.5, and which arrives, in particular, in the interesting case $p > 1/2$. Indeed, if $p > 1/2$, since $\xi_0(\lambda) \in [0,1]$ for all $\lambda > 0$, the root $\tilde{\lambda}_0$ is non positive, and a fortiori $\lambda_1^* > \tilde{\lambda}_0$. For that case, however, we can use the results derived for the establishment probability in Section 4.3 to obtain the following monotonicity result, proven in Section 4.11.

Proposition 4.5.6. *Under the supplementary Assumption 4.2.4, for all $\alpha \geq 0$ there exists a unique critical value $\bar{p} \leq 1/2$ such that for all $\gamma \in (0,1)$*

$$\partial_\gamma \lambda_{\alpha,\gamma} > 0 \iff p < \bar{p},$$
$$\partial_\gamma \lambda_{\alpha,\gamma} < 0 \iff p > \bar{p}.$$

The proof is postponed to Section 4.11. Figure 4.6 summarises the results of Propositions 4.5.4 and 4.5.6.

Corollary 4.5.7. *For all $\alpha > 0$ and $\gamma \in (0,1)$, we have $h_{\alpha,\gamma}(0,1) > h_{\alpha,\gamma}(0,0)$ if $p > \bar{p}$, and $h_{\alpha,\gamma}(0,1) \leq h_{\alpha,\gamma}(0,0)$ otherwise.*

Proof. It follows directly from Proposition 4.5.6 and the explicit form of $\partial_\gamma \lambda_{\alpha,\gamma}$ obtained in Proposition 4.5.3. □

Corollary 4.5.7 shows that under high stress, the reproductive value $h_{\alpha,\gamma}(0,0)$ of newborn individuals of type 0, i.e., the contribution of type 0 individuals to the asymptotic size of the population, is always less important than the reproductive value of individuals of type 1. Indeed, even if they take a long time to divide and if the switch events are rare, the

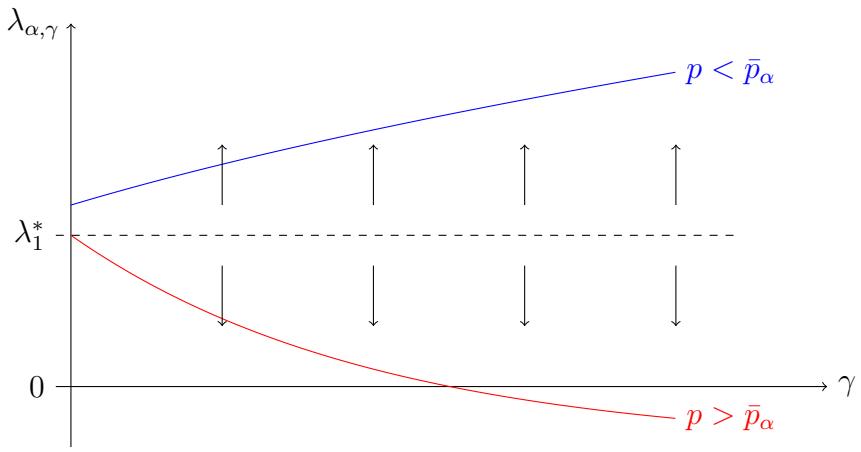

Figure 4.6: Illustration of Propositions 4.5.4 and 4.5.6.

fact that type 1 individuals are *perfectly adapted* to the stress environment (in the sense that they reproduce without dying), make that they end up contributing statistically more to the population size. It is not hard to imagine that this is not generally true when individuals of type 1 happen to be less adapted. For example, under a changing environment, the subpopulation of type 0 can be allowed to proliferate if the stress is reduced ($p < \bar{p}$) at some intervals of time. This could be sufficient to make the contribution of type 0 larger in the asymptotic population. In the next section we explore an extension of the model where this happens. We will consider the case where the death probability p is allowed to vary periodically in time.

Surprisingly, if we look at the establishment probability, we do not necessarily observe the same variations with respect to γ. Proposition 4.5.8 below shows that increasing γ will increase the extinction probability, for all $p \in [0,1]$ (and thus even for $p < \bar{p}$):

Proposition 4.5.8. *For all $p \in [0,1]$, $\alpha > 0$, $\gamma \in [0,1[$, let $(\pi_0^{\alpha,\gamma}, \pi_1^{\alpha,\gamma}) \in [0,1]^2$ the minimal solution to (4.13a)-(4.13b). Then*

$$\partial_\gamma \pi_0^{\alpha,\gamma} > 0 \quad \textit{and} \quad \partial_\gamma \pi_1^{\alpha,\gamma} > 0.$$

Proof. Note that in the system (4.13a)-(4.13b) characterising the extinction probability, only (4.13b) depends on the value of γ. Moreover, for $(\pi_0, \pi_1) \in (0,1)^2$ verifying (4.13b) we have

$$\pi_1 = \frac{1 - 2\gamma(1-\gamma)\pi_0 - \sqrt{1 - 4\gamma(1-\gamma)\pi_0}}{2(1-\gamma)^2},$$

and therefore, for all fixed value of π_0 we have

$$\partial_\gamma \pi_1 = \frac{\sqrt{1 - 4\gamma(1-\gamma)\pi_0} + (1-\gamma)\pi_0\left(1 + 2\gamma - \sqrt{1 - 4\gamma(1-\gamma)\pi_0}\right) - 1}{(1-\gamma)^3\sqrt{1 - 4\gamma(1-\gamma)\pi_0}},$$

which is always non-negative for $\gamma \in [0,1]$ and $\pi_0 \in [0,1]$, since in that case $\pi_0 \leq 1/(4\gamma(1-\gamma))$. Moreover, from (4.13a) we obtain that π_1 is an increasing function of π_0. Thus, for (π_0, π_1) solution of the system, we have both $\partial_\gamma \pi_0 > 0$ and $\partial_\gamma \pi_1 > 0$. □

In particular, only in the case $p > \bar{p}$, both the survival probability $1 - \pi_i^{\alpha,\gamma}$ and the Malthusian parameter $\lambda_{\alpha,\gamma}$ decrease with respect to γ. Fig. 4.4 and 4.7 give a quantitative idea of this behaviour. Fig. 4.4 shows numerical solutions of the system (4.13a)-(4.13b), where we observe the monotonicity with respect to the parameter γ. On the other hand, Fig. 4.7 shows numerical approximations of $\lambda_{\alpha,\gamma}$ obtained from the numerical solution to PDE 4.25. This result is in contrast to [59], where the monotonic dependence observed in the survival probability translated to a monotonic dependence also in the population fitness. In that sense, our result is similar to [25], where a non-monotonic dependence of the population fitness was found on the growth and reproduction parameters in a size-structured growth-fragmentation model. As discussed by [59], this can be explained by a loss of monotonicity in the survival probabilities. In our case, albeit the survival probability varies monotonically with respect to γ (Proposition 4.5.8), the monotonicity is lost by the coexistence of two types. In Section 4.11.6 we exhibit this loss of monotonicity using probabilistic arguments.

4.6 Sensitivity of the population fitness under periodic stress

We consider at last the case where the death probability p evolves periodically in time. Let $T > 0$ a time period and $t \in [0, T[\mapsto p(t) \in [0, 1]$ a T-periodic function. Only this term is allowed to fluctuate in time; α and γ are considered fixed traits of the population and remain constant. Since deaths occur at birth, only the birth matrix $\mathbf{B}$ is affected and we define thereby

$$\mathbf{B}(t,a) := \begin{bmatrix} (1-p(t))\beta_0(a) & 0 \\ \gamma\beta_1(a) & (1-\gamma)\beta_1(a) \end{bmatrix}.$$

Analogously, we define the time-inhomogeneous generator

$$\mathcal{Q}(t)\mathbf{f}(a) := \mathbf{f}'(a) + 2\mathbf{B}(t,a)\mathbf{f}(0) - \mathbf{D}(a)\mathbf{f}(a), \tag{4.35}$$

whose adjoint operator is for every $t \geq 0$

$$\mathcal{Q}^*(t)\mathbf{n}(a) := -\mathbf{n}'(a) - \mathbf{D}^\top(a)\mathbf{n}(a),$$

and has time-dependent domain

$$\mathcal{D}(\mathcal{Q}^*(t)) = \left\{ \mathbf{n} \in W^{1,\infty}(\mathbb{R}_+) : \mathbf{n}(0) = 2\int_0^{+\infty} \mathbf{B}^\top(t,a)\mathbf{n}(a)da \right\}.$$

We consider as well the time-inhomogenenous associated matrices

$$\mathbf{F}(t,\lambda) := 2\int_0^{+\infty} e^{-\lambda a}\mathbf{\Psi}(0,a)\mathbf{B}(t,a)da.$$

As Perron-Frobenious Theorem in the previous case, now Floquet's Theorem (see for example [119], p.163) allows us to construct the eigenelements that will drive the long-time behaviour of the periodic dynamics.

Proposition 4.6.1. *Let $p : \mathbb{R}_+ \to [0,1]$ a T-periodic continuous function. Under the same set of Assumptions 4.2.1 there exists a unique triplet of eigenelements $(\lambda_T, \boldsymbol{\nu}, \mathbf{h})$ where $\lambda_T \in \mathbb{R}$ and $\boldsymbol{\nu} = \boldsymbol{\nu}(t, da)$ and $\mathbf{h} = \mathbf{h}(t, da)$ are time-dependent T-periodic positive continuous functions such that*

$$\begin{cases} -\partial_t \mathbf{h}(t,a) = \mathcal{Q}(t)\mathbf{h}(t,a) - \lambda_T \mathbf{h}(t,a), & (4.36a) \\ \partial_t \boldsymbol{\nu}(t,a) = \mathcal{Q}^*(t)\boldsymbol{\nu}(t,a) - \lambda_T \boldsymbol{\nu}(t,a)\ ,\ \boldsymbol{\nu}(t,\cdot) \in \mathcal{D}(\mathcal{Q}^*(t)), & (4.36b) \\ \int_0^T \int_0^{+\infty} \boldsymbol{\nu}(t,a)dadt = 1\ ,\ \int_0^T \int_0^{+\infty} \mathbf{h}(t,a)\boldsymbol{\nu}(t,a)dadt = 1. & (4.36c) \end{cases}$$

Remark 4.6.2. We recall that the Floquet dominant eigenvalue λ_T gives indeed the growth rate of the population. Set

$$M_{s,t} f(a,i) = \mathbb{E}\left[\langle Z_t, f\rangle \middle| Z_s = \delta_{(a,i)}\right]$$

the time-inhomogenenous semigroup associated to $\mathcal{Q}(t)$ and denote $\mathbf{M}_{s,t}$ its vectorial form, as in the previous sections. Then, for $\mathbf{h}(t,\cdot)$ solving (4.36a), we have immediately that

$$\mathbf{M}_{s,t}\mathbf{h}(s,a) = e^{\lambda_T(t-s)}\mathbf{h}(t,a).$$

Now, as in Section 4.5, we study the variations of λ_T with respect to the model parameters. Using the normalisation conditions (4.36c) and repeating the same calculations as in the proof of Lemma 4.5.1 and Proposition 4.5.3 we obtain the Proposition 4.6.3 below.

Proposition 4.6.3. *Let $(\lambda_{T,\alpha,\gamma}, \boldsymbol{\nu}_{\alpha,\gamma}, \mathbf{h}_{\alpha,\gamma})$ the triplet of Floquet eigenelements associated to T-periodic $\mathcal{Q}_{\alpha,\gamma}(t)$. We have*

$$\partial_\alpha \lambda_{\alpha,\gamma} = \int_0^T \int_0^{+\infty} \left(h_{\alpha,\gamma}(t,a,1) - h_{\alpha,\gamma}(t,a,0)\right) \nu_{\alpha,\gamma}(t,a,0)dadt, \quad (4.37)$$

$$\partial_\gamma \lambda_{\alpha,\gamma} = 2\int_0^T \left(h_{\alpha,\gamma}(t,0,0) - h_{\alpha,\gamma}(t,0,1)\right)\left(\int_0^{+\infty} \beta_1(a)\nu_{\alpha,\gamma}(t,a,1)da\right)dt \quad (4.38)$$

Proof. Follows directly from (4.36c) and repeating the same calculations as in the proof of Proposition 4.5.3 . The continuity of $(\alpha,\gamma) \in \mathbb{R}_+ \times [0,1] \mapsto \mathbf{h}_{\alpha,\gamma}(t,\cdot)$ for all fixed $t \geq 0$; follows also directly from Lemma 4.5.1. □

Remark 4.6.4. We compare this result with the one obtained in the constant environment case. We focus in the variations with respect to parameter γ. In the constant environment case we saw that if $p > 1/2$ then increasing γ is always detrimental from a Malthusian point of view (see Proposition 4.5.6 and Fig. 4.7), since the reproductive value $h_{\alpha,\gamma}(0,1)$ of type 1 is always larger than the reproductive value $h_{\alpha,\gamma}(0,0)$ of type 0 when the level of stress is constant. However, we see now that in the fluctuating case the sign of $\partial_\gamma \lambda_{\alpha,\gamma}$ depends on some time-average of the reproductive value difference. In particular, this difference is weighted proportionally to the mean division rate of type 1, $\bar{\beta}_1(t) := \int_0^{+\infty} \beta_1(a)\nu_{\alpha,\gamma}(t,a,1)da$, observed at that time. Hence, if there are times t at which

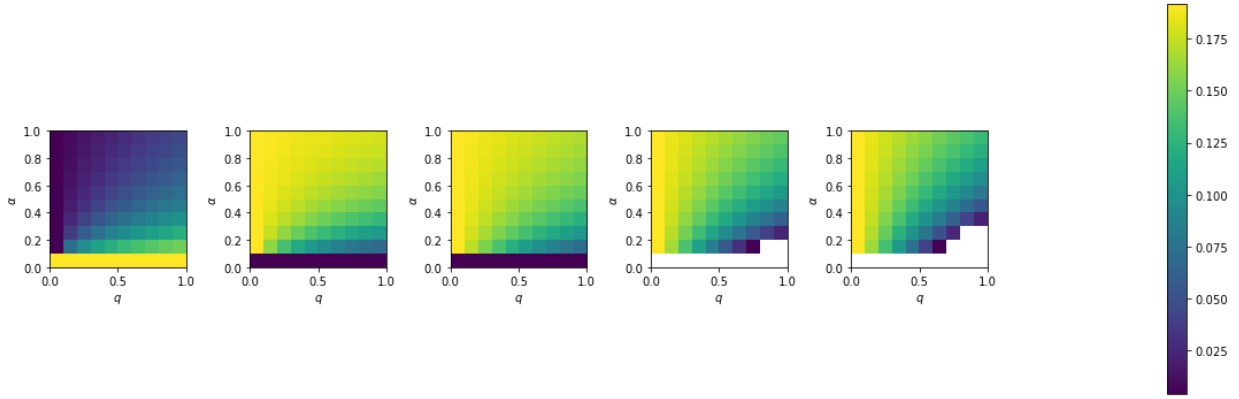

Figure 4.7: Value of the Perron-Frobenius eigenvalue λ as function of γ (abscissa) and q (ordinate), obtained from numerical simulations of (4.25) under fixed p varying from $p = 0$ to $p = 1$, from left to right.

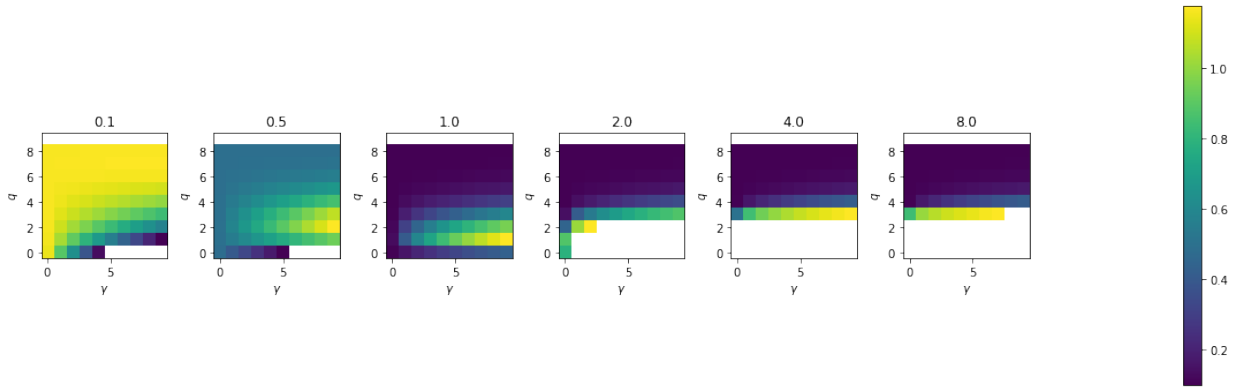

Figure 4.8: Value of the Floquet eigenvalue λ_T for the value of T indicated in the head of the panel, as function of γ (abscissa) and q (ordinate), obtained from numerical simulations of (4.25). The death probability p oscillates between 0 and 1 (*good* and *bad* phases), passing a period $T/2$ in each value. The division times are exponentially distributed with $\beta_0 \equiv 10$ and $\beta_1 \equiv 0.1$. We see how the *optimal* set of parameters and the non-establishment region change in a non-trivial way. In particular, increasing the value of γ becomes interesting from a Malthusian point of view as the length of *good* and *bad* phases increases. However this increments the extension of the non-viability region.

$p(t) \leq 1/2$, such that the reproductive value of type 0 is able to be larger than the reproductive value of type 1, it is possible for the average difference to be positive. In particular, the coincidence of these times with times at which the mean type 1 division rate $\bar{\beta}_1(t)$ is large, can lead to positive values of $\partial_\gamma \lambda_{\alpha,\gamma}$. This comes off naturally from a heuristic reasoning. Indeed, big values of $\bar{\beta}_1(t)$ and γ would lead to a burst in the creation of individuals of type 0 at time t, which possesses the biggest relative advantage at that time. In Fig. 4.8 , simulations of PDE (4.25) with T-periodic p illustrate this qualitative observation for different values of T.

Finally, we can also compute the extinction probabilities. However, the time-dependent

value of p breaks the Markovian property at the division stopping times that allows us to reduce the problem to a simple algebraic system in the constant environment case, and obtain the explicit description of the survival region. The new system however can be solved numerically.

Proposition 4.6.5. *Let*

$$\pi_i(s,a) := \mathbb{P}\left(\exists t \geq s : N_t = 0 | Z_s = \delta_{(i,a)}\right).$$

Then, we have that (π_0, π_1) *is the minimal solution on* $[0,1]^2$ *of the system*

$$\begin{aligned}
\pi_0(s,a) = &\int_0^{+\infty} p(s+t)\beta_0(a+t)\psi_0(a,a+t)dt \\
&+ \int_0^{+\infty} \pi_1(s+t,a+t)\alpha\psi(a,a+t)dt \\
&+ \int_0^{+\infty} (\pi_0(s+t,0))^2 (1-p(s+t))\beta_0(a+t)\psi_0(a,a+t)dt \\
\pi_1(s,a) = &\int_0^{+\infty} (\gamma\pi_0(s+t,0) + (1-\gamma)\pi_1(s+t,0))^2 \beta_1(a+t)\psi_1(a,a+t)dt
\end{aligned}$$

Moreover $t \mapsto \pi_i(t,\cdot)$ *is* T*-periodic.*

Proof. It follows directly repeating the steps in Prop. 4.3.5

□

4.7 Discussion and outlook

We have introduced a stochastic bi-type age-structured population model to describe the stress-response dynamics of *E. coli*. Some experimental studies have been able to quantify the fitness response of *E. coli* populations under low-genotoxicity environment ($p \leq 1/2$) and perturbations of the SOS response genetic circuit, providing some hints of validation for our approach. In the recent work [92], the authors measure the population growth rates (λ) and survival probability ($1-\pi$) in a panel of *E. coli* strains with different SOS response activation parameters, by introducing mutations into the *lexA* promoter, responsible for the transcriptional inhibition of SOS proteins trought the expression of the repressor protein LexA. The authors analyse their experimental results within the framework of a low dimensional chemical reaction model with three parameters that they estimate, producing survival curves (Fig. 4A ibid.) and a quantitative parameter-fitness landscape from the empirical population growth rates (Figs. 4B, 4C and 5 ibid.). Two main effective biomolecular parameters drive the model considered by the authors. The first one is the effective expression rate of *lexA* (β/α therein), which can be related to our switching rate α, since it quantifies the speed at which the SOS response can be initiated. The second parameter is the repression affinity of LexA for its own promoter (k therein), which quantifies the strength at which the SOS response "turns off" when the stress is removed. Thus, it can be related to our

coarse-grain parameter γ that conveys the "repair" probability with which tolerant individuals of type 1 switch back to vulnerable individuals of type 0. Although these links are only suggestive at the very most, specially since in our specific and minimal model the type switches are coupled to the division dynamics, they allow to interpret Fig. 5 of [92] under the light of our Figs. 4.7 and 4.8 and our general results. Interestingly, [92] suggests the existence of a trade-off between the SOS repression and SOS expression rates, that produces two distinct regimes in the variations of the empirical relative fitness, in a way that it is similar to the trade-off observed between our parameters γ and q. Indeed, they show that lowering the steady-state concentration of LexA (linked to our switching rate α) and altering the repressive activity of LexA (their k, linked to our γ) can increase fitness after a critical dose of DNA damage (in our words, when $p > \bar{p}_\alpha$), but results in decreased fitness with lower amounts of DNA damage ($p < \bar{p}_\alpha$), echoing the result of Proposition 4.5.6. This might indicate a much more general parameter-fitness trade-off for other stress-response and negatively autoregulated response mechanisms.

We have shown in Propositions 4.5.6 and 4.5.8 that measuring the dependence of the extinction probability of a population issued from a single cell and of the population growth rate on variations in the *stress repair* probability γ can lead to seemingly opposite conclusions, even in our very simplistic model. Albeit increasing γ will always increase the extinction probability, even under sublethal stress, it might increase the population fitness if p is low enough, so that creating vulnerable but fast-proliferating type 0 individuals is advantageous. This raises some methodological questions about the non trivial equivalence of measuring the response of bacterial proliferation using single-cell and bulk techniques in sublethal conditions. For instance, in the context of antibiotic susceptibility studies, parameter variations might not have the same effects when looking at the population growth rate in longitudinal experiments, and when looking at the survival outcome of microcolonies. Our mathematical results highlight the differences that might emerge from these two acquisitions. Indeed, this difference can then be explained by the bias shown here, rather than by actual biological discrepancies.

Finally, we have seen that the fitness landscape change when the environmental stress is allowed to fluctuate. In particular, it is possible that phenotypic plasticity strategies that would have lead to almost sure extinction in constant environment, become advantageous in the periodic case. The evolutionary paths over this fitness landscape should then take into account this variability. This will be subject of future works.

4.8 Construction and well-posedness of Z_t

Definition 4.8.1 (Pathwise representation of the population process)**.** Let Z_0 be a counting measure on $\mathbb{R}_+ \times \{0,1\}$, of the form of (4.1), and $\mathcal{N}(du, dk, dz, d\omega)$ an independent Poisson point measure over $\mathbb{R}_+ \times \mathbb{N}_* \times \mathbb{R}_+ \times [0,1]^2$ with intensity $du\, n(dk)\, dz\, d\omega$, with n the counting measure on $\mathbb{N}_*$. Z_0 represents the initial population and $\mathcal{N}$ clocks the division and switching times that occur in some time interval measured by the integrating variable u. These events are measured for each individual k independently and happen proportionally to their division and switching rates, which are measured by the integrating variable z. Finally, the two

independent uniform random variables $\omega = (\omega_1, \omega_2)$ determine, respectively, the outcome of the first and the second daughter.

Thus, under the canonical filtration $(\mathcal{F}_t)_{t\geq 0}$ generated by $(Z_0, \mathcal{N})$, we define the process $(Z_t)_{t\geq 0}$ as

$$\begin{aligned} Z_t = &\sum_{k=1}^{N_0} \delta_{(A_k(0)+t, I_k(0))} \\ &+ \int_0^t \int_{\mathbb{N}^*\times\mathbb{R}_+\times[0,1]^2} \mathbb{1}_{\{k\leq N_{u^-}\}} \Bigg\{ \mathbb{1}_{\{z\leq \alpha(1-I_k(u^-))\}} \left[\delta_{(A_k(u^-)+(t-u),1)} - \delta_{(A_k(u^-)+(t-u),I_k(u^-))}\right] \\ &+ \mathbb{1}_{\left\{0<z-\alpha(1-I_k(u^-))\leq \beta_{I_k(u^-)}(A_k(u^-))\right\}} \Big(- \delta_{(A_k(u^-)+(t-u),I_k(u^-))} \\ &+ \mathbb{1}_{I_k(u^-)=0} \left[\mathbb{1}_{\omega_2>p}\delta_{(t-u,0)} + \mathbb{1}_{\omega_3>p}\delta_{(t-u,0)}\right] \\ &+ \mathbb{1}_{I_k(u^-)=1}\left[\mathbb{1}_{\omega_2\leq\gamma}\delta_{(t-u,0)} + \mathbb{1}_{\omega_2>\gamma}\delta_{(t-u,1)} + \mathbb{1}_{\omega_3\leq\gamma}\delta_{(t-u,0)} + \mathbb{1}_{\omega_3>\gamma}\delta_{(t-u,1)}\right]\Big)\Bigg\} \mathcal{N}(du, dk, dz, d\omega). \end{aligned} \tag{4.39}$$

Note that

$$Z_t(da, di) = Z_t(da, \{0\})\delta_0(di) + Z_t(da, \{1\})\delta_1(di).$$

We explain now each term of the RHS of (4.8.1). The first line represents the deterministic evolution of the population when no random events happen before time t. The second line represents the switching events, that occur only for individuals of type $I_k = 0$ at rate α, and gives a new individual of type 1 with identical age while removing the previous individual of type 0 from the population. The third and four lines represent the divisions, which remove the divided cell from the population. If the mother type is 0 (third line), we add independently two cells of type 0, but only with probability $1-p$ each. If the mother type is 1 (fourth line) we add independently two cells whose type is decided by a Bernoulli random variable of parameter $1-\gamma$.

We show that the stochastic process $(Z_t)_t$ is well-defined under Assumptions 4.2.1:

Proposition 4.8.2 (Well-posedness and first-moment control). *Under Assumptions 4.2.1, and if* $\mathbb{E}\left[\int (Z_0(da,\{0\}) + Z_0(da,\{1\}))\right] < \infty$ *and* $\mathbb{E}\left[\int a(Z_0(da,\{0\}) + Z_0(da,\{1\}))\right] < \infty$, *then the SDE (4.8.1) has a well-posed solution* $(Z_t)_{t\geq 0} \in \mathbb{D}\left(\mathbb{R}_+, \mathcal{M}\left(\{0,1\}\times\mathbb{R}_+\right)\right)$ *which verifies for every* $t > 0$

$$\begin{aligned} \mathbb{E}\left[\sup_{s\in[0,t]} \int (1+a)(Z_s(da,\{0\}) + Z_s(da,\{1\}))\right] \leq &\mathbb{E}\left[\int (1+a)(Z_0(da,\{0\}) + Z_0(da,\{1\}))\right] \\ &\times \exp\left((\bar{b}+1)t\right) < +\infty. \end{aligned} \tag{4.40}$$

Proof. The proof is classical for populations with uniformly bounded birth rates, a suitable sequence of stopping times and Gronwall inequality to conclude. See for example [140], and Appendix A.1 for the case with unbounded birth rates under the adder assumption. □

Using the Compensated Poisson Point Measure associated to $\mathcal{N}$ and Ito's formula for semi-martingales [80] we can derive the following representation for $\langle Z_t, f\rangle$.

Proposition 4.8.3 (Semi-martingale decomposition)**.** *Under control assumptions for the moments of Z_0 and for control assumptions for β 2.1, Z_t is well-posed for $t \in [0,T]$ for any $T > 0$. Moreover, for any $f \in C^{1,\cdot}(\mathbb{R}_+ \times \{0,1\})$, we can write for any $t \geq 0$*

$$\begin{aligned}\int (f(a,0)Z_t(da,\{0\}) + f(a,1)Z_t(da,\{1\})) = \int (f(a,0)Z_0(da,\{0\}) + f(a,1)Z_0(da,\{1\}))\\ + \int_0^t \int (\mathcal{Q}f(a,0)Z_s(da,\{0\}) + \mathcal{Q}f(a,1)Z_s(da,\{1\}))ds + \mathcal{M}_t^f\end{aligned} \tag{4.41}$$

where $\mathcal{M}_t^f$ is a squared-integrable $\mathcal{F}_t$-martingale and the infinitesimal generator $\mathcal{Q}$ is defined as

$$\begin{aligned}\mathcal{Q}f(a,i) = \partial_a f(a,i) + (1-i)\alpha(f(a,1) - f(a,0)) - \beta_i(a)f(a,i)\\ + 2(1-i)(1-p)\beta_i(a)f(0,0) + 2i\beta_i(a)(\gamma f(0,0) + (1-\gamma)f(0,1))\end{aligned} \tag{4.42}$$

We can write Proposition 4.8.3 in an abbreviated vectorial form. For all $f : \mathbb{R}_+ \times \{0,1\} \to \mathbb{R}$ which is C^1 in the first coordinate, we pose $\mathbf{f}(a) = (f(a,0), f(a,1))$ and analogously $\mathbf{f}'(a) = (\partial_a f(a,0), \partial_a f(a,1))$. Then, we can write for $\mathbf{f} \in (C^1(\mathbb{R}_+))^2$, $\mathcal{Q}\mathbf{f} = (\mathcal{Q}f(a,0), \mathcal{Q}f(a,1))$ with $\mathcal{Q}$ given by (4.19).

4.9 Proofs of Section 4.3

4.9.1 Proof of Theorem 4.3.2

We compute the extinction probability in a general way that will be useful when time inhomogeneity is included in Sections 4.6 and 4.12, this is, when p is a periodic function instead of a constant. Note however that since for now p is fixed, we could have shown that the extinction probability of Z_t equals the extinction probability of some embedded discrete-time branching process giving the number of particles at the n-th generation, which is no other than a multitype Galton-Watson process [5].

Proof. Conditioning with respect to the possible outcomes of the first jump, we have

$$\begin{aligned}\pi(a,i) &= \mathbb{P}_{\delta_{(a,i)}}(Z_T = 0) + \mathbb{P}_{\delta_{(a,i)}}(\exists t > T : N_t = 0, Z_T \neq 0)\\ &= \mathbb{P}_{\delta_{(a,i)}}(Z_T = 0) + \mathbb{P}_{\delta_{(a,i)}}(\exists t > T : N_t = 0, Z_T = \delta_{a+T,1})\\ &\quad + \mathbb{P}_{\delta_{(a,i)}}\left(\exists t > T : N_t = 0, Z_T = \delta_{(0,I_1)} + \delta_{(0,I_2)}\right).\end{aligned}$$

Applying the strong Markov property on the stopping time T gives

$$\begin{aligned}\pi(a,i) = \mathbb{P}_{\delta_{(a,i)}}(Z_T = 0) + \mathbb{E}_{\delta_{(a,i)}}\left[\mathbb{P}_{\delta_{(a+T,1)}}(\exists t > 0 : N_t = 0)\,\mathbb{1}_{Z_T = \delta_{a+T,1}}\right]\\ + \mathbb{E}_{\delta_{(a,i)}}\left[\mathbb{P}_{\delta_{(0,I_1)}+\delta_{(0,I_2)}}(\exists t > 0 : N_t = 0)\,\mathbb{1}_{Z_T = \delta_{(0,I_1)}+\delta_{(0,I_2)}}\right],\end{aligned}$$

which by the independence of the processes starting from $\delta_{(0,I_1)}$ and $\delta_{(0,I_2)}$, gives

$$\begin{aligned}
&= \mathbb{P}_{\delta_{(a,i)}}\left(Z_T = 0\right) + \mathbb{E}_{\delta_{(a,i)}}\left[\mathbb{P}_{\delta_{(a+T,1)}}\left(\exists t > 0 : N_t = 0\right) \mathbb{1}_{Z_T = \delta_{a+T,1}}\right] \\
&\quad + \mathbb{E}_{\delta_{(a,i)}}\left[\mathbb{P}_{\delta_{(0,I_1)}}\left(\exists t > 0 : N_t = 0\right) \mathbb{P}_{\delta_{(0,I_2)}}\left(\exists t > 0 : N_t = 0\right) \mathbb{1}_{Z_T = \delta_{(0,I_1)} + \delta_{(0,I_2)}}\right] \\
&= \mathbb{P}_{\delta_{(a,i)}}\left(Z_T = 0\right) + \mathbb{E}_{\delta_{(a,i)}}\left[\pi(a+T,1)\mathbb{1}_{Z_T = \delta_{a+T,1}}\right] + \mathbb{E}_{\delta_{(a,i)}}\left[\pi(0,I_1)\pi(0,I_2)\mathbb{1}_{Z_T = \delta_{(0,I_1)} + \delta_{(0,I_2)}}\right].
\end{aligned}$$

Now, using Lemma 4.2.3, we obtain that

$$\begin{aligned}
\pi(a,i) = \mathbb{1}_{i=0}\, p \int_0^{+\infty} \beta_0(a+t) \exp\left(-\int_0^t \beta_0(a+u)du - \alpha t\right) dt \\
+ \mathbb{1}_{i=0} \int_0^{+\infty} \pi(a+t,1)\, \alpha \exp\left(-\int_0^t \beta_0(a+u)du - \alpha t\right) dt \\
+ \int_0^{+\infty} \beta_i(a+t) \exp\left(-\int_0^t \beta_i(a+u)du - (1-i)\alpha t\right) dt \left\{\mathbb{1}_{i=0}(1-p)\pi(0,0)^2 \right. \\
\left. + \mathbb{1}_{i=1}\left(\gamma\pi(0,0) + (1-\gamma)\pi(0,1)\right)^2\right\}. \qquad (4.43)
\end{aligned}$$

In particular, doing $a = 0$, we obtain

$$\begin{cases}
\pi_0 = \pi(0,0) = pq' + (1-p)q'\pi_0^2 + \displaystyle\int_0^{+\infty} \pi(t,1)\, \alpha \exp\left(-\int_0^t \beta_0(u)du - \alpha t\right) dt, & (4.44) \\
\pi_1 = \pi(0,1) = (\gamma\pi_0 + (1-\gamma)\pi_1)^2, & (4.45)
\end{cases}$$

with

$$q' = \int_0^{+\infty} \beta_0(t) \exp\left(-\int_0^t \beta_0(u)du - \alpha t\right) dt = 1 - q,$$

for q defined by (4.12), since

$$q' + q = \int_0^{+\infty} (\alpha + \beta_0(t)) \exp\left(-\int_0^t \beta_0(u)du - \alpha t\right) dt = \mathbb{P}_{\delta_{(0,0)}}\left(T < +\infty\right) = 1.$$

Moreover, from (4.43) we have that for all $t \geq 0$

$$\begin{aligned}
\pi(t,1) &= (\gamma\pi_0 + (1-\gamma)\pi_1)^2 \int_0^{+\infty} \beta_1(t+u) \exp\left(-\int_0^u \beta_1(t+w)dw\right) du \\
&= (\gamma\pi_0 + (1-\gamma)\pi_1)^2 \left(1 - \exp\left(-\int_0^{+\infty} \beta_1(t+u)du\right)\right).
\end{aligned}$$

Hence using the integrabilty condition Assumptions 4.2.1 (A1), we obtain for all $t \geq 0$

$$\pi(t,1) = (\gamma\pi_0 + (1-\gamma)\pi_1)^2 = \pi_1,$$

which gives immediately (4.15). Finally, after injecting these results back in (4.44) we get the system (4.13a)-(4.13b):

$$\begin{cases} \pi_0 = (1-q)p + (1-q)(1-p)\pi_0^2 + q\pi_1 \\ \pi_1 = (\gamma\pi_0 + (1-\gamma)\pi_1)^2. \end{cases}$$

Analogously, injecting these results back in (4.43) with $i = 0$ we get (4.14) for all $a \geq 0$.

Next, we prove that (π_0, π_1) is the minimal solution of this system. Set $(T_n)_{n\in\mathbb{N}}$ the jump times of Z, with $T_0 = 0$, so in our previous notation $T_1 = T$. Define the extinction probabilities at the n-th jump by

$$\pi^{(n)}(a,i) = \mathbb{P}_{\delta_{(a,i)}}\left(N_{T_n} = 0\right).$$

Therefore

$$\lim_{n\to+\infty} \pi^{(n)}(a,i) = \mathbb{P}_{\delta_{(a,i)}}\left(\bigcup_{n\in\mathbb{N}} \{N_{T_n} = 0\}\right) = \mathbb{P}_{\delta_{(a,i)}}\left(\exists t > 0 : N_t = 0\right) = \pi(a,i).$$

Now, suppose that we have some positive real solution $\tilde{\pi}$ of (4.13a)-(4.13b). Then for both $i \in \{0,1\}$, $\tilde{\pi}_i \geq \pi^{(0)}(0,i) = 0$. We now show inductively that the same is verified for each $n \in \mathbb{N}_*$ and in the limit $n \to +\infty$. As before, we condition with respect to the first jump and use the strong Markov property to obtain the following recursive equation

$$\begin{aligned} \pi^{(n)}(a,i) &= \mathbb{P}_{\delta_{(a,i)}}\left(Z_T = 0\right) + \mathbb{E}_{\delta_{(a,i)}}\left[\mathbb{P}_{\delta_{(a+T,1)}}\left(N_{T_{n-1}} = 0\right)\mathbb{1}_{Z_T=\delta_{a+T,1}}\right] \\ &\quad + \mathbb{E}_{\delta_{(a,i)}}\left[\mathbb{P}_{\delta_{(0,I_1)}+\delta_{(0,I_2)}}\left(N_{T_{n-1}} = 0\right)\mathbb{1}_{Z_T=\delta_{(0,I_1)}+\delta_{(0,I_2)}}\right] \\ &= \pi^{(1)}(a,i) + \mathbb{E}_{\delta_{(a,i)}}\left[\pi^{(n-1)}(a+T,1)\mathbb{1}_{Z_T=\delta_{a+T,1}}\right] \\ &\quad + \mathbb{E}_{\delta_{(a,i)}}\left[\pi^{(n-1)}(0,I_1)\pi^{(n-1)}(0,I_2)\mathbb{1}_{Z_T=\delta_{(0,I_1)}+\delta_{(0,I_2)}}\right], \qquad n \in \mathbb{N}_* \end{aligned}$$

where we have again

$$\pi^{(1)}(a,i) = \mathbb{1}_{i=0}\, p \int_0^{+\infty} \beta_0(a+t)\exp\left(-\int_0^t \beta_0(a+u)du - \alpha t\right)dt.$$

Suppose that $\pi^{(n-1)} \leq \tilde{\pi}$. Then

$$\begin{aligned} \pi^{(n)}(a,i) &\leq \pi^{(1)}(a,i) + \mathbb{E}_{\delta_{(a,i)}}\left[\tilde{\pi}(T,1)\mathbb{1}_{Z_T=\delta_{T,1}}\right] + \mathbb{E}_{\delta_{(a,i)}}\left[\tilde{\pi}(0,I_1)\tilde{\pi}(0,I_2)\mathbb{1}_{Z_T=\delta_{(0,I_1)}+\delta_{(0,I_2)}}\right] \\ &= \tilde{\pi}(a,i), \end{aligned}$$

since $\tilde{\pi}$ is a solution of (4.43). Therefore, by induction, for all $n \in \mathbb{N}$, $\pi^{(n)} \leq \tilde{\pi}$. Moreover, since $\left\{\pi^{(n)}(a,i)\right\}_{n\in\mathbb{N}}$ is a sequence of probabilities of monotonic increasing events, we pass to the limit and conclude that $\pi \leq \tilde{\pi}$. Finally, notice that $\pi_0 = \pi_1 = 1$ is always an admissible solution, therefore the extinction probability are well contained in $[0,1]$. □

4.9.2 Proof of Theorem 4.3.5

Proof. First, note that (4.13a) and (4.13b) define two parabolic curves in the plane (π_0, π_1) which intersect at least at the point $(1,1)$, since $\pi_0 = \pi_1 = 1$ is always solution of the system. The proof consists in showing that other intersection occurs in the unit square $[0,1[\times[0,1[$ if and only if Condition (4.16) is verified. As in the classical characterisation of the extinction probability in Galton-Watson branching processes, this property can be obtained as a consequence of the value of the derivatives of the curves at the intersection point $(1,1)$.

Note that the parametric curve defined by (4.13a) is a concave parabola whose intercept is located at $\pi_1 = -p\frac{1-q}{q} < 0$ and whose derivative is given by

$$\frac{d\pi_1}{d\pi_0}(\pi_0) = \frac{1-2(1-p)(1-q)\pi_0}{q}.$$

In particular, the derivative in $(1,1)$ equals

$$\frac{d\pi_1}{d\pi_0}(1) = \frac{1-2(1-p)(1-q)}{q}.$$

Note that the curve defined by (4.13a) admits two solutions at $\pi_0 = 1$. However, using the implicit function theorem around $(1,1)$, we obtain a locally well defined function such that, by the implicit differentiation of (4.13b), it has derivative

$$\frac{d\pi_1}{d\pi_0}(\pi_0) = 2\left(\gamma\pi_0 + (1-\gamma)\pi_1(\pi_0)\right)\left(\gamma + (1-\gamma)\frac{d\pi_1}{d\pi_0}(\pi_0)\right),$$

and therefore at $(1,1)$ we have

$$\frac{d\pi_1}{d\pi_0}(1) = \frac{2\gamma}{2\gamma-1}.$$

We can show that there is a second solution $\bar{\pi}_1$ of (4.13b) at $\pi_0 = 1$ comprised strictly between 0 and 1 if and only if $0 < \gamma < 1/2$. Moreover, (4.13b) also admits $(0,0)$ as solution. Thus, the trace of the curve described by (4.13b) connects $(0,0)$ to $(1,1)$ if $\gamma \geq 1/2$, or to $(1,\bar{\pi}_1)$, if $\gamma < 1/2$. Meanwhile, the curve of (4.13a) connects the negative ordinate $(0, -p\frac{1-q}{q})$ with $(1,1)$. Therefore, no intersection other than $(1,1)$ can occur inside the unit square if and only if $\gamma \geq 1/2$, and (4.13a) arrives at $(1,1)$ with non-negative derivative and whose value is at least as much as the value of the derivative of (4.13b). Otherwise, by the continuity and strict monotonicity of the curves we would have some other intersection point below $(1,1)$ (see Fig. 4.3). This is then:

$$\gamma \geq 1/2 \quad , \quad 1-2(1-p)(1-q) \geq 0 \quad \text{and} \quad \frac{1-2(1-p)(1-q)}{q} \geq \frac{2\gamma}{2\gamma-1},$$

which gives finally, for $p \neq 1/2$

$$\gamma \geq \frac{1}{2}\left(1 + \frac{q}{(2p-1)(1-q)}\right).$$

In particular, the condition cannot be verified if $p < 1/2$. In the case $p = 1/2$, the previous conditions cannot be verified either. Thus finally, extinction occurs almost surely if and only if $p > 1/2$ and condition (4.16) is verified, which gives the result. □

4.10 Proofs of Section 4.4

4.10.1 Proof of Proposition 4.4.2

Proof. Let $(a,i) \in \mathbb{R}_+ \times \{0,1\}$, $f \in \mathcal{B}_b(\mathbb{R}_+ \times \{0,1\})$. Conditioning on the first jump event, we develop $M_t f(a,i)$ using Lemma 4.2.3 to compute the expectations at each jump case, and the strong Markov property, similarly as we did in the Proof of Proposition 3.5. We obtain the following Duhamel's representation:

$$\begin{aligned} M_t f(a,i) =& f(a+t,i)\psi_i(a,a+t) \\ &+ (1-i)\alpha \int_0^t M_{t-s} f(a+s,1)\psi_i(a,a+s)ds \\ &+ 2\int_0^t \beta_i(a+s)\psi_i(a,a+s)\Big\{(i-1)(1-p)M_{t-s}f(0,0) \\ &\quad i\left(\gamma M_{t-s}f(0,0) + (1-\gamma)M_{t-s}f(0,1)\right)\Big\}ds, \end{aligned} \tag{4.46}$$

where the first term of the RHS corresponds to the deterministic evolution when there are no events before time t, the second term corresponds to the case when the first jump is a type switch, and the third one to the case when the first jump is a division.

We iterate Duhamel's formula once more for the second line of the RHS, using (4.46) with $i = 1$ and $a = a + s$, and then re-injecting the obtained result. We obtain therefore a representation that uses only the semigroup valuated at initial age 0. Rearranging the terms for $i = 0$ and $i = 1$ in a vector, we obtain (4.21). □

4.10.2 Proof of Lemma 4.4.6

Proof. We start by the direct integration of (4.23) to obtain $\mathbf{K}_\infty$. The integration of the composition $\psi_0 \star \psi_1$ requires some attention. First, we can easily remark that for all $s < a$, $\psi_1(s,a) = \psi_1(0,a)/\psi_1(0,s)$, and then using Fubini's theorem we obtain that

$$\begin{aligned} \int_0^{+\infty} \alpha\beta_1(a)\psi_0 \star \psi_1(0,a)da &= \int_0^{+\infty} \alpha\beta_1(a)\int_0^a \psi_0(0,s)\psi_1(s,a)dsda \\ &= \int_0^{+\infty} \alpha\frac{\psi_0(0,s)}{\psi_1(0,s)}\left(\int_s^{+\infty}\beta_1(a)\psi_1(0,a)da\right)ds. \end{aligned}$$

But, by definition of the survival function, we know that $\psi_1(0,s) = \int_s^{+\infty}\beta_1(a)\psi_1(0,a)da$. Thus, using the definition of q introduced by (4.12) we have that

$$\int_0^{+\infty} \alpha\beta_1(a)\psi_0 \star \psi_1(0,a)da = \int_0^{+\infty}\alpha\psi_0(0,s)ds = q.$$

Thus, we obtain finally

$$\mathbf{K}_\infty = 2\begin{bmatrix} (1-p)(1-q)+\gamma q & (1-\gamma)q \\ \gamma & 1-\gamma \end{bmatrix},$$

which is a 2×2 matrix of non-negative terms. In particular, it has non-negative discriminant and non-negative eigenvalues which are given by

$$\frac{1}{2}\left(\mathrm{tr}(\mathbf{K}_\infty) \pm \sqrt{\mathrm{tr}(\mathbf{K}_\infty)^2 - 4\det(\mathbf{K}_\infty)}\right).$$

with

$$\begin{aligned}\mathrm{tr}(\mathbf{K}_\infty) &= 2\left(1 + (1-p-\gamma)(1-q)\right);\\ \det(\mathbf{K}_\infty) &= 4(1-p)(1-q)(1-\gamma).\end{aligned}$$

In particular, the largest eigenvalue is larger than 1 if and only if

$$\sqrt{\mathrm{tr}(\mathbf{K}_\infty)^2 - 4\det(\mathbf{K}_\infty)} > 2 - \mathrm{tr}(\mathbf{K}_\infty) = (\gamma - (1-p))(1-q). \tag{4.47}$$

1. Case $\gamma \le 1-p$: Since the RHS of (4.47) is non-positive, (4.47) is trivially verified and we have immediately $\rho(\mathbf{K}_\infty) > 1$

2. Case $\gamma > 1-p$: Since the RHS of (4.47) is positive, by taking squares we have that (4.47) is equivalent to the following inequalities:

$$\begin{aligned}&\mathrm{tr}(\mathbf{K}_\infty)^2 - 4\det(\mathbf{K}_\infty) > 4 + \mathrm{tr}(\mathbf{K}_\infty)^2 - 4\mathrm{tr}(\mathbf{K}_\infty)\\ \iff &\mathrm{tr}(\mathbf{K}_\infty) - \det(\mathbf{K}_\infty) - 1 > 0\\ \iff &2 + 2(1-p-\gamma)(1-q) - 4(1-p)(1-q)(1-\gamma) - 1 > 0\\ \iff &2(1-q)((1-\gamma)(1-2(1-p)) - p) + 1 > 0.\end{aligned}$$

   Then, isolating the value of γ we obtain

$$(2p-1)\gamma < \frac{(2p-1)(1-q)+q}{2(1-q)}. \tag{4.48}$$

   We study the case $p > 1/2$ and $p \le 1/2$ separately. If $p > 1/2$, the factor $2p-1$ is positive, and then dividing (4.48) by $2p-1$ we obtain directly condition (4.16):

$$\gamma < \frac{1}{2}\left(1 + \frac{q}{(2p-1)(1-q)}\right).$$

   If $p = 1/2$, then (4.48) is trivially verified. Finally, if $p < 1/2$, the factor $2p-1$ is negative and dividing (4.48) by $2p-1$ we obtain

$$\gamma > \frac{1}{2}\left(1 + \frac{q}{(2p-1)(1-q)}\right).$$

   However, since we are under the assumption $\gamma > 1-p$ and $p < 1/2$, we have $\gamma > 1/2$ and the inequality above is verified a fortiori.

Summarising,

$$\begin{aligned}\rho(\mathbf{K}_\infty) > 1 \iff &\{\gamma \le 1-p\} \cup (\{\gamma > 1-p\} \cap \{p > 1/2\} \cap \{(4.16) \text{ is true}\})\\ &\cup (\{\gamma > 1-p\} \cap \{p \le 1/2\})\\ \iff &\{p \le 1/2\} \cup (\{p > 1/2\} \cap \{(4.16) \text{ is true}\}),\end{aligned}$$

which is exactly the condition assuring survival with positive probability in Theorem 4.3.5. □

4.10.3 Proof of Lemma 4.4.7

Proof. Notice that for all $\lambda \in \mathbb{R}$ the matrix $\mathbf{F}(\lambda)$ is a 2×2 matrix with all strictly positive entries. In particular, this assures irreducibility and by Perron-Frobenius Theorem we have the existence, for all fixed $\lambda \in \mathbb{R}$, of a unique triplet of eigenelements $(\mu(\lambda), \mathbf{n}(\lambda), \mathbf{h}(\lambda))$ such that

$$\begin{cases} \mathbf{F}(\lambda)\mathbf{h}(\lambda) = \mu(\lambda)\mathbf{h}(\lambda) \\ \mathbf{n}(\lambda)^\top \mathbf{F}(\lambda) = \mu(\lambda)\mathbf{n}(\lambda)^\top \\ \mathbf{n}(\lambda)^\top \mathbf{h}(\lambda) = 1 \\ \mathbf{n}(\lambda)^\top (1,1) = 1. \end{cases}$$

We start by the sufficiency direction of the equivalence. To show that there is a unique $\lambda > 0$ such that $\rho(\mathbf{F}(\lambda)) = 1$ we will use a classical monotonicity argument. First, we notice that $\mathbf{F}(0) = \mathbf{K}_\infty$, which under the survival conditions and thanks to Lemma 4.4.6 has spectral radius $\rho(\mathbf{F}(0)) = \mu(0) > 1$. Second, notice that as $\lambda \to +\infty$, $e^{-\lambda s}\mathbf{K}(0,s)$ decreases coordinate by coordinate to the null matrix. Thus, we have by monotone convergence that $\mathbf{F}(+\infty) = \mathbf{0}_{2\times 2}$ and therefore $\lim_{\lambda\to+\infty} \mu(\lambda) = 0$. It remains to show that $\lambda \mapsto \mu(\lambda)$ is a decreasing continuous function. This is a classical property that comes from Lemma 4.12.2. The monotonicity is given by the assertion (i) of the Lemma, whilst the continuity comes from the estimation (ii) and the continuity of $\lambda \mapsto e^{-\lambda s}$. Finally, this implies that there exists a unique $\lambda^* > 0$ such that $\mu(\lambda^*) = 1$.

The necessity direction of the equivalence follows easily from the previous remarks. Since $\lambda \mapsto \mu(\lambda)$ is a continuous decreasing function, if $\lambda^* \in \mathbb{R}$ such that $\mu(\lambda^*) = 1$ is strictly positive, then $\rho(\mathbf{F}(0)) = \mu(0) > 1$. Finally, by Lemma 4.4.6, this is equivalent to verify the survival condition (4.16). □

4.10.4 Proof of Proposition 4.4.5

Proof. The proof follows classical arguments, presented for example in Section 4.3 of [143]. The first part of the proof consists on showing the existence of a spectral gap, this is, of a positive constant ω such that for the value of λ defined by (4.32) we have

$$\max\left\{-\underline{b}, \sup_{z\in\sigma(\mathcal{Q})\setminus\sigma_{ess}(\mathcal{Q})\setminus\{\lambda\}} \mathrm{Re}(z)\right\} < \omega < \lambda.$$

To do so, we show in Section 4.10.5 further below that the *growth bound* $\omega_1(\mathbf{M}_t)$ associated with the measure of non-compactness of the semigroup $\mathbf{M}_t$ (see Definition 4.10.2) is bounded by $-\underline{b}$. Then, by Theorem 4.6 of [143] we have that the essential spectrum of $\mathcal{Q}$ must be contained within $\{z \in \mathbb{C} : \mathrm{Re}(z) \leq -\underline{b}\}$. Therefore, for any $\lambda \in \mathbb{C}$ such that $\mathrm{Re}(\lambda) > -\underline{b}$ which is a root of the characteristic equation (4.32), we have that λ is an eigenvalue of $\mathcal{Q}$. This is, there exists a non-zero $\mathbf{h} \in (L^1(\mathbb{R}_+))^2$ such that $\mathcal{Q}\mathbf{h} = \lambda\mathbf{h}$.

Indeed, suppose that the pair $(\lambda, \mathbf{h})$ is solution to $\mathcal{Q}\mathbf{h} = \lambda\mathbf{h}$, then $\mathbf{h}' \in (L^1(\mathbb{R}_+))^2$ and is given almost everywhere by

$$\mathbf{h}'(a) = (\lambda\mathbf{I} + \mathbf{D}(a))\mathbf{h}(a) - 2\mathbf{B}(a)\mathbf{h}(0).$$

Then, we notice that

$$\begin{aligned}\partial_a\left(e^{-\lambda a}\mathbf{\Psi}(0,a)\mathbf{h}(a)\right) &= \partial_a\left(e^{-\lambda a}\mathbf{\Psi}(0,a)\right)\mathbf{h}(a) + e^{-\lambda a}\mathbf{\Psi}(0,a)\mathbf{h}'(a)\\ &= -e^{-\lambda a}\mathbf{\Psi}(0,a)(\lambda\mathbf{I}+\mathbf{D}(a))\mathbf{h}(a) + e^{-\lambda a}\mathbf{\Psi}(0,a)(\lambda\mathbf{I}+\mathbf{D}(a))\mathbf{h}(a)\\ &\quad - 2e^{-\lambda a}\mathbf{\Psi}(0,a)\mathbf{B}(a)\mathbf{h}(0)\\ &= -2e^{-\lambda a}\mathbf{K}(0,a)\mathbf{h}(0). \end{aligned} \tag{4.49}$$

Therefore, since $\mathbf{h}\in(L^1(\mathbb{R}_+))^2$ and $\lim_{a\to+\infty}\mathbf{\Psi}(0,a)=\mathbf{0}$, we have

$$\mathbf{h}(0) = -\int_0^{+\infty}\partial_a\left(e^{-\lambda a}\mathbf{\Psi}(0,a)\mathbf{h}(a)\right)da = 2\int_0^{+\infty}e^{-\lambda a}\mathbf{K}(0,a)\mathbf{h}(0)\,da = \mathbf{F}(\lambda)\mathbf{h}(0).$$

This linear equation has a non-trivial solution $\mathbf{h}(0)$ if and only if $\det(\mathbf{F}(\lambda)-\mathbf{I})=0$. Conversely if λ is the largest root of $\det(\mathbf{F}(\lambda)-\mathbf{I})=0$ and is simple and associated with some eigenvector $\mathbf{h}(0)\in\mathbb{R}^2_+$, we have that

$$\mathbf{h}(a) := e^{\lambda a}\mathbf{\Psi}^{-1}(0,a)\left(\mathbf{I}-2\int_0^a e^{-\lambda s}\mathbf{\Psi}(0,s)\mathbf{B}(s)\,ds\right)\mathbf{h}(0) \tag{4.50}$$

$$= 2e^{\lambda a}\int_a^{+\infty}e^{-\lambda s}\mathbf{\Psi}(a,s)\mathbf{B}(s)\,ds\mathbf{h}(0) \tag{4.51}$$

is a $(L^1(\mathbb{R}_+))^2$ solution to $\mathcal{Q}\mathbf{h}=\lambda\mathbf{h}$ (both representations will be useful in the sequel). Finally, Lemma 4.4.7 allows us to conclude for the simplicity of the eigenvalue λ.

Then, thanks to Proposition 4.65 of [143], we can identify $\ker(\lambda\mathbf{I}-\mathcal{Q})$ to the image of the projection operator $\mathbf{P}:(L^1(\mathbb{R}_+))^2\to(L^1(\mathbb{R}_+))^2$ given by the resolvent

$$\mathbf{P}\mathbf{f}(a) := \frac{1}{2\pi i}\oint_{C_\lambda}(z\mathbf{I}-\mathcal{Q})^{-1}\mathbf{f}(a)\,dz,$$

where C_λ is a closed counterclockwise oriented curve of the complex plane enclosing λ but no other point of the spectrum of $\mathcal{Q}$.

Then, since λ is a simple root of (4.32), we have a unique pair $(\lambda,\mathbf{h})$ (up to normalisation of $\mathbf{h}$) such that $\mathcal{Q}\mathbf{h}=\lambda\mathbf{h}$, and so $\mathbf{P}$ is of rank 1. Therefore, for all $\mathbf{f}$ we can write $\mathbf{P}\mathbf{f}(a)=\bar\nu(\mathbf{f})\mathbf{h}(a)$, where $\bar\nu(\mathbf{f})$ is a normalisation constant depending on $\mathbf{f}$.

Moreover, by the linearity of $\mathbf{P}$, we have that $\boldsymbol{\nu}:(C_c(\mathbb{R}_+))^2\to\mathbb{R}^2_+$ given for all $\mathbf{f}$ of the form $\mathbf{f}=(f(\cdot,0),f(\cdot,1))$ by

$$\boldsymbol{\nu}(\mathbf{f}) = (\bar\nu(f(\cdot,0),0),\bar\nu(0,f(\cdot,1)))$$

is a linear application. Therefore, Riesz–Markov–Kakutani representation Theorem allows us to write $\bar\nu(\mathbf{f})=\int_0^{+\infty}\mathbf{f}(a)^\top\boldsymbol{\nu}(da)$ where $\boldsymbol{\nu}\in(\mathcal{M}(\mathbb{R}_+))^2$ is a (vector) positive Radon measure. Furthermore, by duality we can conclude that this measure $\boldsymbol{\nu}$ is the limiting distribution of the population ages in the sense that for all initial distribution $\boldsymbol{\mu}$ and all $\mathbf{f}\in(L^1(\mathbb{R}_+))^2$ we have

$$\begin{aligned}e^{-\lambda t}\langle\boldsymbol{\mu}\mathbf{M}_t,\mathbf{f}\rangle = \int_0^{+\infty}\mathbf{f}(a)\,e^{-\lambda t}\boldsymbol{\mu}\mathbf{M}_t(da) &= \int_0^{+\infty}e^{-\lambda t}\mathbf{M}_t\mathbf{f}(a)\,\boldsymbol{\mu}(da)\\ &\xrightarrow[t\to+\infty]{}\left(\int_0^{+\infty}\mathbf{h}(a)\boldsymbol{\mu}(da)\right)\left(\int_0^{+\infty}\mathbf{f}(a)\boldsymbol{\nu}(da)\right)\end{aligned}$$

Finally, by Proposition 4.15 of [143] we have

$$||\mathbf{M}_t\mathbf{f} - \mathbf{P}\mathbf{f}||_1 \leq ce^{\omega t}||\mathbf{f} - \mathbf{P}\mathbf{f}||_1$$

from where we conclude the exponential rate of convergence. □

4.10.5 Compactness estimates

We start our analysis by studying some estimates about the boundness and compactness of $\mathbf{M}_t$. To that purpose, we write the decomposition

$$\mathbf{M}_t\mathbf{f}(a) = \mathbf{U}_t\mathbf{f}(a) + \mathbf{W}_t\mathbf{f}(a),$$

where $\mathbf{U}_t$ is destinated to be small and $\mathbf{W}_t$ is destinated to be compact, in the senses that will be detailed further below (see for example Section 3.4 of [143] for a detailed motivation of this decomposition). In our case, the natural decomposition is given by Lemma 4.10.1.

Lemma 4.10.1. *Consider the semigroup $\mathbf{M}_t$ on $(L^1(\mathbb{R}_+))^2$ introduced by Def. 4.4.1. Then, for all $\mathbf{f} \in (L^1(\mathbb{R}_+))^2$ we can write $\mathbf{M}_t\mathbf{f}(a) = \mathbf{U}_t\mathbf{f}(a) + \mathbf{W}_t\mathbf{f}(a)$ where*

$$\mathbf{U}_t\mathbf{f}(a) := \mathbf{\Psi}(a, a+t)\mathbf{f}(a+t) \tag{4.52a}$$

$$\mathbf{W}_t\mathbf{f}(a) := 2\int_0^t \mathbf{K}(a, a+t-s)(\mathbf{I} - \mathbf{S}_1)^{-1}\mathbf{S}_2\mathbf{f}(s)ds, \tag{4.52b}$$

where $\mathbf{S}_1 : (L^1(\mathbb{R}_+))^2 \to (L^1(\mathbb{R}_+))^2$ is a locally compact linear operator of spectral radius 0, and $\mathbf{S}_2 : (L^1(\mathbb{R}_+))^2 \to (L^1(\mathbb{R}_+))^2$ is a bounded linear operator, both defined by

$$\mathbf{S_1}\mathbf{f}(t) := 2\int_0^t \mathbf{K}(0, t-s)\mathbf{f}(s)ds$$
$$\mathbf{S_2}\mathbf{f}(t) := \mathbf{\Psi}(0, t)\mathbf{f}(t).$$

Moreover, for all fixed $t > 0$, $\mathbf{W}_t : (L^1([0,t]))^2 \to (L^1([0,t]))^2$ is a compact operator.

Proof. Fix $t > 0$ and let $\mathbf{f} \in (L^1([0,t]))^2$. When needed, we extend $\mathbf{f}$ to $(L^1(\mathbb{R}))^2$ as $\mathbf{f}(s) = (0,0)$ whenever $s > t$ or $s < 0$. The Duhamel representation obtained in (4.21), along with (4.24) give that for all $a \geq 0$,

$$\mathbf{M}_t\mathbf{f}(a) = \mathbf{\Psi}(a, a+t)\mathbf{f}(a+t) + 2\int_0^t \mathbf{K}(a, a+t-s)\mathbf{g}(s)ds,$$

where $\mathbf{g}$ solves the fixed point problem

$$\begin{aligned}\mathbf{g}(s) &= \mathbf{\Psi}(0, s)\mathbf{f}(s) + 2\int_0^s \mathbf{K}(0, s-u)\mathbf{g}(u)du \\ &= \mathbf{S_2}\mathbf{f}(s) + \mathbf{S_1}\mathbf{g}(s)\end{aligned}$$

Therefore, if $(\mathbf{I}-\mathbf{S}_1)^{-1}$ is well defined, we have that $\mathbf{g}$ can be obtained as

$$\mathbf{g} = (\mathbf{I}-\mathbf{S}_1)^{-1}\mathbf{S}_2\mathbf{f},$$

from where we get (4.52b).

Hence, we start proving that $\mathbf{S_1} : (L^1([0,t]))^2 \to (L^1([0,t]))^2$ is a compact linear operator, to then conclude thanks to the Fredholm alternative.

1. **Compactness of $\mathbf{S}_1$.** Since we are restricted to the compact interval $[0,t]$ we only need to check the equicontinuity assumption of the Riesz-Fréchet-Kolmogorov Theorem. Consider some bounded sequence $\{\mathbf{f}_n\}_n$ on the unit ball of $(L^1([0,t]))^2$. For all $\mathbf{f} \in (L^1([0,t]))^2$ we have

$$\begin{aligned}
\int_0^t ||\mathbf{S}_1\mathbf{f}(s+a)-\mathbf{S}_1\mathbf{f}(s)||_1 ds &= 2\int_0^t ||\int_0^{s+a}\mathbf{K}(0,s+a-u)\mathbf{f}(u)du - \int_0^s \mathbf{K}(0,s-u)\mathbf{f}(u)du||_1 ds \\
&\le 2\int_0^t\int_0^s ||\mathbf{K}(0,s-u+a)-\mathbf{K}(0,s-u)||_1||\mathbf{f}(u)||_1 duds \\
&\quad + 2\int_0^t\int_s^{a+s} ||\mathbf{K}(0,s-u+a)||_1||\mathbf{f}(u)||_1 duds \\
&\le 2\int_0^t\int_0^s ||\mathbf{K}(0,s-u+a)-\mathbf{K}(0,s-u)||_1||\mathbf{f}(u)||_1 duds \\
&\quad + 2\int_0^a \left(\int_0^u ||\mathbf{K}(0,s-u+a)||_1 ds\right)||\mathbf{f}(u)||_1 du \\
&\quad + 2\int_a^t \left(\int_{u-a}^u ||\mathbf{K}(0,s-u+a)||_1 ds\right)||\mathbf{f}(u)||_1 du \\
&\le 2\int_0^t\int_0^s ||\mathbf{K}(0,s-u+a)-\mathbf{K}(0,s-u)||_1||\mathbf{f}(u)||_1 duds \\
&\quad + 2|a|\sup_{0<s<t}||\mathbf{K}(0,s)||_1||\mathbf{f}||_1
\end{aligned}$$

The second term of the RHS can be controlled uniformly as $|a| \to 0$. We focus in the first term. By construction, as shown in (4.9), the jump times are absolutely continuous random variables. Therefore $s \mapsto \mathbf{K}(0,s)$, which contains the probability densities of the different jump events at time s, is a continuous application from $\mathbb{R}_+$ to the vector space of positive 2×2 matrices. In particular, it is uniformly continuous over the compact $[0,t]$, this is, for all $\varepsilon > 0$, there exists $\delta > 0$ such that

$$||\mathbf{K}(0,s-a)-\mathbf{K}(0,s)||_1 < \varepsilon \qquad \text{for all } s \in [0,t[\quad \text{whenever } a < \delta$$

Therefore, for all $a < \delta$ we have

$$\int_0^t ||\mathbf{S}_1\mathbf{f}(s-a)-\mathbf{S}_1\mathbf{f}(s)||_1 ds \le 2\varepsilon t + 2|a|\sup_{0<s<t}||\mathbf{K}(0,s)||_1 =: \tilde{\varepsilon},$$

uniformly with respect to $\mathbf{f}$. Therefore $\{\mathbf{S}_1\mathbf{f}_n\}$ is relatively compact.

2. **Fredholm alternative.** Since $\mathbf{S_1} : (L^1([0,t]))^2 \to (L^1([0,t]))^2$ is compact, any $\lambda \neq 0$ is either an eigenvalue of $\mathbf{S_1}$ or otherwise lies in the domain of the resolvent. Let's suppose by absurd that $\lambda \neq 0$ is an eigenvalue associated to some nonzero eigenfunction $\mathbf{u} \in (L^1([0,t]))^2$ such that $\mathbf{S}_1\mathbf{u} = \lambda\mathbf{u}$, this is, for all $a \in [0,t]$,

$$\mathbf{u}(a) = \frac{2}{\lambda}\int_0^a \mathbf{K}(0, a-s)\mathbf{u}(s)ds,$$

and thereby,

$$||\mathbf{u}(a)||_1 \leq \frac{2}{\lambda}\sup_{0<s<t}||\mathbf{K}(0,s)||_1 \int_0^a ||\mathbf{u}(s)||_1 ds.$$

Thus, by Grönwall's inequality $||\mathbf{u}(a)||_1 = 0$ for all $a \in [0,t]$, and therefore $\mathbf{u} \equiv 0$, which is a contradiction. Therefore the spectrum of $\mathbf{S}_1$ consists only on $\{0\}$. In particular the constant $\lambda = 1$ is in the domain of the resolvent and $(\mathbf{I} - \mathbf{S}_1)^{-1}$ is then well defined bounded linear operator.

We prove that $\mathbf{S}_2 : (L^1([0,t]))^2 \to (L^1([0,t]))^2$ is bounded and then, rejoining all the previous results, we obtain the compactness of $\mathbf{W}_t : (L^1([0,t]))^2 \to (L^1([0,t]))^2$ which allow us to conclude the Lemma.

3. **Boundness of $\mathbf{S}_2$.** For all $\mathbf{f} \in (L^1([0,t]))^2$ we have

$$\int_0^t ||\mathbf{S}_2\mathbf{f}(s)||_1 ds \leq \int_0^t ||\mathbf{\Psi}(0,s)||_1 ||\mathbf{f}(s)||_1 ds \leq ||\mathbf{f}||_1,$$

since $t \mapsto \mathbf{\Psi}(0,t)$ is decreasing in each coordinate and therefore $\sup_{t>0}||\mathbf{\Psi}(0,t)||_1 = ||\mathbf{\Psi}(0,0)||_1 = 1$.

4. **Compactness of $\mathbf{W}_t$.** As we did for $\mathbf{S}_1$, for all $\mathbf{f} \in (L^1([0,t]))^2$ we have

$$\int_0^t (\mathbf{W}_t\mathbf{f}(a+s) - \mathbf{W}_t\mathbf{f}(a))\, da = 2\int_0^t \int_0^t (\mathbf{K}(a+s, a+s+t-u) - \mathbf{K}(a, a+t-u)) \\ (\mathbf{I} - \mathbf{S}_1)^{-1}\mathbf{S}_2\mathbf{f}(u)\, du\, da,$$

and therefore

$$||\mathbf{W}_t\mathbf{f}(\cdot + s) - \mathbf{W}_t\mathbf{f}(\cdot)||_1 \leq 2\int_0^t \left(\int_0^t ||\mathbf{K}(a+s, a+s+t-u) - \mathbf{K}(a, a+t-u)||_1 da\right) \\ ||(\mathbf{I} - \mathbf{S}_1)^{-1}\mathbf{S}_2\mathbf{f}(u)||_1 du$$

By our previous calculations, we can bound $||(\mathbf{I} - \mathbf{S}_1)^{-1}\mathbf{S}_2\mathbf{f}(u)||_1$ uniformly for $u \in [0,t]$ by some constant $M > 0$ times $||\mathbf{f}||_1$. By the absolutely continuity of the jump time densities, $(a,s) \mapsto \mathbf{K}(a,s)$ is a continuous application in both coordinates, and therefore uniformly continuous on $[0,t]$. Thus, for all $\varepsilon > 0$ there exists a $\delta > 0$ such that whenever $|s| < \delta$, then

$$||\mathbf{W}_t\mathbf{f}(\cdot + s) - \mathbf{W}_t\mathbf{f}(\cdot)||_1 \leq 2Mt^2\varepsilon,$$

uniformly for all $\mathbf{f} \in (L^1([0,t]))^2$ with $||\mathbf{f}||_1 \leq 1$. Therefore $\mathbf{W}_t$ maps bounded set to relatively compact sets and we conclude the proof.

□

We recall now some useful definitions:

Definition 4.10.2 (Measure of non-compactness and growth bounds)**.** We define the Kuratowski's measure of non-compactness of a bounded set A of a Banach space $\mathcal{X}$ as

$$\alpha(A) := \inf\{\varepsilon > 0 : A \text{ can be covered by a finite number of subsets of } \mathcal{X} \text{ of diameter} \leq \varepsilon\},$$

and the associated measure of non-compactness of a bounded operator S in $\mathcal{X}$ as

$$\alpha(S) := \inf\{\varepsilon > 0 : \alpha(S(A)) \leq \varepsilon\alpha(A) \text{ for all bounded sets } A \subset \mathcal{X}\}.$$

Finally we define the α-growth bound of the semigroup $\mathbf{M}_t$ as

$$\omega_1(\mathbf{M}_t) := \lim_{t\to+\infty} \frac{1}{t}\log\left(\alpha\left(\mathbf{M}_t\right)\right).$$

Now, thanks to the decomposition proven in Lemma 4.10.1, we obtain the following estimate on the non-compactness of $\mathbf{M}_t$:

Proposition 4.10.3. *Under Assumptions 4.2.1 we have that* $\omega_1(\mathbf{M}_t) \leq -\bar{b} < 0$.

Proof. From Proposition 4.12.1 applied to the decomposition proven on Lemma 4.10.1, since $\mathbf{W}_t$ is compact we have that

$$\alpha(\mathbf{M}_t) \leq \alpha(\mathbf{U}_t) \leq ||\mathbf{U}_t||.$$

Now, for all fixed $t \geq 0$, and for all $a \geq 0$, we have term by term

$$\mathbf{\Psi}(a, a+t) \leq \begin{bmatrix} e^{-(\alpha+\underline{b})t} & e^{-\underline{b}t}(1-e^{-\alpha t}) \\ 0 & e^{-\underline{b}t} \end{bmatrix},$$

so $||\mathbf{\Psi}(a, a+t)||_1 \leq e^{-\underline{b}t}\left(2 - e^{-\alpha t}\right)$. Therefore, for all $\mathbf{f} \in (L^1(\mathbb{R}_+))^2$ we have,

$$\begin{aligned} ||\mathbf{U}_t\mathbf{f}||_1 &= \int_0^{+\infty} ||\mathbf{\Psi}(a, a+t)\mathbf{f}(a+t)||_1 da \\ &\leq e^{-\underline{b}t}\left(2 - e^{-\alpha t}\right)||\mathbf{f}||_1, \end{aligned}$$

and therefore

$$\omega_1(\mathbf{M}_t) \leq \lim_{t\to+\infty} \frac{1}{t}\log\left(e^{-\underline{b}t}\left(2 - e^{-\alpha t}\right)\right) = -\underline{b}$$

□

Then we conclude with the rest of the proof of Proposition 4.4.5 as stated in the main text.

4.10.6 Proof of Remark 4.4.8

Proof. Notice that taking as test function $\mathbf{f} \equiv \mathbf{1} = (1,1)$, we get

$$\begin{aligned}\mathbf{M}_t\mathbf{1}(a) &= \mathbf{1} + \int_0^t \mathbf{M}_s\left(\mathcal{Q}\mathbf{1}\right)(a)ds = \mathbf{1} + \int_0^t \mathbf{M}_s\left((2\mathbf{B}(\cdot) - \mathbf{D}(\cdot))\mathbf{1}\right)(a)ds \\ &= \mathbf{1} + \int_0^t \begin{bmatrix}\mathbf{M}_s(\beta_0,0)(a)^\top \\ \mathbf{M}_s(0,\beta_1)(a)^\top\end{bmatrix} ds \begin{pmatrix}1-2p \\ 1\end{pmatrix} ds.\end{aligned}$$

Therefore for both coordinates $i \in \{0,1\}$ we have

$$M_t1(a,i) \leq 1 + \bar{b}\int_0^t \mathbf{M}_s1(a,i)ds.$$

Hence, by Grönwall 's inequality, for all $a \geq 0$, $M_t1(a,u) \leq e^{\bar{b}t}$.

Therefore, by duality, and since $\boldsymbol{\nu}\mathbf{M}_t(da) = e^{\lambda t}\boldsymbol{\nu}(da)$,

$$e^{\lambda t}\left\langle \boldsymbol{\nu}, \mathbf{1}\right\rangle = \left\langle \boldsymbol{\nu}\mathbf{M}_t, \mathbf{1}\right\rangle = \left\langle \boldsymbol{\nu}, \mathbf{M}_t\mathbf{1}\right\rangle \leq e^{\bar{b}t}\left\langle \boldsymbol{\nu}, \mathbf{1}\right\rangle.$$

Finally, $\langle \boldsymbol{\nu}, \mathbf{1}\rangle = 1 \neq 0$ and the result follows.

□

4.11 Proofs of Section 4.5

4.11.1 Proof of Lemma 4.5.1

Proof. Since $\mathbf{h}$ is solution to the eigenproblem $\mathcal{Q}\mathbf{h} = \lambda\mathbf{h}$, representation (4.51) gives us

$$\mathbf{h}(a) = 2\int_0^{+\infty} e^{-\lambda s}\mathbf{\Psi}(a, a+s)\mathbf{B}(a+s)\mathbf{h}(0)ds.$$

We deduce the result by Dominated Convergence in each coordinate of the expression above. Set $\boldsymbol{\ell}(a,s) := 2e^{-\lambda s}\mathbf{\Psi}(a,a+s)\mathbf{B}(s)\mathbf{h}(0)$. Note that only matrix $\mathbf{\Psi}$ (defined in (4.22), and with $\psi_0, \psi_1, \psi_0 \star \psi_1$ in (4.2)-(4.4)) depends on a. First, we know by construction of the Perron eigenelements that for all $a \geq 0$, $\boldsymbol{\ell}(a,\cdot) \in (L^1(\mathbb{R}_+))^2$. Indeed:

$$||\boldsymbol{\ell}(a,s)||_\infty \leq 2\bar{b}||\mathbf{h}(0)||_\infty e^{-\lambda s} \in L^1(\mathbb{R}_+, ds).$$

Moreover, since we assume additionally that β_0, β_1 are continuous, we deduce that for all $s \geq 0$, $\boldsymbol{\ell}(\cdot, s) \in C^1\left(\mathbb{R}_+, \mathbb{R}_+^2\right)$. Indeed, for all $a \geq 0, s \geq 0$, we have explicitly

$$\begin{aligned}\partial_a\psi_0(a,a+s) &= (\beta_0(a) - \beta_0(a+s))\psi_0(a,a+s), \\ \partial_a\psi_1(a,a+s) &= (\beta_1(a) - \beta_1(a+s))\psi_1(a,a+s), \\ \partial_a(\psi_0 \star \psi_1)(a,a+s) &= (\alpha + \beta_0(a) - \beta_1(a+s))\psi_0 \star \psi_1(a,a+s) + \psi_0(a,a+s) - \psi_1(a,a+s),\end{aligned}$$

where all the terms at the RHS are well defined and continuous for all $a \geq 0$. Finally, all these terms are uniformly bounded by $\bar{b} + \alpha + 1$, and therefore

$$||\partial_a\boldsymbol{\ell}(a,s)||_\infty \leq 4\bar{b}(\bar{b} + \alpha + 1)||\mathbf{h}(0)||_\infty e^{-\lambda s} \in L^1(\mathbb{R}_+, ds).$$

Hence, by the Dominated Convergence Theorem, $\mathbf{h} \in C^1(\mathbb{R}_+,\ \mathbb{R}_+^2)$. □

4.11.2 Proof of Lemma 4.5.2

Proof. Writing the dependencies on α and γ explicitly, we express $\mathbf{h}_{\alpha,\gamma}(a)$ for all $a \geq 0$ as

$$\mathbf{h}_{\alpha,\gamma}(a) = 2\int_0^{+\infty} e^{-\lambda_{\alpha,\gamma} s}\mathbf{\Psi}_\alpha(a, a+s)\mathbf{B}_\gamma(a+s)\mathbf{h}_{\alpha,\gamma}(0)ds. \tag{4.53}$$

Again by Dominated Convergence, it suffices to prove the continuity and domination by an integrable function of both coordinates of

$$(\alpha,\gamma) \mapsto \boldsymbol{\ell}_a(\alpha,\gamma) := 2e^{-\lambda_{\alpha,\gamma} s}\mathbf{\Psi}_\alpha(a, a+s)\mathbf{B}_\gamma(a+s)\mathbf{h}_{\alpha,\gamma}(0) \ \in \mathbb{R}_+^2.$$

Hence, we show first that $||\mathbf{h}_{\alpha,\gamma}(0)||_\infty$ is uniformly bounded in every open neighborhood of $(\alpha,\gamma) \in \mathbb{R}_+ \times (0,1)$. Using the normalisation condition $\langle \boldsymbol{\nu}_{\alpha,\gamma}, \mathbf{h}_{\alpha,\gamma}\rangle = 1$ with $\boldsymbol{\nu}_{\alpha,\gamma}$ the left eigenmeasure, we have that for all $a \geq 0$,

$$1 = \langle \boldsymbol{\nu}_{\alpha,\gamma}, \mathbf{h}_{\alpha,\gamma}\rangle = \mathbf{u}_{\alpha,\gamma}^\top \mathbf{h}_{\alpha,\gamma}(0),$$

where

$$\mathbf{u}_{\alpha,\gamma} := 2\int_0^{+\infty}\left(\int_0^{+\infty} e^{-\lambda_{\alpha,\gamma}\tau}\mathbf{B}_\gamma(a+\tau)^\top \mathbf{\Psi}_\alpha(a, a+\tau)^\top d\tau\right)\boldsymbol{\nu}_{\alpha,\gamma}(a)\, da.$$

Therefore, to bound each coordinate of $\mathbf{h}_{\alpha,\gamma}(0) \in \mathbb{R}_+^2$ it suffices to bound by below both coordinates of $\mathbf{u}_{\alpha,\gamma}$. Set $\mathbf{u}_{\alpha,\gamma} = (u^0_{\alpha,\gamma}, u^1_{\alpha,\gamma})$, such that

$$u^0_{\alpha,\gamma} = 2\iint_{\mathbb{R}_+^2} e^{-\lambda_{\alpha,\gamma}\tau}\boldsymbol{\nu}_{\alpha,\gamma}(a)^\top \begin{pmatrix}(1-p)\beta_0(a+\tau)\psi_0(a+\tau) + \gamma\beta_1(a+\tau)\alpha\psi_0 \star \psi_1(a, a+\tau)\\ \gamma\beta_1(a+\tau)\psi_1(a+\tau)\end{pmatrix} d\tau\, da,$$
$$u^1_{\alpha,\gamma} = 2\iint_{\mathbb{R}_+^2} e^{-\lambda_{\alpha,\gamma}\tau}\boldsymbol{\nu}_{\alpha,\gamma}(a)^\top \begin{pmatrix}(1-\gamma)\beta_1(a+\tau)\alpha\psi_0 \star \psi_1(a, a+\tau)\\ (1-\gamma)\beta_1(a+\tau)\psi_1(a+\tau)\end{pmatrix} d\tau\, da.$$

By Remark 4.4.8, the value of $\lambda_{\alpha,\gamma}$ is bounded by $\bar{b}$ for all (α,γ). Then, using Assumptions 4.2.1 to bound the division rates in matrix $\mathbf{B}$ and the survival functions in matrix $\mathbf{\Psi}$ we obtain :

$$u^0_{\alpha,\gamma} \geq 2\gamma\int_0^{+\infty}\left(\int_{a_0}^A \underline{b}e^{-2\bar{b}\tau}(1-e^{-\alpha\tau})d\tau\right)\boldsymbol{\nu}_{\alpha,\gamma}(a)^\top \mathbf{1}\, da,$$
$$u^1_{\alpha,\gamma} \geq 2(1-\gamma)\int_0^{+\infty}\left(\int_{a_0}^A \underline{b}e^{-2\bar{b}\tau}(1-e^{-\alpha\tau})d\tau\right)\boldsymbol{\nu}_{\alpha,\gamma}(a)^\top \mathbf{1}\, da,$$

for some fixed arbitrary quantity $A > a_0$ with a_0 being given by (A3) in Assumptions 4.2.1. Then, the integral with respect to τ can be uniformly bounded by below by some positive constant $\tilde{c}_{\alpha,A}$ dependent on α and the choice of A. Finally, by the normalisation condition $\langle \boldsymbol{\nu}, \mathbf{1}\rangle = 1$, we obtain

$$u^0_{\alpha,\gamma} \geq 2\gamma\tilde{c}_{\alpha,A}, \qquad u^1_{\alpha,\gamma} \geq 2(1-\gamma)\tilde{c}_{\alpha,A},$$

and therefore,

$$h_{\alpha,\gamma}(0,0) \leq \frac{1}{2\gamma\tilde{c}_{\alpha,A}}, \qquad h_{\alpha,\gamma}(0,1) \leq \frac{1}{2(1-\gamma)\tilde{c}_{\alpha,A}}.$$

Thus, for all fixed $a \geq 0$

$$\ell^0_{\alpha,\gamma}(a,s) \leq 2\tilde{c}^{-1}_{\alpha,A}\left(\frac{1-p}{\gamma}\beta_0(a+s)\psi_0(a,a+s) + \beta_1(a+s)\alpha\psi_0 \star \psi_1(a,a+s)\right) \in L^1(\mathbb{R}_+, ds),$$
$$\ell^1_{\alpha,\gamma}(a,s) \leq 2\tilde{c}^{-1}_{\alpha,A}\beta_1(a+s)\psi_1(a,a+s) \in L^1(\mathbb{R}_+, ds),$$

which can be bound uniformly in any neighbourhood around (α,γ), whenever $\alpha,\gamma \notin \{0,1\}$. Finally, we show that $(\alpha,\gamma) \mapsto \boldsymbol{\ell}_a(\alpha,\gamma)$ is continuous for the uniform norm. Fix some couple $(\alpha,\gamma) \in \mathbb{R}_+ \times (0,1)$ and let $(\alpha_n,\gamma_n)_{n\in\mathbb{N}}$ be some sequence converging to (α,γ) as $n \to +\infty$. We know already that $\mathbf{h}_{\alpha_n,\gamma_n}(0)$ and $\lambda_{\alpha_n,\gamma_n}$ are bounded for all n. Therefore we can extract some convergent subsequences with adherence values

$$\lambda_{\alpha_{n_k},\gamma_{n_k}} \to \lambda_\infty \geq 0, \qquad \mathbf{h}_{\alpha_{n_k},\gamma_{n_k}}(0) \to \boldsymbol{\eta}_\infty \in \mathbb{R}^2_+.$$

Moreover, note that for all fixed vector $\mathbf{x} \in \mathbb{R}^2_+$, the linear application $(\alpha,\gamma) \mapsto \mathbf{K}_{\alpha,\gamma}(a,a+s)\mathbf{x} = \boldsymbol{\Psi}_\alpha(a,a+s)\mathbf{B}_\gamma(a+s)\mathbf{x}$ is a continuous function of (α,γ) for the uniform norm. Therefore, we have that entry-wise

$$[\mathbf{K}_{\alpha_n,\gamma_n}(a,a+s)]_{i,j} \to [\mathbf{K}_{\alpha,\gamma}(a,a+s)]_{i,j}.$$

To conclude, we identify λ_∞ and $\boldsymbol{\eta}_\infty$ to the Perron eigenelements of the associated limit matrix $\mathbf{K}_{\alpha,\gamma}(a,a+s)$. Indeed, let

$$\mathbf{h}_\infty(a) := e^{\lambda_\infty a}\boldsymbol{\Psi}^{-1}_\alpha(0,a)\left(\mathbf{I} - 2\int_0^a e^{-\lambda_\infty s}\boldsymbol{\Psi}_\alpha(0,s)\mathbf{B}_\gamma(s)\,ds\right)\boldsymbol{\eta}_\infty.$$

Therefore

$$\mathbf{h}_\infty(0) = \boldsymbol{\eta_\infty},$$

and differentiating $\mathbf{h}_\infty(a)$ we obtain that

$$\mathbf{h}'_\infty(a) = \lambda_\infty\mathbf{h}_\infty(a) - 2\mathbf{B}_\gamma(a)\boldsymbol{\eta}_\infty + \mathbf{D}_\alpha(a)\mathbf{h}_\infty(a),$$

or equivalently

$$\mathcal{Q}_{\alpha,\gamma}\mathbf{h}_\infty(a) = \lambda_\infty\mathbf{h}_\infty(a).$$

By uniqueness of the solution to the eigenvalue problem associated to $\mathcal{Q}_{\alpha,\gamma}$ (see previous sections) we conclude that

$$\mathbf{h}_\infty(a) = \mathbf{h}_{\alpha,\gamma}(a), \qquad \lambda_\infty = \lambda_{\alpha,\gamma}.$$

This allow us to conclude that for all fixed values of $a, s \geq 0$ both coordinates of $\boldsymbol{\ell}_{\alpha_n,\gamma_n}(a,s)$ converge to $\boldsymbol{\ell}_{\alpha,\gamma}(a,s)$. Thus, by Dominated Convergence we can conclude the continuity of $(\alpha,\gamma) \mapsto \int_0^{+\infty}\boldsymbol{\ell}_{\alpha,\gamma}(a,s)ds = \mathbf{h}_{\alpha,\gamma}(a)$. □

4.11.3 Proof of Proposition 4.5.3

Proof. First, since $\mathbf{h}_{\alpha,\gamma}$ is normalised by $\langle \boldsymbol{\nu}_{\alpha,\gamma}, \mathbf{h}_{\alpha,\gamma}\rangle = 1$, we can write

$$\lambda_{\alpha,\gamma} = \langle \boldsymbol{\nu}_{\alpha,\gamma}, \mathcal{Q}_{\alpha,\gamma}\mathbf{h}_{\alpha,\gamma}\rangle = \langle \boldsymbol{\nu}_{\alpha,\gamma}\mathcal{Q}_{\alpha,\gamma}, \mathbf{h}_{\alpha,\gamma}\rangle\,.$$

Then, for all $\delta \in \mathbb{R}$ we have

$$\begin{aligned}\langle \boldsymbol{\nu}_{\alpha,\gamma}, (\mathcal{Q}_{\alpha+\delta,\gamma} - \mathcal{Q}_{\alpha,\gamma})\,\mathbf{h}_{\alpha+\delta,\gamma}\rangle &= \langle \boldsymbol{\nu}_{\alpha,\gamma}, \lambda_{\alpha+\delta}\mathbf{h}_{\alpha+\delta,\gamma}\rangle - \langle \lambda_{\alpha,\gamma}\boldsymbol{\nu}_{\alpha,\gamma}, \mathbf{h}_{\alpha+\delta,\gamma}\rangle \\ &= \langle \boldsymbol{\nu}_{\alpha,\gamma}, \mathbf{h}_{\alpha+\delta,\gamma}\rangle\,(\lambda_{\alpha+\delta,\gamma} - \lambda_{\alpha,\gamma})\end{aligned}$$

and therefore

$$\begin{aligned}\lambda_{\alpha+\delta,\gamma} - \lambda_{\alpha,\gamma} &= \frac{\langle \boldsymbol{\nu}_{\alpha,\gamma}, (\mathcal{Q}_{\alpha+\delta,\gamma} - \mathcal{Q}_{\alpha,\gamma})\,\mathbf{h}_{\alpha+\delta,\gamma}\rangle}{\langle \boldsymbol{\nu}_{\alpha,\gamma}, \mathbf{h}_{\alpha+\delta,\gamma}\rangle} \\ &= \frac{1}{\langle \boldsymbol{\nu}_{\alpha,\gamma}, \mathbf{h}_{\alpha+\delta,\gamma}\rangle}\int_0^{+\infty} \boldsymbol{\nu}_{\alpha,\gamma}(da)^\top \begin{bmatrix}-\delta & \delta\\ 0 & 0\end{bmatrix}\mathbf{h}_{\alpha+\delta,\gamma}(a) \\ &= \frac{\delta}{\langle \boldsymbol{\nu}_{\alpha,\gamma}, \mathbf{h}_{\alpha+\delta,\gamma}\rangle}\int_0^{+\infty} (h_{\alpha+\delta,\gamma}(a,1) - h_{\alpha+\delta,\gamma}(a,0))\,\nu_{\alpha,\gamma}(da,0).\end{aligned}$$

Thanks to Lemma 4.5.1, and once more by Dominated Convergence, we have that $\langle \boldsymbol{\nu}_{\alpha,\gamma}, \mathbf{h}_{\alpha+\delta,\gamma}\rangle \to \langle \boldsymbol{\nu}_{\alpha,\gamma}, \mathbf{h}_{\alpha+\delta,\gamma}\rangle$ and $\langle \nu_{\alpha,\gamma}(\cdot,0), h_{\alpha+\delta,\gamma}(\cdot,1) - h_{\alpha+\delta,\gamma}(\cdot,0)\rangle \to \langle \nu_{\alpha,\gamma}(\cdot,0), h_{\alpha,\gamma}(\cdot,1) - h_{\alpha,\gamma}(\cdot,0)\rangle$ as $\delta \to 0$. Then, dividing by δ and making $\delta \to 0$, t we obtain (4.33). Analogously for any $\delta \in \mathbb{R}$ small enough we have

$$\begin{aligned}\lambda_{\alpha,\gamma+\delta} - \lambda_{\alpha,\gamma} &= \frac{\langle \boldsymbol{\nu}_{\alpha,\gamma}, (\mathcal{Q}_{\alpha,\gamma+\delta} - \mathcal{Q}_{\alpha,\gamma})\,\mathbf{h}_{\alpha,\gamma+\delta}\rangle}{\langle \boldsymbol{\nu}_{\alpha,\gamma}, \mathbf{h}_{\alpha,\gamma+\delta}\rangle} \\ &= \frac{1}{\langle \boldsymbol{\nu}_{\alpha,\gamma}, \mathbf{h}_{\alpha,\gamma+\delta}\rangle}\int_0^{+\infty} \boldsymbol{\nu}_{\alpha,\gamma}(da)^\top 2\begin{bmatrix}0 & 0\\ \delta\beta_1(a) & -\delta\beta_1(a)\end{bmatrix}\mathbf{h}_{\alpha,\gamma+\delta}(0) \\ &= \frac{\delta}{\langle \boldsymbol{\nu}_{\alpha,\gamma}, \mathbf{h}_{\alpha,\gamma+\delta}\rangle}\,(h_{\alpha,\gamma+\delta}(0,0) - h_{\alpha,\gamma+\delta}(0,1))\int_0^{+\infty} \beta_1(a)\nu_\alpha(da,1),\end{aligned}$$

from where (4.34) is obtained by the same arguments. □

4.11.4 Proof of Proposition 4.5.4

Proof. From the proof of Theorem 4.4.5, if (α,γ) is in the survival region, then

$$\det\left(\mathbf{I} - \mathbf{F}(\lambda_{\alpha,\gamma})\right) = 0,$$

and $\mathbf{h}_{\alpha,\gamma}(0)$ is the unique non-trivial solution to the linear problem

$$\left(\mathbf{I} - \mathbf{F}(\lambda_{\alpha,\gamma})\right)\mathbf{h}_{\alpha,\gamma}(0) = 0.$$

From the expression of $\mathbf{F}(\lambda)$ and the first equation, we have that for $\lambda = \lambda_{\alpha,\gamma}$

$$\det\begin{bmatrix}2(1-p)\xi_0(\alpha+\lambda) + 2\gamma\xi_{01}(\lambda) - 1 & 2(1-\gamma)\xi_{01}(\lambda)\\ 2\gamma\xi_1(\lambda) & 2(1-\gamma)\xi_1(\lambda) - 1\end{bmatrix} = 0,$$

where $\xi_0(\lambda) = \int_0^{+\infty} e^{-\lambda a}\beta_0(a)\exp(-\int_0^a \beta(s)ds)da$, $\xi_1(\lambda) = \int_0^{+\infty} e^{-\lambda a}\beta_1(a)\psi_1(0,a)da$ are the Laplace transforms associated to the division times of types 0 and 1, and $\xi_{01}(\lambda) = \int_0^{+\infty} e^{-\lambda a}\psi_0 \star \psi_1(0,a)da$. This implies the following implicit relation characterising $\lambda_{\alpha,\gamma}$:

$$\xi_{01}(\lambda_{\alpha,\gamma}) = \frac{(1-2(1-p)\xi_0(\alpha+\lambda_{\alpha,\gamma}))(1-2(1-\gamma)\xi_1(\lambda_{\alpha,\gamma}))}{2\gamma},$$

which allows to simplify the matrix $\mathbf{F}(\lambda_{\alpha,\gamma})$ in order to obtain that

$$\mathbf{h}_{\alpha,\gamma}(0) \in \text{span}\left\{\begin{pmatrix} 1-2\xi_1(\lambda_{\alpha,\gamma})+2\gamma\xi_1(\lambda_{\alpha,\gamma}) \\ 2\gamma\xi_1(\lambda_{\alpha,\gamma}) \end{pmatrix}\right\}.$$

Since $\mathbf{h}_{\alpha,\gamma}(0)$ is a non-negative vector, we have finally that

$$\text{sign}\left(h_{\alpha,\gamma}(0,0) - h_{\alpha,\gamma}(0,1)\right) = \text{sign}\left(1-2\xi_1(\lambda_{\alpha,\gamma})\right).$$

Notice that $\lambda \mapsto \xi_1(\lambda)$ is a continuous decreasing function, such that $\xi_1(0) = 1$ and $\xi_1 \to 0$ as $\lambda \to +\infty$. Moreover, the Malthusian parameter associated to ξ_1, λ_1^*, is the unique solution to $\xi_1(\lambda_1^*) = 1/2$ (this is classical, see for example [143]. Therefore, if $\lambda_{\alpha,\gamma} > \lambda_1^*$, then $\xi_1(\lambda_{\alpha,\gamma}) < 1/2$ and by (4.34), $\partial_\gamma \lambda_{\alpha,\gamma} > 0$. Analogously, if $\lambda_{\alpha,\gamma} < \lambda_1^*$, then $\partial_\gamma \lambda_{\alpha,\gamma} < 0$.

□

4.11.5 Proof of Proposition 4.5.6

Proof. We study the sign of $\partial_\gamma \lambda_{\alpha,\gamma}$ in the case where p is big or small enough, and then relate this two partial analysis by continuity. Assumption 4.2.4 plays a key role.

(i) Case $p > 1/2$. From Proposition 4.8.2 and the equivalence established in Lemmas 4.4.6 and 4.4.7, if $p > 1/2$ we have that

$$\text{sign}\left(\frac{1}{2}\left(1+\frac{(2p-1)q}{1-q}\right)-\gamma\right) = \text{sign}\left(\rho(\mathbf{K}_\infty^{\alpha,\gamma})-1\right) = \text{sign}(\lambda_{\alpha,\gamma}).$$

In particular, for all $\alpha \geq 0$ it exists

$$\bar{\gamma}_\alpha := \frac{1}{2}\left(1+\frac{(2p-1)q}{1-q}\right)$$

such that $\lambda_{\alpha,\bar{\gamma}_\alpha} = 0$. Recall from Corollary 4.5.5 and Fig. 4.5 that $\lambda_{\alpha,0} \geq \lambda_1^* > 0$. Therefore, by the continuity of $\gamma \mapsto \lambda_{\alpha,\gamma}$, for some $\hat{\gamma} > 0$ we must have $\lambda_{\alpha,\hat{\gamma}} < \lambda_1^*$, and by Proposition 4.5.4, $\partial_\gamma \lambda_{\alpha,\gamma}|_{\gamma=\hat{\gamma}} < 0$. This implies that for all $\gamma \geq \hat{\gamma}$, $\partial_\gamma \lambda_{\alpha,\gamma} < 0$. and $\partial_\gamma \lambda_{\alpha,\gamma} = 0$ for all $\gamma < \hat{\gamma}$. Thus, whenever $p > 1/2$, we have for all α, γ, $\partial_\gamma \lambda_{\alpha,\gamma} \leq 0$.

(ii) Small p case. Now we prove that for all α, if p is small enough, then we have the opposite, namely: for all $\gamma \geq 0$, $\partial_\gamma \lambda_{\alpha,\gamma} \geq 0$. Consider the limit case $p = 0$ at $\gamma = 1$. The characteristic equation for $\lambda_{\alpha,\gamma=1}$ becomes

$$\xi_0(\alpha + \lambda) + \xi_{01}(\lambda) = \frac{1}{2}.$$

Recall that T_{div} is the division time of a non-switching cell. By Jensen's inequality,

$$\begin{aligned}\xi_0(\alpha + \lambda) &= \mathbb{E}_{\delta_{(0,0)}}\left[\exp(-(\lambda + \alpha)T_{div})\right] \\ &\geq \exp\left(-(\lambda + \alpha)\mathbb{E}_{\delta_{(0,0)}}\left[T_{div}\right]\right) = \xi_0(\lambda)\xi_0(\alpha).\end{aligned}$$

In particular, for $\lambda = \lambda_1^*$, and since $\xi_0(\lambda) > \xi_1(\lambda)$ by Remark 4.2.5,

$$\xi_0(\alpha + \lambda_1^*) \geq \xi_0(\alpha)\xi_0(\lambda_1^*) > \xi_0(\alpha)\xi_1(\lambda_1^*) = \frac{1-q}{2}.$$

On the other hand, letting $\tau \sim \mathrm{Exp}(\alpha)$ independent from T_{div} be the switching time of type 0, and recalling the definition of $\psi_0 \star \psi_1$ from (4.4), by Fubini's theorem we can write

$$\begin{aligned}\xi_{01}(\lambda) &:= \int_0^{+\infty} e^{-\lambda a}\alpha\beta_1(a)\psi_0 \star \psi_1(0,a)\, da \\ &= \int_0^{+\infty}\left(\frac{1}{\psi_1(0,\tau)}\int_\tau^{+\infty} e^{-\lambda a}\beta_1(a)\psi_1(0,a)\, da\right)\alpha\psi_0(0,\tau)\, d\tau \\ &= q\,\mathbb{E}_{\delta_{(0,0)}}\left[\mathbb{E}_{\delta_{(0,1)}}\left[e^{-\lambda T_{div}}\middle|\, T_{div} \geq \tau\right]\middle|\, \tau < T_{div}\right].\end{aligned}$$

By Assumption 4.2.4, consider a monotone coupling $(\hat{T}^0_{div}, \hat{T}^1_{div})$ on a common probability space such that for all $i \in \{0,1\}$, $\hat{T}^i_{div}$ has the same distribution under $\mathbb{P}$ as T_{div} under $\mathbb{P}_{\delta(0,i)}$, and $\mathbb{P}(\hat{T}^1_{div} > \hat{T}^0_{div}) = 1$. In particular $\{\tau \leq \hat{T}^0_{div}\} \subseteq \{\tau \leq \hat{T}^1_{div}\}$. Therefore

$$\begin{aligned}\xi_{01}(\lambda) &= q\,\mathbb{E}\left[\mathbb{E}\left[e^{-\lambda\hat{T}^1_{div}}\middle|\, \hat{T}^1_{div} \geq \tau\right]\middle|\, \tau < \hat{T}^0_{div}\right] \\ &= q\,\mathbb{E}\left[\mathbb{E}\left[e^{-\lambda\hat{T}^1_{div}}\right]\middle|\, \tau < \hat{T}^0_{div}\right] \\ &= q\,\xi_1(\lambda).\end{aligned}$$

In particular, at $\lambda = \lambda_1^*$, $\xi_{01}(\lambda_1^*) = q/2$. Finally,

$$\xi_0(\alpha + \lambda_1^*) + \xi_{01}(\lambda_1^*) > \frac{1}{2}$$

and hence $\lambda_{\alpha,\gamma=1} > \lambda_1^*$. Then, analogously to Corollary 4.5.5, we have that $\partial_\gamma^- \lambda_{\alpha,\gamma}\big|_{\gamma=1} > 0$, where ∂_γ^- is the left derivative with respect to γ (whose values are restricted to $[0,1]$), and by Proposition 4.5.4, for all $\gamma \geq 0$, $\partial_\gamma \lambda_{\alpha,\gamma} \geq 0$.

(iii) Conclusion. The continuity of $p \mapsto \partial_\gamma \lambda_{\alpha,\gamma}$ can be exhibited following the same arguments presented in the proof of Lemma 4.5.2. Moreover, as we did in Proposition 4.5.4 we can further show that $p \mapsto \partial_\gamma \lambda_{\alpha,\gamma}$ is continuously differentiable and that for all $\alpha, \gamma, p \in (0,1)$,

$$\partial_p \lambda_{\alpha,\gamma} = \langle \boldsymbol{\nu}, (\partial_p \mathcal{Q})\, \mathbf{h} \rangle = -2h(0,0) \int \beta_0(a)\nu(a,0)da < 0.$$

Hence, for all α, γ, $p \mapsto \partial_\gamma \lambda_{\alpha,\gamma}$ is continuous and strictly decreasing. Therefore, for all $\alpha \geq 0$, there is a unique $\bar{p}_{\alpha,\gamma}$ such that $\lambda_{\alpha,\gamma} = \lambda_1^*$ and $\partial_\gamma \lambda_{\alpha,\gamma} = 0$ for all $\gamma \in (0,1)$. In particular, this $\bar{p}_{\alpha,\gamma}$ is then constant in γ, and uniquely determined by α, which gives the result. The conclusion is presented in Figure 4.6.

□

4.11.6 Links between $\gamma \mapsto \lambda_{\alpha,\gamma}$ and the establishment probability conditions

Fix $\gamma^* \in (0,1)$. We will introduce an auxiliary process $\tilde{Z}_t$ that will allow to rederive Proposition 4.5.6 using the microscopic establishment conditions. Let $\tilde{Z}_t$ be the measure-valued process characterised under $\mathbb{P}_\mu^{\alpha,\gamma}$ by an initial condition $\tilde{Z}_0 = \mu$ and by the infinitesimal generator $\tilde{\mathcal{Q}}_{\alpha,\gamma}$ defined as

$$\tilde{\mathcal{Q}}_{\alpha,\gamma}\mathbf{f}(a) := \mathbf{f}'(a) + 2\mathbf{B}_\gamma(a)\mathbf{f}(0) - (\mathbf{D}_\alpha(a) + \lambda_{\alpha,\gamma^*}\mathbf{I})\mathbf{f}(a).$$

The only difference with respect to $\mathcal{Q}_{\alpha,\gamma}$ defined in (4.19) is an additional death rate of value $\lambda_{\alpha,\gamma^*}$ for both types. Consider the associated survival functions

$$\tilde{\psi}_i(s,t) := \psi_i(s,t)e^{-\lambda_{\alpha,\gamma^*}(t-s)}.$$

Then, following the proof of Theorem 4.3.2 we have that the extinction probabilities

$$\tilde{\pi}_i^{\alpha,\gamma} := \mathbb{P}_{\delta_{(0,i)}}^{\alpha,\gamma}\left(\exists t \geq 0 : \tilde{Z}_t = 0\right)$$

are the minimal solutions in $[0,1]^2$ to the quadratic system

$$\begin{cases} \tilde{\pi}_0^{\alpha,\gamma} = \omega_0 + (1-\tilde{q}-\omega_0)p + (1-\tilde{q}-\omega_0)(1-p)(\tilde{\pi}_0^{\alpha,\gamma})^2 + \tilde{q}\tilde{\pi}_1^{\alpha,\gamma}, & \text{(4.54a)} \\ \tilde{\pi}_1^{\alpha,\gamma} = \omega_1 + (1-\omega_1)\left(\gamma\tilde{\pi}_0^{\alpha,\gamma} + (1-\gamma)\tilde{\pi}_1^{\alpha,\gamma}\right)^2, & \text{(4.54b)} \end{cases}$$

where

$$\omega_i := \mathbb{P}_{\delta_{(0,i)}}^{\alpha,\gamma}(\text{Die by death rate}) = \lambda_{\alpha,\gamma^*}\int_0^{+\infty} \tilde{\psi}_i(0,s)ds, \tag{4.55}$$

$$\tilde{q} := \mathbb{P}_{\delta_{(0,0)}}^{\alpha,\gamma}(\text{Switch before dividing}) = \alpha\int_0^{+\infty} \tilde{\psi}_0(0,s)ds. \tag{4.56}$$

We can further reduce (4.54a) to

$$\tilde{\pi}_0^{\alpha,\gamma} = (1-\tilde{q})\tilde{p} + (1-\tilde{q})(1-\tilde{p})(\tilde{\pi}_0^{\alpha,\gamma})^2 + \tilde{q}\tilde{\pi}_1^{\alpha,\gamma}, \tag{4.57}$$

where

$$\tilde{p} := p + (1-p)\frac{\omega_0}{1-q}$$

is the *effective* death probability at division of type 0 induced by the additional death rate $\lambda_{\alpha,\gamma^*}$. Note that since $0 \leq \omega_0 + q \leq 1$ we have indeed $0 \leq \tilde{p} \leq 1$. This way, (4.57) has the same form as (4.13a) studied previously. Then, following the proof of Theorem 4.3.5, system (4.54a)-(4.54b) admits a minimal solution different than $(1,1)$ if and only if

$$\left\{\tilde{p} \leq \frac{1}{2}\right\} \text{ or } \left\{\tilde{p} > \frac{1}{2} \text{ and } \omega_1 \leq \frac{1}{2} \text{ and } \gamma < \frac{(1-2\omega_1)(\tilde{q} + (1-\tilde{q})(2\tilde{p}-1)}{2(\omega_1\tilde{q} + (1+\omega_1)(1-\tilde{q})(2\tilde{p}-1))}\right\}. \tag{4.58}$$

We can recover the previous case (condition (4.16)) by making $\omega_1 = 0$.

We exhibit a monotonicity result analogous to Proposition 4.5.8, but for the system (4.54a)-(4.54b) that has an additional extinction probability ω_1, absent in the previously studied system (4.13a)-(4.13b).

Lemma 4.11.1. *For any solution of* (4.54a)-(4.54b), *for any* $i \in \{0,1\}$*:*

- *If* $\omega_1 = \tilde{p}$, *then for all* $\gamma \in (0,1)$, $\partial_\gamma \tilde{\pi}_i^{\alpha,\gamma} = 0$.
- *If* $\omega_1 > \tilde{p}$, *then for all* $\gamma \in (0,1)$, $\partial_\gamma \tilde{\pi}_i^{\alpha,\gamma} \leq 0$.
- *If* $\omega_1 < \tilde{p}$, *then for all* $\gamma \in (0,1)$, $\partial_\gamma \tilde{\pi}_i^{\alpha,\gamma} \geq 0$.

Proof. Fix $x \in (0,1)$. To study (4.54b), we consider the minimal solution to the quadratic equation

$$y = \omega + (1-\omega)(\gamma x + (1-\gamma)y)^2, \quad y \in [0,1], \tag{E_1}$$

which is given by

$$y_x(\gamma,\omega) = \frac{1 - 2\gamma(1-\gamma)(1-\omega)x - \sqrt{1 - 4\gamma(1-\gamma)(1-\omega)x - 4(1-\gamma)^2(1-\omega)\omega}}{2(1-\omega)(1-\gamma)^2}. \tag{4.59}$$

We show first that there exists a unique $\bar{\omega}_x \in (0,1)$ such that for all $\gamma \in (0,1)$, $\partial_\gamma y_x(\gamma, \bar{\omega}_x) = 0$. By differentiation of (4.59) we have that, for $x \neq 1$, $\partial_\gamma y_x(\gamma, \bar{\omega}_x) = 0$ for all $\gamma \in (0,1)$ if and only if

$$\bar{\omega}_x = \frac{x}{1+x}.$$

Now, to determine the value of $p = p_x$ compatible with $y_x(\gamma, \bar{\omega}_x) = x$, we study the equation

$$x = (1-q)p_x + (1-q)(1-p_x)x^2 + q y_x(\gamma,\omega), \tag{E_0}$$

which admits a solution $x = y_x(\gamma, \omega)$ if and only if

$$p_x = \frac{x}{1+x},$$

from where we deduce $\bar{\omega}_x = p_x$. Then, by implicit differentiation of (E_0), valuating under $x = y_x(\gamma, \omega)$, we have for all $\gamma \in (0,1)$,

$$\partial_\omega \left(\partial_\gamma y_x(\gamma, \bar{\omega}_x)\right) = -\frac{2(1-x)x(1+x)^2}{(1-(1-2\gamma)x)^2} < 0.$$

In the final case, if $x = 1$ then from (E_0), for all $\gamma \in (0,1)$, $y_x(\gamma, \omega) = 1$ too. In particular, $\partial_\gamma y_x(\gamma, \omega) = 0$ for all $\gamma \in (0,1)$ and $\omega \in (0,1)$.

Finally, since from (E_0), $x \in (0,1) \mapsto y_x(\gamma, \omega) \in (0,1)$ is increasing, if $\partial_\omega \partial_\gamma y_x(\gamma, \bar{\omega}_x) \leq 0$ for all fixed x, by the implicit function theorem, $\partial_\omega \partial_\gamma \tilde{\pi}_1^{\alpha,\gamma} \leq 0$. □

Then, as in Lemma 4.4.6, we show now that there is an equivalence relation between condition (4.58) and the spectral properties of the matrix

$$\tilde{\mathbf{K}}_\infty^{\alpha,\gamma} := 2\int_0^{+\infty} \tilde{\mathbf{\Psi}}_\alpha(0,a)\mathbf{B}_\gamma(a)da.$$

As in Lemma 4.4.6 we obtain

$$\tilde{\mathbf{K}}_\infty^{\alpha,\gamma} = 2\begin{bmatrix} (1-\tilde{p})(1-\tilde{q}) + \gamma\tilde{q} & (1-\gamma)\tilde{q} \\ (1-\omega_1)\gamma & (1-\omega_1)(1-\gamma) \end{bmatrix},$$

from which we can compute explicitly the eigenvalues, so that we are able to show that

$$\rho(\tilde{\mathbf{K}}_\infty^{\alpha,\gamma}) > 1 \iff (4.58) \text{ is verified} \iff \tilde{\pi}_0^{\alpha,\gamma^*}, \tilde{\pi}_1^{\alpha,\gamma^*} < 1. \qquad (\star)$$

Then, following Lemma 4.4.7, there is a unique $\tilde{\lambda}_{\alpha,\gamma} \in \mathbb{R}$ such that $\rho(\tilde{\mathbf{F}}_{\alpha,\gamma}(\tilde{\lambda}_{\alpha,\gamma})) = 1$. By construction, $\tilde{\lambda}_{\alpha,\gamma} = \lambda_{\alpha,\gamma} - \lambda_{\alpha,\gamma^*}$. Indeed, $\lambda_{\alpha,\gamma}$ is the largest solution to (4.32) and then:

$$\det\left(2\int_0^{+\infty} e^{-(\lambda_{\alpha,\gamma}-\lambda_{\alpha,\gamma^*})s}\tilde{\mathbf{K}}_{\alpha,\gamma}(a,s)\,ds\; - \mathbf{I}\right) = \det\left(2\int_0^{+\infty} e^{-\lambda_{\alpha,\gamma}s}\mathbf{K}_{\alpha,\gamma}(a,s)\,ds\; - \mathbf{I}\right) = 0$$

In particular, for $\gamma = \gamma^*$, $\tilde{\lambda}_{\alpha,\gamma^*} = 0$, and therefore by ($\star$),

$$\tilde{\pi}_0^{\alpha,\gamma^*} = \tilde{\pi}_1^{\alpha,\gamma^*} = 1.$$

Now, suppose that γ^* is such that $\omega_1 < \tilde{p}$. Then, by Lemma 4.11.1, for all $\gamma \geq \gamma^*$, $\tilde{\pi}_0^{\alpha,\gamma} = \tilde{\pi}_1^{\alpha,\gamma} = 1$. Then, by ($\star$), $\rho(\tilde{\mathbf{K}}_\infty^{\alpha,\gamma}) \leq 1$ for all $\gamma \geq \gamma^*$. Therefore, again by Lemma 4.4.7, we have $\tilde{\lambda}_{\alpha,\gamma} \leq 0$ for all $\gamma \geq \gamma^*$, or equivalently, $\lambda_{\alpha,\gamma} \leq \lambda_{\alpha,\gamma^*}$ for all $\gamma \geq \gamma^*$. We proceed analogously for the case $\omega_1 > \tilde{p}$ and $\omega_1 = \tilde{p}$. Finally, recalling from Proposition 4.5.3 that $\gamma \mapsto \lambda_{\alpha,\gamma}$ is continuously differentiable, we obtain that

$$\text{sign}\left(\partial_\gamma\, \lambda_{\alpha,\gamma}|_{\gamma=\gamma^*}\right) = \text{sign}\,(\omega_1 - \tilde{p}) = \text{sign}\left(\mathbb{P}^{\alpha,\gamma^*}_{\delta_{(0,1)}}\left(\tilde{Z}_{T_1} = 0\right) - \mathbb{P}^{\alpha,\gamma^*}_{\delta_{(0,0)}}\left(\tilde{Z}_{T_1} = 0 \middle| \text{ Do not switch}\right)\right).$$

Finally, from (4.55) an (4.56) and by an integration by parts we obtain

$$\omega_1 = \tilde{p} \iff p = \bar{p}(\alpha,\gamma) := \frac{\alpha\xi_0(\lambda_{\alpha,\gamma})\xi_1(\lambda_{\alpha,\gamma}) + \lambda_{\alpha,\gamma}(\xi_0(\lambda_{\alpha,\gamma}) + \xi_1(\lambda_{\alpha,\gamma}) - 1)}{(\alpha+\lambda_{\alpha,\gamma})\xi_0(\lambda_{\alpha,\gamma})},$$

where

$$\xi_i(\lambda) := \int_0^{+\infty} e^{-\lambda a}\beta_i(a)\exp\left(-\int_0^a \beta_i(s)ds\right)da$$

is the Laplace transform of the division time distribution of type $i \in \{0,1\}$. Thus, for all α,γ, $\bar{p}(\alpha,\gamma)$ is uniquely defined.

4.12 Proofs of Section 4.6

4.12.1 Proof of Proposition 4.6.1

Proof. We adapt the general ideas developed on Section 5 of [113] and in Appendix A of [32], extending Section 4.4 to the case where $t \mapsto p(t)$ is a continuous T-periodic function. If we wish to allow discontinuities (for example to account for piecewise constant treatments) we might follow the approach of [32], that requires to estimate supplementary controls.

By variation of parameters, if $(\lambda_T, \boldsymbol{\nu}, \mathbf{h})$ are solutions to (4.36a)-(4.36c) then

$$\mathbf{h}(t,a) = 2\int_a^{+\infty} e^{-\lambda_T(s-a)}\boldsymbol{\Psi}(a,s)\mathbf{B}(t+s-a,s)\mathbf{h}(t+s-a,0)ds, \tag{4.60}$$

$$\boldsymbol{\nu}(t,a) = e^{-\lambda_T a}\boldsymbol{\Psi}^\top(0,a)\boldsymbol{\nu}(t-a,0), \tag{4.61}$$

For the first equation, valuated the integral at $a=0$ we obtain that $\mathbf{h}(t,0)$ is solution to the integral fixed point problem

$$\mathbf{h}(t,0) = \mathcal{F}_{\lambda_T}(t)\mathbf{h}(\cdot,0) := 2\int_0^{+\infty} e^{-\lambda_T a}\boldsymbol{\Psi}(0,a)\mathbf{B}(t+a,a)\mathbf{h}(t+a,0)da. \tag{4.62}$$

Analogously, since $\boldsymbol{\nu}$ must verify the boundary condition imposed by $\boldsymbol{\nu}(t,\cdot) \in \mathcal{D}(\mathcal{Q}^*(t))$, at $a=0$ we obtain that $\mathbf{h}(t,0)$ is solution to the integral fixed point problem

$$\boldsymbol{\nu}(t,0) = \mathcal{G}_{\lambda_T}(t)\boldsymbol{\nu}(\cdot,0) := 2\int_0^{+\infty} e^{-\lambda_T a}\mathbf{B}^\top(t,a)\boldsymbol{\Psi}^\top(0,a)\boldsymbol{\nu}(t-a,0)da. \tag{4.63}$$

The sequel is classical. By Arzela-Ascoli Theorem, one shows that under the Assumptions 4.2.1, for all $\lambda > 0$ and $t \geq 0$ the operators $\mathcal{F}_\lambda(t)$ and $\mathcal{G}_\lambda(t)$ are continuous, strictly positive and compact. Thus, by Krein-Rutman Theorem there is a simple dominant eigenvalue $\mu_\lambda > 0$ associated to eigenfunctions $\boldsymbol{\nu}_\lambda(t,0)$ and $\mathbf{h}_\lambda(t,0)$. Then, by the maximum principle and analogously as done in the proof of Lemma 4.4.7, we obtain that $\lambda \mapsto \mu_\lambda$ is a continuous and strictly decreasing map. Hence there is a unique λ_T such that $\mu_{\lambda_T} = 1$ with associated eigenfunctions $\boldsymbol{\nu}_{\lambda_T}(t,0)$ and $\mathbf{h}_{\lambda_T}(t,0)$. We can finally recover $\boldsymbol{\nu}(t,a)$ and $\mathbf{h}(t,a)$ using the reconstruction formulae (4.60) and (4.61).

□

4.12.2 Technical lemmas

We recall some useful classical properties:

Proposition 4.12.1. *Let S, T be two bounded linear operators in a Banach space $\mathcal{X}$ and let $\alpha(S)$ the measure of non-compactness of S as defined in Definition 4.10.2. Then:*

(i) $\alpha(S) \leq ||S||_{op}$.

(ii) $\alpha(TS) \leq \alpha(T)\alpha(S)$.

(iii) $\alpha(T + S) \leq \alpha(T) + \alpha(S)$.

(iv) $\alpha(S) = 0$ *if and only if* S *is compact.*

Lemma 4.12.2. *Let A and B two positive matrices such that $A_{ij} \geq B_{ij}$ for all pairs (i, j), then:*

(i) $\rho(A) \geq \rho(B)$, *and*

(ii) $\rho(B) \geq \rho(A)\left(1 - \dfrac{\max_{i,j}(A_{i,j} - B_{i,j})}{\min_{i,j} A_{i,j}}\right)$.

Chapter 5

Regime switching on the propagation speed of travelling waves of some size-structured Myxobacteria population models

This chapter is based on work conducted during CEMRACS 2022, in collaboration with Vincent Calvez, Adil El Abdouni, Maxime Estavoyer, Florence Hubert, Julien Olivier and Magali Tournus. It has been submitted to *ESAIM: Proceedings and Surveys*.

Abstract. The spatial propagation of complex populations can depend on some structuring variables. In particular, recent developments in microscopy have revealed the impact of bacteria heterogeneity on the population motility. Biofilms of *Myxococcus xanthus* bacteria have been shown to be structured in clusters of various sizes, which remarkably, tend to move faster when they consist of a larger number of bacteria. We propose a minimal reaction-diffusion discrete size-structured model modelling a population of *Myxococcus* with two possible cluster sizes: isolated and paired bacteria. Numerical experiments show that this model exhibits travelling waves whose propagation speed depends on the increased motility of clusters, and the exchange rates between isolated bacteria and clusters. Notably, we evince the existence of a characteristic threshold level θ^* on the ratio between cluster motility and isolated bacteria motility, which separates two distinct regimes of propagation speed. When the ratio is below θ^*, the propagation speed of the population is constant. However, when the ratio is above θ^*, the propagation speed takes higher values. We also consider a generalised model with continuous-size structure, which also shows the same behaviour. We extend the model to include interactions with a prey population, which show qualitative behaviours in agreement to the biological experiments.

5.1 Introduction

Recent development in high-throughput cell segmentation techniques have allow microbiologist to closely follow complexly structured bacterial populations [118]. Interactions between individuals, both cooperative and competitive, and the emergence of subpopulations with distinct behaviours, have revealed the streaking effects that this underlying structure might have across the different scales of the population dynamics [127, 6]. One important dimension that might be affected is the way they explore their surroundings.

One interesting example of this is the behaviour of *Myxococcus xanthus*, a motile predatory bacterium found on soil which forms multicellular biofilms to predate on other microorganisms [146]. Thanks to high-throughput microscopy techniques, it has been shown that this biofilm has not a homogeneous structure, but that it is in fact composed of bacteria clusters of various sizes, from isolated individuals, to large swarms of closely adhered bacteria. In particular, recent works have shown that this clusters can exhibit distinct motility behaviours, which depend on their size and composition, and that affect the macroscopic motility of the population ensemble during the predatory incursions [123].

In particular, the cluster structure of *M. xanthus* populations has been shown to be determined by the phenotypic heterogeneity among individual cells [123]. Indeed, *M. xanthus* cells are capable to switch between two different motility regimes, namely: the adventurous A-motility, and the social S-motility, which result from the expression of two distinct set of genes [76]. A-motile cells can glide over the surface, using a complex protein machinery that anchors and pushes the cell forward. S-type motion, on the other hand, is contact-dependent. S-motile cells move thanks to the projection of pili, hair-like structures that grow from the cell and can attach to other cells or the surrounding extracellular matrix, to then retrace and drag the cell. This movement depends on the presence of one key component of the extracellular matrix: the exopolysaccharides (EPS). EPS are secreted and laid as a chemical trail by *M. xanthus* as it moves, which allows the adhesion and cohesion of cells, thus favouring the emergence of swarms of bacteria which move collectively.

Importantly, the proportion of A-motile and S-motile cells, and therefore, the distribution of the cluster sizes, has been show to impact the fitness of *M. xanthus* populations. On the one hand, the collective motion of S-motile cells can increase the efficiency of predation, since killing is seemingly contact-dependent, and then is favoured by *M. xanthus* cell density in the predation forefront. On the other hand, predation is initiated by pioneer A-motile cells that explore the area around the colony first (wolf-pack predation). Therefore, both motility systems play synergistic roles [123].

In this work we aim to study the impact of cellular cohesion in the global motility of the population. In particular, we will be interested in population dynamics in which individuals have an advantage when coagulating (social synergy), which is expressed as a higher motility. To that extent, we will consider some spatial structured population models, where besides a spatial variable coding for the the bacteria positions, we consider a structuring variable which corresponds to the cluster size. Clusters of different sizes may grow, divide

and coagulate, and from previous observations, larger clusters will diffuse at higher rates [19].

In the paragraphs that follow we will introduce three models which will give some insight into the phenomenons described above. In first place, a discrete-structure model, in which we only consider two cluster sizes: singletons of isolated A-motile bacteria, and clusters of two S-motile bacteria. In second place, we present a continuous cluster-size model that generalises this model, accounting for the possibility to produce, by fragmentation and coagulation, clusters of any size. Finally, we consider a derived predator-prey model, where the bi-type clustered population introduced in the first model will interact with a prey population of *E. coli*.

5.2 Proposed models and main results

5.2.1 Discrete size model

Let us consider first a minimal model in which we have isolated bacteria (i.e. clusters of size one) and paired bacteria (clusters of size two) that move in the real line. We suppose that both species are well mixed and call $p_1(x,t)$ the number density of isolated bacteria, and $p_2(x,t)$ the number density of clusters of size two, at a given location in space $x \in \mathbb{R}$ and at a given time $t \geq 0$. We suppose that p_1 and p_2 solve the following system of two reaction–diffusion partial differential equations

$$\partial_t p_1 = \theta_1 \Delta p_1 - \tau_1 p_1^2 + 2\tau_2 p_2 + \alpha p_1 \left(1 - \frac{p}{K}\right), \tag{5.1}$$

$$\partial_t p_2 = \theta_2 \Delta p_2 + \frac{\tau_1}{2} p_1^2 - \tau_2 p_2, \tag{5.2}$$

with p the total number of bacteria, $p = p_1 + 2p_2$.

The first term in the right-hand side of Equations (5.1) and (5.2) is a diffusion term, and describes respectively the spatial random movement of isolated bacteria and clusters of bacteria. We assume that $\theta_2 > \theta_1$, *i.e.* clusters spread faster than isolated bacteria. The second term $\tau_1 p_1^2$ represents the coagulation of isolated bacteria, which happens at rate $\tau_1 > 0$ and changes two isolated bacteria into one cluster of size two. The term $\tau_2 p_2$ corresponds to the fragmentation of clusters of size two, which happens at rate $\tau_2 > 0$ and produces two isolated bacteria. Moreover, we assume that only isolated bacteria can divide. This growth term is assumed to be logistic, with growth rate $\alpha > 0$ and carrying capacity K. As such, the model (5.1)-(5.2) is an extension of the Fisher-KPP model [54, 90], which reduces to Fisher-KPP when $\tau_2 = 0$, decoupling the two equations.

Numerical simulations of this system allow us to conclude the existence of travelling waves solutions for all positive parameters. Moreover, we observe two distinct regimes separated by a constant threshold level θ^* for the ratio θ_2/θ_1. When $\theta_2/\theta_1 < \theta^*$, the propagation front consists on *pulled* waves. This is, the propagation speed is equal to the Fisher-KPP speed. In this case, the population propagation is limited by the motility of the isolated bacteria, so the cluster structure does not affect the speed. However, when $\theta_2/\theta_1 > \theta^*$, the

propagation front consists on so-called *pushed* waves. In this case, the propagation speed is strictly bigger than the Fisher-KPP speed, thanks to the non negligible effect of the non-linearity introduced by the coagulation term. In layman's terms, we conclude that when the motility of clusters is big enough with respect to the motility of isolated bacteria, the collective behaviour of *M. xanthus* allows the whole population to propagate faster than in the asocial case. We also observe that θ^* is independent from the coagulation and fragmentation rates. In particular, we can reduce the system to the case $\tau_1, \tau_2 \to +\infty$, which gives us a scalar equation that we study numerically.

5.2.2 Continuous cluster-size model

In real life, the cluster structure of *M. xanthus* swarms can vary from lonely scout cells to thousands of densely packed social bacteria. We can extend the model (5.1)-(5.2) to a general Diffusion-Growth-Fragmentation-Coagulation model, described by (5.3)-(5.6), where we define $\rho(t, x, z)$ as the density number of clusters of size $z \in [0, z_{max}]$ (or more precisely, the total mass or volume of the cluster, which is a continuous variable) at position $x \in \mathbb{R}$ and time $t \geq 0$. The model is defined by the following integro-differential equation:

$$\partial_t \rho(t,x,z) = \partial_{xx}\left[\theta(z)\rho(t,x,z)\right] - \partial_z\left[v(z,m)\rho(t,x,z)\right] + \mathcal{F}[\rho](t,x,z) + \mathcal{G}[\rho](t,x,z), \quad (5.3)$$

with

$$\mathcal{F}[\rho](t,x,z) = 2\int_z^{z_{\max}} \beta(z')k(z',z)\rho(t,x,z')\,dz' - \beta(z)\rho(t,x,z), \quad (5.4)$$

$$\mathcal{G}[\rho](t,x,z) = \frac{1}{2}\int_0^z \gamma(z-z',z')\rho(t,x,z-z')\rho(t,x,z')\,dz' - \rho(t,x,z)\int_0^{z_{\max}-z} \gamma(z',z)\rho(t,x,z')dz', \quad (5.5)$$

and

$$m(t,x) = \int_0^{z_{\max}} z'\rho(t,x,z')\,dz'. \quad (5.6)$$

As before, the first term in (5.3) corresponds to the spatial diffusion of the clusters, though here the diffusion coefficient of a cluster is a function of its size. The second term in (5.3) is a transport term and corresponds to the growth of cluster size by cell division within each cluster. The function $v(z, m) \geq 0$ is the instantaneous growth speed of a cluster of size z when the total mass at its spatial position is m, as defined by (5.6). The third term in (5.3), which is defined in (5.4), corresponds to the fragmentation of clusters, which occurs at a fragmentation rate $\beta(z) \geq 0$, which is a function of the cluster size. When a cluster of size z fragmentates, it produces two clusters of respective sizes z' and $z - z'$ with probability $k(z, z')dz' = k(z, z - z')dz'$. The first term in (5.4) corresponds to the creation of clusters of size z by the fragmentation of cluster of larger sizes, while the second term corresponds

to the loss of clusters of size z by fragmentation into clusters of smaller size. Finally, the last term in (5.3) corresponds to the coagulation of clusters, as defined by the operator in (5.6). Two clusters of respective sizes z an z' coagulate at rate $\gamma(z, z')$, which we call the coagulation rate. The first term in (5.6) corresponds to the creation of clusters of size z by the coagulation of clusters of sizes z' and $z - z'$, with $z' < z$. The second term corresponds to the loss of clusters of size z by coagulation with clusters of any other size.

The existence of travelling waves in spatial models with continuous structure has been studied by various authors in many particular cases (for example [49, 21, 2, 67]). However, to our humble knowledge, the existence of travelling waves in structured populations involving a coagulation operator is being studied numerically for the first time in this work. Under certain assumptions, we exhibit numerically the existence of travelling waves connecting the null function to the stationary solution of the problem without diffusion. As for the discrete model, we notice the existence of a diffusion coefficient value corresponding to a threshold. That is, for a smaller diffusion coefficient, the wave speed is constant with respect to this parameter and for a larger value, the wave speed increases.

5.2.3 Predator-prey model

M. xanthus are predator bacteria. This predation is initiated by isolated cells called *scouts*, which explore the surroundings of the colony to identify possible nutrient sources [87]. Their attack strategy depends on several parameters, but it depends crucially on the prey density [75]. This way, as prey become scarce, *M. xanthus* increase their scouting capabilities and once the prey has been found, they can switch behaviours to start killing the prey and consuming the nutriments they have released. Though the exact mechanism used by *M. xanthus* to kill its prey remains badly understood, it is known that cell killing can only occur at close proximity of *M. xanthus* (contact-dependent) [106, 15]. Moreover, cluster size structure also play an important role in predation: whereas the forefront of the assault is constituted mainly by singletons or small groups of scouts, the rear of the front is constituted by rather big clusters with some distinct macroscopic behaviours, called *swarms* [124].

To model this phenomenon, we extend the model (5.1)-(5.2) and suppose the existence of another two bacterial types: diffusive individuals which move around alone or in clusters; and eating individuals which are isolated bacteria and clusters capable to kill and eat the prey, but which are kept immobile. This supplementary structure gives a total of 4 subtypes. We call $\rho_1^D(x, y, t)$ the density number of isolated bacteria in diffusing state, and $\rho_1^E(x, y, t)$ of isolated bacteria in eating state, which are solutions of

$$\partial_t \rho_1^D = \theta_1 \Delta \rho_1^D + \alpha \rho_1^D (1 - \rho) - \tau_1^{DE}(e)\rho_1^D + \tau_1^{ED}(e)\rho_1^E - \tau_1 (\rho_1^D)^2 + 2\tau_2 \rho_2^D, \tag{5.7}$$

$$\partial_t \rho_1^E = \tau_1^{DE}(e)\rho_1^D - \tau_1^{ED}(e)\rho_1^E + \alpha \rho_1^E (1 - \rho) - \tau_1 (\rho_1^E)^2 + 2\tau_2 \rho_2^E. \tag{5.8}$$

On the other hand, the density of clusters of two bacteria in diffusing state, $\rho_2^D(x, y, t)$, and those which eat, $\rho_2^E(x, y, t)$, are given by

$$\partial_t \rho_2^D = \theta_2 \Delta \rho_2^D + \frac{\tau_1}{2} (\rho_1^D)^2 - \tau_2 \rho_2^D - \tau_2^{DE}(e)\rho_2^D + \tau_2^{ED}(e)\rho_2^E, \tag{5.9}$$

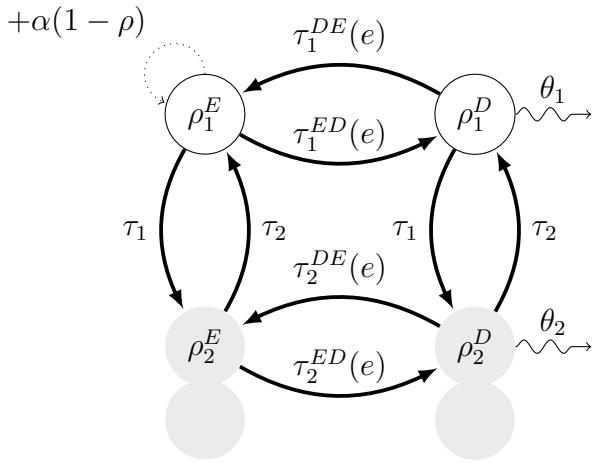

Figure 5.1: Schematic representation of the model (5.7)-(5.11)

$$\partial_t\, \rho_2^E = \tau_2^{DE}(e)\rho_2^D - \tau_2^{ED}(e)\rho_2^E + \frac{\tau_1}{2}(\rho_1^E)^2 - \tau_2\rho_2^E. \tag{5.10}$$

As previously we are interested in the situation in which clusters have got an enhanced motility, so $\theta_2 > \theta_1$. Finally, the density of the prey, which is supposed to be immobile, is given by

$$\partial_t\, e = -\delta_1\rho_1^E - \delta_2\rho_2^E\rho = \rho_1^D + \rho_1^E + 2\left(\rho_2^D + \rho_2^E\right). \tag{5.11}$$

We define ρ as the total of predatory bacteria, *i.e.* $\rho = \rho_1^E + \rho_1^D + 2\rho_2^E + 2\rho_2^D$. The model (5.7)-(5.11) is schematized in figure 5.1. We assume that the change between the "diffusion" state and the "eating" state is dependent on the local amount of prey. Diffusing bacteria can change state with a certain rate τ_i^{DE}, and conversely bacteria become diffusing with a rate τ_i^{ED}, with $i = 1$ or $i = 2$ which corresponds to the size of the cluster. We assume that only isolated bacteria that eat can divide. The transitions between the clusters of two bacteria and the isolated bacteria are the same as in the previous model. The proliferation term is assumed to be logistic with a carrying capacity dependent on the total number of bacteria, ρ. For the model (5.7)-(5.11), the Laplacian operator only depends on space, *i.e.*, $\Delta u(x,y,t) = \partial_{xx}u(x,y,t) + \partial_{yy}u(x,y,t)$. This term corresponds to the movement of bacteria. For the biological reasons mentioned above, it is assumed that the clusters of two bacteria have a faster diffusion than the isolated bacteria, i.e. $\theta_2 > \theta_1$.

We assume that the rates of transitions between the "diffusion" and the "eating" state are linearly dependent on the density of the prey e, i.e. τ_i^{DE} and τ_i^{ED} are given by

$$\tau_i^{DE}(e) = \tau_i^{DE}e, \quad \text{and} \quad \tau_i^{ED}(e) = \tau_i^{ED}(e_{\max} - e), \tag{5.12}$$

with $e_{\max}$ the maximum in space of $e(x,y,t=0)$. As the density of the prey e decreases over time, $e_{\max}$ corresponds to the maximum of e in time and in space.

We perform a numerical analysis of this model. The simulations for different parameters show that the model admits similarities with the biological experiments of predation by the

Myxococcus xanthus bacterium. We notice that, as expected, the sociability and the strong diffusion of the clusters play an important role in the speed of predation.

5.3 Discrete size model

5.3.1 Some properties of the mathematical model

We consider the equivalent nondimensional system given by

$$\partial_\tau \rho_1 = \Delta\rho_1 - k_1\rho_1^2 + 2k_2\rho_2 + \rho_1\,(1-\rho)\,, \tag{5.13}$$

$$\partial_\tau \rho_2 = \theta\Delta\rho_2 + \frac{1}{2}k_1\rho_1^2 - k_2\rho_2, \tag{5.14}$$

where $\theta = \theta_2/\theta_1$, $k_1 = K\tau_1/\alpha$ and $k_2 = \tau_2/\alpha$ are the only three free parameters.

This model has a unique positive equilibrium point $\rho^\star = (\rho_1^\star, \rho_2^\star)$, given by

$$\rho_1^\star = 1 - 2\rho_2^\star, \quad \text{and} \quad \rho_2^\star = \frac{2k_1 + k_2 - \sqrt{k_2(4k_1+k_2)}}{4k_1},$$

with $\rho^\star = \rho_1^\star + 2\rho_2^\star = 1$.

The point $(0,0)$ is another equilibrium point of the system (5.13)-(5.14). Linearising around these equilibrium points, we obtain the following Jacobian matrices

$$J(0,0) = \begin{pmatrix} \alpha & 2k_2 + 2\alpha \\ 0 & -k_2 \end{pmatrix}, \quad \text{and,} \quad J(\rho_1^\star, \rho_2^\star) = \begin{pmatrix} -2k_1\rho_1^\star - \alpha & 2k_2 - 2\alpha \\ k_1\rho_1^\star & -k_2 \end{pmatrix}.$$

The point $(0,0)$ is unstable while the point $\rho^\star$ is stable we are in a monostable case.

Asymptotics in fast fragmentation-coagulation regime.

In order to simplify the theoretical study of the system (5.13)-(5.14), we look at the limit where both rates k_1 and k_2 go towards infinity at the same speed (in the sense that $k_1/k_2 < +\infty$). This means that both cluster fragmentation and the coagulation of isolated bacteria happen at the same time scale, which is much faster than the growth and diffusion time scale. Equation (5.14) can be written

$$\partial_t \rho_2 - \theta\Delta\rho_2 = k_1\left(\frac{1}{2}\rho_1^2 - \frac{k_2}{k_1}\rho_2\right). \tag{5.15}$$

Since $k_1 \to +\infty$, we must have $\frac{1}{2}\rho_1^2 - \frac{k_2}{k_1}\rho_2 = 0$ in the RHS of Eq. (5.15). Then, recalling that $\rho = \rho_1 + 2\rho_2$ we obtain

$$\rho_1 = f(\rho) := \frac{-1 + \sqrt{1 + 4\frac{k_1}{k_2}\rho}}{2\frac{k_1}{k_2}}.$$

Therefore, since $2\rho_2 = \frac{k_1}{k_2}\rho_1^2 = \frac{k_1}{k_2}f(\rho)^2$, adding equations (5.13) and (5.14)

$$\partial_t \rho - \Delta\phi(\rho) = F(\rho), \tag{5.16}$$

with $\phi(\rho) := f(\rho) + \theta\frac{k_1}{k_2}f(\rho)^2$ and $F(\rho) := f(\rho)(1-\rho)$. Thus,

$$\phi''(x) = \frac{\frac{k_1}{k_2}(\theta-1)}{2\left(1+4\frac{k_1}{k_2}x\right)^{3/2}} \quad \text{and} \quad F''(x) = \frac{-2\frac{k_1}{k_2}}{(1+4\frac{k_1}{k_2}x)^{3/2}}(1-x) - \frac{2}{\sqrt{1+4\frac{k_1}{k_2}x}}.$$

Thereby, F is concave, positive and verifies $F(0) = F(1) = 0$. Moreover, we have that ϕ is convex if $\theta > 1$.

For the equation $\partial_t\rho - \theta\Delta\rho = F(\rho)$ with F concave, the minimal speed front is given by $c^* = 2\sqrt{\theta F'(0)}$ (see for instance [90]). On the other hand, the non-linear diffusion term of Eq. (5.16) does not allow to directly apply this theory. Instead, we approach numerically the minimal speed employing a shooting method. The method is build upon the analysis of the phase plane $(\rho, (\phi(\rho))')$. We start by looking for solutions of the form

$$\rho(x,t) = p(x-ct), \quad (t,x) \in \mathbb{R}^2,$$

with c the unknown front speed that we want to determine. We are interested in solutions connecting the equilibrium state $p = 1$ (in $-\infty$) with the equilibrium state $p = 0$ (in $+\infty$). Then, from (5.16), we obtain

$$-cp' - (\phi(p))'' = F(p), \tag{5.17}$$

and if we set $q = (\phi(p))'$ we obtain the following system

$$\begin{cases} p' = \dfrac{1}{\phi'(p)}q, \\ q' = \dfrac{-c}{\phi'(p)}q - F(p), \\ \lim\limits_{\xi\to-\infty} p(\xi) = 1, \quad \lim\limits_{\xi\to+\infty} p(\xi) = 0. \end{cases}$$

So the problem is to find the wave speed $c \in \mathbb{R}$ and the $\mathcal{C}^2$ wave profile $p : \mathbb{R} \longrightarrow [0,1]$ which solve the previous system. For this, we performed a shooting method. We test proposal values of c, and simulate the associated profile p. If p become negative at a certain moment, we reject the value of c and try a larger one, until obtaining an admissible profile. We will compare this speed with the one obtained by numerical simulations of the population dynamics. The method used and the results are given in the next paragraph and Figure 5.2, which is discussed further below.

5.3.2 Numerical simulations

We simulate Eq. (5.13)-(5.14) using a splitting method with a semi-implicit finite difference scheme. This is, we the diffusion and reaction terms in two separate steps. For the first one,

we use an implicit numerical scheme, and for the latter we use the RK4 explicit scheme. We extend the same method to simulate the two-dimensional model of Eq. (5.7)-(5.11), which is presented further below.

Using this method, we approximate numerically the solutions of (5.13)-(5.14) for different values of the cluster's relative diffusion coefficient $\theta > 1$ and for equal fragmentation and coagulation rates $k = k_1 = k_2 = k$. We let vary k and θ and study whether the total population density ρ behaves as a wave of the form $\rho(x,t) = u(x-ct)$ with $u(\xi) \sim \exp(-\lambda\xi)$. The coefficient λ is the rate of exponential decay towards the stable state 0 and gives the form of the front. When the system admits indeed travelling wave solutions, we extract numerically the values of c and λ from the simulated solutions to (5.13)-(5.14). We explain below the methods used.

In first place, to obtain the wavespeed we compute at each time-step t_n the estimator $\hat{c}_n$ defined by

$$\hat{c}_n := \sum_{j=1}^{J} \frac{\rho^n(x_j) - \rho^{n-1}(x_j)}{\Delta t} \Delta x, \tag{5.18}$$

where $\{x_j = j\Delta x\}_{j\in\{0,\dots,J\}}$ is the space grid. As $\Delta x, \Delta t \to 0$, c_n converges to the wavespeed. Indeed, if we suppose that we admit wave solutions which are of the form $\rho(t,x) = u(x-ct)$, with $u(\xi) \to 1$ as $\xi \to -\infty$, and $u(\xi) \to 0$ as $\xi \to +\infty$, then $\partial_t \rho = -c\partial_x \rho$. Integration of this equation with respect to x gives

$$c = \int_{-\infty}^{+\infty} \partial_t \rho(t,x) dx. \tag{5.19}$$

Equation (5.18) is then a finite difference discretisation of the the time derivative and the spatial integral in the latter expression.

In second place, the value λ of the exponential decay constant is computed by fitting an exponential curve to the wavefront, using a least squares estimator.

Fig. 5.2 gives the results of c (panel A and C) and λ (panel B) extracted for $\theta \in [0, 30]$ and $k_1 = k_2 = k \in [0, 15]$. We recall that in the Fisher-KPP case we have $c = 2$ and $\lambda = 1$. In particular, this values correspond to the regime where the cluster structure do not affect the propagation speed of the population. In this case, the population front is said to be *pulled* by the isolated bacteria, which are the leading component at the front. Fig. 5.2-A and 5.2-C shows the existence of a critical diffusion coefficient θ^* near the value $\theta = 3$ such that for all $\theta < \theta^*$ the wave speed correspond to the Fisher-KPP (pulled) case, and that for all $\theta > \theta^*$, the speed is strictly bigger than the Fisher-KPP speed. In the latter case, the population wave is said to be *pushed*. The speed of propagation is determined by the whole front, including the clusters of bacteria, which therefore contribute to the overall acceleration. A formal definition of pulled and pushed waves in the context of the *inside dynamics* of the population can be consulted in [63]. So, to summarise, if the diffusion coefficient of the clusters is sufficiently larger than the diffusion coefficient of isolated bacteria (around 3 times bigger), the whole population advances faster than in the Fisher-KPP case, switching from a pulled regime, where the speed is limited by the isolate bacteria speed, to a pushed regime, where the speed is enhanced by the social behaviour of the bacteria. Moreover,

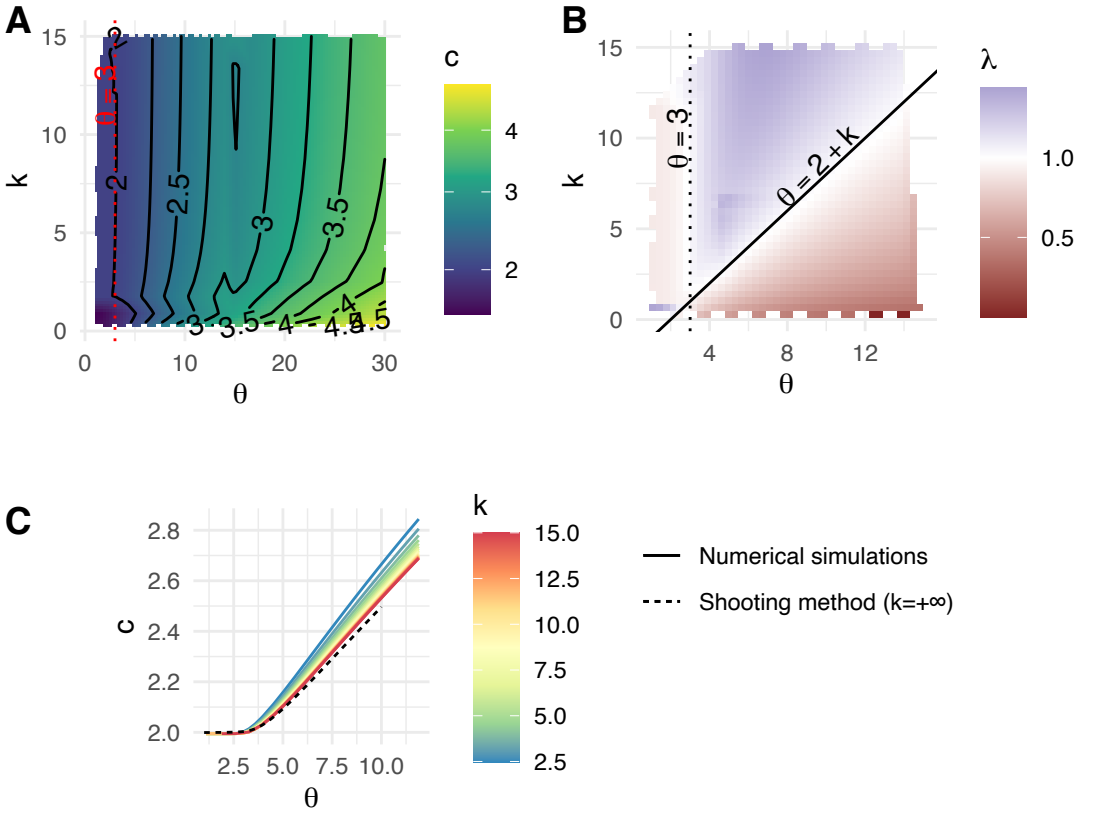

Figure 5.2: Numerical results of the nondimensional system of Eq. (5.13)-(5.14) for different values of the cluster's relative diffusion coefficient $\theta > 1$ and for equal fragmentation and coagulation rates $k = k_1 = k_2$. **A.** Wavefront propagation speed c as function of θ and k. Contour levels are also indicated along the coloured heatmap. The speed is obtained using (5.18). The critical value of $c = 2$ is reached near the ordinate $\theta = 3$, highlighted in red. **B.** Exponential decay rate λ of the total population wavefront. The line $\theta = 2 + k$ corresponds to the regime change expected by the heuristic (Section 5.7). **C.** Value of the wavefront speed c as function of the clusters' diffusion coefficient θ, for various values of k (solid line). The value predicted by the shooting method described in Section 5.3.1 in the limit $k \to +\infty$ is also presented (dotted line).

the value of this critical θ^* appears to be constant for all $k > 0$, so this regime switch is independent of the fragmentation-coagulation rate.

The analysis of the exponential decay of the front λ can shed some light about the regime switching in speed. Fig. 5.2-B shows that the critical Fisher-KPP value of $\lambda = 1$ is reached in our simulations around two lines: first, around the constant $\theta = 3$, which corresponds to the actual threshold observed for the speed regimes; and second, around the line $\theta = 2 + k$. In particular, some heuristic calculations make it possible to explain formally this threshold (see Section 5.7). We see however that this line is not associated with a change of regime in the speed.

Finally, in Fig.5.2-C we can see the value of c approximated by the shooting method in the asymptotic $k \to +\infty$. This results, which are obtained trough a completely different

numerical approach, confirm the independence of the threshold θ^* with respect to k and help validate also the results obtained from our numerical scheme.

5.4 Continuous cluster-size model

We make the following assumptions about the functions of the model (5.3)-(5.6)

$$\gamma(z', z) = \gamma z' z, \qquad \beta(z) = \beta z, \qquad v(z, m) = \alpha z(1 - m/\kappa), \quad \forall z \in [0, z_{\max}], \tag{5.20}$$

with $\gamma > 0$ a constant coagulation rate by squared unit of size, $\beta > 0$ a constant fragmentation rate by unit of size, $\kappa > 0$ a carrying capacity with respect to the sum of the individual sizes of the population, and $\alpha > 0$ some constant growth rate by unit of size, and m is the total mass of the system as defined by Eq. (5.6).

To begin with, we assume that the diffusion coefficient is defined by

$$\theta(z) = \theta_1, \qquad \text{for all } \; z \in [0, z_{\max}] \; . \tag{5.21}$$

Under the assumptions (5.20) and (5.21), we have the following equations on n and m:

$$\partial_t n = \theta \partial_{xx} n + \beta m \left(1 - \frac{\alpha}{2\beta} m\right), \tag{5.22}$$

and

$$\partial_t m = \theta \partial_{xx} m + m\alpha(1 - m/\kappa). \tag{5.23}$$

Note that Eq. (5.23) corresponds to a Fisher-KPP equation. This equation admits traveling wave type solutions. Searching for a travelling wave for the model (5.3)-(5.6), we define the variable $\xi(z) = x - c(z)t$, where $c(z)$ is a function of z corresponding to the unknown invasion speed. We denote, ρ, the wave profile, given by

$$\rho(t, x, z) = p(\xi(z)), \tag{5.24}$$

with the following limits

$$p(-\infty) = f(z), \qquad p(+\infty) = \tilde{0}(z.) \tag{5.25}$$

Where $\tilde{0}$ corresponds to the null function and $f(z)$ to a stationary stable solution of the following system

$$\partial_t q(t, z) = -\partial_z \left[v(z, m) q(t, z)\right] + \mathcal{F}[q](t, z) + \mathcal{G}[q](t, z). \tag{5.26}$$

The equation (5.26) corresponds to the system (5.3)-(5.6) without diffusion. In theory we do not know the function f, we approximate it using a numerical simulation. For our parameter values the shape of $f(z)$ is a peak close to $z = 0$.

In figure 5.3-A, we see an example of a traveling wave type solution for the model (5.3)-(5.6). The initial data is given by $\rho(x, z, 0) = \tilde{f}(z)\mathbf{1}_{x \leq 30}$, where $\tilde{f}(z)$ is the numerical solution of the equation (5.26). Between the time $t = 30$ and $t = 50$, the state $\tilde{f}(z)$ spatially

invades the null state. According to our numerical simulations, for these parameter values, the speed of the traveling wave solutions of the equation (5.24) seems to be independent of z and is similar to the speed of the traveling waves of the moments of order 0 and 1 given by the equations (5.22) and (5.23). Traveling waves for the term m and n are illustrated in the panel B of figure 5.3. The colorimetry represents the progression of time, blue for $t = 0$ and red for $t = 80$. For this initial data, it is known that the selected speed of the traveling wave for m corresponds to the critical wave speed, *i.e.* $2\sqrt{\alpha\theta}$. In theory, if the system (5.3)-(5.6) admits solutions of traveling waves, the moments have them too. Moreover, the speed of the traveling waves of the moments is necessarily less than or equal to the speed of the traveling wave of the model (5.3)-(5.6).

Now, for the biological reasons mentioned above, we assume that θ is an increasing function of z. For numerical reasons, we define θ as

$$\theta(z) = \begin{cases} \theta_1 \ , & \text{si } z \leq s, \\ \theta_2 \ , & \text{si } z > s, \end{cases} \tag{5.27}$$

with θ_1, θ_2 two positive constant such that $\theta_2 > \theta_1$ and s a positive constant.

The figure 5.4 corresponds to the evolution of the numerical speed of the traveling wave of the moment of order 1 as a function of θ_2, for the model (5.3)-(5.6) with θ defined by (5.27). We observe, once again, the existence of a threshold $\tilde{\theta}_2$. Indeed, for $\theta_2 \leq \tilde{\theta}_2$, we notice that the speed of the traveling wave seems to be very close to the speed $c_{\text{KPP}} = 2\sqrt{\theta_1\alpha}$ and becomes strictly larger for $\theta_2 > \tilde{\theta}_2$. For θ_2 sufficiently large, we notice that the growth is of order $\sqrt{\theta_2}$, as for the discrete model (5.1)-(5.2).

5.5 Prey-predator model

Figure 5.5 corresponds to the numerical simulation of the system (5.7)-(5.11) which takes into account two types of bacteria, the first type ρ_i^E is immobile and can consume its prey while the second ρ_i^E diffuses. The density of the prey, for example *E. coli*, is shown in red. The green color corresponds to the density of bacteria which diffuse, $\rho_1^D + 2\rho_1^D$, and in blue the bacteria which consume the prey, $\rho_1^E + 2\rho_1^E$. The initial data, represented in the figure 5.5 (top panel) are chosen to be as close as possible to the biological experiments. At first the bacteria are in the "diffusion" state, looking for prey. Some of the diffusing bacteria will, on contact with the prey, change state to become bacteria that consume the prey. This behavior will tend to reduce the spread of predation in areas with high prey density. For example, the propagation of predatory bacteria is faster in the middle of *E. coli* than on these edges with a higher initial density (See Figure 5.5 lower left panel). Gradually, the prey will be consumed and will disappear.

To understand the importance of sociability in predator propagation, we define a model similar to the system (5.7)-(5.11) for which isolated cells cannot regroup to form a cluster.

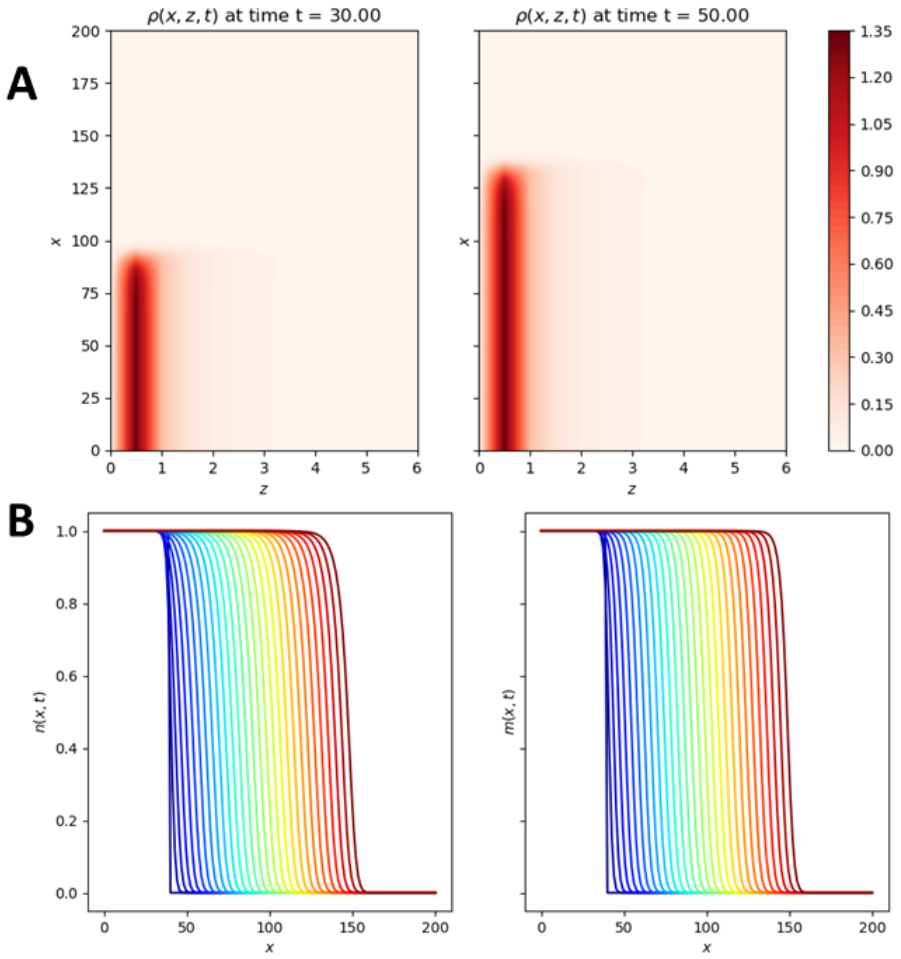

Figure 5.3: A. Example of traveling wave for the model (5.3)-(5.6) under the assumptions (5.20) and (5.21). The state $f(z)$ spatially invades the state $\tilde{0}(z)$ for all z. Concerning the initial data, we assume that, at time $t = 0$, the density is given by $\rho(x, z, 0) = f(z)\mathbf{1}_{x \leq x_0}$ with some positive constant x_0. The parameter values are $\theta_1 = 1$, $\alpha = 1$, $\beta = 1$, $\gamma = 1$, $\kappa = 1$. **B.** Representation over time of the numerical solutions $m(x, t)$ and $n(x, t)$ (Left n and right m). The color represents the time, blue $t = 0$ and red $t = T_{\text{end}}$ and the colorimetry is linear. The initial data and parameters value are the same as above.

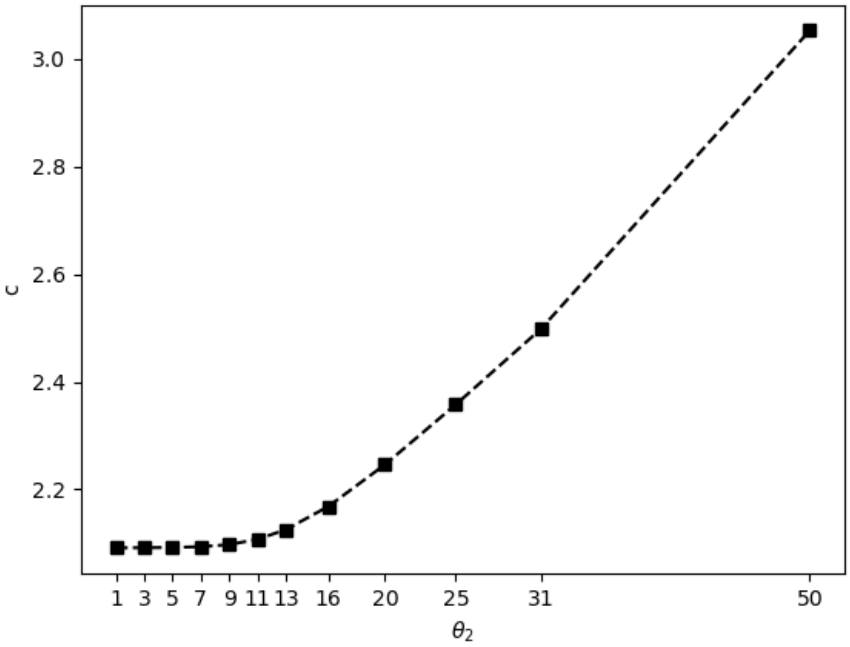

Figure 5.4: Speed of the traveling wave of the equation (5.23), obtained by numerical simulations, for different θ_2, under assumption (5.27). Similarly to the discrete model, there is a threshold $\tilde{\theta}_2$ such that for all $\theta_2 \leq \tilde{\theta}_2$ the speed of the wave is $c_{\text{KPP}} = 2\sqrt{\alpha\theta_1} = 2$, and for $\theta_2 > \tilde{\theta}_2$, the speed becomes strictly higher than the speed c_{KPP}. The parameter values are similar to those in Figure 5.3.

The model is defined by

$$\begin{cases} \partial_t\ \rho_1^D = \theta_1 \Delta \rho_1^D + \alpha \rho_1^D (1-\rho) - \tau_1^{DE}(e)\rho_1^D + \tau_1^{ED}(e)\rho_1^E, \\ \partial_t\ \rho_1^E = \tau_1^{DE}(e)\rho_1^D - \tau_1^{ED}(e)\rho_1^E + \alpha \rho_1^E (1-\rho), \\ \partial_t\ e = -\delta_1 \rho_1^E, \\ \rho = \rho_1^D + \rho_1^E. \end{cases} \tag{5.28}$$

In the figure 5.6 we observe the importance of sociability on the speed of predation. The left part corresponds to the numerical simulation of the model (5.28) at time $t = 0$ and at time $t = 8$ and on the right it corresponds to the numerical simulation of the system (5.7)-(5.11) at the same times. For both simulations we take similar initial data and parameters shared by both models have the same values. For equations (5.8) and (5.10), the parameter values for the bacteria clusters are similar to the values for the isolated bacteria, except for the diffusion coefficient. Under these assumptions, we observe in Figure 5.6 (bottom panel) that for the (5.7)-(5.11) model, the prey, shown in red, is consumed more quickly. This increase in the speed of invasion is due to the diffusion advantage of the clusters. Indeed, in the case $\theta_2 = \theta_1$ for the (5.7)-(5.11) model, the speed of predation appears to be the same as the speed obtained with the associated (5.28) model.

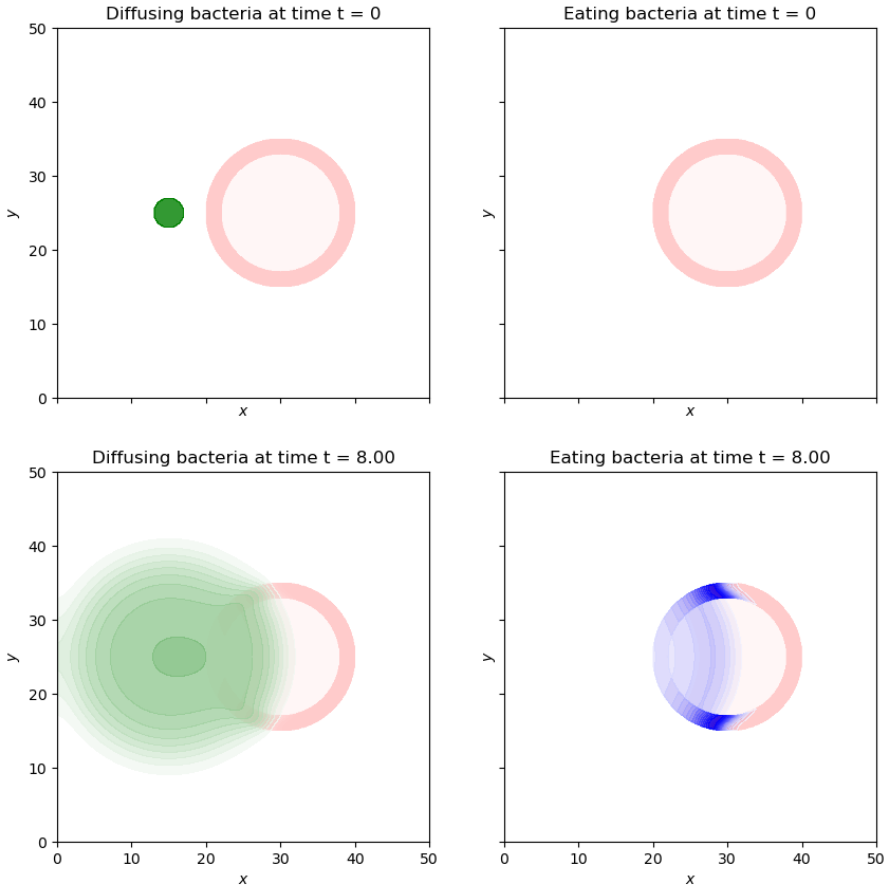

Figure 5.5: Numerical simulations of the model (5.7)-(5.11), under the assumption (5.12). The density of bacteria which diffuse, $\rho_1^D + 2\rho_2^D$, is represented in green and the density of bacteria which consume the prey, $\rho_1^E + 2\rho_2^E$, is represented in blue. The prey density, e, is represented shown in red. The initial data are shown in the top panel, they are chosen to be as close as possible to the biological experiments. The initial distribution of predatory bacteria is assumed to be homogeneous on a circle, while the initial distribution of prey is assumed to be arranged on a circle with a higher density on the edges. At time $t = 0$, there are no predatory bacteria in the "eating" state. The bottom panel represents the densities at time, $t = 8$, the predatory bacteria spread and reached the prey, which then began to consume the prey. The parameter values for this numerical simulation are $\theta_1 = 1$, $\theta_2 = 2$, $\alpha = 1$, $\tau_1 = 2$, $\tau_2 = 1$, $\tau_1^{DE} = \tau_2^{DE} = 1$, $\tau_1^{ED} = \tau_2^{ED} = 1$, $\delta_1 = \delta_2 = 2$.

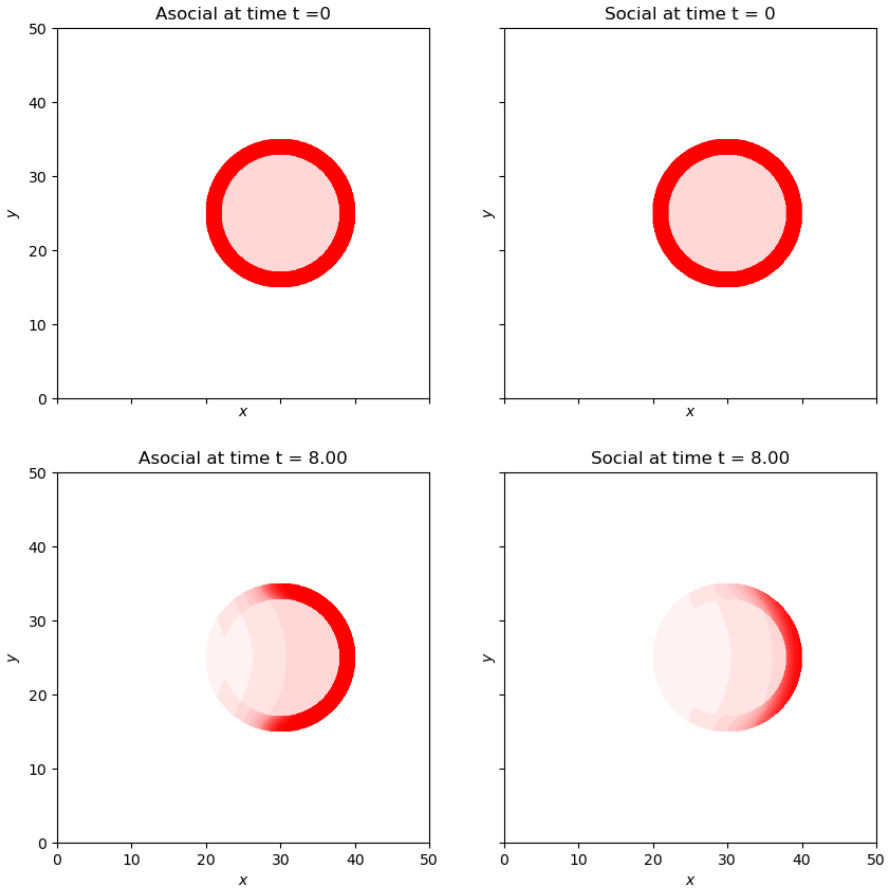

Figure 5.6: The distribution of *E. coli* at time $t = 0$ (top) and $t = 8$ (bottom) is represented in red, for the model (5.28) (left) and for the model (5.7)-(5.11) (right). For both simulations, we assume the linear transition hypothesis (5.12). We assume that there are no benefits other than diffusion, therefore $\delta_2 = \delta_1$, $\tau_2^{ED} = \tau_1^{ED}$ and $\tau_2^{DE} = \tau_1^{DE}$. Under this assumption, predation is faster for the model (5.7)-(5.11) than for the model (5.28). The values of the parameters are the same as in the figure 5.5

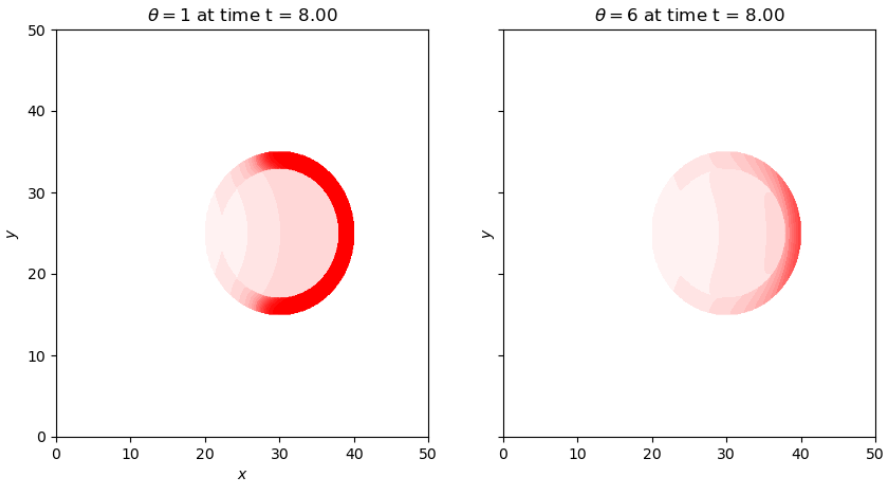

Figure 5.7: Numerical simulations of the model (5.7)-(5.11) with different diffusion coefficients. The distribution of *E. coli* is represented in red at time $t = 8$ with the same initial data. The coefficient θ is defined as the ratio of θ_2 and θ_1, *i.e.* $\theta := \theta_2/\theta_1$ and corresponds to the advantage/disadvantage of cluster diffusion. For the simulation on the left, we assume that $\theta = 1$ and for the simulation on the right we assume that $\theta = 6$. The values of the other parameters are the same for both simulations and are those in figure 5.5.

The speed of predation is strongly correlated with the value of the parameter θ_2. Contrary to the previous model, the lesser advantage given to clusters has an effect on the predation speed. The figure 5.7 corresponds to two numerical simulations of the system (5.7)-(5.11) at time $t = 8$ for two different coefficients θ_2. The other parameter values and the initial data are similar. The prey density, represented in red, is much lower for a larger θ_2 coefficient. We see that the speed of predation is an increasing function of $\theta := \theta_2/\theta_1$, for $\theta > 1$.

5.6 Conclusions and perspectives

We studied the effect of social behaviour on the motility of *Myxococcus xanthus* populations. Previous *in vitro* experiments have showed that the capacity to constitute clusters of bacteria that move collectively begets an enhanced predation efficiency. Our numerical experiments shed some light onto this phenomenon. We have first considered a minimal model in which isolated bacteria are able to form clusters of two bacteria which diffuse collectively. The simulations suggest that when the clusters diffuse at least 3 times faster than the isolated individuals, the speed of propagation of the whole population is bigger than the critical Fisher-KPP speed (pushed wave). Otherwise, if clusters do not diffuse fast enough, the speed of the population is limited by the propagation speed of isolated individuals (pulled wave). The threshold separating the pushed and pulled regimes seems to be unique and independent from the rates of fragmentation and coagulation. In particular, using a shooting method, the same regime separation was found numerically in the asymptotic

case of infinitely fast fragmentation and coagulation.

We also considered two extensions. First, we considered a continuous cluster-size model written as an integro-differential equation with some fragmentation and coagulation operators. Under some biologically meaningful choices of parameterisation for these operators, we show that the total number of individuals (zero-th order moment) and total sum of cluster sizes (first order moment) of the structured population exhibit travelling waves whose speed is also characterised by a threshold in the diffusion coefficient, below which the speed coincides with Fisher-KPP critical speed. This result seems to extend the regime separation observed in the discrete case to a more general class of population dynamics. In this case, as the population wavefront progresses, the cluster structure of the rear of the wave is distributed according to the steady-state distribution of cluster sizes, and the travelling wave connects the steady-state to the null function.

Finally, we considered an extended model in which isolated and clustered bacteria are both able to switch towards an *eating* state when they encounter a positive density of prey. However, they become immobile in this state. With the purpose of observing the effect of clusters in the predatory efficiency, we compared the propagation fronts obtained in presence and absence of clustering. The numerical simulations indicate that the prey is consumed faster when the bacteria are allowed to cluster. In that case, the speed of predation is an increasing function of the ratio of the diffusion coefficients of clusters and isolated bacteria.

Regime separation in the discrete case, particularly in the fast fragmentation-coagulation asympototic, can motivate some theoretical investigations which are not explored here. For example, approaches relying in the variational characterisation of the wave speed can be adapted to obtain bounds on the diffusion threshold θ^*. The numerical simulations can also be extended to include some more realistic cases, accounting for the complex cluster structure of swarms and scouts.

5.7 Heuristics on the $\theta = 2 + k$ threshold line

We give some explanations on the critical threshold $\theta = 2 + k$ observed in Fig. 5.2-B at which $\lambda = 1$. To that extent, suppose the existence of a wavefront solution $\rho(t, x) = \rho(x - ct)$ with unknown speed c. Let $z = x - ct$. PDE system (5.13)-(5.14) reduces to the following system of second-order ODE on the variable z:

$$\begin{cases} -c\partial_z\rho_1 = \partial_{zz}\rho_1 - k_1\rho_1^2 - 2k_2\rho_2 + \rho_1\left(1 - \rho\right), \\ -c\partial_z\rho_2 = \theta\partial_{zz}\rho_2 + \frac{1}{2}k_1\rho_1^2 - k_2\rho_2, \\ \rho = \rho_1 + 2\rho_2. \end{cases}$$

Now, let's suppose that in the forefront of the population the number of isolated individuals and clusters is such that we are under the following heuristic hypothesis

$$(H_0): \qquad \rho_1^2 \ll \rho_2 \ll \rho_1,$$

such that under (H_0) the first ODE becomes

$$-c\rho_1 = \partial_{zz}\rho_1 - \rho_1.$$

This is equivalent to the linearisation of Fisher-KPP Equation, for which the critical speed is $c = 2$. Moreover, the solution profile is of the form $\rho_1(z) = C_1 \exp(-\lambda z)$, with $\lambda = 1$. Now, let's come back to the second ODE and replace ρ_1. We get

$$-c\partial_z \rho_2 - \theta \partial_{zz} \rho_2 + k_2 \rho_2 = \frac{k_1}{2} C_1^2 e^{-2\lambda z.}$$

We solve this equation finding a solution of the form

$$\rho_2(z) = Ae^{-\mu z} + Be^{-2\lambda z},$$

for some unknown value μ. In particular, for the particular solution, the constant B is such that

$$\left(2\lambda c - 4\theta\lambda^2 + k_2\right) B = \frac{k_1}{2} C_1^2.$$

Thus, at the critical value $\lambda = 1$ we obtain

$$\left(2c - 4\theta + k_2\right) B = \frac{k_1}{2} C_1^2,$$

which for $2c - 4\theta + k_2 \neq 0$ begets

$$B = \frac{C_1^2 k_1}{2\left(2c - 4\theta + k_2\right)}.$$

On the other hand, for the constant μ, we have:

$$c\mu - \theta\mu^2 + k_2 = 0.$$

Thus, for a discriminant $\Delta = c^2 + 4\theta k_2 > 0$, we obtain the solutions:

$$\mu_\pm = \frac{-c \pm \sqrt{c^2 + 4\theta k_2}}{-2\theta} = \frac{c \mp \sqrt{c^2 + 4\theta k_2}}{2\theta}.$$

Since $\mu_+ < 0$, we consider only the solution with $\mu = \mu_-$. The critical transition should occur at the moment when H_0 is not verified anymore, and thus the non-linear effects are not negligible. In particular, when we are just at the threshold level, we also have the critical Fisher-KPP values $\mu = 1$ and $c = 2$ which gives

$$\sqrt{1 + \theta k_2} = \theta - 1,$$

from which we derive the relation $\theta = 2 + k_2$. Therefore we should expect that, at fixed k_2, (H_0) is violated for all $\theta > 2 + k_2$, and thus we transit from a pulled to a pushed regime.

Acknowledgements

This project has received funding from the European Research Council (ERC) under the European Union's Horizon 2020 research and innovation programme (grant agreement No 865711). M.E. was funded by the ANR via the project PLUME under grant agreement ANR-21-CE13-0040. The authors would also like to thank the organisers of CEMRACS 2022 (Emmanuel Franck, Hélène Hivert, Guillaume Latu, Hélène Leman, Bertrand Maury, Michel Mehrenberger, Laurent Navoret) for the stimulating research environment in the context of which this work was developed. We acknowledge particularly Hélène Hivert for our fruitful discussions concerning the numerical schemes.

Bibliography

[1] M. Acar, J. T. Mettetal, and A. Van Oudenaarden. "Stochastic switching as a survival strategy in fluctuating environments". In: *Nature Genetics* 40.4 (2008), pp. 471–475. ISSN: 10614036. DOI: 10.1038/NG.110.

[2] M. Alfaro, J. Coville, and G. Raoul. "Travelling waves in a nonlocal reaction-diffusion equation as a model for a population structured by a space variable and a phenotypic trait". In: *Communications in Partial Differential Equations* 38.12 (2013), pp. 2126–2154.

[3] R. N. Alnahhas and M. J. Dunlop. "Advances in linking single-cell bacterial stress response to population-level survival". In: *Current Opinion in Biotechnology* 79 (2023), p. 102885. ISSN: 09581669. DOI: 10.1016/j.copbio.2022.102885.

[4] A. Amir. "Cell Size Regulation in Bacteria". In: *Physical Review Letters* 112.20 (2014), p. 208102. ISSN: 0031-9007. DOI: 10.1103/PhysRevLett.112.208102.

[5] K. B. Athreya and P. E. Ney. *Branching Processes*. Berlin, Heidelberg: Springer Berlin Heidelberg, 1972. ISBN: 978-3-642-65373-5. DOI: 10.1007/978-3-642-65371-1.

[6] S. V. Avery. "Microbial Cell Individuality & the Underlying Sources of Heterogeneity". In: *Nature Reviews. Microbiology* 4.8 (2006), 577–87.

[7] E. Baake and H. O. Georgii. "Mutation, selection, and ancestry in branching models: a variational approach". In: *J. Math. Biol.* 54 (2007), pp. 257–303. DOI: 10.1007/s00285-006-0039-5.

[8] N. Q. Balaban, J. Merrin, R. Chait, L. Kowalik, and S. Leibler. "Bacterial persistence as a phenotypic switch". In: *Science* 305.5690 (2004), pp. 1622–1625. ISSN: 00368075. DOI: 10.1126/SCIENCE.1099390.

[9] D. Balagué, J. A. Cañizo, and P. Gabriel. "Fine asymptotics of profiles and relaxation to equilibrium for growth-fragmentation equations with variable drift rates". In: *Kinetic and Related Models* 6 (2013), p. 219. DOI: 10.3934/KRM.2013.6.219.

[10] V. Bansaye, B. Cloez, P. Gabriel, and A. Marguet. "A non-conservative Harris ergodic theorem". In: *Journal of the London Mathematical Society* 106.3 (2022), pp. 2459–2510. DOI: 10.1112/jlms.12639.

[11] V. Bansaye, B. Cloez, and P. Gabriel. "Ergodic behavior of non-conservative semigroups via generalized Doeblin's conditions". In: *Acta Applicandae Mathematicae* 166.1 (2020), pp. 29–72. DOI: 10.1007/S10440-019-00253-5.

[12] G. Bell. "Evolutionary Rescue". In: *Annual Review of Ecology, Evolution, and Systematics* 48 (2017), pp. 605–627. ISSN: 15452069. DOI: 10.1146/annurev-ecolsys-110316-023011.

[13] R. Bellman and T. Harris. "On Age-Dependent Binary Branching Processes". In: *The Annals of Mathematics* 55.2 (1952), p. 280. ISSN: 0003486X. DOI: 10.2307/1969779.

[14] M. Benaïm and T. Hurth. "Harris Ergodic Theorem". In: *Markov Chains on Metric Spaces: A Short Course*. Cham: Springer International Publishing, 2022, pp. 161–179. ISBN: 978-3-031-11822-7. DOI: 10.1007/978-3-031-11822-7_8.

[15] J. E. Berleman and J. R. Kirby. "Deciphering the hunting strategy of a bacterial wolfpack". In: *FEMS microbiology reviews* 33.5 (2009), pp. 942–957.

[16] J. Bierkens, G. O. Roberts, and P. A. Zitt. "Ergodicity of the zigzag process". In: *The Annals of Applied Probability* 20.4 (2019), pp. 2266–2301. DOI: 10.1214/18-AAP1453.

[17] J. Blath, F. Hermann, and M. Slowik. "A branching process model for dormancy and seed banks in randomly fluctuating environments". In: *Journal of Mathematical Biology* 83.2 (2021), pp. 1–40. ISSN: 14321416. DOI: 10.1007/S00285-021-01639-6/FIGURES/9.

[18] J. Blath and A. Tóbiás. "Invasion and fixation of microbial dormancy traits under competitive pressure". In: *Stochastic Processes and their Applications* 130.12 (2020), pp. 7363–7395. ISSN: 03044149. DOI: 10.1016/j.spa.2020.07.018.

[19] H. Bloch, B. Gaudeul, M. Romanos, and J. Saulnier. "CEMRACS 2022 Proceedings (to appear)". In: (2022).

[20] F. Bouguet. "A Probabilistic Look at Growth-Fragmentation Equations". In: *Séminaire de Probabilités XLIX. Lecture Notes in Mathematics* 2215 (2018), pp. 57–74. DOI: 10.1007/978-3-319-92420-5_2.

[21] E. Bouin and V. Calvez. "Travelling waves for the cane toads equation with bounded traits". In: *Nonlinearity* 27.9 (2014), p. 2233.

[22] T. Bourgeron, Z. Xu, M. Doumic, and M. T. Teixeira. "The asymmetry of telomere replication contributes to replicative senescence heterogeneity". In: *Scientific Reports* 5 (2015), p. 15326. DOI: 10.1038/srep15326.

[23] A. Brauner, O. Fridman, O. Gefen, and N. Q. Balaban. "Distinguishing between resistance, tolerance and persistence to antibiotic treatment". In: *Nature Reviews Microbiology* 14.5 (2016), pp. 320–330. ISSN: 17401534. DOI: 10.1038/nrmicro.2016.34.

[24] J. Broughton. "Ph. D. dissertation (in progress)". PhD thesis. University of Edinburgh, Jan. 2024.

[25] V. Calvez, M. Doumic, and P. Gabriel. "Self-similarity in a general aggregation-fragmentation problem. Application to fitness analysis". In: *Journal des Mathematiques Pures et Appliquees* 98.1 (2012), pp. 1–27. ISSN: 00217824. DOI: 10.1016/J.MATPUR.2012.01.004.

[26] F. Campillo, N. Champagnat, and C. Fritsch. "Links between deterministic and stochastic approaches for invasion in growth-fragmentation-death models". In: *Journal of Mathematical Biology* 73.6-7 (2016), pp. 1781–1821. ISSN: 14321416. DOI: 10.1007/S00285-016-1012-6/METRICS.

[27] F. Campillo, N. Champagnat, and C. Fritsch. "On the variations of the principal eigenvalue with respect to a parameter in growth-fragmentation models". In: *Communications in Mathematical Sciences* 15.7 (2017), pp. 1801–1819. ISSN: 19450796. DOI: 10.4310/CMS.2017.v15.n7.a1.

[28] M. Campos, I. V. Surovtsev, S. Kato, A. Paintdakhi, B. Beltran, S. E. Ebmeier, and C. Jacobs-Wagner. "A Constant Size Extension Drives Bacterial Cell Size Homeostasis". In: *Cell* 159.6 (2014), pp. 1433–1446. ISSN: 00928674. DOI: 10.1016/j.cell.2014.11.022.

[29] O. Carja and J. B. Plotkin. "Evolutionary rescue through partly heritable phenotypic variability". In: *Genetics* 211.3 (2019), pp. 977–988. ISSN: 19432631. DOI: 10.1534/genetics.118.301758.

[30] J. Cayron, A. Dedieu-Berne, and C. Lesterlin. "Bacterial filaments recover by successive and accelerated asymmetric divisions that allow rapid post-stress cell proliferation". In: *Molecular Microbiology* 119.2 (2023), pp. 237–251. ISSN: 0950-382X. DOI: 10.1111/mmi.15016.

[31] J. A. Cañizo, P. Gabriel, and H. Yoldaş. "Spectral gap for the growth-fragmentation equation via Harris's theorem". In: *SIAM Journal on Mathematical Analysis* 53.5 (2021), pp. 5185–5214. DOI: 10.1137/20M1338654.

[32] J. Clairambault, S. Gaubert, and T. Lepoutre. "Comparison of Perron and Floquet Eigenvalues in Age Structured Cell Division Cycle Models". In: *Mathematical Modelling of Natural Phenomena* 4.3 (2009), pp. 183–209. ISSN: 0973-5348. DOI: 10.1051/MMNP/20094308.

[33] J. Clairambault, S. Gaubert, and B. Perthame. "An inequality for the Perron and Floquet eigenvalues of monotone differential systems and age structured equations". In: *Comptes Rendus Mathematique* 345.10 (2007), pp. 549–554. ISSN: 1631073X. DOI: 10.1016/J.CRMA.2007.10.001/.

[34] B. Cloez and P. Gabriel. “On an irreducibility type condition for the ergodicity of nonconservative semigroups”. In: *Comptes Rendus. Mathématique* 358.6 (2020), pp. 733–742. DOI: 10.5802/crmath.92.

[35] B. Cloez, B. de Saporta, and T. Roget. “Long-time behavior and Darwinian optimality for an asymmetric size-structured branching process”. In: *Journal of Mathematical Biology* 83.6 (2021). DOI: 10.1007/s00285-021-01695-y.

[36] M. Costa. “A piecewise deterministic model for a prey-predator community”. In: *The Annals of Applied Probability* 26.6 (2016), pp. 3491–3530. ISSN: 1050-5164. DOI: 10.1214/16-AAP1182.

[37] C. Cox, H. Chu, M. F. Schneider, and A. Muñoz. “Parametric survival analysis and taxonomy of hazard functions for the generalized gamma distribution”. In: *Statistics in Medicine* 26.23 (2007), pp. 4352–4374. ISSN: 0277-6715. DOI: 10.1002/sim.2836.

[38] G. Deligiannidis, A. Bouchard-Côté, and A. Doucet. “Exponential ergodicity of the bouncy particle sampler”. In: *The Annals of Statistics* 47.3 (2019), pp. 1268–1287. DOI: 10.1214/18-AOS1714.

[39] U. Dieckmann and R. Law. “The dynamical theory of coevolution: a derivation from stochastic ecological processes”. In: *J Math Biol* 34.5 (1996), pp. 579–612. ISSN: 14321416. DOI: 10.1007/bf02409751.

[40] W. Doeblin. “Éléments d’une théorie générale des chaînes simples constantes de Markoff”. fre. In: *Annales scientifiques de l’École Normale Supérieure* 57 (1940), pp. 61–111.

[41] S. Donnet and A. Samson. “Parametric inference for mixed models defined by stochastic differential equations”. In: *ESAIM: Probability and Statistics* 12 (2008), pp. 196–218. ISSN: 1292-8100. DOI: 10.1051/ps:2007045.

[42] M. Doumic. “Analysis of a population model structured by the cells molecular content”. In: *Math. Model. Nat. Phenom* 2 (2007), pp. 121–152. DOI: 10.1051/mmnp:2007006.

[43] M. Doumic and P. Gabriel. “Eigenelements of a general aggregation-fragmentation model”. In: *Mathematical Models and Methods in Applied Sciences* 20.05 (2010), pp. 757–783. DOI: 10.1142/S021820251000443X.

[44] M. Doumic, A. Olivier, and L. Robert. “Estimating the division rate from indirect measurements of single cells”. In: *Discrete and Continuous Dynamical Systems - B* 25.10 (2020), pp. 3931–3961. DOI: 10.3934/dcdsb.2020078.

[45] M. Doumic and B. van Brunt. “Explicit Solution and Fine Asymptotics for a Critical Growth-Fragmentation Equation”. In: *ESAIM: ProcS* 62 (2018), pp. 30–42. DOI: 10.1051/proc/201862030.

[46] M. Doumic and M. Hoffmann. “Individual and population approaches for calibrating division rates in population dynamics: Application to the bacterial cell cycle”. In: *Modeling and Simulation for Collective Dynamics*. World Scientific, 2023, pp. 1–81. DOI: 10.1142/13136.

[47] M. Doumic, M. Hoffmann, N. Krell, and L. Robert. “Statistical estimation of a growth-fragmentation model observed on a genealogical tree”. In: *Bernoulli* 21.3 (2015). ISSN: 1350-7265. DOI: 10.3150/14-BEJ623.

[48] D. Down, S. P. Meyn, and R. L. Tweedie. “Exponential and Uniform Ergodicity of Markov Processes”. In: *Ann. Probab.* 23.4 (1995), pp. 1671–1691. DOI: 10.1214/aop/1176987798.

[49] A. Ducrot and P. Magal. “Travelling wave solutions for an infection-age structured model with diffusion”. In: *Proceedings of the Royal Society of Edinburgh Section A: Mathematics* 139.3 (2009), pp. 459–482.

[50] M. Durinx and J. A. Metz. “Multi-type Branching Processes and Adaptive Dynamics of Structured Populations”. In: *Branching Processes*. Cambridge University Press, 2005. Chap. 7, pp. 266–277. DOI: 10.1017/CBO9780511629136.007.

[51] K.-J. Engel and R. Nagel. “One-parameter semigroups for linear evolution equations”. In: *Semigroup Forum* 63 (1999), pp. 278–280.

[52] P. Fearnhead, J. Bierkens, M. Pollock, and G. O. Roberts. “Piecewise Deterministic Markov Processes for Continuous-Time Monte Carlo”. In: *Statist. Sci.* 33.3 (2018), pp. 386–412. DOI: 10.1214/18-STS648.

[53] R. Ferriere and V. C. Tran. “Stochastic and deterministic models for age-structured populations with genetically variable traits”. In: *ESAIM: Proceedings*. Vol. 27. EDP Sciences. 2009, pp. 289–310.

[54] R. A. Fisher. “The wave of advance of advantageous genes”. In: *Annals of eugenics* 7.4 (1937), pp. 355–369.

[55] R. A. Fisher. *The genetical theory of natural selection*. Oxford: Clarendon Press, 1930. DOI: 10.5962/bhl.title.27468.

[56] C. Fonte and V. Schmutz. “Long time behavior of an age- and leaky memory-structured neuronal population equation”. In: *SIAM Journal on Mathematical Analysis* 54.4 (2022), pp. 4721–4756. DOI: 10.1137/21M1428571.

[57] N. Fournier and S. Méléard. “A microscopic probabilistic description of a locally regulated population and macroscopic approximations”. In: *Ann. Appl. Probab.* 14.4 (2004), pp. 1880–1919. DOI: 10.1214/105051604000000882.

[58] N. Friedman, S. Vardi, M. Ronen, U. Alon, and J. Stavans. “Precise temporal modulation in the response of the SOS DNA repair network in individual bacteria”. In: *PLoS Biology* 3.7 (2005), pp. 1261–1268. ISSN: 15457885. DOI: 10.1371/journal.pbio.0030238.

[59] C. Fritsch, F. Campillo, and O. Ovaskainen. “A numerical approach to determine mutant invasion fitness and evolutionary singular strategies”. In: *Theoretical Population Biology* 115 (2017), pp. 89–99. ISSN: 0040-5809. DOI: 10.1016/J.TPB.2017.05.001.

[60] N. Fétique. “Long-time behaviour of generalised Zig-Zag process”. In: *arXiv preprint arXiv:1710.01087* (2017). DOI: arXiv:1710.01087.

[61] P. Gabriel. “Measure solutions to the conservative renewal equation”. In: *ESAIM: ProcS* 62 (2018), pp. 68–78. DOI: 10.1051/proc/201862186206.

[62] P. Gabriel and H. Martin. “Steady distribution of the incremental model for bacteria proliferation”. In: *Networks and Heterogeneous Media*. Special issue on mathematical methods in systems biology 14.1 (Mar. 2019), pp. 149–171. DOI: 10.3934/nhm.2019008.

[63] J. Garnier, T. Giletti, F. Hamel, and L. Roques. “Inside dynamics of pulled and pushed fronts”. In: *Journal de Mathématiques Pures et Appliquées* 98.4 (2012), pp. 428–449.

[64] V Genon-Catalot. “Cours de statistique des diffusions”. In: *MSc. Lecture Notes, Université Paris Cité* (2012).

[65] M. Godin, F. F. Delgado, S. Son, W. H. Grover, A. K. Bryan, A. Tzur, P. Jorgensen, K. Payer, A. D. Grossman, M. W. Kirschner, and S. R. Manalis. “Using buoyant mass to measure the growth of single cells”. In: *Nature Methods* 7.5 (2010), pp. 387–390. ISSN: 15487091. DOI: 10.1038/nmeth.1452.

[66] A. Golubev. “Applications and implications of the exponentially modified gamma distribution as a model for time variabilities related to cell proliferation and gene expression”. In: *Journal of Theoretical Biology* 393 (2016), pp. 203–217. ISSN: 00225193. DOI: 10.1016/j.jtbi.2015.12.027.

[67] Q. Griette. “Singular measure traveling waves in an epidemiological model with continuous phenotypes”. In: *Transactions of the American Mathematical Society* 371.6 (2019), pp. 4411–4458.

[68] J. Guyon. “Limit theorems for bifurcating Markov chains. Application to the detection of cellular aging”. In: *The Annals of Applied Probability* 17.5-6 (2007). ISSN: 1050-5164. DOI: 10.1214/105051607000000195.

[69] M. Hairer and J. C. Mattingly. “Yet Another Look at Harris’ Ergodic Theorem for Markov Chains”. In: *Seminar on Stochastic Analysis, Random Fields and Applications VI. Progress in Probability*. Vol. 63. Springer, Basel, 2011. DOI: 10.1007/978-3-0348-0021-1_7.

[70] A. J. Hall, G. C. Wake, and P. W. Gandar. “Steady size distributions for cells in one-dimensional plant tissues”. In: *Journal of Mathematical Biology* 30 (1991), pp. 101–123. DOI: 10.1007/BF00160330.

[71] T. E. Harris. “The existence of stationary measures for certain Markov processes”. In: *Proceedings of the Third Berkeley Symposium on Mathematical Statistics and Probability*. Vol. 2. 1956, pp. 113–124.

[72] M. Hashimoto, T. Nozoe, H. Nakaoka, R. Okura, S. Akiyoshi, K. Kaneko, E. Kussell, and Y. Wakamoto. “Noise-driven growth rate gain in clonal cellular populations”. In: *Proceedings of the National Academy of Sciences* 113.12 (2016), pp. 3251–3256. ISSN: 0027-8424. DOI: 10.1073/pnas.1519412113.

[73] H. J. A. M. Heijmans. “The dynamical behaviour of the age-size-distribution of a cell population”. In: *The Dynamics of Physiologically Structured Populations*. Berlin, Heidelberg: Springer, 1986, pp. 185–202. DOI: 10.1007/978-3-662-13159-6_5.

[74] L. Hilbert, D. Albrecht, and M. C. Mackey. “Small delay, big waves: a minimal delayed negative feedback model captures Escherichia coli single cell SOS kinetics”. In: *Mol. BioSyst.* 7.9 (2011), pp. 2599–2607. ISSN: 1742-206X. DOI: 10.1039/C1MB05122A.

[75] K. L. Hillesland, G. J. Velicer, and R. E. Lenski. “Experimental evolution of a microbial predator’s ability to find prey”. In: *Proceedings of the Royal Society B: Biological Sciences* 276.1656 (2009), pp. 459–467.

[76] J. Hodgkin and D. Kaiser. “Genetics of Gliding Motility in Myxococcus Xanthus (Myxobacterales): Two Gene Systems Control Movement”. In: *Molecular and General Genetics MGG* (1979). https://doi.org/10.1007/bf00270004.

[77] M. Hoffmann and A. Marguet. “Statistical estimation in a randomly structured branching population”. In: *Stochastic Processes and their Applications* 129.12 (2019), pp. 5236–5277. ISSN: 03044149. DOI: 10.1016/j.spa.2019.02.015.

[78] M. Hoffmann and A. Olivier. “Nonparametric estimation of the division rate of an age dependent branching process”. In: *Stochastic Processes and their Applications* 126.5 (2016), pp. 1433–1471. ISSN: 03044149. DOI: 10.1016/j.spa.2015.11.009.

[79] P. Hougaard. “Frailty models for survival data”. In: *Lifetime data analysis* 1 (1995), pp. 255–273.

[80] N. Ikeda and S. Watanabe. *Stochastic Differential Equations and Diffusion Processes*. Ed. by North-Holland. 2nd ed. 1989, p. 555. ISBN: 9780444873781.

[81] C. Jackson. “flexsurv: A Platform for Parametric Survival Modeling in R”. In: *Journal of Statistical Software* 70.8 (2016), pp. 1–33. DOI: 10.18637/jss.v070.i08.

[82] S. Jaramillo-Riveri, J. Broughton, A. McVey, T. Pilizota, M. Scott, and M. El Karoui. “Growth-dependent heterogeneity in the DNA damage response in Escherichia coli”. In: *Molecular Systems Biology* 18.5 (2022), e10441. DOI: 10.15252/msb.202110441.

[83] E. C. Jones and S. Uphoff. "Single-molecule imaging of LexA degradation in Escherichia coli elucidates regulatory mechanisms and heterogeneity of the SOS response". In: *Nature Microbiology 2021 6:8* 6.8 (2021), pp. 981–990. ISSN: 2058-5276. DOI: 10.1038/s41564-021-00930-y.

[84] S. Jun, F. Si, R. Pugatch, and M. Scott. "Fundamental principles in bacterial physiology—history, recent progress, and the future with focus on cell size control: a review". In: *Reports on Progress in Physics* 81.5 (2018), p. 056601. ISSN: 0034-4885. DOI: 10.1088/1361-6633/aaa628.

[85] S. Jun and S. Taheri-Araghi. "Cell-size maintenance: Universal strategy revealed". In: *Trends in Microbiology* 23.1 (2015), pp. 4–6. ISSN: 18784380. DOI: 10.1016/j.tim.2014.12.001.

[86] D. C. Karasz, A. I. Weaver, D. H. Buckley, and R. C. Wilhelm. "Conditional filamentation as an adaptive trait of bacteria and its ecological significance in soils". In: *Environmental Microbiology* 24.1 (2022), pp. 1–17. ISSN: 1462-2912. DOI: 10.1111/1462-2920.15871.

[87] R. Keane and J. Berleman. "The predatory life cycle of Myxococcus xanthus". In: *Microbiology* 162.1 (2016), pp. 1–11.

[88] C. D. Kelly and O. Rahn. "The Growth Rate of Individual Bacterial Cells". In: *Journal of Bacteriology* 23.2 (1932), pp. 147–153. ISSN: 0021-9193. DOI: 10.1128/jb.23.2.147-153.1932.

[89] D. Kendall. "Les processus stochastiques de croissance en biologie". fr. In: *Annales de l'institut Henri Poincaré* 13.1 (1952), pp. 43–108.

[90] A. N. Kolmogorov, I. G. Petrovsky, and N. S. Piskunov. "A study of the equation of diffusion with increase in the quantity of matter, with application to a biological problem". In: *Bull. Moscow Univ. Sec. A (1)* 1 (1937), p. 1.

[91] I. Kontoyiannis and S. P. Meyn. "Large Deviations Asymptotics and the Spectral Theory of Multiplicatively Regular Markov Processes". In: *Electronic Journal of Probability* 10 (2005), pp. 61–123. DOI: 0.1214/EJP.v10-231.

[92] B. C. Kozuch, M. G. Shaffer, and M. J. Culyba. " The Parameter-Fitness Landscape of lexA Autoregulation in Escherichia coli ". In: *mSphere* 5.4 (2020). ISSN: 23795042. DOI: 10.1128/MSPHERE.00718-20/SUPPL_FILE/MSPHERE.00718-20-ST002.PDF.

[93] S. Krishna, S. Maslov, and K. Sneppen. "UV-Induced Mutagenesis in Escherichia coli SOS Response: A Quantitative Model". In: *PLOS Computational Biology* 3.3 (2007), e41. ISSN: 1553-7358. DOI: 10.1371/JOURNAL.PCBI.0030041.

[94] E. Kussell, R. Kishony, N. Q. Balaban, and S. Leibler. "Bacterial persistence: A model of survival in changing environments". In: *Genetics* 169.4 (2005), pp. 1807–1814. ISSN: 00166731. DOI: 10.1534/genetics.104.035352.

[95] E. Kussell and S. Leibler. "Phenotypic diversity, population growth, and information in fluctuating environments". In: *Science* 309.5743 (2005), pp. 2075–2078. ISSN: 00368075. DOI: 10.1126/SCIENCE.1114383/SUPPL_FILE/KUSSELL.SOM.PDF.

[96] V. Lagage and S. Uphoff. "Pulses and delays, anticipation and memory: seeing bacterial stress responses from a single-cell perspective". In: *FEMS Microbiology Reviews* 44.5 (2020), pp. 565–571. ISSN: 0168-6445. DOI: 10.1093/femsre/fuaa022.

[97] M. Lavielle. *Mixed Effects Models for the Population Approach*. Chapman and Hall/CRC, 2014. ISBN: 9781482226515. DOI: 10.1201/b17203.

[98] J. M. Lee. *Introduction to Smooth Manifolds*. Graduate Texts in Mathematics. Springer, 2003. DOI: 10.1007/978-1-4419-9982-5.

[99] J. T. Lennon, F. den Hollander, M. Wilke-Berenguer, and J. Blath. "Principles of seed banks and the emergence of complexity from dormancy". In: *Nature Communications* 12.1 (2021), p. 4807. ISSN: 2041-1723. DOI: 10.1038/s41467-021-24733-1.

[100] J. Lin and A. Amir. "From single-cell variability to population growth". In: *Physical Review E* 101.1 (2020), p. 012401. ISSN: 24700053. DOI: 10.1103/PhysRevE.101.012401.

[101] P. L. Lions. *Équations paraboliques et ergodicité*. 2014-2015.

[102] J. W. Little and D. W. Mount. *The SOS regulatory system of Escherichia coli*. 1982. DOI: 10.1016/0092-8674(82)90085-X.

[103] I. Madrid. "Exponential Ergodicity of a Degenerate Age-Size Piecewise Deterministic Process". In: *Acta Applicandae Mathematicae* 187.1 (2023), p. 5. ISSN: 0167-8019. DOI: 10.1007/s10440-023-00597-z.

[104] T. Malik and H. L. Smith. "Does dormancy increase fitness of bacterial populations in time-varying environments?" In: *Bulletin of Mathematical Biology* 70 (4 2008), pp. 1140–1162. DOI: 10.1007/s11538-008-9294-5.

[105] A. Marguet. "Uniform sampling in a structured branching population". In: *Bernoulli* 25.4A (2019), pp. 2649–2695. ISSN: 1350-7265. DOI: 10.3150/18-BEJ1066.

[106] M. J. McBride and D. R. Zusman. "Behavioral analysis of single cells of Myxococcus xanthus in response to prey cells of Escherichia coli". In: *FEMS microbiology letters* 137.2-3 (1996), pp. 227–231.

[107] H. Meinhardt and P. A. J. de Boer. "Pattern formation in Escherichia coli : A model for the pole-to-pole oscillations of Min proteins and the localization of the division site". In: *Proceedings of the National Academy of Sciences* 98.25 (2001), pp. 14202–14207. ISSN: 0027-8424. DOI: 10.1073/pnas.251216598.

[108] S. Méléard, M. Rera, and T. Roget. "A birth–death model of ageing: from individual-based dynamics to evolutive differential inclusions". In: *Journal of Mathematical Biology* 79.3 (2019), pp. 901–939. ISSN: 14321416. DOI: 10.1007/S00285-019-01382-Z/METRICS.

[109] J. A. Metz, R. M. Nisbet, and S. A. Geritz. "How should we define 'fitness' for general ecological scenarios?" In: *Trends Ecol Evol* 7.6 (1992), pp. 198–202. ISSN: 01695347. DOI: 10.1016/0169-5347(92)90073-k.

[110] A. Meunier, F. Cornet, and M. Campos. "Bacterial cell proliferation: from molecules to cells". In: *FEMS Microbiology Reviews* 45.1 (2021). ISSN: 1574-6976. DOI: 10.1093/femsre/fuaa046.

[111] S. P. Meyn and R. L. Tweedie. "Stability of Markovian Processes III: Foster-Lyapunov criteria for continuous-time processes". In: *Advances in Applied Probability* 25 (1993), pp. 518–548. DOI: 10.2307/1427522.

[112] S. P. Meyn and R. L. Tweedie. *Markov Chains and Stochastic Stability*. Second. Cambridge University Press, 2009. DOI: 10.1007/978-1-4471-3267-7.

[113] P. Michel. "Fitness optimization in a cell division model". In: *Comptes Rendus Mathematique* 341.12 (2005), pp. 731–736. ISSN: 1631073X. DOI: 10.1016/j.crma.2005.10.012.

[114] S. Mischler and J. Scher. "Spectral analysis of semigroups and growth-fragmentation equations". In: *Annales de l'Institut Henri Poincaré C, Analyse non linéaire* 33.3 (2016), pp. 849–898. ISSN: 0294-1449. DOI: 10.1016/J.ANIHPC.2015.01.007.

[115] N. Ojkic, E. Lilja, S. Direito, A. Dawson, R. J. Allen, and B. Waclaw. "A Roadblock-and-Kill Mechanism of Action Model for the DNA-Targeting Antibiotic Ciprofloxacin". In: *Antimicrobial Agents and Chemotherapy* 64.9 (2020). ISSN: 0066-4804. DOI: 10.1128/AAC.02487-19.

[116] J. Ollion, M. Elez, and L. Robert. "High-throughput detection and tracking of cells and intracellular spots in mother machine experiments". In: *Nature Protocols* 14.11 (2019), pp. 3144–3161. ISSN: 1754-2189. DOI: 10.1038/s41596-019-0216-9.

[117] M. Osella, E. Nugent, and M. C. Lagomarsino. "Concerted control of Escherichia coli cell division". In: *Proceedings of the National Academy of Sciences of the United States of America* 111.9 (2014), pp. 3431–3435. ISSN: 00278424. DOI: 10.1073/pnas.1313715111.

[118] S. Panigrahi, D. Murat, A. Le Gall, E. Martineau, K. Goldlust, J.-B. Fiche, S. Rombouts, M. Nöllmann, L. Espinosa, and T. Mignot. "Misic, a general deep learning-based method for the high-throughput cell segmentation of complex bacterial communities". In: *eLife* 10 (2021), e65151.

[119] B. Perthame. *Transport Equations in Biology*. Frontiers in Mathematics. Basel: Birkhäuser Basel, 2007. ISBN: 978-3-7643-7841-7. DOI: 10.1007/978-3-7643-7842-4.

[120] R. L. Prentice. "A Log Gamma Model and Its Maximum Likelihood Estimation". In: *Biometrika* 61.3 (1974), p. 539. ISSN: 00063444. DOI: 10.2307/2334737.

[121] S. Raghunathan, A. Chimthanawala, S. Krishna, A. G. Vecchiarelli, and A. Badrinarayanan. "Asymmetric chromosome segregation and cell division in DNA damage-induced bacterial filaments". In: *Molecular Biology of the Cell* 31 (26 Dec. 2020). Ed. by E. Goley, pp. 2920–2931. ISSN: 1059-1524. DOI: 10.1091/mbc.E20-08-0547.

[122] T. Roget. "On the long-time behaviour of age and trait structured population dynamics". In: *Discrete and Continuous Dynamical Systems - Series B* 24.6 (2017), pp. 2551–2576.

[123] S. Rombouts. "Advanced microscopies for the study of motility behavior in predating Myxococcus xanthus". PhD thesis. Sciences Chimiques et Biologiques pour la Santé, Montpellier, 2021.

[124] S. Rombouts, A. Mas, A. Le Gall, J.-B. Fiche, T. Mignot, and M. Nollmann. "Multiscale dynamic imaging reveals that cooperative motility behaviors promote efficient predation in bacteria". In: *Nature Communications* 14.1 (2023), p. 5588. ISSN: 2041-1723. DOI: 10.1038/s41467-023-41193-x.

[125] N. M. Sampaio, C. M. Blassick, V. Andreani, J. B. Lugagne, and M. J. Dunlop. "Dynamic gene expression and growth underlie cell-to-cell heterogeneity in Escherichia coli stress response". In: *Proceedings of the National Academy of Sciences of the United States of America* 119.14 (2022), e2115032119. ISSN: 10916490. DOI: 10.1073/PNAS.2115032119/SUPPL_FILE/PNAS.2115032119.SM05.MP4.

[126] D. Serbanescu, N. Ojkic, and S. Banerjee. "Cellular resource allocation strategies for cell size and shape control in bacteria". In: *The FEBS Journal* 289.24 (2022), pp. 7891–7906. ISSN: 1742-464X. DOI: 10.1111/febs.16234.

[127] J. A. Shapiro. "Thinking about Bacterial Populations as Multicellular Organisms". In: *Annual Review of Microbiology* 52 (1998), 81–104.

[128] Y. Shimoni, S. Altuvia, H. Margalit, and O. Biham. "Stochastic analysis of the SOS response in Escherichia coli". In: *PLoS ONE* 4.5 (2009). Ed. by M. Isalan, e5363. ISSN: 19326203. DOI: 10.1371/journal.pone.0005363.

[129] F. Si, G. Le Treut, J. T. Sauls, S. Vadia, P. A. Levin, and S. Jun. "Mechanistic Origin of Cell-Size Control and Homeostasis in Bacteria". In: *Current Biology* 29.11 (2019), 1760–1770.e7. ISSN: 09609822. DOI: 10.1016/j.cub.2019.04.062.

[130] O. K. Silander, N. Nikolic, A. Zaslaver, A. Bren, I. Kikoin, U. Alon, and M. Ackermann. "A genome-wide analysis of promoter-mediated phenotypic noise in Escherichia coli". In: *PLoS Genetics* 8.1 (2012). ISSN: 15537390. DOI: 10.1371/JOURNAL.PGEN.1002443.

[131] E. W. Stacy. "A Generalization of the Gamma Distribution". In: *The Annals of Mathematical Statistics* 33.3 (1962), pp. 1187–1192. ISSN: 0003-4851. DOI: 10.1214/aoms/1177704481.

[132] P. Szekely, H. Sheftel, A. Mayo, and U. Alon. "Evolutionary Tradeoffs between Economy and Effectiveness in Biological Homeostasis Systems". In: *PLoS Computational Biology* 9.8 (2013). Ed. by A. Rzhetsky, e1003163. ISSN: 1553-7358. DOI: 10.1371/journal.pcbi.1003163.

[133] S. Taheri-Araghi, S. Bradde, J. T. Sauls, N. S. Hill, P. A. Levin, J. Paulsson, M. Vergassola, and S. Jun. "Cell-size control and homeostasis in bacteria". In: *Current Biology* 25.3 (2015), pp. 385–391. ISSN: 09609822. DOI: 10.1016/j.cub.2014.12.009.

[134] C. Y. Tang and S. X. Chen. "Parameter estimation and bias correction for diffusion processes". In: *Journal of Econometrics* 149.1 (2009), pp. 65–81.

[135] T. M. Therneau and P. M. Grambsch. *Modeling Survival Data: Extending the Cox Model*. Statistics for Biology and Health. New York, NY: Springer New York, 2000. ISBN: 978-1-4419-3161-0. DOI: 10.1007/978-1-4757-3294-8.

[136] P. Thomas. "Analysis of Cell Size Homeostasis at the Single-Cell and Population Level". In: *Frontiers in Physics* 6 (2018). ISSN: 2296-424X. DOI: 10.3389/fphy.2018.00064.

[137] D. Thompson. *On Growth and Form*. On Growth and Form vol. 1. Cambridge University Press, 1942. ISBN: 0521066220.

[138] M. Tomašević, V. Bansaye, and A. Véber. "Ergodic behaviour of a multi-type growth-fragmentation process modelling the mycelial network of a filamentous fungus". In: *ESAIM: PS* 26 (2022), pp. 397–435. DOI: 10.1051/ps/2022013.

[139] N. Torres, B. Perthame, and D. Salort. "A multiple time renewal equation for neural assemblies with elapsed time model". In: *Nonlinearity* 35.10 (2022), p. 5051. DOI: 10.1088/1361-6544/ac8714.

[140] V. C. Tran. "Large population limit and time behaviour of a stochastic particle model describing an age-structured population". In: *ESAIM* 12 (2008), pp. 345–386. ISSN: 12928100. DOI: 10.1051/ps:2007052.

[141] J. H. Van Heerden, H. Kempe, A. Doerr, T. Maarleveld, N. Nordholt, and F. J. Bruggeman. "Statistics and simulation of growth of single bacterial cells: illustrations with B. subtilis and E. coli". In: *Scientific Reports 2017 7:1* 7.1 (2017), pp. 1–11. ISSN: 2045-2322. DOI: 10.1038/s41598-017-15895-4.

[142] P. Wang, L. Robert, J. Pelletier, W. L. Dang, F. Taddei, A. Wright, and S. Jun. "Robust growth of escherichia coli". In: *Current Biology* 20.12 (2010), pp. 1099–1103. ISSN: 09609822. DOI: 10.1016/j.cub.2010.04.045.

[143] G. Webb. *Theory of Nonlinear Age-Dependent Population Dynamics*. Chapman & Hall Pure and Applied Mathematics. Taylor & Francis, 1985. ISBN: 9780824772901.

[144] M. Wehrens, D. Ershov, R. Rozendaal, N. Walker, D. Schultz, R. Kishony, P. A. Levin, and S. J. Tans. "Size Laws and Division Ring Dynamics in Filamentous Escherichia coli cells". In: *Current Biology* 28.6 (2018), 972–979.e5. ISSN: 0960-9822. DOI: https://doi.org/10.1016/j.cub.2018.02.006.

[145] E. M. Witkin. “The radiation sensitivity of Escherichia coli B: a hypothesis relating filament formation and prophage induction.” In: *Proceedings of the National Academy of Sciences of the United States of America* 57.5 (1967), pp. 1275–1279. ISSN: 00278424. DOI: 10.1073/PNAS.57.5.1275/ASSET/82C97389-68CC-40A3-8163-4D1AED831613/ASSETS/PNAS.57.5.1275.FP.PNG.

[146] Y. Zhang, A. Ducret, J. Shaevitz, and T. Mignot. “From Individual Cell Motility to Collective Behaviors: Insights from a Prokaryote, Myxococcus Xanthus”. In: *FEMS Microbiology Reviews* 36.1 (2012), 149–64.

Appendix A

Construction and well-posedness of the measure-valued stochastic process Z_t

We consider the rigurous trajectorial construction of the measure-valued process Z_t described in Chapter 2, but extended to allow two discrete SOS types, as in Chapter 4. Although the model considered in Chapter 4 is structured in age only, and not within the adder framework, the construction gives us the foundations for future works considering multitype age-and-size structured populations.

We follow closely the approach of Tran [140] for age-structured populations, where the assumption of uniformly bounded division rates is made by the author. In our case however, the divison rate $\beta(a, y) = \lambda y B(a)$ is inherently unbounded, since it is at least linear in y.

A.1 Construction of the process

Let $\mathcal{X} = \{(a, y) : a \geq 0, a \leq y\}$ and $\tilde{\mathcal{X}} = \mathcal{X} \times \{0, 1\}$. The state of the structured population at any instant t is given by the point measure $Z_t \in \mathcal{M}_p(\tilde{\mathcal{X}})$

$$Z_t = \sum_{i=1}^{N_t} \delta_{\xi_i(t)} \tag{A.1}$$

where $N_t = \langle Z_t, 1 \rangle$ is the population size at time t, and each cell i is characterised by the vector $\xi_i(t) = (x_i(t), a_i(t), y_i(t)) \in \tilde{\mathcal{X}}$ where:

- $x_i(t) \in \{0, 1\}$ is the **SOS level** of cell i at time t.
- $a_i(t) \in \mathbb{R}_+$ is the **added size** from birth to current time t
- $y_i(t) \in \mathbb{R}_+$ is the **current size** at time t

We introduce the following functions which will parametrise the process:

- We consider the case of exponential growth $y'(t) = g(y(t)) = \lambda y(t)$. Let $\Phi_t : \tilde{\mathcal{X}} \to \tilde{\mathcal{X}}$ the deterministic flow associated to growth along some time t, as given by Eq. (2.2) and (2.3) (see Fig. 2.2):

$$\Phi_t(x, a, y) = (x, a + y\exp(\lambda t) - y, y\exp(\lambda t)) \tag{A.2}$$

- $B : \{0, 1\} \times \mathbb{R}_+ \to \mathbb{R}_+$ is the **adder division rate** which is a function of the added size a and the SOS type x:

$$B(x, a) = (1 - x)B_0(a) + xB_1(a), \tag{A.3}$$

  where B_0 is the low SOS adder division rate and B_1 is thigh SOS adder division rate.

- $d : \mathbb{R}_+ \times \{0, 1\} \times \mathbb{R}_+ \to \mathbb{R}_+$ is the **death rate** which is function of the antibiotic concentration, the SOS type and the current size. We let

$$d(c, x, y) = (1 - x)d_0(c) + xd_1(y), \tag{A.4}$$

  with d_0 the low SOS death rate, which depends on the antibiotic concentration c only, and d_1 the high SOS death rate, which depends on the cell size only.

- $\alpha(c) \geq 0$ is the switch rate from low SOS to high SOS type, which is function of the antibiotic concentration c.

- We call

$$\Gamma(c, x) = \Gamma(c, x, a, y) := (1 - x)\alpha(c) + \lambda y B(x, a) + d(c, x, y) \tag{A.5}$$

  the **individual cumulative rate**, which is the sum of the three individual rates of the independent events introduced above.

- $F_x : [0, 1] \to \mathbb{R}_+$ is the probability density function of the ratio between the size of the first daughter (which is always low SOS) and the size of the mother. It depends on the the SOS type x.

  For low SOS cells ($x = 0$), F_x is symmetrical with respect to $\frac{1}{2}$, such that $F_0(\rho) = F_0(1 - \rho)$.

The concentration of the antibiotic is fixed at c, and for now we will allow us to drop the variable c in the functions defined above.

We introduce some auxiliary variables to help the writing of the dynamics of Z_t.

Definition A.1.1. On a probability space $(\Omega, \mathcal{F}, \mathbb{P})$ large enough, let $\theta \sim Unif[0, 1]$, $\rho \sim F_0$, $\chi \sim F_1$, all mutually independent random variables and $\xi = (x, a, y)$ the traits of the individual chosen to be replaced. We define the following variables:

- $\mathcal{A}(\theta, x)$ is the replacement event which occurs:

$$\mathcal{A}(\theta,x) := \begin{cases} \text{switch} & \text{if } \theta \leq \frac{(1-x)\alpha}{\Gamma(\xi)} \\ \text{division} & \text{if } \frac{(1-x)\alpha}{\Gamma(\xi)} < \theta \leq \frac{(1-x)\alpha+\lambda y B(x,a)}{\Gamma(\xi)} \\ \text{death} & \text{if } \theta \geq \frac{(1-x)\alpha+\lambda y B(x,a)}{\Gamma(\xi)} \end{cases} \tag{A.6}$$

- $J(\mathcal{A})$ is the number of substitutes obtained in each replacement:

$$J(\mathcal{A}) := \begin{cases} 1 & \text{if } \mathcal{A} = \text{switch} \\ 2 & \text{if } \mathcal{A} = \text{division} \\ 0 & \text{if } \mathcal{A} = \text{death} \end{cases} \tag{A.7}$$

- $H_j^{\mathcal{A}}(x|\rho,\chi) \in \mathcal{X}$, for $1 \leq j \leq J(\mathcal{A})$, is a random vector with the traits of the j-th substitute among the $J(\mathcal{A})$ substitutes obtained when the chosen event is $\mathcal{A}$.

  For the switch we have:

$$H_1^{\text{switch}}(x,a,y|\rho,\chi) = (1-x,a,y) \tag{A.8}$$

  In the case of division:

$$H_1^{\text{division}}(x,a,y|\rho,\chi) = (0,0,((1-x)\rho + x\chi)\, y) \tag{A.9}$$
$$H_2^{\text{division}}(x,a,y|\rho,\chi) = (x,0,(1-((1-x)\rho + x\chi))\, y) \tag{A.10}$$

  where the first child is always low SOS ($x = 0$) and the second child inherit the type of its mother. Notice that if the mother is low SOS ($x = 0$) the ratio between the size of the first child and its mother is ρ which follow the distribution given by F_0. Otherwise, if the mother is high SOS ($x = 1$) the ratio is χ which is distributed according to F_1.

  Since $J(\text{death}) = 0$ we let H_1^{death} undefined, and use the convention $\sum_{j=1}^{0} H_j = 0$.

Definition A.1.2. Let $Y_t^i := Y_i(Z_t)$ where Y_i is the i-th coordinate of the projection

$$Y\left(\sum_{i=1}^{n} \delta_{(x_i,a_i,y_i)}\right) := (y_1, y_2, ..., y_n, 0, 0, ...) \tag{A.11}$$

where the particles are ordered with respect to a certain pre-established order $\preccurlyeq$ of $\tilde{\mathcal{X}}$ (e.g. lexicographical order or by vertical position when we include the variable h as in Chapter 2). And analogously let A_i, X_i be respectively the i-th coordinate (also under $\preccurlyeq$) of the projections

$$A\left(\sum_{i=1}^{n} \delta_{(x_i,a_i,y_i)}\right) := (a_1, a_2, ..., a_n, 0, 0, ...) \tag{A.12}$$

$$X\left(\sum_{i=1}^{n} \delta_{(x_i,a_i,y_i)}\right) := (x_1, x_2, ..., x_n, 0, 0, ...) \tag{A.13}$$

And let $X_t^i := X_i(Z_t)$, $A_t^i := A_i(Z_t)$. We define finally $\boldsymbol{\xi}_t^i = (X_t^i, A_t^i, Y_t^i)$.

We construct the process Z_t as follows

Definition A.1.3. On $(\Omega, \mathcal{F}, \mathbb{P})$ consider the definitions introduced above and

1. Let $\mathcal{E} = \mathbb{N}_* \times \mathbb{R}^+ \times [0,1]^2$ and $\mathcal{N}$ a Poisson point measure over $\mathbb{R}^+ \times \mathcal{E}$ with intensity $ds \otimes n(di) \otimes du \otimes d\theta \otimes F_0(\rho)d\rho \otimes F_1(\chi)d\chi$, where dx is the Lebesgue measure and n is the counting measure over $\mathbb{N}_*$.
2. Let $Z_0 \in \mathcal{M}_p\left(\tilde{\mathcal{X}}\right)$ such that

$$\mathbb{E}\left[\langle Z_0, 1\rangle\right] < \infty \qquad \mathbb{E}\left[\langle Z_0, Y\rangle\right] < \infty \tag{A.14}$$

We construct of $Z_t \in \mathcal{M}_p\left(\tilde{\mathcal{X}}\right)$ as the solution to the Stochastic Differential Equation (SDE)

$$\begin{aligned} Z_t = &\sum_{i=1}^{\langle Z_0,1\rangle} \delta_{\Phi_t(\boldsymbol{\xi}_0^i)} \\ &+ \int_0^t \int_{\mathcal{E}} \mathbb{1}_{\{i \le \langle Z_{s^-},1\rangle, u \le \Gamma(\boldsymbol{\xi}_{s^-}^i)\}} \left[\sum_{j=1}^{J(\mathcal{A}(\theta,\boldsymbol{\xi}_{s^-}^i))} \delta_{\Phi_{t-s} \circ H_j^{\mathcal{A}(\theta,\boldsymbol{\xi}_{s^-}^i)}(\boldsymbol{\xi}_{s^-}^i|\rho,\chi)} - \delta_{\Phi_{t-s}(\boldsymbol{\xi}_{s^-}^i)} \right] \\ &\mathcal{N}(ds, di, du, d\theta, d\rho, d\chi) \end{aligned} \tag{A.15}$$

The interpretation of Eq. (A.15) is as follows: the first term indicates that we let the initial population evolve until time t according to the deterministic dynamics Φ_t which are given by the growth dynamics. Then, if at time $s < t$ a jump event occurs for the individual i, we remove it from the remaining time $t - s$ (term $-\delta_{\Phi_{t-s}(\boldsymbol{\xi}_s^i)}$) and we add the eventual substitutes, which evolve deterministically for the remaining time $t-s$, until the next jump. Remark that the process thus constructed is Markovian. Moreover, in Proposition A.1.7 and in the subsequent Eq. (A.47) we show that the infinitesimal generator of Z_t captures the desired dynamics.

Definition A.1.4. Let $R \in \mathbb{R}_+$ and Z_t defined by (A.15) . For every $t \ge 0$ we define the total number N_t and the total mass M_t of the population as

$$N_t = \langle Z_t, 1\rangle \tag{A.16}$$

$$M_t = \langle Z_t, Y\rangle = \int_{\tilde{\mathcal{X}}} y Z_t(dx, da, dy) \tag{A.17}$$

Since for any $t \ge 0$ these quantities are finite but unbounded we introduce the stopping time

$$\tau_R = \inf\{t \ge 0 : N_t \vee M_t \ge R\} \tag{A.18}$$

The next proposition gives the dynamics of a test function applied to population.

Proposition A.1.5. *For any test function $f \in C_b^{0,0,1,1}(\tilde{\mathcal{X}})$, Z_t defined by (A.15) solves the SDE*

$$\begin{aligned}\langle Z_t, f\rangle = \langle Z_0, f\rangle &+ \int_0^t \Big\langle Z_{s^-}, g\cdot(\partial_a f + \partial_y f)\Big\rangle ds \\ &+ \int_0^t \int_{\mathcal{E}} \mathbb{1}_{\{i\le \langle Z_{s^-},1\rangle, u\le \Gamma(\boldsymbol{\xi}^i_{s^-})\}} \left[\sum_{j=1}^{J(\mathcal{A}(\theta,\boldsymbol{\xi}^i_{s^-}))} f\left(H_j^{\mathcal{A}(\theta,\boldsymbol{\xi}^i_{s^-})}\left(\boldsymbol{\xi}^i_{s^-}|\rho,\chi\right)\right) - f\left(\boldsymbol{\xi}^i_{s^-}\right)\right] \\ &\qquad \mathcal{N}(ds,di,du,d\theta,d\rho,d\chi)\end{aligned} \tag{A.19}$$

Proof. Let $f \in C_b^{0,0,1,1}(\tilde{\mathcal{X}})$. Applying Z_t defined by (A.15) to f gives directly:

$$\begin{aligned}\langle Z_t, f\rangle = &\sum_{i=1}^{\langle Z_0,1\rangle} f\left(\Phi_t(\boldsymbol{\xi}^i_0)\right) \\ &+ \int_0^t \int_{\mathcal{E}} \mathbb{1}_{\{i\le \langle Z_{s^-},1\rangle, u\le \Gamma(\boldsymbol{\xi}^i_{s^-})\}} \left[\sum_{j=1}^{J(\mathcal{A}(\theta,\boldsymbol{\xi}^i_{s^-}))} f\left(\Phi_{t-s}\circ H_j^{\mathcal{A}(\theta,\boldsymbol{\xi}^i_{s^-})}\left(\boldsymbol{\xi}^i_{s^-}|\rho,\chi\right)\right)\right. \\ &\left. - f\left(\Phi_{t-s}\left(\boldsymbol{\xi}^i_{s^-}\right)\right)\right] \mathcal{N}(ds,di,du,d\theta,d\rho,d\chi)\end{aligned} \tag{A.20}$$

Since the growth is given by the deterministic dynamics (A.2), recalling that $a'(t) = y'(t)$, the Fundamental Theorem of Calculus gives for any $t \ge 0$:

$$\begin{aligned} f\circ\Phi_t(x,a,y) &= f(x,a,y) + \int_0^t \frac{d}{du} f\circ\Phi_u(x,a,y)\,du \\ &= f(x,a,y) + \int_0^t g(y(u))\left(\partial_a f\left(x,a(u),y(u)\right) + \partial_y f\left(x,a(u),y(u)\right)\right) du \\ &= f(x,a,y) + \int_0^t \left(g\cdot(\partial_a+\partial_y) f\right)\circ\Phi_u(x,a,y)du \end{aligned} \tag{A.21}$$

Moreover after a simple substitution we get

$$f\circ\Phi_{t-r}(x,a,y) = f(x,a,y) + \int_r^t \left(g\cdot(\partial_a+\partial_y) f\right)\circ\Phi_{u-r}(x,a,y)du \tag{A.22}$$

Applying it to (A.20) we obtain

$$\begin{aligned}\langle Z_t, f\rangle = &\sum_{i=1}^{\langle Z_0,1\rangle} f\left(\boldsymbol{\xi}^i_0\right) + I_1 + I_2 \\ &+ \int_0^t \int_{\mathcal{E}} \mathbb{1}_{\{i\le \langle Z_{s^-},1\rangle, u\le \Gamma(\boldsymbol{\xi}^i_{s^-})\}} \left[\sum_{j=1}^{J(\mathcal{A}(\theta,\boldsymbol{\xi}^i_{s^-}))} f\left(H_j^{\mathcal{A}(\theta,\boldsymbol{\xi}^i_{s^-})}\left(\boldsymbol{\xi}^i_{s^-}|\rho,\chi\right)\right) - f\left(\boldsymbol{\xi}^i_{s^-}\right)\right] \\ &\mathcal{N}(ds,di,du,d\theta,d\rho,d\chi)\end{aligned} \tag{A.23}$$

where

$$I_1 = \sum_{i=1}^{\langle Z_0,1\rangle} \int_s^t \lambda Y_0^i e^{\lambda s} \cdot (\partial_a + \partial_y) \left(f \circ \Phi_s(\boldsymbol{\xi}_0^i)\right) ds \tag{A.24}$$

and

$$\begin{aligned} I_2 = \int_0^t \int_{\mathcal{E}} \mathbb{1}_{\{i \le \langle Z_{s^-},1\rangle, u \le \Gamma(\boldsymbol{\xi}_{s^-}^i)\}} \Bigg[& \\ \sum_{j=1}^{J(\mathcal{A}(\theta,\boldsymbol{\xi}_{s^-}^i))} & \int_s^t \lambda Y_s^i e^{\lambda(r-s)} \cdot (\partial_a + \partial_y) \left(f \circ \Phi_{r-s} \left(H_j^{\mathcal{A}(\theta,\boldsymbol{\xi}_{s^-}^i)} \left(\boldsymbol{\xi}_{s^-}^i | \rho, \chi\right)\right)\right) dr \\ - \int_s^t & \lambda Y_s^i e^{\lambda(r-s)} \cdot (\partial_a + \partial_y) \left(f \circ \Phi_{r-s}(\boldsymbol{\xi}_{s^-}^i)\right) dr \Bigg] \mathcal{N}(ds, di, du, d\theta, d\rho, d\chi) \end{aligned} \tag{A.25}$$

Since $\partial_a f$ and $\partial_y f$ are bounded, applying Fubini-Tonnelli Theorem on I_2 we have

$$\begin{aligned} I_2 = \int_0^t \int_0^r \int_{\mathcal{E}} \mathbb{1}_{\{i \le \langle Z_{s^-},1\rangle, u \le \Gamma(\boldsymbol{\xi}_{s^-}^i)\}} \Bigg[& \\ \sum_{j=1}^{J(\mathcal{A}(\theta,\boldsymbol{\xi}_{s^-}^i))} & \lambda Y_s^i e^{\lambda(r-s)} \cdot (\partial_a + \partial_y) \left(f \circ \Phi_{r-s} \left(H_j^{\mathcal{A}(\theta,\boldsymbol{\xi}_{s^-}^i)} \left(\boldsymbol{\xi}_{s^-}^i | \rho, \chi\right)\right)\right) \\ - \lambda Y_s^i & e^{\lambda(r-s)} \cdot (\partial_a + \partial_y) \left(f \circ \Phi_{r-s}(\boldsymbol{\xi}_{s^-}^i)\right) \Bigg] \mathcal{N}(ds, di, du, d\theta, d\rho, d\chi) dr \end{aligned} \tag{A.26}$$

Therefore

$$\begin{aligned} I_1 + I_2 = \int_0^t \Bigg\{ \sum_{i=1}^{\langle Z_0,1\rangle} & (g \cdot (\partial_a f + \partial_y f)) \circ \Phi_r(\boldsymbol{\xi}_0^i) dr + \int_0^r \int_{\mathcal{E}} \mathbb{1}_{\{i \le \langle Z_{s^-},1\rangle, u \le \Gamma(\boldsymbol{\xi}_{s^-}^i)\}} \Bigg[\\ \sum_{j=1}^{J(\mathcal{A}(\theta,\boldsymbol{\xi}_{s^-}^i))} & (g \cdot (\partial_a f + \partial_y f)) \circ \Phi_{r-s} \left(H_j^{\mathcal{A}(\theta,\boldsymbol{\xi}_{s^-}^i)} \left(\boldsymbol{\xi}_{s^-}^i | \rho, \chi\right)\right) \\ - (g \cdot (\partial_a f + \partial_y f)) & \circ \Phi_{r-s}(\boldsymbol{\xi}_{s^-}^i) \Bigg] \mathcal{N}(ds, di, du, d\theta, d\rho, d\chi) \Bigg\} dr \\ = \int_0^t \Big\langle Z_r, g \cdot (\partial_a f + \partial_y f) \Big\rangle dr & \end{aligned} \tag{A.27}$$

where in the last line we identified Z_t applied to function $g \cdot (\partial_a f + \partial_y f)$ as defined by (A.20). Finally, replacing (A.27) in (A.23) gives the result. □

A.1.1 Existence and uniqueness of Z_t

Let consider the following control hypothesis on the division and death rates:

(B1) There is a positive constant $\bar{b}$ such that $B_r(a) \leq \bar{b}$ for both $s \in \{0,1\}$ and every $a \geq 0$;

(B2) There is a positive constant c such that $d_r(y) \leq c(1+y)$ for both $s \in \{0,1\}$ and every $y \geq 0$.

Proposition A.1.6. *If (B1), (B2) and (A.14) are verified, then the SDE has a well-defined solution* $(Z_t)_{t\geq 0} \in \mathbb{D}\left(\mathbb{R}_+, \mathcal{M}_p\left(\tilde{\mathcal{X}}\right)\right)$ *which verifies for every* $T > 0$

$$\mathbb{E}\left[\sup_{s\in[0,T]} \langle Z_s, 1\rangle + \langle Z_s, Y\rangle\right] \leq \mathbb{E}\left[\langle Z_0, 1\rangle + \langle Z_0, Y\rangle\right] \exp\left(\lambda(\bar{b}+1)T\right) < \infty \tag{A.28}$$

Proof. Let $X > 0$. We can almost surely construct algorithmically a solution $(Z_t)_{t\geq 0}$ to (A.15), by means of the procedure detailled in Section A.2 until the stopping time τ_X defined by (A.18). Now, we check that the sequence of jump instants $(T_k)_{k\in\mathbb{N}}$ goes to $+\infty$ a.s. as $k \to \infty$. Consider the stopped process $\bar{Z}_t = Z_{t\wedge\tau_X}$. By (A.19) applied to $f \equiv 1$ we have:

$$\langle \bar{Z}_t, 1\rangle = \langle \bar{Z}_0, 1\rangle + \int_0^t \int_{\mathcal{E}_1} \mathbb{1}_{\{i\leq \langle \bar{Z}_{s^-}, 1\rangle, u\leq \Gamma(\boldsymbol{\xi}^i_{s^-})\}} \left[J(\mathcal{A}(\theta, \boldsymbol{\xi}^i_{s^-})) - 1\right] \mathcal{N}(ds, di, du, d\theta) \tag{A.29}$$

$$\leq \langle \bar{Z}_0, 1\rangle + \int_0^t \int_{\mathcal{E}_0} \mathbb{1}_{\{i\leq \langle \bar{Z}_{s^-}, 1\rangle, u\leq \lambda Y^i_{s^-} B(R^i_{s^-}, A^i_{s^-})\}} \mathcal{N}(ds, di, du) \tag{A.30}$$

where $\mathcal{E}_0 = \mathbb{N}_* \times \mathbb{R}^+$ and $\mathcal{E}_1 = \mathcal{E}_0 \times [0,1]$. The last inequality is obtained thanks to $J(\mathcal{A}) > 1$ only for the division event, and the measures $F_0(\rho)d\rho$, $F_1(\chi)d\chi$, and $d\theta$ are all probability measures. Then, taking expectation we get

$$\mathbb{E}\left[\sup_{s\in[0,t\wedge\tau_X]} \langle \bar{Z}_s, 1\rangle\right] \leq \mathbb{E}\left[\langle \bar{Z}_0, 1\rangle\right] + \int_0^t \mathbb{E}\left[\sup_{u\in[0,s\wedge\tau_X]} \sum_{i=1}^{\langle \bar{Z}_u, 1\rangle} \lambda Y_i B_{x_i}(A_i)\right] ds \tag{A.31}$$

$$\leq \mathbb{E}\left[\langle \bar{Z}_0, 1\rangle\right] + \lambda\bar{b} \int_0^t \mathbb{E}\left[\sup_{u\in[0,s\wedge\tau_X]} \sum_{i=1}^{\langle \bar{Z}_u, 1\rangle} Y_i\right] ds \tag{A.32}$$

Moreover, now applying (A.19) to $Y(x,a,y) = y$ we have

$$\langle \bar{Z}_t, Y\rangle = \langle \bar{Z}_0, Y\rangle + \int_0^t \langle \bar{Z}_s, \lambda y\rangle\, ds - \int_0^t \int_{\mathcal{E}_0} \mathbb{1}_{\{i\leq \langle \bar{Z}_{s^-}, 1\rangle, u\leq d(X^i_{s^-}, Y^i_{s^-})\}} Y^i_{s^-} \mathcal{N}(ds, di, du) \tag{A.33}$$

Deprecating the negative term and taking expectation we obtain

$$\mathbb{E}\left[\sup_{s\in[0,t\wedge\tau_X]} \langle \bar{Z}_s, Y\rangle\right] \leq \mathbb{E}\left[\langle \bar{Z}_0, Y\rangle\right] + \lambda \int_0^t \mathbb{E}\left[\sup_{u\in[0,s\wedge\tau_X]} \langle \bar{Z}_u, Y\rangle\right] ds \tag{A.34}$$

Thus, adding (A.32) and (A.34) we obtain

$$\mathbb{E}\left[\sup_{s\in[0,t\wedge\tau_X]}\langle\bar{Z}_s,1\rangle+\langle\bar{Z}_s,Y\rangle\right]\leq\mathbb{E}\left[\langle\bar{Z}_0,1\rangle+\langle\bar{Z}_0,Y\rangle\right]+\lambda(\bar{b}+1)\int_0^t\mathbb{E}\left[\sup_{u\in[0,s\wedge\tau_X]}\langle\bar{Z}_u,Y\rangle\right]ds \tag{A.35}$$

Therefore, by Grönwall Lemma, for all $T<\infty$ we get

$$\mathbb{E}\left[\sup_{s\in[0,T\wedge\tau_X]}\langle\bar{Z}_s,1\rangle+\langle\bar{Z}_s,Y\rangle\right]\leq\mathbb{E}\left[\langle\bar{Z}_0,1\rangle+\langle\bar{Z}_0,Y\rangle\right]\exp\left(\lambda(\bar{b}+1)T\right)<\infty \tag{A.36}$$

In particular we deduce that $\tau_X\to\infty$ a.s. as $X\to\infty$. Indeed, suppose the contrary. In this case, one may find $T_0<\infty$ such that $\mathbb{P}\left(\sup_X\tau_X<T_0\right)=\varepsilon>0$. However, this implies $\mathbb{E}\left[\sup_{s\in[0,T_0\wedge\tau_X]}\langle\bar{Z}_s,1\rangle+\langle\bar{Z}_s,Y\rangle\right]\geq 2\varepsilon X$ for every X which contradicts (A.36), since the RHS couldn't be bounded independently to X.

Now, we can make $X\to\infty$ with the Fatou Lemma to obtain the bound (A.28):

$$\mathbb{E}\left[\liminf_{X\to\infty}\sup_{s\in[0,t\wedge\tau_X]}\langle\bar{Z}_s,1\rangle+\langle\bar{Z}_s,Y\rangle\right]\leq\liminf_{X\to\infty}\mathbb{E}\left[\sup_{s\in[0,t\wedge\tau_X]}\langle\bar{Z}_s,1\rangle+\langle\bar{Z}_s,Y\rangle\right] \tag{A.37}$$

$$\leq\mathbb{E}\left[\langle\bar{Z}_0,1\rangle+\langle\bar{Z}_0,Y\rangle\right]\exp\left(\lambda(\bar{b}+1)t\right)<\infty \tag{A.38}$$

Finally, we deduce that also $T_k\to+\infty$ a.s. As before, we show it by an absurd argument. Suppose that we may find $T_0<\infty$ such that $\mathbb{P}\left(\sup_k T_k<T_0\right)>0$. Now, suppose that this implies $\mathbb{P}\left(\lim_{k\to\infty}\langle Z_{T_k},1\rangle\vee\langle Z_{T_k},Y\rangle=+\infty\right)>0$. In that case, for every $X>0$ we should have $\tau_X\leq T_0$ which contradicts $\tau_x\to\infty$ a.s. as proven above. So, let's prove now that under the absurd assumption we have indeed $\mathbb{P}\left(\lim_{k\to\infty}\langle Z_{T_k},1\rangle\vee\langle Z_{T_k},Y\rangle=+\infty\right)>0$. Suppose it's not true. Then, we should have $X'>0$ such that $\mathbb{P}\left(\sup_k\langle Z_{T_k},1\rangle\vee\langle Z_{T_k},Y\rangle<X'\right)>0$. Thus, we can construct the sequence $(T_k)_k$ as a subsequence of the jumping times of a homogeneous Poisson process with intensity $\bar{\Gamma}=\alpha+\lambda\bar{b}X'+c(1+X')$ by an acceptance-rejection method. But this should give $\lim_k T_k=+\infty$ a.s., which is absurd if $\mathbb{P}\left(\sup_k T_k<T_0\right)>0$.

□

A.1.2 Infinitesimal generator and martingale problem

Proposition A.1.7. *Let $\nu\in\mathcal{M}_p(\tilde{\mathcal{X}})$ deterministic such that*

$$\langle\nu,1\rangle=N_0<\infty \tag{A.39}$$

$$\langle\nu,Y\rangle=M_0<\infty \tag{A.40}$$

Then, the process defined by (A.15) with initial condition $Z_0 = \nu$ is a Markovian process with infinitesimal generator given by : for any $U \in C_b^1(\mathbb{R})$ and $f \in C_b^{0,0,1,1}(\tilde{\mathcal{X}})$:

$$\begin{aligned}\mathcal{Q}U_f(\nu) = U'(\langle \nu, f\rangle)\langle \nu, g\cdot(\partial_a f + \partial_y f)\rangle + \\ \int_{\tilde{\mathcal{X}}} \Big\{ (1-r)\alpha \left[U\left(\langle \nu, f\rangle - f(x,a,y) + f(1-x,a,y)\right) - U\left(\langle \nu, f\rangle\right)\right] \\ + \int_0^1 \lambda y B(x,a) F_x(\rho)[U(\langle \nu, f\rangle - f(x,a,y) \\ + f(0,0,\rho y) + f(x,0,(1-\rho)y)) - U\left(\langle \nu, f\rangle\right)]\, d\rho \\ + d(x,y)\left[U\left(\langle \nu, f\rangle - f(x,a,y)\right) - U\left(\langle \nu, f\rangle\right)\right] \Big\} \nu(dx,da,dy)\end{aligned} \tag{A.41}$$

where we have defined $U_f(Z) := U(\langle Z, f\rangle)$. In particular the law of $(Z_t)_{t\geq 0}$ does not depend on the chosen order $\preccurlyeq$.

Proof. Let $U \in C_b^1(\mathbb{R})$ and $f \in C_b^{0,1,1}(\tilde{\mathcal{X}})$. Let $X \in \mathbb{R}_+$ such that $X > N_0 \vee M_0$ and consider the stopped process $Z_{t\wedge\tau_X}$ with τ_X introduced by (A.18). Applying Itô's formula with jumps [80] to (A.19) we get:

$$\begin{aligned}U_f(Z_{t\wedge\tau_X}) &:= U\left(\langle Z_{t\wedge\tau_X}, f\rangle\right) \\ &= U(\langle Z_0, f\rangle) + \int_0^{t\wedge\tau_X} U'(\langle Z_s, f\rangle)\langle Z_s, g\cdot(\partial_a f + \partial_y f)\rangle ds \\ &+ \int_0^t \int_{\mathcal{E}} \mathbb{1}_{\{i\leq\langle Z_s,1\rangle, u\leq\Gamma(\boldsymbol{\xi}_s^i)\}} \Bigg[U\left(\langle Z_s, f\rangle - f(\boldsymbol{\xi}_s^i) + \sum_{j=1}^{J(\mathcal{A}(\theta,\boldsymbol{\xi}_s^i))} f\left(H_j^{\mathcal{A}(\theta,\boldsymbol{\xi}_s^i)}\left(\boldsymbol{\xi}_s^i|\rho,\chi\right)\right)\right) \\ &\quad - U\left(\langle Z_s, f\rangle\right)\Bigg] \mathcal{N}(ds,di,du,d\theta,d\rho,d\chi)\end{aligned} \tag{A.42}$$

Then

$$\begin{aligned}\mathbb{E}_\nu\left[U_f(Z_{t\wedge\tau_X})\right] &= \langle \nu, f\rangle + \mathbb{E}_\nu\left[\int_0^{t\wedge\tau_X} U'(\langle Z_s, f\rangle)\langle Z_s, g\cdot(\partial_a f + \partial_y f)\rangle ds\right] \\ &\quad + \mathbb{E}_\nu\Bigg[\int_0^{t\wedge\tau_X}\int_{\mathcal{E}} \mathbb{1}_{\{i\leq\langle Z_s,1\rangle, u\leq\Gamma(\boldsymbol{\xi}_s^i)\}} \Bigg\{ U\Bigg(\langle Z_s, f\rangle - f(\boldsymbol{\xi}_s^i) \\ &\quad + \sum_{j=1}^{J(\mathcal{A}(\theta,\boldsymbol{\xi}_s^i))} f\left(H_j^{\mathcal{A}(\theta,\boldsymbol{\xi}_s^i)}\left(\boldsymbol{\xi}_s^i|\rho,\chi\right)\right)\Bigg) - U\left(\langle Z_s, f\rangle\right)\Bigg\} \\ &\quad \mathcal{N}(ds,di,du,d\theta,d\rho,d\chi)\Bigg] \\ &= \langle \nu, f\rangle + \mathbb{E}_\nu\left[\int_0^{t\wedge\tau_X} \psi_{U_f}(s,Z) ds\right]\end{aligned} \tag{A.43}$$

where

$$\begin{aligned}\psi_{U_f}(s,Z) = U'(\langle Z_s,f\rangle)\langle Z_s, g\cdot(\partial_a f+\partial_y f)\rangle+\\ \int_{\tilde{\mathcal{X}}}\int_{[0,1]^2}\Big\{(1-x)\alpha\left[U\left(\langle Z_s,f\rangle - f(x,a,y)+f(1-x,a,y)\right)-U\left(\langle Z_s,f\rangle\right)\right]\\ +\lambda y B(x,a)[U(\langle Z_s,f\rangle - f(x,a,y)+f(0,0,((1-x)\rho+x\chi)y)\\ \quad + f(x,0,(1-((1-x)\rho+x\chi))y))-U\left(\langle Z_s,f\rangle\right)]\\ +d(x,y)\left[U\left(\langle Z_s,f\rangle - f(x,a,y)\right)-U\left(\langle Z_s,f\rangle\right)\right]\Big\}F_0(\rho)F_1(\chi)\\ d\rho\, d\chi\;\; Z_s(dr,da,dy)\end{aligned} \tag{A.44}$$

Since F_0, F_1, G are probability distributions the previous expression simplifies into

$$\begin{aligned}\psi_{U_f}(s,Z) = U'(\langle Z_s,f\rangle)\langle Z_s, g\cdot(\partial_a f+\partial_y f)\rangle+\\ \int_{\tilde{\mathcal{X}}}\Big\{(1-x)\alpha\left[U\left(\langle Z_s,f\rangle - f(x,a,y)+f(1-x,a,y)\right)-U\left(\langle Z_s,f\rangle\right)\right]\\ +\int_0^1 \lambda y B(x,a)F_x(\rho)[U(\langle Z_s,f\rangle - f(x,a,y)\\ \quad + f(0,0,\rho y)+f(x,0,(1-\rho)y))-U\left(\langle Z_s,f\rangle\right)]\,d\rho\\ +d(x,y)\left[U\left(\langle Z_s,f\rangle - f(x,a,y)\right)-U\left(\langle Z_r,f\rangle\right)\right]\Big\}\,Z_s(dr,da,dy)\end{aligned} \tag{A.45}$$

Now, we want to calculate

$$\mathcal{Q}U_f(\nu) = \frac{\partial}{\partial t}\mathbb{E}_\nu\left[U_f(Z_t)\right]\Big|_{t=0} = \frac{\partial}{\partial t}\mathbb{E}_\nu\left[\int_0^t \psi_{U_f}(s,Z)ds\right]\Big|_{t=0}$$

Let $T>0$ and consider the application $\Psi_\nu : [0,T]\ni t\mapsto \int_0^{t\wedge\tau_X}\psi_{U_f}(s,\nu)ds$. Since, by Hyp. (B1) and (B2) we have

i. $\Psi_v(t)\le TX\left(\lambda X||(\partial_a f+\partial_y f)||_\infty||U'||_\infty+(\alpha+\lambda\bar{b}X+c(1+X))||U||_\infty\right)<+\infty$ a.s.

ii. Since $\tau_X>0$ a.s. and ν is a right-continuous measure, $\Psi_v(t)$ is a.s. differentiable at $t=0$ with derivative:
$$\frac{\partial}{\partial t}\Psi_\nu(0)=\psi_{U_f}(0,\nu)$$
given by (A.45) evaluated in $r=0$, $Z=\nu$.

iii. Moreover, since ν verifies (A.39) and (A.40), $\psi_{U_f}(0,\nu)$ is a.s. dominated by
$$\lambda M_0 N_0||(\partial_a f+\partial_y f)||_\infty||U'||_\infty+N_0(\alpha+\lambda\bar{B}M_0+c(1+M_0))||U||_\infty<+\infty$$

So, by the dominated convergence theorem, the application $t \mapsto \mathbb{E}_\nu [\Psi_\nu(t)]$ is differentiable in $t = 0$, and the derivative commutes with the expectation, obtaining

$$\mathcal{Q}U_f(\nu) = \mathbb{E}[\partial_t \Psi_\nu(0)] = \psi_{U_f}(0, \nu) \tag{A.46}$$

which gives indeed the infinitesimal generator of (A.41).

□

In particular if we take $U = Id$ the identity function in (A.41) we obtain

$$\begin{aligned}
\mathcal{Q}\langle \nu, f\rangle = \int_{\tilde{\mathcal{X}}} \Big\{ & \lambda y (\partial_a + \partial_y) f(x,a,y) + (1-x)\alpha [f(1-x,a,y) - f(x,a,y)] \\
& + \int_0^1 \lambda y B_x(a) F_x(\rho) [f(0,0,\rho y) + f(x,0,(1-\rho)y) - f(x,a,y)] d\rho \\
& - d(x,y) f(x,a,y) \Big\} \nu(dx,da,dy) \\
= & \int_{\tilde{\mathcal{X}}} \mathcal{Q} f(x) \nu(dx)
\end{aligned} \tag{A.47}$$

This expression evinces that the process defined by (A.15) follows the Markovian dynamics we are interested in. The first term captures the deterministic growth, and the summands of the integral capture the effect of SOS type switching, cell division and death, respectively.

Proposition A.1.8. *Let $Z_0 \in \mathcal{M}_p(\tilde{\mathcal{X}})$ such that $\mathbb{E}[\langle Z_0, 1\rangle] < +\infty$ and $\mathbb{E}[\langle Z_0, Y\rangle] < +\infty$. Then for every $f \in C_b^{0,0,1,1}(\tilde{\mathcal{X}})$ we have that*

$$\left(M_t^f\right)_{t\geq 0} := \left(\langle Z_t, f\rangle - \langle Z_0, f\rangle - \int_0^t \langle Z_s, \mathcal{Q} f\rangle \, ds\right)_{t\geq 0} \tag{A.48}$$

is a square-integrable càdlàg martingale with zero expectation, with $\mathcal{Q}$ defined by (A.47), and whose quadratic variation is

$$\begin{aligned}
\langle M^f \rangle_t = \int_0^t \int_{\tilde{\mathcal{X}}} \Big\{ & (1-x)\alpha [f(1-x,a,y) - f(x,a,y)]^2 \\
& + \int_0^1 \lambda y B_x(a) F_x(\rho) [f(0,0,\rho y) + f(x,0,(1-\rho)y) - f(x,a,y)]^2 d\rho \\
& + d(x,y) f^2(x,a,y) \Big\} Z_s(dr,da,dy) ds
\end{aligned} \tag{A.49}$$

Proof. Starting from (A.19), and introducing the compensated Poisson punctual measure $\tilde{\mathcal{N}}$ associated to $\mathcal{N}$ we have:

$$\begin{aligned}\langle Z_t, f\rangle = \langle Z_0, f\rangle + M_t^f + \int_0^t \int_{\tilde{\mathcal{X}}} g(\xi)\left(\partial_a f(\xi) + \partial_y f(\xi)\right) Z_s(d\xi)ds \\ + \int_0^t \int_{\tilde{\mathcal{X}}} \int_{[0,1]^3} \Gamma(\xi) \left[\sum_{j=1}^{J(\mathcal{A}(\theta,\xi))} f\left(H_j^{\mathcal{A}(\theta,\xi)}(x|\rho,\chi)\right) - f(\xi)\right] d\theta d\rho d\chi Z_s(d\xi)ds\end{aligned} \tag{A.50}$$

where

$$M_t^f = \int_0^t \int_{\mathcal{E}} \mathbb{1}_{\{i\le\langle Z_{s^-},1\rangle, u\le\Gamma(\boldsymbol{\xi}_{s^-}^i)\}} \left[\sum_{j=1}^{J(\mathcal{A}(\theta,\boldsymbol{\xi}_{s^-}^i))} f\left(H_j^{\mathcal{A}(\theta,\boldsymbol{\xi}_{s^-}^i)}\left(\boldsymbol{\xi}_{s^-}^i|\rho,\chi\right)\right) - f\left(\boldsymbol{\xi}_{s^-}^i\right)\right] \tilde{\mathcal{N}}(ds,di,du,d\theta,d\rho,d\chi) \tag{A.51}$$

is a local martingale associated to the stopping times $(\tau_k)_k$ defined by (A.18).

Then, integrating in θ and using the definitions introduced in A.1.1 we obtain:

$$\begin{aligned}\langle Z_t, f\rangle &= \langle Z_0, f\rangle + M_t^f + \int_0^t \int_{\tilde{\mathcal{X}}} g(x)\left(\partial_a f(x) + \partial_y f(x)\right) Z_s(dx)ds \\ &\quad + \int_0^t \int_{\tilde{\mathcal{X}}} \Bigg\{(1-x)\alpha\left[f(1-x,a,y) - f(x,a,y)\right] \\ &\quad + \int_0^1 \lambda y B_x(a) F_x(\rho)[f(0,0,\rho y) + f(x,0,(1-\rho)y) - f(x,a,y)]d\rho \\ &\quad - d(x,y)f(x,a,y)\Bigg\} Z_s(dr,da,dy)ds \\ &= \langle Z_0, f\rangle + M_t^f + \int_0^t \int_{\tilde{\mathcal{X}}} \mathscr{Q}f(\xi) Z_s(d\xi)ds\end{aligned} \tag{A.52}$$

where we recognised the generator $\mathscr{Q}$ from Eq. (A.47).

Now, to obtain the bracket of M_t^f let's begin by applying Itô's formula to $(M_{t\wedge\tau_k}^f)^2$:

$$\begin{aligned}(M_{t\wedge\tau_k}^f)^2 = \langle Z_{t\wedge\tau_k}, f\rangle^2 - \langle Z_0, f\rangle^2 \\ - 2\int_0^{t\wedge\tau_k} \langle Z_s, f\rangle \int_{\tilde{\mathcal{X}}} \Bigg\{g(x)\left(\partial_a f(x) + \partial_y f(x)\right) + (1-x)\alpha\left(f(1-x,a,y) - f(x,a,y)\right) \\ + \int_0^1 \lambda y B_x(a) F_r(\rho)\left(f(0,0,\rho y) + f(x,0,(1-\rho)y) - f(x,a,y)\right) \\ - d(x,y)f(x,a,y)\Bigg\} Z_s(dx,da,dy)ds\end{aligned} \tag{A.53}$$

Moreover, by using Itô's formula (A.42) applied to $U : x \mapsto x^2$ we obtain:

$$\begin{aligned}\langle Z_{t\wedge\tau_k}, f\rangle^2 = \langle Z_0, f\rangle^2 &+ \int_0^{t\wedge\tau_k} 2\langle Z_s, f\rangle\langle Z_s, g\cdot(\partial_a f + \partial_y f)\rangle ds \\ &+ \int_0^{t\wedge\tau_k}\int_{\mathcal{E}} \mathbb{1}_{\{i\le\langle Z_s,1\rangle, u\le\Gamma(\boldsymbol{\xi}^i_s)\}}\Bigg[\left(\langle Z_s, f\rangle - f(\boldsymbol{\xi}^i_s) + \sum_{j=1}^{J(\mathcal{A}(\theta,\boldsymbol{\xi}^i_s))} f\left(H_j^{\mathcal{A}(\theta,\boldsymbol{\xi}^i_s)}\left(\boldsymbol{\xi}^i_s|\rho,\chi\right)\right)\right)^2 \\ &\quad - \langle Z_s, f\rangle^2\Bigg]\mathcal{N}(ds, di, du, d\theta, d\rho, d\chi)\end{aligned} \tag{A.54}$$

Therefore

$$\begin{aligned}&\langle Z_{t\wedge\tau_k}, f\rangle^2 - \langle Z_0, f\rangle^2 - \int_0^{t\wedge\tau_k} 2\langle Z_s, f\rangle\langle Z_s, g\cdot(\partial_a f + \partial_y f)\rangle ds \\ &- \int_0^{t\wedge\tau_k}\int_{\tilde{\mathcal{X}}}\Bigg\{(1-x)\alpha\Big[\left(\langle Z_s, f\rangle - f(x,a,y) + f(1-x,a,y)\right)^2 - \langle Z_s, f\rangle^2\Big] \\ &+ \int_0^1 \lambda y B_x(a) F_x(\rho)\Big[\left(\langle Z_s, f\rangle - f(x,a,y) + f(0,0,\rho y) + f(x,0,(1-\rho)y)\right)^2 - \langle Z_s, f\rangle^2\Big] \\ &+ d(x,y)\Big[\left(\langle Z_s, f\rangle - f(x,a,y)\right)^2 - \langle Z_s, f\rangle^2\Big]\Bigg\} Z_s(dr, da, dy)ds\end{aligned} \tag{A.55}$$

is a martingale, which is equal to

$$\begin{aligned}&\langle Z_{t\wedge\tau_k}, f\rangle^2 - \langle Z_0, f\rangle^2 - \langle M^f\rangle_t \\ &- 2\int_0^{t\wedge\tau_k}\langle Z_s, f\rangle\int_{\tilde{\mathcal{X}}}\Bigg\{\lambda y\left(\partial_a f(x,a,y) + \partial_y f(x,a,y)\right) + (1-x)\alpha\left(f(1-x,a,y) - f(x,a,y)\right) \\ &+ \int_{\mathcal{K}}\int_0^1 \lambda y B_x(a) F_x(\rho)\left(f(0,0,\rho y) + f(x,0,(1-\rho)y) - f(x,a,y)\right) \\ &- d(x,y) f(x,a,y)\Bigg\} Z_s(dr, da, dy)ds\end{aligned} \tag{A.56}$$

which equals $(M^f_{t\wedge\tau_k})^2 - \langle M^f\rangle_{t\wedge\tau_k}$ with $\langle M^f\rangle_t$ as defined by Eq. (A.49). The uniqueness of Doob decomposition shows then that $\langle M^f\rangle_{t\wedge\tau_k}$ is indeed the quadratic variation of $M^f_{t\wedge\tau_k}$.

Finally, to conclude, since $\tau_k \to +\infty$ a.s. when $k \to \infty$ (see proof of Prop. 4.8.2), we

can make $k \to \infty$ with the Fatou lemma, which gives thanks to Hypothesis (B1) and (B2):

$$\mathbb{E}\left[\langle M^f\rangle_t\right] \leq \liminf_{k\to\infty} \mathbb{E}\left[\langle M^f\rangle_{t\wedge\tau_k}\right] \leq ||f||_\infty^2 \Big(2\alpha \sup_{s\in[0,t]} \langle Z_s, 1\rangle + 3\lambda\bar{b} \sup_{s\in[0,t]} \langle Z_s, Y\rangle + c(\sup_{s\in[0,t]} \langle Z_s, 1\rangle \sup_{s\in[0,t]} \langle Z_s, Y\rangle) \Big)$$

which is finite by Prop. 4.8.2. Therefore $\mathbb{E}\left[\langle M^f\rangle_t\right] < \infty$ and thus M_t^f is a square-integrable true martingale with quadratic variation as defined by Eq. (A.49). □

A.2 Simulation of the process

Since the adder-dependent jump rates are unbounded, a classic acceptance-rejection algorithm to construct an exact solution $(Z_t)_{t\geq 0}$ of (A.15) on $[0, \infty[$, based on the simulation of a Poisson process that dominates Z_t is not possible.

Remark however that, to build a solution Z_t over a bounded interval $[0, T]$ we can use a homogeneous Poisson process with intensity

$$\bar{\Gamma} = N_0 \sup_{y\leq \bar{y}_0 \exp \lambda T} \{\alpha + \lambda(B_0(y) \vee B_1(y)) + d_0(y) \vee d_1(y)\} \tag{A.57}$$

where $\bar{y}_0$ is the size of the biggest initial cell. This is a very coarse bound, especially for large values of T. So acceptance-rejection schemes based on this bound could result in too frequent rejections.

Alternatively, one can simulate first, for each newborn individual, random realizations of the division and death sizes thanks to Proposition A.2.1 below. Then, since the growth is deterministic, the jump times will be deterministic functions of the division/death size, the initial size and the elongation rate. Thereby, using the distributions for the final sizes we can exactly simulate the jumping times for each individual cell. We give the details of this scheme in the next paragraph.

A.2.1 An exact simulation algorithm

We compute the conditional distributions of the sizes at division and death:

Proposition A.2.1. *For every individual :*

- *Conditionally to the division event, the probability density of having added some size a before division, given the SOS type r, is*

$$\eta(a|x) = B_x(a) \exp\left(-\int_0^a B_x(x)dx\right) \tag{A.58}$$

- *Conditionally to the death event, the probability density of having size y at the moment of death, given the SOS type r, the initial size y_0 and the elongation rate λ is*

$$\zeta(y|x, y_0) = \frac{d_x(y)}{\lambda y} \exp\left(-\int_{y_0}^y \frac{d_x(s)}{\lambda s} ds\right) \mathbb{1}_{y\geq y_0} \tag{A.59}$$

Proof. Fix $x \in \{0,1\}, y_0 > 0$. η is obtained by direct differentiation of (A.2). Now, since the death rate is a function d_x of the size, we have that, conditionally to the death event, the lifetime τ of the cell, given the SOS type x and the initial size y_0 is distributed by

$$\mathbb{P}(\tau \leq t|x, y_0) = \exp\left(-\int_0^\tau d_x(y(u))du\right) = \exp\left(-\int_0^\tau d_x(y_0 \exp(\lambda u))du\right) \tag{A.60}$$

Therefore, the conditional size at death is random variable Y defined by

$$Y = y_0 \exp(\lambda\tau) \tag{A.61}$$

Then, by (A.60):

$$\mathbb{P}(Y \leq y|x, y_0) = \mathbb{P}\left(\tau \leq \frac{1}{\lambda}\log\left(\frac{y}{y_0}\right)\middle| x, y_0\right) \tag{A.62}$$

$$= \exp\left(-\int_0^{\frac{1}{\lambda}\log\left(\frac{y}{y_0}\right)} d_x(y_0 \exp(\lambda u))du\right) \tag{A.63}$$

$$= \exp\left(-\int_{y_0}^{y} \frac{d_r(y')}{\lambda y'}dy'\right) \tag{A.64}$$

and we obtain ζ by differentiation. □

Now we construct a solution to (A.19) as follows.

1. Take a initial cell $i \leq N_0$, let $\xi_i = (x, a, y)$ the vector of its traits.
2. Draw $Y \sim \zeta(\cdot|x)$ which is the presumed death size, and draw $A \sim \eta(\cdot|x, y)$ which is the presumed added size before division.
3. Then, the time to death is given by

$$T_{\text{death}} = \frac{1}{\lambda}\log\left(\frac{Y}{y}\right) \tag{A.65}$$

The time to division is given by

$$T_{\text{division}} = \frac{1}{\lambda}\log\left(\frac{y + A - a}{y}\right) \tag{A.66}$$

And the time to switch is obtained by drawing an exponential random variable of parameter $(1-x)\alpha$

$$T_{\text{switch}} \sim Exp((1-x)\alpha) \tag{A.67}$$

4. The jumping time for i is $T_i = T_{\text{death}} \wedge T_{\text{division}} \wedge T_{\text{switch}}$ and the jumping event is ℓ_i which realises the minimum, i.e. such that $T_i = T_{\ell_i}$.
5. Repeat (1-4) for any other initial cell.

6. Let $j \leq N_0$ such that $T_j = \min_{i \leq N_0} \{T_i\}$. $S_1 = T_j$ is the first instant of jump.

7. a) If $\ell_j =$ switch, remove $x_j = (x, a, y)$ from Z_{T_j} and add $x' = (1 - x, a, y)$.
   b) If $\ell_j =$ division, remove $x_j = (x, a, y)$ from Z_{T_j} and draw $\rho \sim F_r$. Add $x' = (0, 0, \rho y)$ and $x'' = (x, 0, (1 - \rho)y)$ to Z_{T_j}.
   c) If $\ell_j =$ death, remove $x_j = (x, a, y)$ from Z_{T_j}

8. For any newly produced cell x_i repeat (1-4).

9. Let $j \leq N_{S_1}$ such that $T_j = \min_{i \leq N_{S_1}} \{T_i\}$. Call $S_2 = T_j$ and repeat (7-8).

10. In general: Let $j \leq N_{S_k}$ such that $T_j = \min_{i \leq N_{S_k}} \{T_i\}$. Call $S_{k+1} = T_j$ the $(k+1)$-th jump and repeat (7-8).

This construction, while exact, requires to draw random variables for each newborn cell which can be computationally extensive. Indeed, *reasonable* bounds on the total jump rate at each step can provide good approximations based on acceptance-rejection schemes. In the next section we provide an example.

A.2.2 Approximate simulation algorithm

We propose an approximate simulation algorithm which uses the following individual bounds: for each living individual i of trait $\xi_i = (x_i, a_i, y_i)$ at time t_k, where $k \in \mathbb{N}$ counts the number of jumps, we put

$$\bar{\Gamma}^i_{t_k} = \sup_{y \leq y_i e^{\lambda \Delta t}} \Gamma(x_i, a_i + y - y_i, y_i) \tag{A.68}$$

with Γ defined by (A.5), and where Δt is a fixed time window. The $(k+1)$-th division event is $t_k + \tau$ where τ is drawn from a Exponential distribution with rate

$$\bar{\Gamma}_{t_k} = \sum_{i=1}^{N_{t_k}} \bar{\Gamma}^i_{t_k} \tag{A.69}$$

The bound is justified if the next event arrives before $t_k + \Delta t$. Thus, we aim to have a Δt big enough to guarantee $\tau \leq \Delta t$, but small enough to avoid frequent rejections. The detailed algorithm is explained in the pseudo-code 1 for a population issued from a single initial cell.

Algorithm 1: Simulation scheme for $(Z_t)_{t\geq 0}$ defined by (A.15)

Data: Initial cell $\xi_0 = (x_0, a_0, y_0)$, simulation time T, calibration time Δt
Result: Ordered list $Z_T = ((x_i, a_i, y_i))_{1\leq i\leq N}$ of living cells ;
List M_T of mother cells which have divided before T

Add (x_0, a_0, y_0) to Z_T ;
Initialise $t = 0$ and the population size $N_0 = 1$;
while $t \leq T$ **do**
  $\bar{\Gamma} \longleftarrow \sum_{i=1}^{N_t} \bar{\Gamma}^i$;
  Draw a random variable $\tau \sim Exp\left(\bar{\Gamma}\right)$;
  foreach $i \in \{1, ..., N_t\}$ **do**
    $y_i \longleftarrow y_i \exp(\lambda\tau)$ (growth dynamics)
  $\Gamma \longleftarrow \sum_{i=1}^{N_t} \lambda y_i B(x_i, a_i) + (1 - x_i)\alpha + d(x_i, y_i)$;
  Draw a random variable $v \sim Unif([0, 1])$;
  if $\Gamma/\bar{\Gamma} \leq v$ **then**
    Calculate individual jump probabilities
    $$p_i = \frac{\lambda y_i B(x_i, a_i) + (1 - x_i)\alpha + d(x_i, y_i)}{\Gamma};$$
    Draw $j \sim Mult(\{p_1, ..., p_{N_t}\})$;
    Draw $\theta \sim Unif([0, 1])$;
    if $\theta \leq \dfrac{\lambda_j y_j B(x_j, a_j)}{\Gamma}$ **then**
      Draw $\rho \sim F(s, \cdot)$;
      Remove cell j from Z_T and add (x_j, a_j, y_j) to M_T;
      Append new individuals $(0, \rho y_j)$ and $(x_j, 0, (f1 - \rho)y_j)$ in the positions j and $j + 1$ in Z_T ;
      $N_{t+\tau} \longleftarrow N_t + 1$;
    else if $\theta \leq \dfrac{\lambda y_j B(x_j, a_j) + (1 - x_j)\alpha}{\Gamma}$ **then**
      Remove cell j from Z_T;
      Append the new individual $(1 - x_j, a_j, y_j)$ at position j in Z_T ;
    else
      Remove cell j from Z_T;
  $t \longleftarrow t + \tau$;

ECOLE
DOCTORALE
DE MATHEMATIQUES
HADAMARD

Titre : Modèle de croissance cellulaire sous l'action d'un stress : Émergence d'hétérogénéité et impact de l'environnement

Mots clés : Populations structurées, Modèles individu-centrés, Données single-cell, Plasticité phénotypique

Résumé : Cette thèse porte sur l'analyse statistique et mathématique de la croissance cellulaire à l'échelle individuelle sous l'effet d'un stress. À partir de l'analyse des données recueillies dans le laboratoire de M. El Karoui, nous avons construit différents modèles permettant une scompréhension à différents niveaux de l'impact que la réponse hétérogène au stress génotoxique (réponse SOS) a sur la croissance d'une population de bactéries *E. coli*. Pour modéliser la dynamique de ces populations on utilise des processus stochastiques à valeurs mesures.
Nous construisons tout d'abord un modèle stochastique basé sur le modèle "adder" de contrôle de la taille, étendu pour incorporer la dynamique de la réponse SOS et son effet sur la division cellulaire. Le cadre choisi est paramétrique et le modèle est ajusté par maximum de vraisemblance aux données de lignées individuelles obtenues en *mother machine*. Cela nous permet de comparer quantitativement les paramètres inférés dans différents environnements.
Nous nous intéressons ensuite aux propriétés ergodiques d'un modèle plus général que "adder", répondant à des questions ouvertes sur son comportement en temps long. On considère un flot déterministe général et un noyau de fragmentation non nécessairement auto-similaire. Nous montrons l'existence des éléments propres. Ensuite, une h-transformée de Doob avec la fonction propre nous ramène à l'étude d'un processus conservatif. Enfin, en montrant une propriété de *petite set* pour les compacts de l'espace d'états, nous obtenons alors la convergence exponentielle du modèle.
Finalement, nous considérons un modèle bitype structuré en âge modélisant la plasticité phénotypique observée dans la réponse au stress. Nous étudions la probabilité de survie et le taux de croissance de la population en environnement constant et périodique. Nous mettons en lumière un trade-off pour avoir la survie de la population, ainsi qu'une sensibilité par rapport aux paramètres du modèle qui n'est pas la même pour la probabilité de survie et pour le taux de croissance.
Nous concluons avec une section indépendante, initiée durant le CEMRACS 2022. Nous étudions numériquement la propagation spatiale des populations structurés en taille modélisant le mouvement collectif de clusters de *Myxobactéries* à travers de systèmes d'équations de réaction-diffusion.

Title : Model of Cellular Growth under Stress: Emergence of Heterogeneity and Impact of the Environment

Keywords : Structured Population Dynamics, Individual-Based Models, Single-cell data, Phenotypic plasticity

Abstract : This thesis focuses on understanding individual-scale cell growth under stress. Starting from the analysis of the data collected in M. El Karoui's lab, we have developed various models to comprehend the impact of the heterogeneous response to genotoxic stress (SOS response) on the growth of a *Escherichia coli* bacteria populations. We employ measure-values stochastic processes to model the dynamics of these populations.
Firstly, we construct a stochastic model based on the "adder" size-control model, extended to incorporate the dynamics of the SOS response and its effect on cell division. The chosen framework is parametric, and the model is fitted by maximum likelihood to individual lineage data obtained in *mother machine*. This allows us to quantitatively compare inferred parameters in different environments.
Next, we explore the ergodic properties of a more general model than the "adder," addressing open questions about its long-time behaviour. We consider a general deterministic flow and a fragmentation kernel that is not necessarily self-similar. We demonstrate the existence of eigenelements. Then, a Doob h-transform with the foud eigenfunction reduces the problem to the study of a conservative process. Finally, by proving a "petite set" property for the compact sets of the state space, we obtain the exponential convergence.
Finally, we consider a bitype age-structured model capturing the phenotypic plasticity observed in the stress response. We study the survival probability of the population and the population growth rate in constant and periodic environments. We evince a trade-off for population establishment, as well as a sensitivity with respect to the model parameters that differs for survival probability and growth rate.
We conclude with an independent section, collaborative work initiated during CEMRACS 2022. We investigate numerically the spatial propagation of size-structured populations modeling the collective movement of *Myxobacteria* clusters via a system of reaction-diffusion equations.

Institut Polytechnique de Paris
91120 Palaiseau, France